Sedimentology and Stratigraphic Architecture of Fluvial to Shallow Marine Deposits

Bassam Hamdan Alshammari

Submitted in accordance with the requirements for the degree of
Master of Philosophy

The University of Leeds
School of Earth and Environment

February, 2021

Intellectual Property and Publication Statements

The candidate confirms that the work submitted is his own and that appropriate credit has been given where reference has been made to the work of others.

Acknowledgements

All praises due to Allah, the most knowledgeable.

I would like to express my gratitude to my research supervisors, Prof. Nigel Mountney and Dr. Luca Colombera for their support, guidance, suggestions and patience during my M.Phil study and related research. The immense knowledge they have, has helped me expand my knowledge and develop my research skills. The outcome of working with them has made a better researcher out of me and surely will make me a more valuable asset to my sponsors, Saudi Aramco.

I would also like to extend my thanks to my sponsors, Saudi Aramco, specifically to the management of Geological Operation Department for giving me the opportunity to pursue my M.Phil study. My thanks also go to my mentor Dr. Mohammed Al-Masrahy, for his guidance and support before and during my M.Phil research. I also would like to thank Mahmud Alkathery for his advice, related to life and study in Leeds.

My sincere thanks go to my mother, father and siblings for their continuous encouragement, prayers and support. My special and warm thanks are due to my loving, supportive and patient wife and two little boys for taking the M.Phil journey with me in Leeds and for their support and patience especially during working from home. My M.Phil would not have been completed without the support of these people. I am eternally grateful.

Preface

Two chapters of the thesis (Chapter 3 and 4) have been written in the style of paper. Chapter 3 has been submitted to the peer-reviewed journal, Journal of Sedimentary Research, and has been accepted for publication on 14th of March, 2021. The accepted version of the paper is included in the appendix. Chapter 4 is planned to be submitted for publication after concluding the M.Phil research.

Abstract

The interaction of fluvial, tidal and wave processes in coastal and paralic environments gives rise to accumulations represented in the sedimentary record by varied types of architectural elements. The internal facies characteristics and external preserved geometry of these sedimentary units is determined by the morphology and the evolutionary behaviour of the range of coastal sub-environments.

This study includes the results of two related projects. The first project analyses fluvial to shallow marine deposits through the consideration of subsurface dataset obtained from the Middle Jurassic lower Dhruma Formation in Saudi Arabia. The dataset comprises facies descriptions based on cores, thin sections, gamma-ray loges and FMI images. It achieves the following: i) it examines and demonstrates sedimentary relationships between various fluvial, nearshore and shallow-marine deposits; ii) it develops depositional models to account for the stratigraphic complexity inherent in fluvial to shallow-marine successions; iii) it documents the sedimentology and the stratigraphic evolutionary patterns of the lower Dhruma Formation in the studied area of Saudi Arabia. The second project examines estuarine tidal bars based on quantitative data extracted from many published studies. The second project i) investigates the geometry and size of tidal bars known from modern systems and their deposits preserved in ancient outcropping successions; ii) illustrates their sedimentological characters (internal facies organisation, external form and architectural geometry); iii) investigates the nature of juxtaposition of tidal bars in association with other estuarine and shallow-marine elements; iv) highlights tidal-bar development and preservation; and vi) presents implications of the results for reservoir prediction and characterisation.

Table of Contents

Intellectual Property and Publication Statements I

Acknowledgements II

Preface III

Abstract IV

List of Tables VIII

List of Figures IX

1 Introduction 17

1.1 Overview 17

1.2 Aims and Objectives 18

1.3 Research Questions 19

1.3.1 What controls sedimentation in fluvial to shallow marine settings? What controls the interaction between siliciclastic and carbonate deposition? 19

1.3.2 What controls the deposition and preservation of tidal bars? How are they different from each other? What scales of lithological heterogeneity exist within them? 21

1.4 Thesis structure 22

1.4.1 Chapter 1: Introduction 22

1.4.2 Chapter 2: Literature review 22

1.4.3 Chapter 3: Sedimentology and Stratigraphic Architecture of a Fluvial to Shallow Marine Succession: The Jurassic Dhruma Formation, Saudi Arabia 23

1.4.4 Chapter 4: Quantitative analysis of tidal bars in tide-dominated estuaries: modern systems and ancient preserved successions 23

1.4.5 Chapter 5: Discussion 24

1.4.6 Chapter 6: Conclusions and Future work 24

2 Literature Review 25

2.1 Fluvial Systems 25

2.2 Coastal depositional systems 27

2.2.1 Coastal process-based classifications 28

2.2.2 Tidal depositional systems 33

2.2.3 Estuaries 36

2.2.4 Deltas 41

2.2.5 Fluvial to marine transition zone 44

2.2.6 Controls on coastal environments 47

2.3 Mixed siliciclastic and carbonate systems 47

2.4 Palaeosols 49
2.5 Ichnology 49
2.6 Importance of analogues and quantitative studies 51
3 Sedimentology and Stratigraphic Architecture of A Fluvial to Shallow Marine Succession: The Jurassic Dhruma Formation, Saudi Arabia 53
3.1 Introduction 53
3.2 Geological setting 57
3.3 Data and methods 59
3.3.1 Subsurface datasets 59
3.3.2 Constraining uncertainty associated with inter-well correlation 61
3.4 Results 62
3.4.1 Fluvial-channel deposits (FA1) 68
3.4.2 Intertidal and pedogenically modified supratidal flat or floodplain (FA2): intertidal flat deposits (FA2a) 70
3.4.3 Intertidal and pedogenically modified supratidal flat or floodplain (FA2):pedogenically modified supratidal flat or floodplains (FA2b) 72
3.4.4 Fluvial-influenced tidal bars (FA3) 75
3.4.5 Shoreface to offshore transition and delta-front to prodelta (FA4): weakly storm-affected shoreface to offshore-transition zone (FA4a) 78
3.4.6 Shoreface to offshore transition and delta-front to prodelta (FA4): storm-dominated river-influenced prodelta to delta-front deposits (FA4b) 80
3.4.7 Open-marine shelf (FA5): carbonate shelf (FA5a) 82
3.4.8 Open-marine shelf (FA5): iron-rich oolitic shoal (FA5b) 84
3.4.9 Palaeocurrent analysis 87
3.4.10 Spatial distribution of facies associations 88
3.5 Discussion 94
3.5.1 Controls on sedimentation in the lower Dhruma Formation 94
3.5.2 Climate and sediment source 97
3.6 Conclusions 98
4 Quantitative analysis of tidal bars in tide-dominated estuaries: modern systems and ancient preserved successions 99
4.1 Introduction 99
4.2 Background 101
4.3 Data and Methods 105
4.3.1 Overview 105
4.3.2 Data Collection and Data Types 110

4.3.3 Statistical Analysis 112
4.4 Results 113
4.4.1 Geomorphic Dataset from Modern Estuaries 113
4.4.2 Architectural Dataset from Modern and Ancient Estuaries 121
4.4.3 Vertical Succession and Nature of Juxtaposition of Elements 126
4.5 Discussion 129
4.5.1 Controls on Tidal Bar Size and Architecture 129
4.5.2 Grain size Distribution within Estuaries 130
4.5.3 Preservation and Reservoir Potential 131
4.6 Conclusions 133
5 Discussion 135
5.1 What controls sedimentation in fluvial to shallow-marine settings? What controls the interaction between siliciclastic and carbonate deposition? 135
5.1.1 Controls on the Deposition of Fluvial to Shallow-Marine Sediments 136
5.1.2 Controls on the Interaction of Siliciclastic and Carbonate Deposits 140
5.1.3 Modern Environments 143
5.2 What controls the deposition and preservation of tidal bars? How are they different from each other? What types of heterogeneity exist within them? 150
5.2.1 Controls on the Deposition and Preservation of Tidal Bars 150
5.2.2 Types of tidal bars 152
5.2.3 Lithological Heterogeneities in Tidal Bars 154
6 Conclusions and future work 159
6.1 Conclusions 159
6.2 Future Work 161
References 163

List of Tables

Table 3.1: Summary of lithofacies observed in the lower Dhruma Formation.. 65

Table 3.2: Summary of the facies associations defined in this study along with their occurrence with respect to well locations. 66

Table 4.1: Showing the geographic location of modern estuaries from which tidal bras were examined. ‘N’ denotes the number of tidal bars. 109

Table 4.2: Shows the name of the formation, the geographic location, age, data type and sources of the case studies considered in this study from the architectural point of view. ‘N’ denotes the number of tidal bars..... 110

Table 4.3: Relationships between tidal-bar dimensions based on Pearson (Rp) and Spearman (Rs) correlation coefficients.‘N’ denotes the number of tidal bars. ‘P’ denotes the statistical significance (P-value)..... 117

List of Figures

Figure 2.1: Simplified plan view diagram showing the arrangement of fluvial system subenvironments..... 26

Figure 2.2: Plan view map depicting the simplified morphology of coastal depositional systems showing their relationships and different geomorphologies, adapted after Harris et al. (2002) and Shiers (2016)..... 28

Figure 2.3: Schematic diagram showing the characterisation of deltas into fluvial-dominated, wave-dominated and tide-dominated types, adapted after Galloway (1975) and Shiers (2016)..... 29

Figure 2.4: Coastal process classification ternary plots, adapted after Ainsworth et al. (2011). F = Fluvial dominated; W = Wave dominated; T = Tide dominated. Capital letters indicate the dominant process, lower case letters indicate a process which influences an environment and lower case letters in italics indicate a process which modifies the environment. 30

Figure 2.5: Representative schematic plan view models of the 15 classification categories in the coastal process classification presented in Figure 2.4, adapted after Ainsworth (2011) and Shiers (2016)..... 31

Figure 2.6: Image of the modern coastline of the Mouth of the Ganges and adjacent region showing how depositional process dominance results in different coastline morphologies and how dominant processes can change laterally over relatively short distances. Images courtesy of Google Earth..... 32

Figure 2.7: A two-tier ternary classification to account for the dominant and influencing processes based on the relative importance of each of the processes. F= Fluvial, T= tidal and W= wave processes. The capital letters indicate the dominant process and the lower case letters indicate the influencing process. Modified after Nyberg and Howell (2016)..... 33

Figure 2.8: A) The arrangement of Moon-Earth-Sun orbital system in a synodic month. B) Schematic representation of depositional response to two spring-neap cycles. Adapted after McLean and Wilson (2016). 36

Figure 2.9: A) Morphology and B) Energy types their distribution in tide-dominated estuaries, adapted from Dalrymple et al. (1992). 39

Figure 2.10: A) Morphology and b) Energy types and their distribution in wave-domianted estuaries, adapted from Dalrymple et al. (1992). 40

Figure 2.11: Modern examples of A) river-dominated, B) tide-dominated and C) wave-dominated deltEarth.as. Images courtesy of Google Earth. 43

Figure 2.12: Environmental subdivision of a deltaic environment, adapted from (Bhattacharya, 2006). 44

Figure 2.13: Diagram showing the changes in facies, energy, grain size, salinity and channel morphology through the fluvial to tidal transition and the processes at work. After Dalrymple et al. (1992), Martinius & Gowland (2011), Dalrymple & Choi (2007), van den Berg & van Gelder (2007), Shanley & McCabe (1994) and Shiers (2016). 45

Figure 2.14: Schematic representation of a semi-quantitative assessment of bioturbation intensity, modified from Bann et al. (2008). 51

Figure 3.1: A) Simplified regional geological map of the Arabian Peninsula adapted from Stewart et al. (2016). B) Well distribution map within the study area. The exact geographic location of the wells cannot be published due to the proprietary nature of the dataset. C) Generalized stratigraphy of Eastern Saudi Arabia. 57

Figure 3.2: Representative sedimentary logs depicting the different facies associations defined in the lower Dhruma Formation and their vertical relationships. A) 'Fluvial channels' and 'intertidal flats and pedogenically modified supratidal or floodplain facies associations B) 'fluvial-influenced tidal bars' facies associations, C) 'weakly storm-affected shoreface and offshore transition zone' and ' fluvial-influenced storm-dominated delta-front and prodelta' facies associations; note the occurrence of the oolitic ironstone facies association Fa5 below the shoreface successions; D) carbonate shelf facies associations occurring in the uppermost part of the cored section; E) simplified paleogeographic map of the lower unit of the lower Dhruma Formation based

on this study; F) Legend with color codes for facies associations and symbols used in the sedimentary logs. See text for further explanation. 67

Figure 3.3: Representative core photographs of 'fluvial channel' facies association (FA1). A-B) massive to faintly bedded sandstone with lag sediments at the bottom and common floating coal debris and mud chips; B) Alternating sandstone and heterolithic facies D-E) transition between sandstone and heterolithic facies (white arrows indicate double mud drapes in (D); F) destratified facies of FA2b overlying the FA1, G-H) thin sections representing the petrography of the sandstone facies (G) and heterolithic facies (H) defined in FA1; note grain size and mud content variation..... 70

Figure 3.4: Representative core photographs of 'tidal flat' (FA2a, A-C) and 'paleosol' (FA2b, D-G) facies associations. A-B) heterolithic sand and mud facies; note the stacked bidirectional ripple forms (black arrows) and double mud drapes (white arrows); C) intense bioturbation within the sand-mud alternation; D-E) kaolinite-rich sandstone, siltstone and mudstone with intense rooting; note the color mottling in photograph E; F-G) coaly mudstone. H-I) representative thin sections of the heterolithic facies of FA2a..... 74

Figure 3.5: Representative core photographs of the 'fluvial-influenced tidal bars' facies association (FA3). A) cross-bedded sandstone with apparent bundled bedsets showing internal mud drapes; B-C) cross-stratified sandstone showing thin beds of very coarse sand within medium-grained sandstone; note the double mud drapes in (B). D-E) heterolithic and kaolinite-rich deposits that overlie the tidal bar deposits; F-G) representative thin sections of tidal-bar facies; note the kaolinite in photograph G. 77

Figure 3.6: Representative core photographs of 'offshore-transition zone to shoreface' (FA4a; A-D) and prodelta to delta-front (FA4b; E-I) facies associations. A) heterolithic facies overlying bioturbated sandstone; B) slightly asymmetrical wave ripple; C) bioturbated sandstone; D) representative thin section showing deformed chamosite ooids within heterolithic facies; E-F) thin sandstone intervals interbedded with heterolithic and mudstone facies; G-H) hummocky cross stratification; I) thin section showing abundant chlorite cement within hummocky cross-stratified sandstone. 82

Figure 3.7: Representative core photographs of 'open-marine shelf carbonate' facies association (FA5). A-B) bioturbated limestone; C) calcareous mudstone; D) calcareous sandstone overlying massive mudstone; E) ooid-rich ironstone; F-G) representative thin section examples showing calcareous sandstone (F) and ooid-rich ironstone (G)..... 86

Figure 3.8: Rose diagrams showing the dominant dip direction of cross-stratification in different sandstone units, based on analysis of image logs. See Figure 4 for keys to facies associations and symbols..... 88

Figure 3.9: Cross plots showing thickness and lateral dip extent for analog sedimentary units that broadly match with the defined facies associations, as derived from a sedimentological database (Colombera et al., 2016a). A) Data relating to parasequence-scale sedimentary units representing the product of regression of shoreface and more generally shallow marine (i.e., encompassing sand-prone offshore transition) sand belts (Colombera et al., 2016a and b); Colombera & Mountney, 2020); B) Data relating to architectural elements classified as 'tidal bar' and 'tidal flat' 89

Figure 3.10: Strike-oriented stratigraphic cross-section (A-A') showing the distribution of facies associations and key stratigraphic surfaces as correlated along strike in a seaward position. 91

Figure 3.11: Strike-oriented stratigraphic cross-section (B-B') showing facies associations and stratigraphic surfaces as correlated along strike in a landward position compared to cross-section A-A'. 92

Figure 3.12: Dip-oriented stratigraphic cross-section (C-C') intersecting the two strike-oriented cross sections (A-A' and B-B') showing the distribution of facies associations and key stratigraphic surfaces as correlated along depositional dip, and documenting the increase in marine deposits towards the northeast (basinward)..... 93

Figure 3.13: A depositional model depicting the evolution of the Middle Jurassic lower Dhruma Formation over five intervals. Each interval represents a synthesis 96

Figure 4.1: Organisation of tidal sand bars in Cobequid Bay, Bay of Fundy, adapted from Dalrymple and Rhod (1995) and B) Bathymetric map showing an oblique landward view of the arrangement of tidal dunes in San Francisco Bay (Barnard et al., 2006). Note the relationship between the dominant flow direction and the organisation of tidal bars and tidal dunes..... 103

Figure 4.2: Comparison of the architecture and vertical succession of A) tidal bars, modified from Dalrymple (2010) and B) tidal dunes, modfied from Mutti et al. (1985). 104

Figure 4.3: Representative sketch of tidal bar types defined in Dalrymple and Choi, (2007) and Luven et al. (2016). A) elongate, B) sidebar, C) lobate and D) complex bars. Modified after Luven et al. (2016)..... 106

Figure 4.4: Geographic location of estuaries considered in this study. Red circles represent locations of geomorphic data and green circles represent locations of architectural data from both modern and ancient estuaries..... 108

Figure 4.5: Satellite images showing examples of modern estuarine tidal bars. Locations are indicated at the top left corner of each example. Images are courtesy of Google Earth..... 111

Figure 4.6: Cross plots showing the relationships of tidal bar dimensions, A) width-length, B) length-height and C) width-height relationships..... 114

Figure 4.7: Box-plots show ranges of readings relating to A) lengths, B) widths and C) heights of tidal bars of different types (Elongate, Complex, Sidebar and Lobate). For each box-plot, boxes represent interquartile ranges, open circles represent mean values, horizontal bars within the boxes represent median values, and black dots represent outliers (values that are more than 1.5 times the interquartile range). ‘N’ denotes the number of readings. ‘σ’ denotes the standard deviation. ‘F’ denotes the one-way analysis of variance (Anova). ‘P’ denotes P-value. 115

Figure 4.8: Cross plots showing the relationships of tidal bar dimensions, A-D) width-length, E-H) length-height and I-L) width-height relationships. 116

Figure 4.9: Cross plots showing the relationships between size of estuaries and tidal bars. A) relationship of mean estuary depth and mean bar height and B) relationship of mean estuary width and mean bar width. ‘N’ denotes the number of readings..... 118

Figure 4.10: Examples of estuary types compared in this study, A) bar-built estuaries (Columbia River, Oregon, USA) and B) coastal-plain (Themes River, UK). 119

Figure 4.11: Box-plots show ranges of size readings relating to A) estuary width, B) estuary depth, C) bar length, D) bar width and E) bar heights across bar-built and coastal-plain estuaries. For each box-plot, boxes represent interquartile ranges, open circles represent mean values, horizontal bars within the boxes represent median values, and black dots represent outliers (values that are more than 1.5 times the interquartile range). ‘N’ denotes the number of readings. ‘σ’ denotes the standard deviation. ‘t’ denotes the two-sample t-test. ‘df’ degrees of freedom. ‘P’ denotes P-value. 121

Figure 4.12: Histogram shows tidal bar thickness distribution across 53 tidal bars. ‘N’ denotes number of readings. ‘σ’ denotes the standard deviation. 122

Figure 4.13: Pie charts illustrating A) proportion of lithiotypes and B) proportion of sand grainsize across tidal bars. ‘N’ denotes the number of readings..... 123

Figure 4.14: A) Pie charts illustrating the proportion of sandstone facies across tidal bars and B) Box-plots illustrating the variation in means of thickness of sandstone facies. the grain size variation in planar and trough-cross bedding sandstone. For each box-plot, boxes represent interquartile ranges, open circles represent mean values, horizontal bars within the boxes represent median values, and black dots represent outliers (values that are more than 1.5 times the interquartile range). ‘N’ denotes the number of readings. ‘σ’ denotes the standard deviation. ‘t’ denotes the two-sample t-test. ‘df’ degrees of freedom. ‘P’ denotes P-value. 124

Figure 4.15: A) Pie chart illustrating the proportion of mudstone facies across tidal bars and B) Box-plots illustrating the variation in means of thickness of mudstone facies. the grain size variation in planar and trough-cross bedding sandstone. For each box-plot, boxes represent interquartile ranges, open

circles represent mean values, horizontal bars within the boxes represent median values, and black dots represent outliers (values that are more than 1.5 times the interquartile range). ‘N’ denotes the number of readings. ‘σ’ denotes the standard deviation. ‘t’ denotes the two-sample t-test. ‘df’ degrees of freedom. ‘P’ denotes P-value. 125

Figure 4.16: Pie charts illustrating the grain size variation in A) planar, B) trough, C) undefined cross-bedded sandstone while D) show the variation in grain size in bioturbated sandstone. ‘N’ denotes the number of readings. 126

Figure 4.17: Graphs show the count of elements that tidal bars interact with in tidal estuaries. A) shows the elements occur below tidal bars and B) show the elements that occur on top of tidal bars..... 128

Figure 4.18: Schematic diagrams showing how marine mud fills the estuary bay and subsequently preserve tidal bars, adapted from (Plink-Björklund, 2005). 133

Figure 5.1: A) generalised vertical section showing the vertical stratigraphic evolution of lower Dhruma Formation, B) series of schematic representation of change in shoreline morphology during the Middle Jurassic in the study area. The letter on the maps indicate the processes by which the shoreline was affected (T= tide, F= fluvial and wave= w. the capital letter indicate the dominant control while the lower case letter indicate the subsequent control. 139

Figure 5.2: Schematic diagram showing the facies-scale interaction between siliciclastic and carbonate deposits, adapted after Chiarella et al. (2017). Refer to Figure 5.1 for key to facies and facies association. 141

Figure 5.3: Schematic diagram showing the architectural element-scale interaction between siliciclastic and carbonate deposits. The interaction can a result of increased rate of sediment supply that outpaces relative sea-level rise or during stilstand periods (Scenario 1) or it can be produce during relative fall in sea level irrespective of rate of sediment supply (scenario 2). Refer to Figure 5.1 for key to facies and facies association. 142

Figure 5.4: A-C) Possible modern example from the Conwy estuary (UK) that is deduced to be analogous to the facies FA1, FA2 and FA3. Note that image B

shows the estuary during low tides while C shows it during high tide. Images are courtesy of Google Earth..... 146

Figure 5.5: Possible modern analogues to A) FA4a and B) FA4b. Images are courtesy of Google Earth..... 147

Figure 5.6: A) Possible modern example for the oolitic shoal deposits defined in FA5a from the west of Great Bahama Bank, B) zoomed-in image of B. Images are courtesy of Google Earth..... 148

Figure 5.7: A) Iron-rich river water flowing into the sea, which may resemble the processes by which the iron was delivered to the oolitc shoals defined in FA5b. B) zoomed-in image of A. Images are courtesy of Google Earth..... 149

Figure 5.8: Schematic diagram presenting the types of tidal bars defined in estuaries. Estuary model modified after Dalrymple et al. (1992). Note the location of each bar with respect to the tidal maximum zone. 153

Figure 5.9: Block diagrams presenting the scale of lithological heterogeneity in tidal bars. The Mesoscopic heterogeneity in Figure C is further discussed in the following Figure (Figure 5.10)..... 157

Figure 5.10: Examples of the occurrence of mud drapes in tidal deposits. A) continuous mud drapes that separate sandstone bedsets in the Trompeloup tidal bar in Gironde estuary, adapted from Fenies and Tastet (1998), B-C) examples showing continuous mud drapes at dunes foresets, after Collinson et al. (2016), D) synthetic example of mud drapes at the front of barform that taper from the bar top and pinchout above its base which provides laterally-connected lower section, adapted from Colombera et al. (2018) and E) discontinuous mud drapes across the top of the Plassac tidal bar in Gironde estuary, adapted from Virolle et al. (2019). 158

1 Introduction

This chapter provides an overview of the thesis and outlines its structure. Two sets of research questions that framed this research are stated herein. To answer these questions, two related investigative projects have been undertaken and their principal results are reported in main body of the thesis. The two discrete projects each form core chapters in this thesis (chapters 3 and 4). The first project is based on subsurface datasets obtained from the Middle Jurassic lower Dhruma Formation in Saudi Arabia. The second project is a quantitative study on estuarine tidal bars and their accumulated deposits based on data collected from published sources.

1.1 Overview

Coastal fluvial and shallow marine systems located adjacent to and offshore from marine shorelines are important depositional settings. Sedimentary successions representing the accumulated deposits of these systems are inherently complex due to the interaction of many different processes that control sediment distribution and stratigraphic architectures. The controls on the sedimentary evolution of these systems are manifested by fluvial, tide and wave processes and, at a larger scale, by the interplay of sediment supply and sea-level change. The deposits of fluvial and shallow marine environments are typically represented by a mosaic of types of architectural elements (Miall, 1985; Olariu et al., 2012; Vakarelov and Ainsworth, 2013). The internal lithofacies composition and external preserved geometry of these sedimentary units is determined in large part by the morphology and the evolutionary

behaviour of the range of formative coastal sub-environments (Dalrymple et al., 2003).

Discerning the controls that influence the resultant accumulated architecture of sedimentary units requires detailed analysis of their characters and sedimentologic expressions from a range of modern settings and ancient preserved successions. Gaining an improved understanding of the controls on fluvial and shallow marine sediment distribution, and sedimentary architecture leads to better-informed approaches to the reconstruction of palaeoenvironments. From an applied standpoint, understanding the sediment distribution and the stratigraphic evolution of such deposits leads to improved characterisation and assessment of subsurface reservoirs.

1.2 Aims and Objectives

The aim of this study is to understand the controls that govern the deposition of fluvial and shallow marine sediments that accumulated in near-coast settings and to investigate their spatial and temporal stratigraphic architecture. Specific objectives are as follows:

I. Examine and demonstrate stratigraphic relationships between fluvial and shallow marine deposits generated by coevally active depositional systems.
II. Document and present the stratigraphic evolutionary patterns and account for the stratigraphic complexity inherent in fluvial and shallow marine settings through the development of bespoke and novel depositional models.
III. Document and investigate the relationships between shallow marine siliciclastic and carbonate deposits.

IV. Investigate the nature of tidal bars in tidal-dominated estuaries, and their resultant deposits accumulated as stratigraphic successions.

V. Present a summary of the heterogeneity types that exist in estuarine tidal bars and their deposits.

1.3 Research Questions

Two sets of questions have been developed to frame the overall research theme. The answers to the questions are stated in the integrated discussion chapter (chapter 5).

1.3.1 What controls sedimentation in fluvial to shallow marine settings? What controls the interaction between siliciclastic and carbonate deposition?

Fluvial to shallow marine settings host a wide range of environments, including estuaries, deltas and strandplains. The sedimentology of teh deposits of fluvial and shallow marine environments is governed by different factors that occur at multiple scales. Sea-level fluctuations, rate of accommodation generation and rate of sediment supply act to control patterns of sedimentation at large scales. The deposits of fluvial and shallow marine environments are also controlled by the interaction of fluvial, tidal and wave processes that govern their lithology distribution and sedimentary architecture at smaller scales. These processes vary through space and time, and the pattern in which they occur is inherently complex. As such, their sedimentological indicators in the rock record requires careful investigation to interpret detailed aspects of the palaeoenvironments represented by preserved successions.

Within the realm of fluvial and coastal environments, there exists a tract known as fluvial to marine transition zone (FMTZ). The FMTZ is defined by the upstream limit of marine processes and the downstream limit of fluvial process (Dalrymple and Choi, 2007; van den Berg et al. 2007). This zone extends for tens to hundreds of kilometres upstream from shorelines at the lower reaches of major rivers, as seen for example in the present-day Fraser River delta, western Canada (Dashtgard et al., 2012), in the Fly River delta, Papua New Guinea (Dalrymple et al., 2003) and in the Amazon River, Brazil, (Dalrymple et. al., 2015). The seaward end of this tract is documented by many studies, including, for example, those that examine gravity-flow deposits of the Fraser River delta front associated with fluvial-tidal interaction (Ayranci et al., 2012) and remote sensing analysis of the outward delta plume of the Mekong River (Loisel et al., 2014).

In shallow marine settings, given appropriate combinations of latitude, climate, water depth, and a limited supply of nutrients and clastic detritus, carbonate deposition may occur in parts of systems that are elsewhere dominated by clastic sedimentation (Vicalvi and Milliman, 1977). Siliciclastic sediments can interact with carbonate sediments in shallow marine settings at a range of scales from the small (facies-unit) scale to the large (stratigraphic-unit) scale (Chiarella et al., 2017).

The interaction of fluvial and shallow marine deposits (including those of carbonate origin) produce complex stratigraphic patterns. Careful investigation of their sedimentological characters and their controls is key to better understand how these deposits operate in space and time. This study seeks to understand the factors that controlled their deposition and their stratigraphic evolutionary patterns in the rock record through the consideration of subsurface

dataset obtained from the Middle Jurassic lower Dhruma Formation in Saudi Arabia.

1.3.2 What controls the deposition and preservation of tidal bars? How are they different from each other? What scales of lithological heterogeneity exist within them?

Tidal bars are notable features of tidal estuaries (e.g. Dalrymple and Rhodes, 1995; Fenies and Tastet, 1998; Dalrymple et al., 2003). They develop over a wide range of scales from tens of metres to several kilometres in length and width, and a few tens of metres in height (Tang et al., 2019).

The first part of this research (Chapter 3) describes fluvial to shallow marine successions based on subsurface datasets from the Middle Jurassic lower Dhruma Formation in Saudi Arabia, where tidal-bar deposits form a component of these successions. Tidal-bar deposits are observed at different spatial locations, at different stratigraphic levels, and at different scales in the Lower Dhruma Formation. However, they are described based on one-dimensional subsurface datasets, which are inherently associated with uncertainties related to their true size and three-dimensional architecture.

As such, applied geoscientists commonly utilise analogous examples from successions exposed in outcrops and from modern systems to predict their three-dimensional geometry and detailed internal facies organisation. However, single analogues may be suitable only in particular, limited cases (Howell et al., 2014). The second part of this research (chapter 4) seeks to understand the controls on the deposition and preservation of estuarine tidal bars, and discusses their internal sedimentological characters through a quantitative study for which data from many published sources were extracted and analysed.

1.4 Thesis structure

The thesis consists of 6 chapters, two of which are the primary data chapters (chapters 3 and 4). The methods used in these two chapters are different; therefore, each of these two chapters contain their own dedicated methods section. Brief descriptions of all chapters are given below:

1.4.1 Chapter 1: Introduction

This chapter introduces the aim and objectives, and the research questions that form the theme of this research.

1.4.2 Chapter 2: Literature review

This chapter provides a brief review of published literature related to key concepts covered in this thesis. This includes aspects of sedimentary geology of coastal fluvial and shallow marine environments, schemes for classifying coastal systems, the fluvial-to-marine transition zone (FMTZ) and palaeosols. The literature review also includes a brief overview on the mixing of siliciclastic and carbonate deposits, and the significance of utilising ichnology in sedimentological studies. The last portion of this chapter highlights the importance and benefits of using quantitative approaches to study certain types of depositional units, especially in relation to gaining improved understanding of the three-dimensional sedimentary architecture of subsurface successions at a scale below seismic resolution.

1.4.3 Chapter 3: Sedimentology and Stratigraphic Architecture of a Fluvial to Shallow Marine Succession: The Jurassic Dhruma Formation, Saudi Arabia

This chapter accomplishes the following: i) it examines and demonstrates the relationships between contemporaneous and genetically related fluvial and shallow marine deposits; ii) it documents and presents the evolutionary patterns and accounts for the stratigraphic complexity inherent in a fluvial and shallow marine setting through development of bespoke and novel depositional models; iii) it investigates the relationships between shallow marine siliciclastic and carbonate deposits.

1.4.4 Chapter 4: Quantitative analysis of tidal bars in tide-dominated estuaries: modern systems and ancient preserved successions

This chapter accomplishes the following: i) it quantitively documents the form and sedimentology of tidal bars in tide-dominated estuaries and their resultant deposits through a quantitative investigation of the geometry and size of tidal bars known from a suite of modern systems and their deposits preserved in ancient outcropping successions; ii) it illustrates the sedimentological characters of tidal bar deposits (internal facies organisation, external form and architectural geometry); iii) it investigates the nature of juxtaposition of tidal bars in association with other estuarine and shallow marine elements; iv) it highlights processes and mechanisms of tidal-bar development and preservation; and vi) it presents implications of the results for reservoir prediction and characterisation.

1.4.5 Chapter 5: Discussion

The discussion chapter integrates the results from the subsurface study of the lower Dhruma Formation (chapter 3) and the quantitative study of estuarine tidal bars and their deposits (chapter 4) to develop and present a discussion of factors that influence patterns of sedimentation and the nature of the stratigraphic record in paralic sedimentary systems. Specifically, this chapter seeks to answer and address the research questions posed herein.

1.4.6 Chapter 6: Conclusions and Future work

This chapter summarises the main findings in this research and provides recommendations for future research.

2 Literature Review

2.1 Fluvial Systems

Fluvial systems are the principal agent for the transportation of weathered debris from continental drainage basins (catchment areas), overland to bodies of water (lakes and seas). Fluvial currents are responsible for eroding, transporting and depositing sediments in different ways and in different environments within the system. Sediments are transported away from the source catchment area via a range of physical transport processes, including debris-flow, bedload and suspended-load transport processes.

Lithofacies units in fluvial systems, and also in other siliciclastic sedimentary systems, are typically classified based on distinct characteristics of grain size, texture and sedimentary structures. These sedimentological characteristics yield information about small-scale depositional processes. For example, certain types of gravel and matrix-supported deposits might be inferred to represent deposition through debris flows (Miall, 2010; Bridge, 1993). Different assemblages of lithofacies occur in association and represent a wide range of architectural elements within confined channels and overbank environments (Miall, 2010). Architectural elements occur at larger scales than lithofacies units, and typically yield information on larger-scale aspects of depositional environment (Bridge, 1993). Miall (1985) described 8 types of fluvial architectural elements based on attributes relating to lower and upper surfaces, internal and external geometry, and lithofacies assemblages. Common architectural elements deposited within confined channels include channel-fill deposits, sandsheets and bar forms, whereas overbank architectural

elements include floodplain fines, levees and crevasse splays (Figure 2.1; Miall, 1985, 2010).

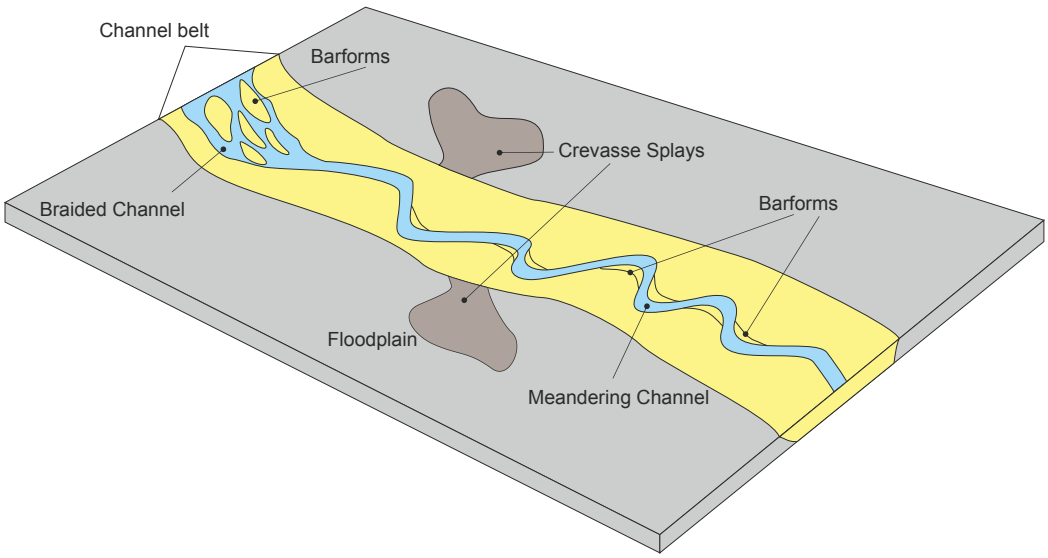

Figure 2.1: Simplified plan view diagram showing the arrangement of fluvial system subenvironments.

Rivers in lower coastal plains carry sediments and deposit them into seas (or lakes). The interface between rivers and seas is characterised by the interaction of fluvial and marine process (tides and waves). Different combination of these processes in marine coastal regions produces different morphological and sedimentary patterns. River-linked coastal environments include deltas and estuaries, which are typically classified based on the dominant process acting upon them. Rivers in coastal areas may contain a tract known as fluvial-to-marine transition zone, where fluvial and marine process interact (Dalrymple and Choi, 2007). Different parts of this zone are dominated by different processes which gives rise to variability of sedimentary expressions from land into the sea. The inner zone of fluvial systems in lower coastal plain are fluvial dominated but become progressively more influenced by marine processes seawards. Fluvial processes weaken towards the shoreline, where marine processes dominate. The decrease in river influence seaward is attributed to a

number of factors including the hydraulic gradient and the funnel shape of an estuary (Dalrymple and Choi, 2007; Dalrymple et al., 2015).

The coastal regions of fluvial systems are also subject to interaction of freshwater and seawater, which has implications on the ecosystem of coastal areas. For examples, marine life is inhibited by the introduction of freshwater into the coastal zones. Further discussion on river-related coastal systems is given below (see 2.2)

2.2 Coastal depositional systems

Coastal depositional systems comprise a wide range of environments including estuaries, deltas, tidal flats, strandplains, barrier islands, beaches. These environments are inherently complex because of the interplay of numerous factors that vary over space and time (e.g., Davis 1985; Reading and Collinson 1996; Harris et al. 2002; Yang et al., 2007; Dalrymple and Choi, 2007). These factors include sediment influx from the land to the sea, the relative importance of the sedimentary processes (fluvial, tidal and wave), the morphology of the coastline, and relative sea-level changes (for example, whether the coastline is undergoing regression or transgression) (Figure 2.2; Harris et al., 2002).

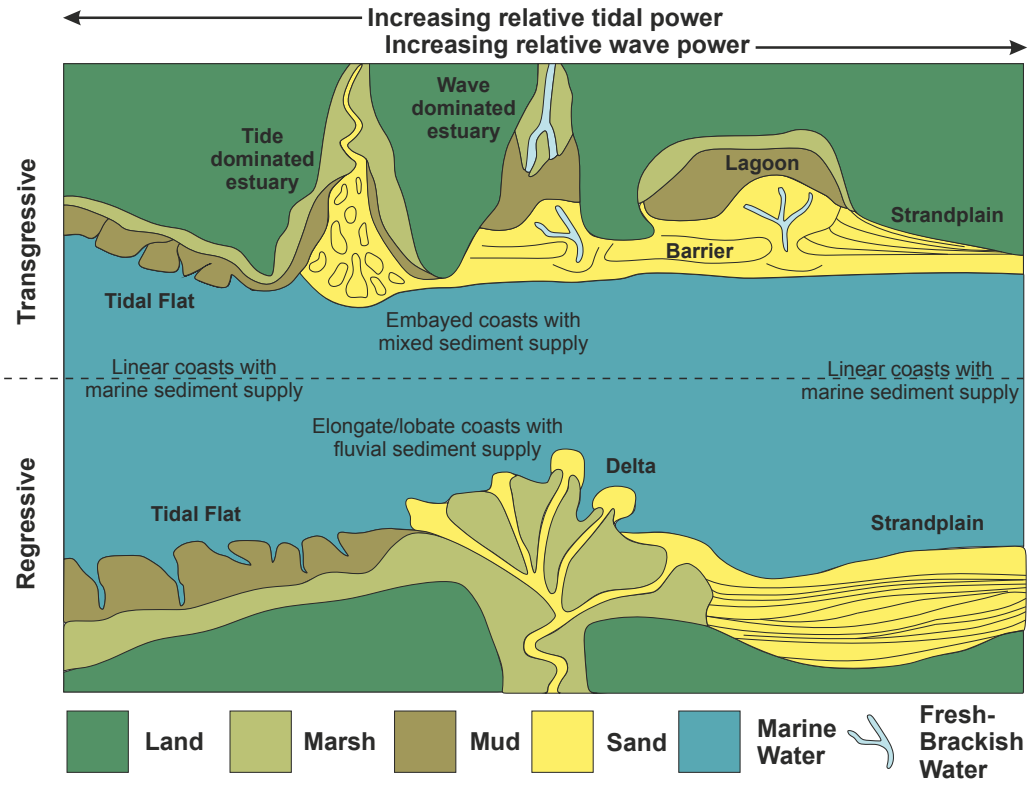

Figure 2.2: Plan view map depicting the simplified morphology of coastal depositional systems showing their relationships and different geomorphologies, adapted after Harris et al. (2002) and Shiers (2016).

2.2.1 Coastal process-based classifications

The deposits of coastal environments are commonly classified based on an effective ternary classification of the relative power of fluvial, tidal and wave processes that act upon shorelines. This ternary classification was first introduced by Galloway (1975) in a scheme that relates to the primary processes acting upon modern deltas (Figure 2.3). This classification was later refined in more recent work by Orton and Reading (1993) to include a third axis that accounts for grain size.

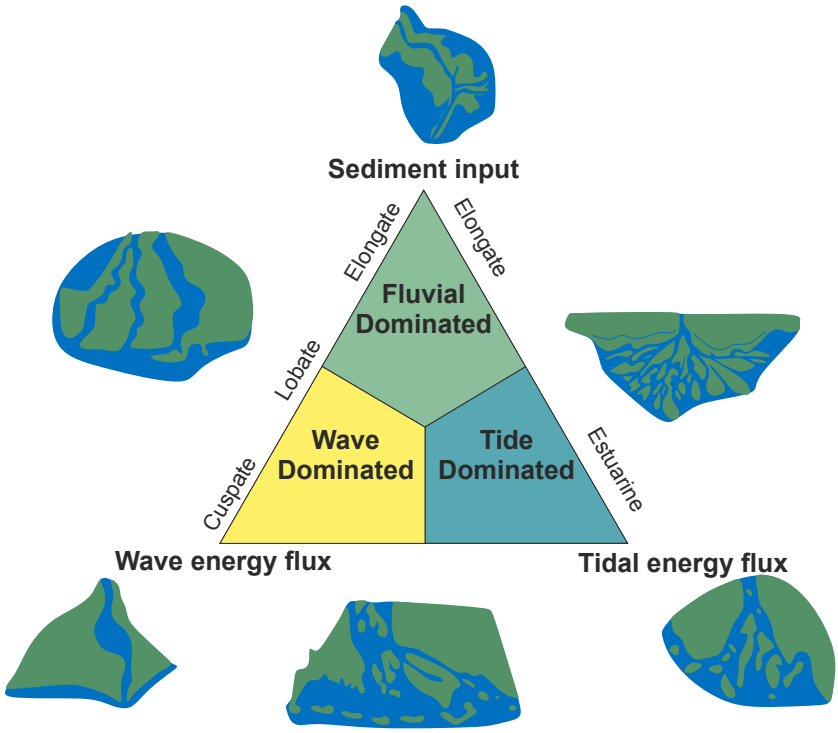

Figure 2.3: Schematic diagram showing the characterisation of deltas into fluvial-dominated, wave-dominated and tide-dominated types, adapted after Galloway (1975) and Shiers (2016).

These classifications were perceived as being overly simple in that they only focus on the dominant process affecting a coastal area. A further refined classification approach (Ainsworth, et al., 2011) provided a scheme that accounts for the dominant process along with a secondary and/or tertiary process (Figure 2.4). Combinations of these processes give rise to 15 possible idealised shoreline morphologies (Figure 2.5). These shoreline morphologies may coevally exist in close proximity to each other. For example, those observed along the northern coast of the Bay of Bengal (Figure 2.6). The eastern region of the shoreline at the north coast of the Bay of Bengal is dominated by tidal processes, whereas fluvial processes play a secondary role in controlling sedimentation. By contrast, the western region of the coast is wave-dominated, fluvial-influenced in some places and fluvial-dominated, wave-influenced in other places (Figure 2.6).

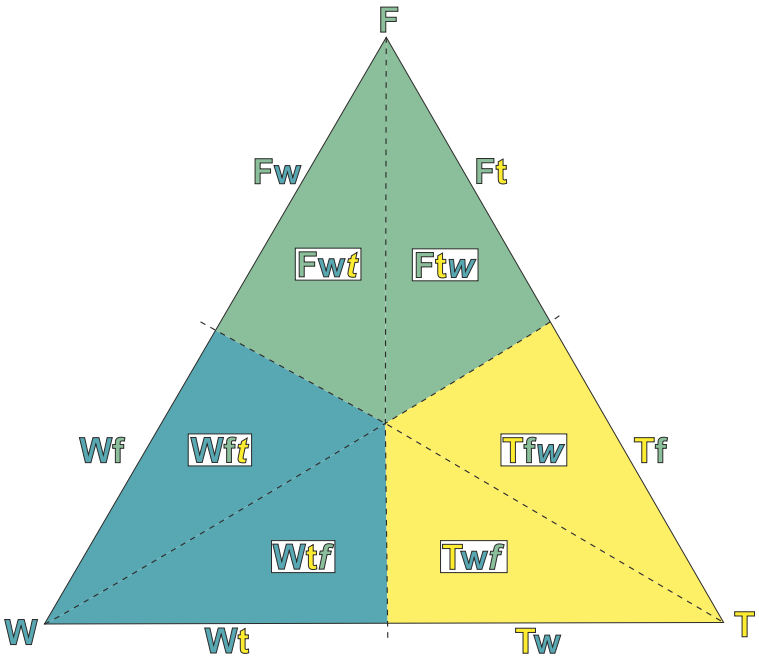

Figure 2.4: Coastal process classification ternary plots, adapted after Ainsworth et al. (2011). F = Fluvial dominated; W = Wave dominated; T = Tide dominated. Capital letters indicate the dominant process, lower case letters indicate a process which influences an environment and lower case letters in italics indicate a process which modifies the environment.

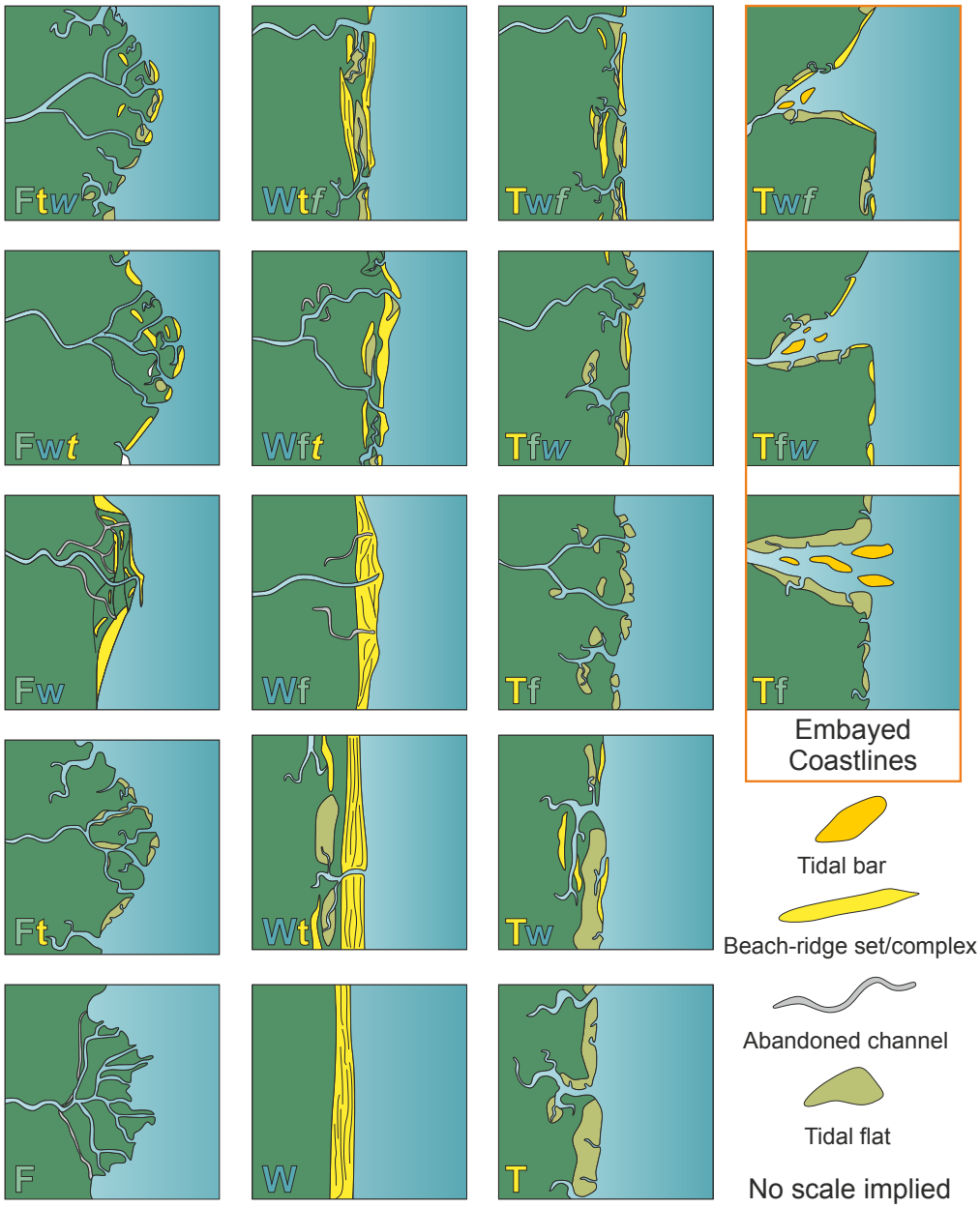

Figure 2.5: Representative schematic plan view models of the 15 classification categories in the coastal process classification presented in Figure 2.4, adapted after Ainsworth (2011) and Shiers (2016).

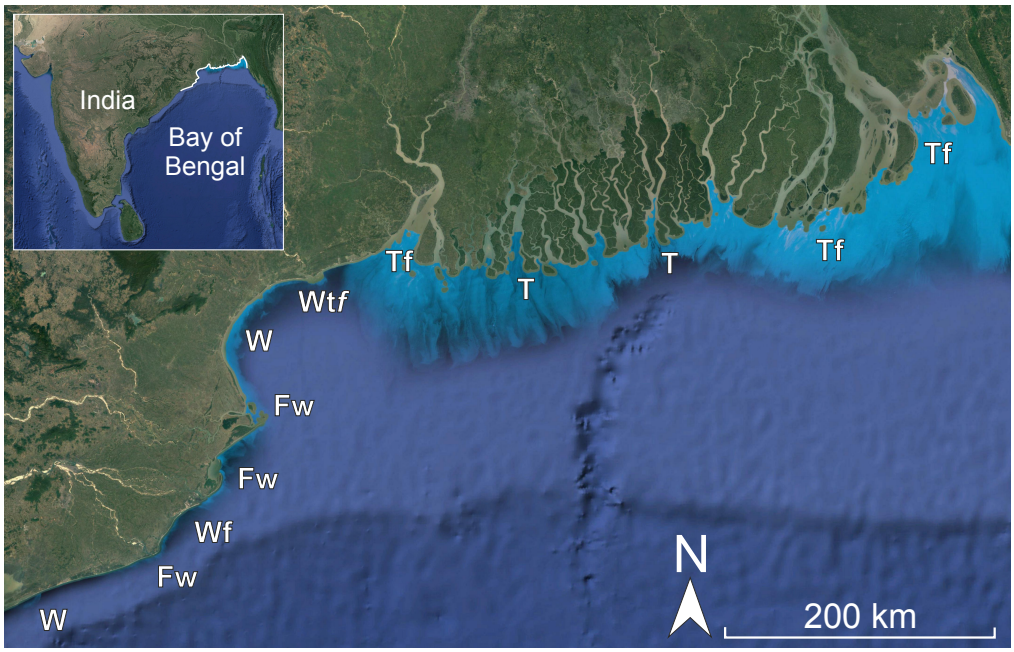

Figure 2.6: Image of the modern coastline of the Mouth of the Ganges and adjacent region showing how depositional process dominance results in different coastline morphologies and how dominant processes can change laterally over relatively short distances. Images courtesy of Google Earth.

The use of different classification approaches is dependent on the purpose of a study and on the scale of interest. For example, Nyberg and Howell (2016) employed a modified version of the classification proposed by Ainsworth et al. (2011). They classified shorelines based only on the dominant process and the secondary process that act upon coastal areas in their study of global shallow marine shorelines (Figure 2.7).

The processes of fluvial and tidal currents and wave activities govern the distribution of sediments and types of sedimentary architecture in the rock record. Understanding the interplay of these processes is therefore important for interpreting palaeoenvironments and also for assessing sedimentary bodies for applied resource geology, including hydrocarbon exploration and development (Ainsworth, 2010).

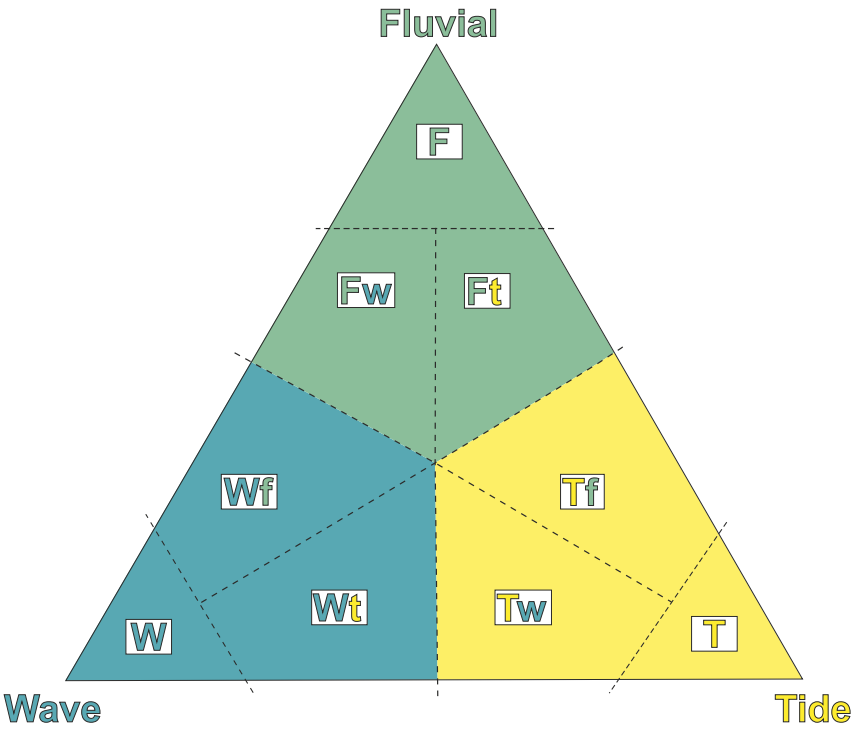

Figure 2.7: A two-tier ternary classification to account for the dominant and influencing processes based on the relative importance of each of the processes. F= Fluvial, T= tidal and W= wave processes. The capital letters indicate the dominant process and the lower case letters indicate the influencing process. Modified after Nyberg and Howell (2016).

2.2.2 Tidal depositional systems

Tides are one of the principal physical processes that influence the coastal depositional settings. They are able to erode, transport and deposit sediments in a variety of ways. Tidal depositional systems are categorised according to the dominant tidal range at the shoreline, as being micro-, meso and macrotidal (Hayes, 1979). In macrotidal systems, tidal range exceeds 4 m. Approximately a third of the world's coastlines are subject to a macrotidal range (Davies, 1964). Estuaries are common examples that are affected by macrotides, for exmaple Cobequid Bay-Salmon River Estuary in Canada (Dalrymple et al., 1990) and South Alligator River in Australia (Woodroffe et al.,1985). Along with sediments brought by river currents, macrotides are able to transport large volumes of sediment landwards, leading to deposition in subtidal and intertidal areas in the

landwards parts of embayments (Dalrymple et al., 1990; Longhitano et al., 2012). Tidal currents in macrotidal settings can cause the accumulation of large sandy bar complexes in shallow environments and tidal dunes in the relatively deeper zones (Longhitano et al., 2012).

The mesotidal coastlines are subject to tides that range between 2 to 4 m. Common environmental examples of this type of setting are barrier-beach coasts, tidal deltas and estuaries (e.g. Hayes, 1979; Boothroyd et al., 1985; Ashley and Zeff, 1988; Nichols, 1989; Oertel et al., 1989). There are numerous end-member examples of this type of setting, including northern Germany (FitzGerald et al., 1984; Hoekstra et al., 2009), the tidal inlet in the Gulf of Maine, eastern USA (Lynch and Naimie, 1993) and the Georgia Bight estuary, Georgia, USA (Frey and Howard, 1986). Examples from the ancient rock record of this type of depositional setting are rarely documented, as their recognition is difficult because sediments preserve signatures of the youngest superimposed influence (Longitano et al., 2012).

Microtidal systems have a tidal range that is less than 2 m. Tidal signatures in such settings are generally rarely preserved (Longhitano, 2011 and Longhitano et al., 2012), or more likely their deposits are rarely recognized.

2.2.2.1 Tidal indicators (Tidal rhythmites)

Tidal rhythmites are considered one of the key tidal indicators in the rock record (Tessier et al. 1993; Dalrymple, 2010; Greb et al. 2011). They represent repeated cycles and continuous deposition of alternating sand and mud layers. These cycles are controlled by the tidal energy and represent deposition by bedload process (deposition of sand) and by settling from suspension (deposition of mud). During flood and ebb currents, coarse sediments are transported and deposited by bedload process whereas during slack water

periods, finer sediments are deposited by settling out of suspension (Reineck and Wunderlich, 1968). This can occur through the course of a single tidal cycles, commonly reported in semi-diurnal regimes (e.g. Steel et al., 2012).

The amount of tidal mud vs sand deposited in an area is partly controlled by spring-neap tidal cycles. The lunar month is the period for the moon to complete one full rotation around the earth which occurs every 29.531 days on average (McLean and Wilson, 2016). Each lunar month has two spring tides (at new moon and full moon) and two neap tides (at first quarter and third quarter) (Figure 2.8A; McLean and Wilson, 2016). During spring cycles, tides have the highest high tides and the lowest low tides, which results in thick sand and thin mud laminae (Figure 2.8B). The deposition of thick sand laminae is attributed to strong tidal current associated with spring tides which is capable of transporting and depositing sand-size particles. By contrast, during neap cycles, tides have the lowest high tides and the highest low tides and results in thick mud and thin sand laminae (Figure 2.8B). Tidal current in this instance is weak compared to spring tides, such that it does not transport and deposit sand and allows for the deposition of mud from settling out of suspension.

The number of sand-mud couplets is governed by the number of high-low tidal cycles, which varies depending on the tidal regime. There is one high-low tidal cycle during a lunar day in a diurnal tidal regime (the cycle occurs every 24 hours and 50 minutes) whereas in the case of semi-diurnal regimes, there are two high-low tidal cycles (one cycle occurs every 12 hours and 25 minutes).

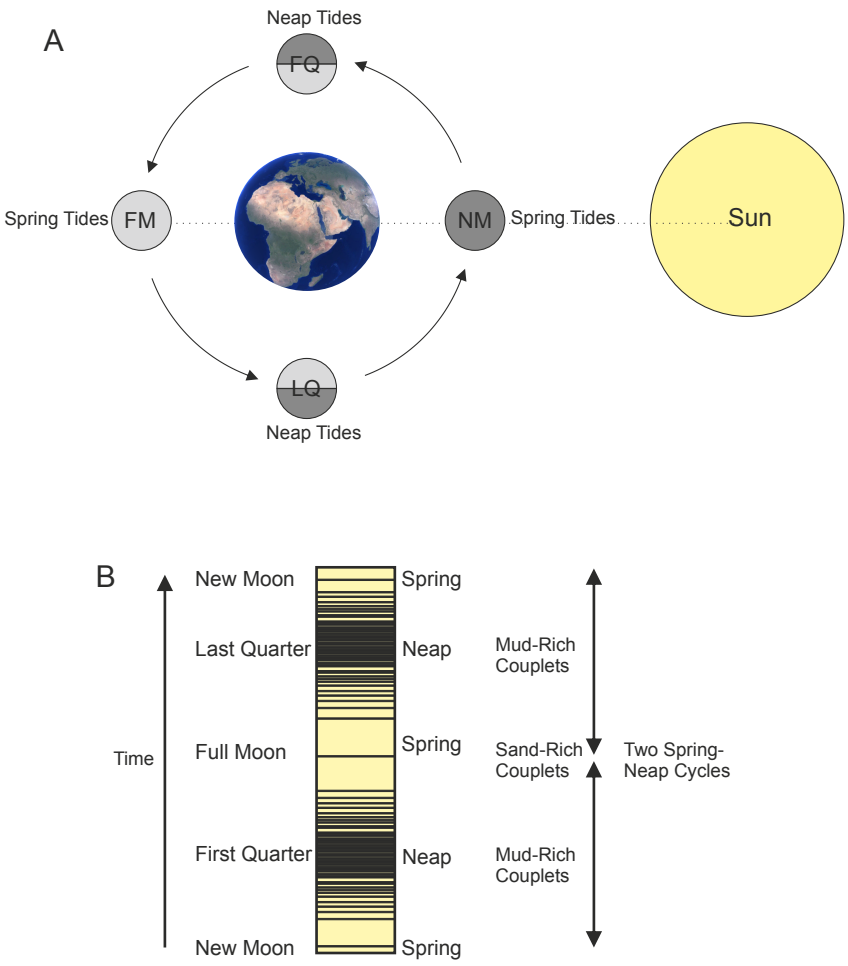

Figure 2.8: A) The arrangement of Moon-Earth-Sun orbital system in a synodic month. B) Schematic representation of depositional response to two spring-neap cycles. Adapted after McLean and Wilson (2016).

2.2.3 Estuaries

An estuary is a drowned river-terminus that has inflowing freshwater from rivers in the upstream end and seawater from the downstream end (Dalrymple and Choi, 2007). Estuaries are important depositional settings along transgressive coastlines. They are efficient sediment traps with high preservation potential (Meade 1972; Biggs and Howell 1984; Demarest and Kraft 1987). The most commonly used geological definition of an estuary is that proposed by Dalrymple et al. (1992), which was more recently refined by Dalrymple (2006). The latter account defined an estuary as "*a transgressive coastal environment at the mouth of a river, that receives sediment from both fluvial and marine*

sources, and that contains facies influenced by tide, wave and fluvial processes. The estuary is considered to extend from the landward limit of tidal facies at its head to the seaward limit of coastal facies at its mouth" (Dalrymple, 2006, p. 11).

Two estuary end-member types are classified based on the dominant sedimentary process: tide- and wave-dominated estuaries (Figure 2.9 and 2.10). Both the morphology and energy distribution of these types of estuaries differ. Sedimentation at the mouth of tide-dominated estuaries is controlled primarily by tides, whereas in wave-dominated estuaries sedimentations is dominated by wave action. The main morphological difference between the two types is that the tide-dominated estuaries have the typical funnel shape that is wider in the seaward position and narrows landwards (Figure 2.9A: Dalrymple et al., 1992). By contrast, wave-dominated estuaries typically have bars built at their mouths giving an enclosed or semi-enclosed morphology (Figure 2.10A: Dalrymple et al., 1992).

Energy types and levels, from land to sea, are different in the two types of estuary, and this has an impact on sediment distribution. Wave-dominated estuaries have a tripartite division of energy types and levels. In the outer part of this estuary type, energy originates predominantly from wave activity. In an ideal wave-dominated estuary, the mouth of the estuary is characterised by barrier islands or spits, which hinder penetration of wave and tidal energy. At high tidal ranges and tidal prism (volume of water entering or leaving an estuary during flood and ebb tides), tides may breach through barrier islands or spits via inlets. In the inner part of wave-dominated estuaries, environmental energy is provided predominantly by river currents, which typically decrease seawards due to the decrease in hydraulic gradient (Dalrymple et a., 1992). This leaves

the middle estuarine zone (i.e. central basin), with minimum energy levels (low marine and fluvial energy) (Figure 2.10B). The resultant sediment distribution corresponds to the high-low-high energy distribution in wave-dominated estuaries, and therefore typically consists of sand-dominated lithology types at the upstream and downstream ends (where fluvial and wave processes dominate, respectively), and mud-dominated lithology types in the central zone (where low energy levels occur) (Dalrymple et al., 1992).

Tidal energy in a tide-dominated estuary is the energy type which exceeds wave energy at the mouth of the estuary (Dalrymple et al., 1992). The tidal energy increases landwards as tides enter an estuary (Figure 2.9B) because tidal waves are compressed into smaller cross-sectional area due to the typical estuary funnel-shape (Dalrymple and Choi, 2007). This increase occurs to a position within the estuary known as tidal maximum (TM; Dalrymple and Choi, 2007). Landwards of the tidal maximum, tidal energy decreases until it reaches zero at the tidal limit (Figure 2.9B; Godin, 1990). River energy, by contrast, decreases progressively seawards because of the hydraulic gradient similar to the case of wave-dominated estuaries (Figure 2.9B).

This energy distribution produces a more complex sediment distribution compared to those of ideal wave-dominated estuaries, such that the aforementioned tripartite facies distribution is not clearly defined (Dalrymple et al., 1992). The outer zone is tide-dominated and is characterised by elongate sand-dominated tidal bars (Dlarymple et al., 1992; Dalrymple and Choi, 2007). The zone where the tidal maximum takes place is described to consist of upper flow regime sand flats with network of dense channels commonly with a braided pattern. These channels are typically confined into a single channel headwards (Hamilton, 1979; Dalrymple et al., 1992).

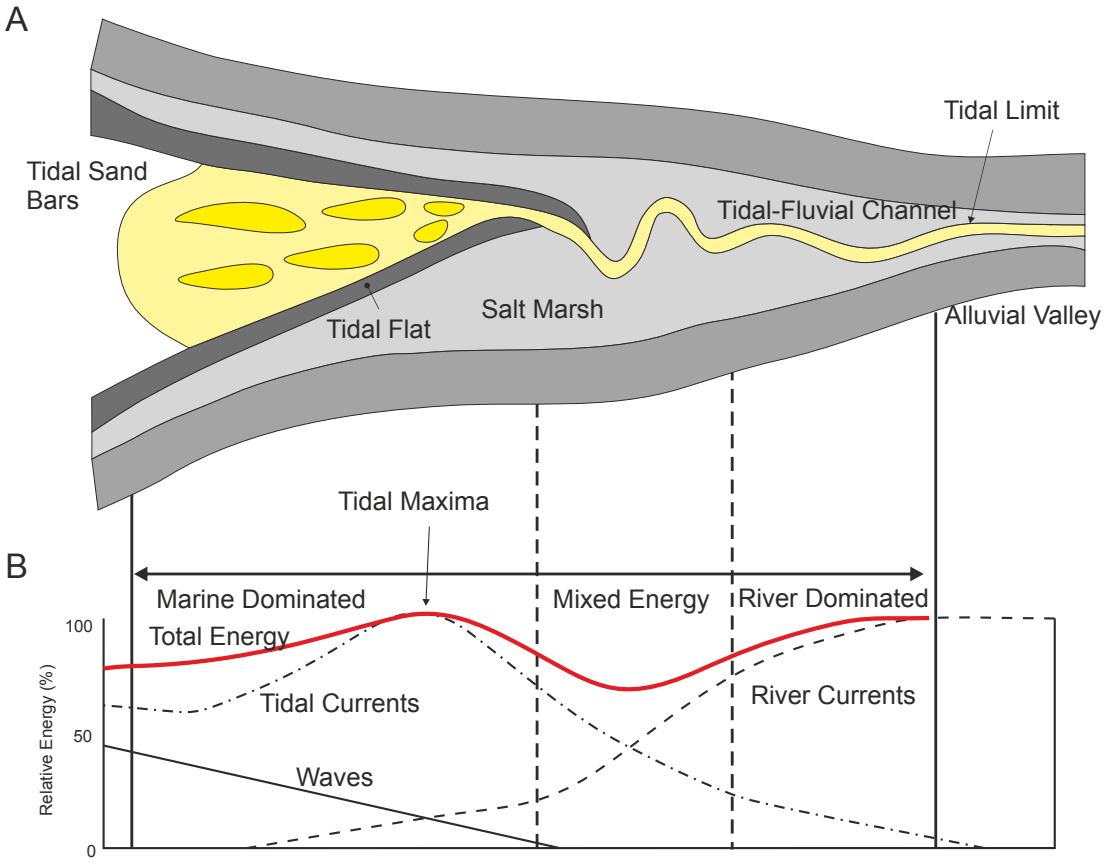

Figure 2.9: A) Morphology and B) Energy types their distribution in tide-dominated estuaries, adapted from Dalrymple et al. (1992).

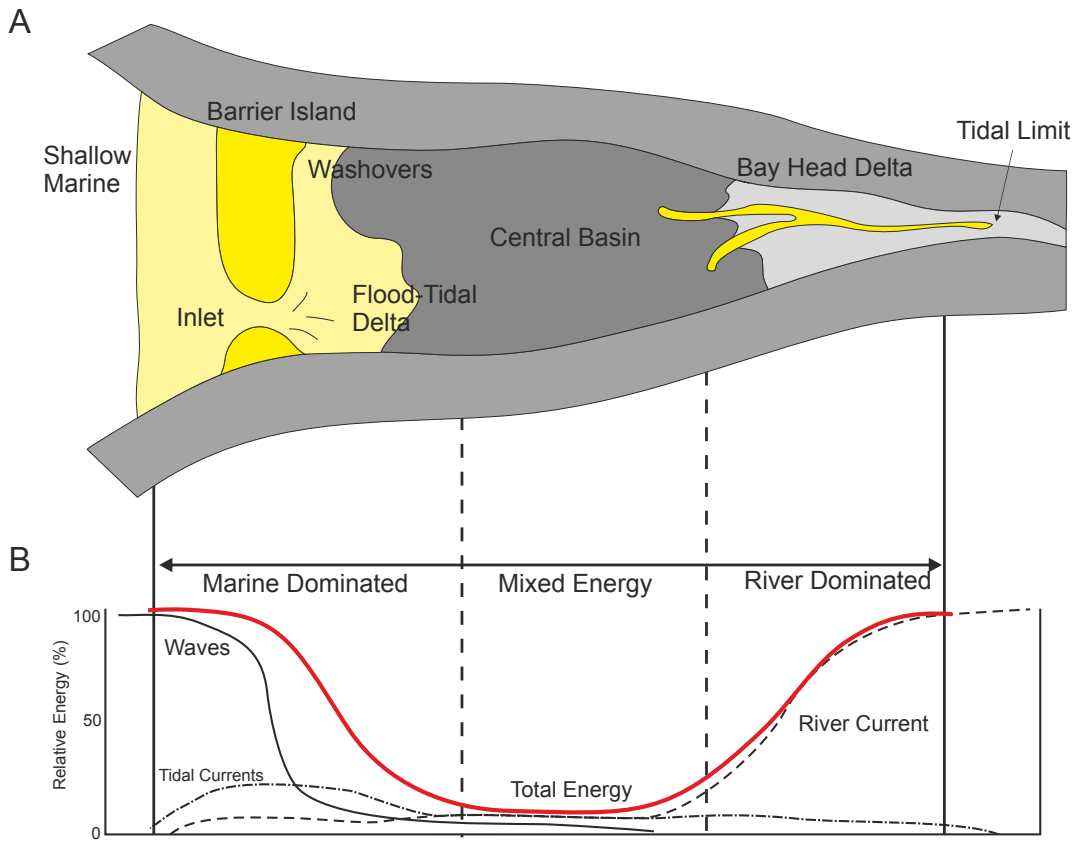

Figure 2.10: A) Morphology and b) Energy types and their distribution in wave-domianted estuaries, adapted from Dalrymple et al. (1992).

Tidal bars are sandbodies that commonly develop within deltaic and estuarine systems and that are built by tidal processes (Dalrymple and Choi, 2007; Olariu et al., 2012). Tidal bars are commonly associated with channels and can be mistaken for tidal compound dunes in ancient deposits (Desjardins et al., 2012a, Olariu et al., 2012). This misconception occurs because both bed form types typically possess similar facies and overall thicknesses. However, the main difference between tidal bars and tidal compound dunes is that tidal bars migrate laterally or obliquely to the dominant flow, whereas compound dunes migrate in the direction of dominant flow (Dalrymple et al., 2003 and Desjardins et al., 2012a, Olariu et al., 2012). Moreover, tidal-bar deposits typically exhibit a fining-upward trend, whereas tidal compound dunes tend to have a coarsening-upward trend. However, the lowermost portions of tidal bars in estuaries may

show coarsening upward trend where the basal deposits are associated with fluid-mud (Dalrymple et al., 2003; Dalrymple and Choi, 2007).

Estuaries are typically characterised by a well-developed zone of turbidity maximum, which inherently allows for the deposition of mud-rich layers within tidal bars (Allen, 1991; Dalrymple and Choi, 2007). The deposition of mud occurs during tidal slacks between ebb and flood tidal currents. From an applied geology standpoint, the deposition of such mud-prone layers can be problematic for hydrocarbon reservoir performance as they can act as baffle zones to hydrocarbon migration pathways. Characterisation of the internal architecture and external geometries of tidal bars is therefore important for reservoir development and characterisation.

2.2.4 Deltas

Ancient deltaic deposits, their sedimentary architecture and facies models have been widely documented in the literature (Fisk et al., 1954; Fisher et al. 1969; Miall, 1976; Coleman and Prior, 1982; Elliott,1986; Bhattacharya, 2006; Bhattacharya, 2010). Present-day deltas are also widely documented and have been the focus of much study. Well-documented examples include the Mekong river delta in Vietnam (Ngyuen et al., 2000), the Fraser delta, in British Columbia, Canada (Dashtgard et al. 2012; Sisulak and Dashtgard 2012; Johnson and Dashtgard 2014; La Croix and Dashtgard 2014), and the Danube delta, in Romania (Bhattacharya and Giosan, 2002; Giosan et al. 2005).

The morphology and sedimentary patterns of deltas are dependent on the dominant processes acting upon the system. For example, delta shoreline morphologies are typically lobate-shaped in river-dominated deltas, funnel-shaped in tide-dominated deltas and have a smooth straight shape in wave-dominated deltas (Figure 2.11).

Deltas are represented in the ancient record by progradational sedimentary bodies arise due to regression. Different areas of a delta are subject to different sedimentary processes that govern their sedimentary distribution and architecture. Deltas are typically subdivided into three main sub-environments: delta plain, delta front and prodelta (Figure 2.12). These divisions can be further subdivided based on the range of processes acting upon different areas, which typically produce different types of deposits.

Delta plains are typically subaerial and dominantly controlled by river processes in their upper parts and by mixed processes (fluvial, tidal and wave processes) in their lower parts (Coleman and Prior,1982). Upper delta plains are characterised by fluvial channels and extensive flood plains similar to those of fluvial environments whereas the lower delta plain is marine influenced and characterised by distributary channels (Gugliotta et a., 2015). Delta fronts form in front of delta plains and can be characterised by mouth bars, tidal bars or shorefaces, depending on whether the delta is river-, tide-or wave-dominated. The delta front forms in the subtidal zone above wave base and is commonly described to have sand-dominated deposits. The prodelta is the distal seaward (offshore) part of the delta front. It also forms in the subtidal area but below wave base where mud deposition is most likely to take place.

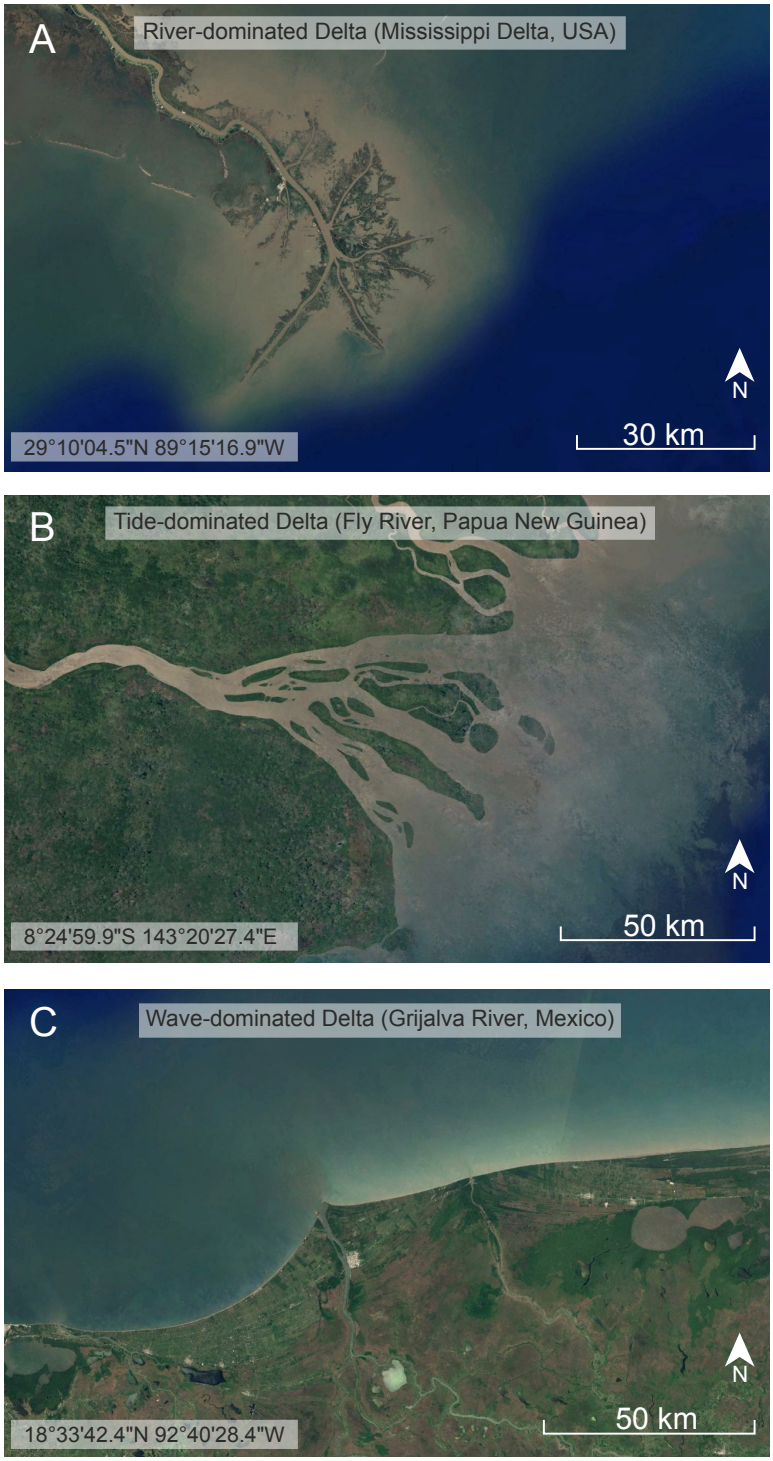

Figure 2.11: Modern examples of A) river-dominated, B) tide-dominated and C) wave-dominated deltEarth.as. Images courtesy of Google Earth.

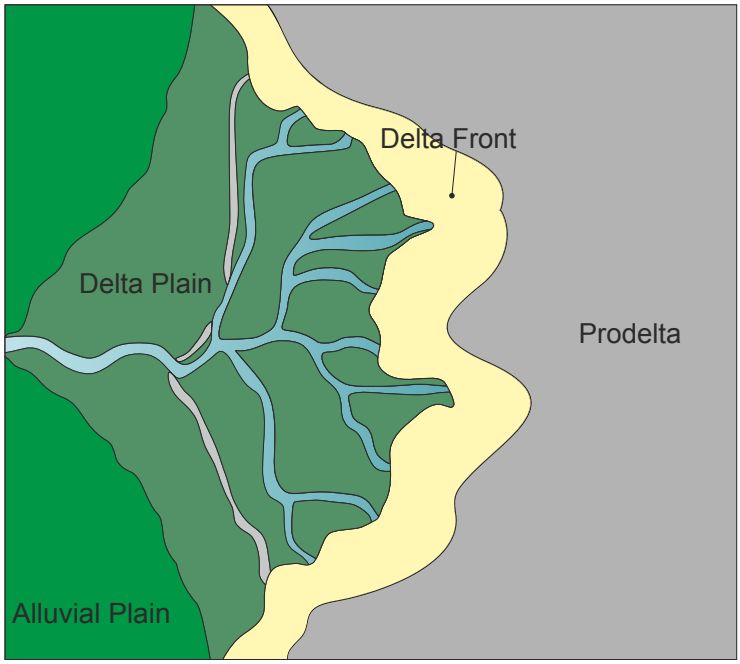

Figure 2.12: Environmental subdivision of a deltaic environment, adapted from (Bhattacharya, 2006).

2.2.5 Fluvial to marine transition zone

The Fluvial to Marine Transition Zone (FMTZ) represents the transition between fully fluvial and fully marine environments (Figure 2.13). The FMTZ is the region that extends from the effective tidal limit up-dip to the bedload convergence zone downstream of estuaries, and to the point where seaward broadening of a channel allows for the formation of elongate bars downstream of deltas (Dalrymple and Choi, 2007). In relation to sediment erosion, transport and deposition, van den Berg et al. (2007, p. 255) defined the FTMZ to comprise *''the part of a river occurring between the landward limit of the effects of tidal flow deceleration on fluvial cross-bedding at low river discharge, and the seaward limit of fluvial signature on sediment texture and structures at high [river] stage''*. This definition was subsequently further revised by Gugliotta et al. (2016) to include all marine influences, as opposed to only tidal ones.

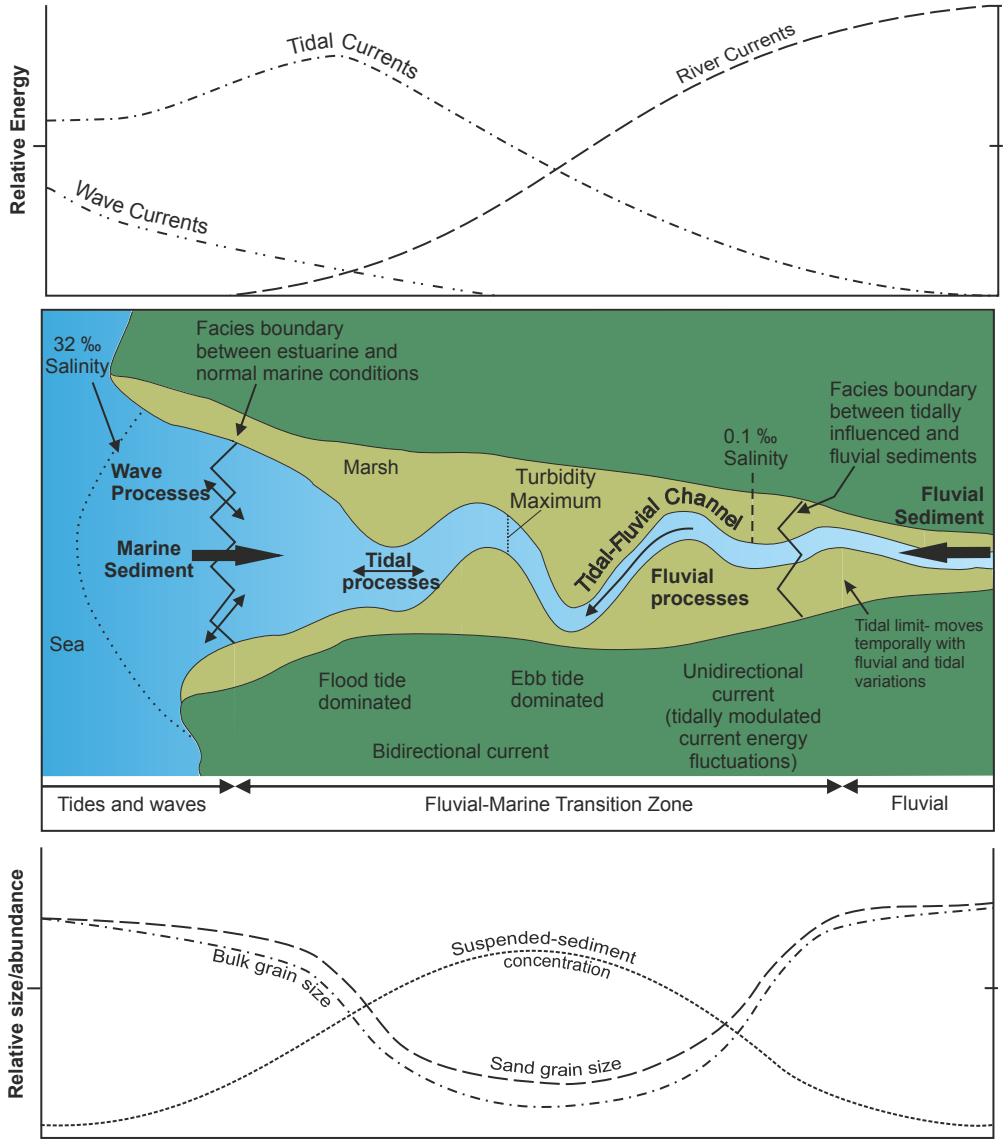

Figure 2.13: Diagram showing the changes in facies, energy, grain size, salinity and channel morphology through the fluvial to tidal transition and the processes at work. After Dalrymple et al. (1992), Martinius & Gowland (2011), Dalrymple & Choi (2007), van den Berg & van Gelder (2007), Shanley & McCabe (1994) and Shiers (2016).

The FMTZ differs hydraulically from the upstream fluvial and downstream marine realms (van den Berg et al., 2007). In recent years, a growing number of studies have examined the detailed sedimentology of FMTZ-related deposits from both modern systems (e.g. La Croix and Dashtgard, 2014; Prokocki et al., 2015; Gugliotta et al., 2016; Gugliotta et al., 2019) and ancient successions

(e.g. van den Berg et al., 2007; Shiers et al., 2014; Martinius et al., 2015; Gugliotta et al., 2017).

Sedimentary environments at the interface between land and sea form a broad zone where fluvial, tide and wave processes interact (Dalrymple and Choi, 2007; van den Berg et al., 2007). This zone can extend for tens to hundreds of kilometres upstream from the shoreline within the lower reaches of rivers. Examples of studies that document such reaches include: the present-day Fraser River delta, in western Canada (Dashtgard et al., 2012), the Fly River delta, in Papua New Guinea (Dalrymple et al., 2003), and the Amazon River, in Brazil (Dalrymple et. al., 2015). The influence of fluvial processes can also extend for hundreds of kilometres seaward from the shoreline in front of the river mouths during high river discharge (Dalrymple and Choi, 2007 and Gugliotta et al., 2019). Several studies have investigated depositional processes taking place in this region, including documentation of the gravity-flow deposits of the Fraser River delta front associated with fluvial-tidal interaction (Ayranci et al., 2012), and remote sensing analysis of the tide-dominated delta of the Mekong River (Loisel et al., 2014).

Ancient successions representative of FMTZ settings are mostly recognized in outcrop and those include the Neslen Formation (e.g. Willis, 2000; Dalrymple, 2015; Colombera et al., 2016b; Shiers, 2016; Shiers et al. 2014, 2017), the Lajas Formation (e.g. Legarreta and Uliana, 1996; Howell et al., 2005; Rossi et al., 2016), the McMurray Formation (e.g. Mossop and Flach, 1983; Musial et al., 2011), the lower Sego Formation (van Cappelle et al., 2016), the Juara Quartzite (e.g Levell et al., 2020), the lower Cambrian (stage 2) units (e.g. Went, 2020) and the Lambir Formation (e.g. Collins et al., 2020). A number of subsurface successions are also interpreted to be representative of the FMTZ:

for example, the subsurface McMurray Formation (e.g. Hein, 2015) and the Tilje Formation, offshore Norway (e.g. Ichaso and Dalrymple, 2009 and Dalrymple et al., 2015).

2.2.6 Controls on coastal environments

Fluvial to shallow marine systems (including the FMTZ) are influenced by many variables, notably the gradient of the coastal plain, the fluvial discharge, and the tidal range at the shoreline (Dalrymple and Choi, 2007; La Croix and Dashtgard, 2014; Dalrymple et al., 2015; Gugliotta et al., 2017). The depth and width of a channel, and the shape of a river-mouth estuary can play important roles in determining the upstream reach of tidal influence. Specifically, tidal currents might be amplified or attenuated depending on the interaction of these variables (Salomon and Allen, 1983; Dalrymple and Choi, 2007; Dalrymple et al., 2015). The region of tidal limit is represented by a dynamic zone that varies in accordance with the relative power of river discharge and tidal currents. During river flows that are strong relative to tidal currents, the tidal limit is pushed downstream (Dalrymple et al., 2015). By contrast, during times of stronger tidal currents relative to river flows, the tidal limit shifts upstream. This relationship gives rise to fluvial-dominated and tide-dominated sedimentation in different parts of the FMTZ (van den Berg et al., 2007 and Dalrymple et al., 2015).

2.3 Mixed siliciclastic and carbonate systems

Siliciclastic and carbonate sedimentary systems are commonly documented separately in the scientific sedimentological literature. This is principally because of the different origin and the different processes that govern their formation. Siliciclastic sediments are transported through the means of water,

wind or gravity and ultimately deposited in sedimentary basins whereas primary carbonate sediments are of chemical and biological origins and may typically form in-situ at certain water depths in lakes and seas, though carbonate allochems may be transported via physical processes too. Carbonate production flourishes in calm, equatorial water conditions and is sensitive to terrigenous influx and nutrients. They can also form at high latitudes and in high energy settings. Increased siliciclastic input to a shelf, which can be caused by tectonic or climatic factors, and nutrients brought along with siliciclastic input negatively impact carbonate production (Tirsgaard, 1996). Siliciclastic influx to a carbonate platform enhances water turbidity and precludes light penetration to the carbonate factory, which can significantly reduce carbonate production or end it.

Mixing of siliciclastic and carbonate deposits occurs in different ways and scales. Siliciclastic and carbonate can mix where siliciclastic and carbonate coevally and adjacently occupy an environment (Dorsey and Kidwell, 1999; Coffey and Read, 2004; Longhitano et al., 2010: Chiarella et al., 2012) and temporally, where they alternate vertically through a single succession (e.g. Gillespie and Nelson, 1997; Moissette et al., 2010; Lee and Chough, 2011). The mixing of siliciclastic and carbonate deposits occurs at multiple scales, ranging from facies-unit scale (e.g. Narva succession of Baltic basin, Eastern Europe; Tanavsuu-Milkeviciene et al., 2009) to stratigraphic-unit, seismic scale (e.g. Miocene of the Lorca Basin, Southeast Spain; Thrana and Talbot, 2006).

The sedimentology of lower Dhruma Formation, documented in chapter 3, records the interaction of siliciclastic and carbonate deposits at multiple scale. This is discussed in detail in the discussion chapter (chapter 5).

2.4 Palaeosols

Palaeosols are ancient soils that have been lithified and preserved in the rock record (Kraus, 1999; Retallack, 2001). Soils typically form when sediments and/or rocks are exposed at the Earth's surface and subjected to pedogenic processes (physical, biological and chemical) that modify and/or alter their characteristics (Kraus, 1999). Palaeosols are commonly described from alluvial settings, but have been documented from deposits that are representative of many sedimentary environments, including terrestrial (e.g. Soreghan et al., 1997; Tandon et al., 1995; Wright and Platt, 1995), marginal marine (e.g. Lander et al., 1991) shallow marine carbonates (Wright, 1994) and even environments that overall are considered to be of marine origin (e.g. Driese et al., 1994 and Webb, 1994).

Palaeosols can be many metres or even tens of metres thick and can be laterally extensive over tens or even hundreds of kilometres in some instances (e.g. Kraus, 2002). As such, they can act as significant stratigraphic markers that enable subdivisions of stratigraphic units (Kraus, 1999). They also play an important role in the analysis of sequence stratigraphy. Palaeosols have been repeatedly associated with unconformities in the rock record. However, not all unconformities show evidence of palaeosols and not all palaeosols mark unconformities (Kraus, 1999). The lower Dhruma Formation records the presence of possibly extensive pedogenically modified deposits (i.e. palaeosols) of fluvial and nearshore origin (Chapter 3).

2.5 Ichnology

Ichnology is the study of traces created by organisms that interact with substrate sediment, as observed in modern environments and preserved in the

rock record. Organisms that live on and or in sediments leave several types of traces that represent their behaviour on the substrate (i.e. grazing, dwelling, filter feeding and escape structures). Organisms are typically sensitive to the conditions of the environment they occupy. The diversity and intensity of organisms' traces (i.e. ichnofossils) can give insights on sedimentation rate, salinity, nutrition etc. For example, a high abundance of ichnofossil types may indicate a combination of low sedimentation rate and many biogenic activities. In contrast, a low abundance of ichnofossil types might imply high sedimentation rate and few infaunal organisms. Also, trace styles can provide information about the sedimentation rate, for example, escape traces (Fugichnia) might be attributed to organisms absconding a high sedimentation rate. Furthermore, the diversity of ichnofossils can bear a record of the environmental conditions during organism colonisation. For example, a high diversity of ichnofossils is typical of favourable and unstressed settings. By contrast, a low diversity of forms might indicate stressed environmental conditions; forms that are present in stressed settings might typically be produced by organisms that are tolerant to harsh conditions.

Bioturbation intensities can be described in qualitative terms: deposits may be classed as slightly or highly bioturbated, for example. However, it is now more common to apply a auantification of bioturbation intensity using the bioturbation index (BI) which has 7 grades of intensity (0 to 6), where 0 is given for cases where bioturbation is absent and 6 is given to entirely reworked substrates (Figure 2.14; Taylor and Goldring, 1993; Bann et al., 2008).

Bioturbation Index (BI)	Schematic Representation	Description
0	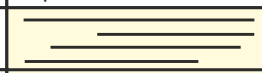	Bioturbation absent
1	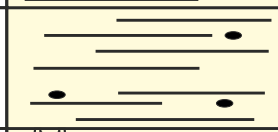	Sparse bioturbation, bedding distinct, few discrete trace fossils
2		Uncommon bioturbation, bedding distinct, low trace fossils diversity
3	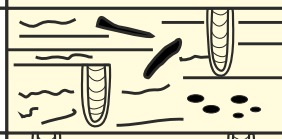	Moderate bioturbation, bedding boundries sharp, trace fossils discrete with rare overlap
4	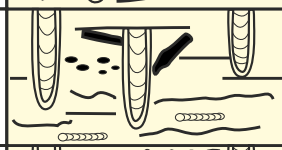	Common bioturbation, bedding boundries indistinct, high trace fossils density with common overlap
5	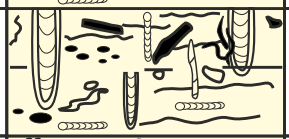	Abundant bioturbation, bedding hardly visible and completely disturbed
6	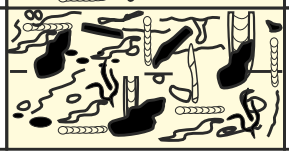	Complete bioturbation, total biogenic homogenization of sediment

Figure 2.14: Schematic representation of a semi-quantitative assessment of bioturbation intensity, modified from Bann et al. (2008).

2.6 Importance of analogues and quantitative studies

Marginal marine sandstone bodies form important reservoirs for natural resources, notably oil and gas. Prediction of their shapes and dimensions is vital for reservoir characterisation and modelling. The analyses of sand bodies from the subsurface relies primarily on core and well log data which are inherently associated with high uncertainties. Establishing dimensions of and relationships between sand bodies requires the use of studies on modern and ancient analogues. Analogues are evidently important in improving our understanding of the geometry and dimensions of subsurface sand bodies. However, each sedimentary system possesses its own unique attributes and accumulated geobodies can be different to those of other analogous systems in

many aspects. Therefore, it is challenging to determine which analogue is most suitable for adoption in subsurface studies. Selecting an inappropriate analogue can lead to inaccurate predictions and assessments of the extent and properties of a reservoir. Approaches based on the use of composite analogues (e.g. Colombera et al., 2012) can account for natural variability and help better predict the geometry, dimensions and sedimentary architecture of subsurface reservoirs. A showcase of the use of this approach is shown in the quantitative study in chapter 4.

3 Sedimentology and Stratigraphic Architecture of A Fluvial to Shallow Marine Succession: The Jurassic Dhruma Formation, Saudi Arabia

3.1 Introduction

Coastal fluvial to shallow-marine settings comprise a range of environments including estuaries, lagoons, tidal flats, strandplains, barrier islands, beaches and deltas; these pass basinward to marine offshore settings. Shoreline environments are defined and further sub-divided by the relative importance of fluvial, wave and tidal processes (Boyd et al., 1992; Harris et al., 2002). These environments are commonly classified using various simple yet widely employed ternary classifications based on dominant and subordinate process regimes (Galloway, 1975; Johnson and Baldwin, 1986; Boyd et al., 1992; Porebsky and Steel, 2006; Ainsworth et al., 2011).

The interaction of fluvial, tidal and wave processes in nearshore coastal environments gives rise to the accumulation of depositional bodies that are represented in the sedimentary record by a variety of types of architectural elements (Miall, 1985; Olariu et al., 2012; Vakarelov and Ainsworth, 2013). The internal facies architecture and external preserved geometry of these sedimentary units is determined by the morphology and the evolutionary behaviour of the range of formative coastal sub-environments (Dalrymple et al., 2003). The coastal terminus of rivers – where many of the aforementioned physical processes interplay – is termed the Fluvial-to-Marine Transition Zone (FMTZ), wherein there typically exists a downstream transition from fluvial dominance to marine dominance (Dalrymple and Choi, 2007; van den Berg et

al., 2007; Gugliotta et al., 2019). This zone can extend for tens to hundreds of kilometres upstream from shorelines at the lower reaches of rivers. Examples of studies that document such reaches include the present-day Fraser River delta, western Canada (Dashtgard et al., 2012), the Fly River delta, Papua New Guinea (Dalrymple et al., 2003), and the Amazon River, Brazil (Dalrymple et. al., 2015). The influence of fluvial processes can also extend for hundreds of kilometres seaward from the shoreline in the region in front of river mouths during episodes of high river discharge (Dalrymple and Choi, 2007 and Gugliotta et al., 2019). Several studies have investigated depositional processes taking place in seaward part of the FMTZ, including documentation of the gravity-flow deposits of the Fraser River delta front associated with fluvial-tidal interaction (Ayranci et al., 2012), and remote sensing analysis of the outward delta plume of the Mekong River (Loisel et al., 2014). In recent years, a growing number of studies have examined the detailed sedimentology of FMTZ-related deposits, from both modern systems (e.g. La Croix and Dashtgard, 2014; La Croix and Dashtgard, 2015, Prokocki et al., 2015; Gugliotta et al., 2017; Gugliotta et al., 2019) and ancient successions (e.g. van den Berg et al., 2007; Shiers et al., 2014; Martinius et al., 2015; Gugliotta et al., 2016; La Croix et al., 2019).

In shallow marine settings, seawards to systems that are dominated by siliciclastic deposits, carbonate accumulation may occur due to factors include the combination of latitude, climate, water depth, water temperature and limited nutrients and siliciclastic supply (Vicalvi and Milliman, 1977). As such, carbonate and siliciclastic sediments coevally and adjacently occupy an environment (Chiarella et al., 2017).

Sand bodies present in various accumulations of fluvial to shallow-marine origin are known in the subsurface chiefly through drill-core and seismic data records. Examples of successions representative of fluvial to shallow-marine sub-environments (including those of the FMTZ) include the Triassic Mungaroo Formation, NW Shelf, Australia (Heldreich, 2017), the Jurassic Brent Group, North Sea, UK (Livera and Caline, 1990), the Cretaceous McMurray Formation, Alberta, Canada (Hubbard et al., 2011; Hein, 2015; Jablonski and Dalrymple, 2015), and the Cretaceous Burgan Formation, Kuwait (Al-Eidan, 2001). In these settings, sand-body accumulations can be laterally extensive over kilometres where they represent large-scale depositional elements (Wightman and Pemberton, 1997; Shchepetkina et al., 2016; Reynolds, 2017). However, although sand-prone overall, these types of successions tend to be internally lithologically heterogeneous at a variety of smaller scales, for example as exemplified by sandstone beds partitioned by thin but numerous mudstone interbeds (e.g., Reineck and Wunderlich, 1968; Reineck and Singh, 1980; Thomas et al., 1987; Nio and Yang, 1991). As such, developing detailed sedimentological models of fluvial to shallow-marine successions known only from the subsurface is challenging (Jackson et al., 2005; Martinius et al., 2005; Ringrose et al., 2005; Massart et al., 2016). Gaining an improved understanding of the sedimentary facies distribution and anatomy of these types of deposits is therefore important for subsurface characterisation. A key part of this is the development of predictive lithofacies models (Dalrymple and Choi, 2007; Burton and Wood, 2013; Al-Masrahy and Mountney, 2015; Dashtgard and La Croix, 2015; Al-Masrahy, 2017; van de Lageweg et al., 2018) based on observations of the lateral extent and continuity of architectural elements in the subsurface, as inferred from subsurface data including cores, wireline logs, seismic data

and, in some cases, pressure data. Nonetheless, it remains a difficult task to reconstruct the geometry and continuity of sandstone bodies representative of fluvial to shallow-marine settings from subsurface data alone. Uncertainty associated with attempts to characterize subsurface successions can be reduced by utilizing analogues based on studies of outcrops and modern systems, and from which quantitative measures of facies and architectural-element proportions, geometries and distributions can be obtained (e.g. Ainsworth et al., 2008, 2011; Colombera et al., 2012, 2016a).

The aim of this chapter is to document the nature of interaction in fluvial to shallow marine systems. Specific objectives of this chapter are as follows: (i) examine and demonstrate the relationships between various fluvial, nearshore and shallow-marine deposits, (ii) construct depositional models to account for the stratigraphic complexity inherent in fluvial to shallow-marine successions (iii) document the sedimentology and the evolutionary patterns of the lower Dhruma Formation in the studied area of Saudi Arabia.

The aim and objectives are fulfilled through the consideration of a subsurface dataset from the lower Dhruma Formation in Saudi Arabia (Figure 3.1; exact well locations cannot be published due to the proprietary nature of the dataset, though well positions relative to one another are indicated). The dataset allows for the characterisation of sedimentary geobodies considered to represent fluvial to shallow-marine palaeoenvironments and allows for prediction of the occurrence and arrangement of those geobodies in the subsurface.

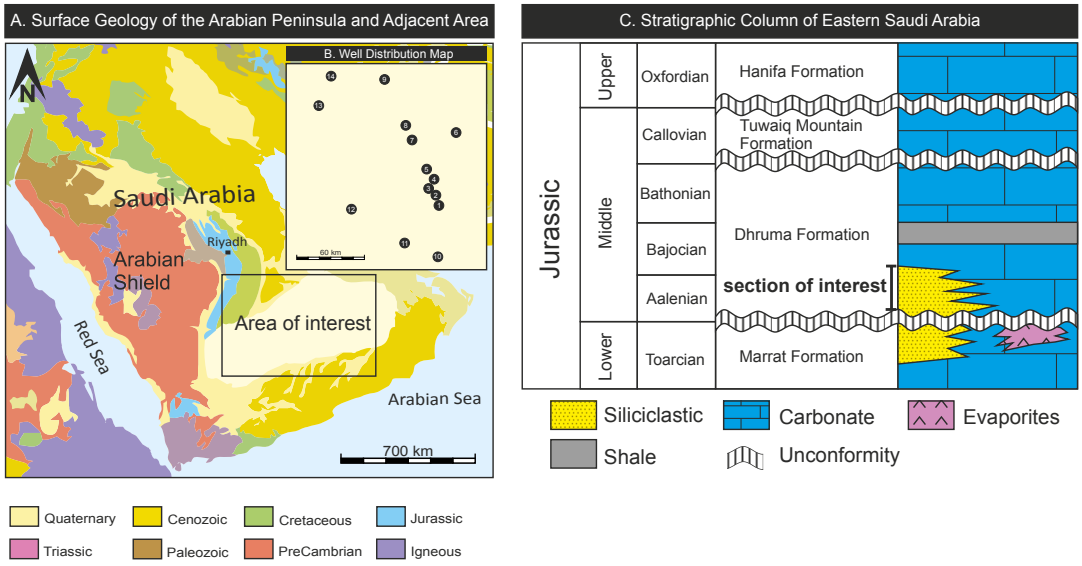

Figure 3.1: A) Simplified regional geological map of the Arabian Peninsula adapted from Stewart et al. (2016). B) Well distribution map within the study area. The exact geographic location of the wells cannot be published due to the proprietary nature of the dataset. C) Generalized stratigraphy of Eastern Saudi Arabia.

3.2 Geological setting

The Arabian plate, which formed part of the north-eastern margin of the Gondwana supercontinent, experienced diastrophic tectonic events throughout much of its geological history (Haq et al., 1988; Haq and Al-Qahtani, 2005; Faqira et al., 2009; Stewart, 2016). It was located close to an equatorial palaeolatitude throughout most of the Mesozoic (Stampfli and Borel, 2002; Golonka, 2007; Seton et al., 2012; Stewart et al., 2016). During the Triassic, it progressively shifted northwards from its previous position of ~25° south of the palaeoequator in the Permian. Throughout much of the Jurassic, it occupied a location close to the palaeoequator (Scotese, 2001; Ziegler, 2001; Schlaich and Aigner, 2017). In the late Permian, the Neo-Tethys Ocean started to form as a result of continental rifting and spreading between the Zagros suture and Gulf of Oman. This led to the formation of a northeast-dipping passive margin (Ziegler, 2001). In the Early Jurassic, back-arc rifting commenced along the eastern

Mediterranean basin, and this induced uplift in the western and southern parts of the Arabian plate. This resulted in the development of a new northward-dipping passive margin to the Neo-Tethys Ocean, with an associated open-marine shelf palaeoenvironment (Ziegler, 2001).

The surface geology of the region is presently covered with aeolian sand dunes, except for bedrock exposures that crop out in the western part of the basin near the Arabian Shield (Figure 3.1). The subsurface succession records the basin fill of an elongate intra-shelf feature that plunges to the northeast from south of the Arabian Shield towards the United Arab Emirates (Soliman and Al-Shamlan, 1980; Haq et al., 1988; Tawfik et al., 2016). The study region is bounded by the Qatar Arch to the north and northwest, and by the Hadhramaut-Oman arches to the south and southeast.

Within the fill of the studied basin, the lower part of the Middle Jurassic Dhruma Formation is the focus of this study. The Dhruma Formation was first identified in outcrop and was originally assigned as a member of the Tuwaiq Mountain Formation by Max Steineke in 1937 (summarized in Powers et al., 1966), but was subsequently ranked as a formation in its own right by Brankamp and Steineke (Arkell, 1952). Later workers have subdivided the Dhruma Formation into Lower, Middle and Upper members based on distinct lithological characters recognized in outcrop (Powers et al., 1966; Powers, 1968). More recently, the formation has been further subdivided into 7 informal units: lowermost D1 to uppermost D7 (Vaslet, et al., 1983; Manivit et al., 1990; Énay et al., 2009). Where exposed in outcrop, the lower Dhruma Formation is subdivided to units D1 and D2, which are referred to in the literature as the Balum Member and Dhibi Limestone Member, respectively (Hughes, 2006; Al-Husseini, 2009).

In the subsurface, the lower Dhruma Formation of the study area is composed dominantly of a siliciclastic accumulation of coastal-plain and shallow-marine origin, equivalent to the D1 unit (or the Balum Member seen in outcrop). This siliciclastic succession passes vertically to a carbonate-dominated succession, which forms the upper part of the lower Dhruma Formation (equivalent to the D2 unit, Dibi Limestone Member seen in outcrop). The lower Dhruma Formation has previously been interpreted to represent marginal-marine to paralic environments by Stewart et al. (2016) as part of their review of the Mesozoic subsurface succession. However, no detailed and systematic sedimentological lithofacies analysis of the formation has been published previously.

3.3 Data and methods

3.3.1 Subsurface datasets

This study integrates techniques in lithofacies analysis, ichnology and sequence stratigraphy based on analysis of subsurface data from 14 wells that penetrate the lower Dhruma Formation in the studied area, in Saudi Arabia. The dataset includes subsurface core data, representative core thin sections, gamma-ray logs and image logs. Cores and thin sections have been described in detail in terms of grain-size distribution, grain texture (clast shape, sorting), sedimentary structures, bed thickness, bed contact types, and bioturbation intensity using the bioturbation index of Taylor and Goldring (1993). Using these descriptive criteria, fourteen distinct lithofacies are identified in the succession. These lithofacies are grouped into five primary facies associations that have been interpreted as being representative of vertical accumulations arising in response to particular suites of depositional processes; each facies association is

considered representative of sedimentation within a particular palaeoenvironment.

Based on correlations between the studied wells, three stratigraphic cross sections (correlation panels) have been constructed, two in an orientation considered close to parallel to the depositional strike of the sedimentary system, and one along a dip-oriented profile. These three panels have been used to determine the spatial distribution of the defined facies associations. Correlation has been undertaken principally based on analysis of the sedimentary logs and the gamma-ray signatures. Well-log gamma-ray data from the studied wells were placed against the descriptive sedimentary core-logs to account for the uncored sections of the lower Dhruma Formation. Logs and cores are commonly mismatched with respect to reported depths due to line stretch and temperature expansion within the deep boreholes (Crain, 2015). To address discrepancy between the reported depths of the sedimentary logs (descriptions of the cores) and the gamma-ray logs, a standard core-to-log calibration technique has been applied by matching the core gamma-ray logs (as obtained in the lab after cutting the core) with the reference (wireline) gamma-ray logs. This typically required a core shift of up to 7 m downward or upward with respect to the reference gamma-ray log. The gamma-ray signature, which is a proxy for sand and shale in the subsurface, was used to derive insight into vertical lithology trends. The gamma-ray signature of the uncored intervals has been interpreted based on the gamma-ray log responses typical of different depositional settings (cf. Emery and Myers, 1996). Age-diagnostic palynomorphs, described by Stewart et al. (2016), were considered in this study to discriminate the relevant successions of the Middle Jurassic lower Dhruma Formation from the underlying lower Jurassic and/or Upper Triassic formations.

Formation Micro-Imager (FMI) image-log analyses from 4 wells have also been used to determine the palaeoflow direction of the defined geobodies (e.g. dip directions of sedimentary structures of different types); results were provided courtesy of Shahzad Ulhaq, Saudi Aramco.

3.3.2 Constraining uncertainty associated with inter-well correlation

This study is based primarily on a comprehensive one-dimensional subsurface dataset from wells distributed over an area of approximately 150 km x 150 km (Figure 3.1B). The two wells that are closest to each other have a spatial separation of 4 km (wells 3 and 4), whereas the two most widely separated wells are ~126 km apart (wells 12 and 13). Therefore, significant uncertainty exists in interpretations of the inter-well areas, especially given the lack of three-dimensional seismic coverage.

In the subsurface study, cores and wireline-log signatures (gamma-ray logs) are the principal data types utilized to infer depositional environments. These types of data indicate the vertical extent of different geobodies, biostratigraphy content, physical properties of the rock (porosity, permeability etc.), and provide age dates through biostratigraphy. However, determining the stacking patterns and the lateral connectivity of geobodies is not straightforward. Uncertainty can be associated with facies interpretation of gamma-ray signatures in cases where cores are unavailable. For example, shoreface and delta-front facies may display similar characteristics and may be difficult to discriminate using well-log data alone.

Geobody geometry has been estimated by employing appropriate modern and ancient analogues from which distributions of geobody length and width can be derived; estimations of geobody lateral extent has been attempted based on

knowledge of their thickness. Analogue data were obtained from a relational database detailing sedimentary architectures: the Shallow Marine Architecture Knowledge Store (SMAKS) (Colombera et al., 2016c). The SMAKS database has here been used to provide quantitative information on the architectures and dimensions of geobodies for ancient shallow-marine and paralic siliciclastic successions deemed analogous to the subsurface Dhruma Formation. The database was filtered and queried to derive analogue data that are the most suitable to this study. For example, data relating to sedimentary units that represent only one part of a tidal flat (i.e. sand flat or mud flat) were disregarded, as tidal-flat deposits described in this study include a full suite of sand-, mixed- and mud-flats. Moreover, data on parasequence-scale shoreface sandstones (cf. Colombera and Mountney, 2020a, 2020b), and on shallow-marine sandstones more generally were considered. Examples of such deposits were filtered on their thicknesses to ensure that only those that are comparable in scale to those observed in core were considered. Relationships between the thickness and lateral dip extent of sedimentary units (i.e. facies associations) as obtained from SMAKS, have been considered to guide well correlations in the studied subsurface succession.

3.4 Results

Fourteen distinctive lithofacies types have been identified from the analysed cores of the lower Dhruma Formation (Table 3.1). These have been grouped into five main facies associations based on their arrangement and genetic relations to one another. The 5 facies associations are categorized as follows: fluvial channels (FA1); intertidal flats and pedogenically modified supratidal or floodplains (FA2); fluvial-influenced tidal bars (FA3); shoreface and delta (FA4);

open-marine shelf (FA5). Facies associations FA2, FA4 and FA5 have been further subdivided into two sub-associations each. FA2 is subdivided into intertidal flats (FA2a) and pedogenically modified supratidal or floodplains (FA2b), FA4 into weakly stormed-influenced shoreface to offshore transition zone (FA4a) and storm-dominated river-influenced delta front to prodelta (FA4b), and (FA5) into carbonate shelf (FA5a) and iron-rich oolitic shoal (FA5b Representative graphical sedimentary log examples from which facies associations have been identified are shown in Figure 3.2.

Code	Facies	Description	Bioturbation Index (0-6)	Process Interpretation	Depositional Environment
F1 Hms	Heterolithic mudstone and sandstone	Light to Dark gray in color, heterolithic silty very fine to fine sandstone and claystone. Grains are angular to subrounded, and poorly to moderately sorted. Characterized by lenticular, wavy and flaser bedding. Pyrite nodule are present and are associated with the presence of mudstone.	0-3	Fluctuating energy levels including ebb and flood tidal processes	Intertidal zone, offshore transition zone
F2 Sx	Trough and planar cross-bedded sandstone	Brown, medium to coarse sandstone with sparse fine sand grains, subrounded to subangular, moderately sorted. Characterized by high and low angle cross bedding, rare irregular lamination.	0-1	Migration of 2D and 3D dunes	Compound bars in estuary, tidal bars (subtidal to intertidal zones)
F3 Ms	Mudstone	Dark gray to black blocky mudstone, non-calcareous, grains are too small to function. Shows planner lamination and abundant pyrite nodules and disseminates.	0-1	Fallout of sediment from suspension in quiet water conditions	Shelf environment, distal prodelta, restricted lagoon, restricted tidal flats
F4 Sd	Destratified, rooted sandstone and siltstone	Light gray, light greenish gray, spotty reddish in color, siltstone and very fine sandstone grained, subangular to subrounded grains, mostly poorly sorted. Shows irregular destratified sedimentary structures and rare horizontal laminations. Also shows common rootlets and reddish to blackish fracture-like structures (likely shrinkage fractures of palaeosols). Rare clustered small pyrite nodules (2-5 mm in diameter).	Rare-3	Chemical alteration during subaerial exposure	Supratidal plain setting
F5 Cm	Coal and coaly mudstone	Black to dark gray, almost homogenous deposits with no pronounced sedimentary structures.	Rare		Supratidal plain setting
F6 Shcs	Hummocky cross-stratified sandstone	Light gray creamy, very fine to medium grained sandstone, subangular to subrounded grains, moderately sorted. Characterized by fine cross lamination, hummocky cross stratification. Alternating mud and sand rythmites present. Single and double mud drapes common. Rare 10-15 cm thick intervals of lag deposits and floating mud chips. Bioturbation can occur but low index value.	1-2	Wave oscillatory currents	Middle and lower shoreface, shelf ridge or barrier island and delta front
F7 Sb	Bioturbated sandstone and silty sandstone	Cream and gray in color, silty to medium sandstone, angular to subrounded grains, poorly to moderately sorted. Shows disrupted and irregular sedimentary structures due to bioturbation. Bioturbation index varies in different wells.	2-5	Borrowing of animals on substrate at low- to high-energy environment	Offshore transition zone, below storm wave base, restricted lagoon, estuarine middle zone (i.e. estuarine central basin), channel associated tidal flats
F8 Sm	Massive structureless to faint laminated sandstone	Grey and Brownish in color, medium to coarse grained sandstone, subrounded grains, moderately to well sorted.	0-2	Rapid or continuous sedimentation	Fluvial deposits (channel fill)

F9 Ls	Limestone	Dark gray in color; packstone and grainstone (Dunham classification). Composed of well-rounded quartz grains, shell fragments, coated grains, ooids, and aggregate grains. Grains range in size from silt to coarse, and are poorly sorted. No pronounced sedimentary structures.	3-5	Biogenic activity	Open-marine shelf environment
F10 Lsd	Dolomitic limestone	Dark gray in color, mudstone to wackstone (Dunham classification). Composed of quartz grains that decrease upwards, coated grains, intraclasts, shell and skeletal fragments. Poorly sorted. No sedimentary structures. Moderate to intense bioturbation.	3-5	Biogenic activity and diagenesis	Open-marine shelf environment
F11 Msc	Calcareous mudstone	Dark gray to black blocky mudstone, mostly calcareous (calcite dissipates towards the top). Abundant replaced shell fragments. Thin interbedding of oolitic siltstone and sandstone. No pronounced sedimentary structures. Pyrite nodules are present.	Rare to 2	Fallout of sediment from suspension in quiet water conditions	Shelf environment with close proximity to carbonate platform, offshore mud, distal prodelta
F12 Sc	Calcareous sandstone and siltstone	Grey to dark gray in color, fine to medium-grained, with common sparse coarse quartz grains, scattered ooids, angular-rounded grains, moderately sorted. Faint planar lamination and common disturbed sedimentary structures with moderate to intense bioturbation.	3-5	Mix of detrital input and marine calcium carbonate	Inner shelf, carbonate platform and oolitic shoal
F13 Ors	Oolitic ironstone	Reddish in color, fine to medium quartz grains, medium to coarse ooid grains. Rare irregular lamination were observed.	1-2	Biogenic activity in a high-energy environment	Shoal complex with periodic subaerial exposure
F14 Lg	Lag sediments	Medium to coarse sandstone with sparse very coarse grains, subangular to rounded grains. Generally, poorly sorted. Fines upwards in some cases.	rare	Sedimentation by high energy currents	Fluvial channels, fluvial-influenced deposits

Table 3.1: Summary of lithofacies observed in the lower Dhruma Formation.

Facies Association	Facies Association Description	Occurrence Location (Well No.)
Fluvial-channel deposits (FA1)	Massive Sandstone (Sm) and/or cross-bedded sandstone (Sx) that are commonly overlain by Heterolithic sandstone and mudstone (Hms) and mudstone (Ms)	1, 2, 4, 7, 10, 12, 13
Intertidal flat deposits (FA2a)	Dominated by (Hms) with a fining-upward trend from sand-dominated to mud-dominated facies. Local soft sediment deformation (Sd) occurs within the sand-dominated part.	1, 2, 4, 5, 7, 8, 12, 13
Pedogenically modified supratidal flat or floodplains (FA2b)	Composed dominantly of intensively destratified sandstone, siltstone and mudstone (Sd) with local presence of coaly mudstone intervals (Cm).	1, 2, 4, 5, 7, 8, 10, 12, 13
Fluvial-influenced tidal bars (FA3)	Massive sandstone (Sm) with scoured bases that grades up to cross-bedded sandstone (Sx) with abundant mud laminae draping the cross stratified sets.	3, 4, 11
Weakly storm-influenced shoreface to offshore transition zone (FA4a)	Coarsening-upward packages of mudstone (Ms) and/or heterolithic mudstone and sandstone (Hms) that grade up to bioturbated (Sb) and/or hummocky cross-stratified sandstone.	1, 2, 5, 6, 7, 8, 11, 14
Storm-dominated delta-front to prodelta (FA4b)	Coarsening-upward packages of (Ms) and/or heterolithic mudstone and sandstone (Hms) that grade up to cross-bedded (Sx) hummocky cross-stratified sandstone.	2
Carbonate shelf (FA5a)	Fining-upward packages in well 2 with limestone (packstone and grainstone) dominating the base of each package that generally grade up to calcareous mudstone (Msc). Conversely, coarsening upward limestone (Ls) packages from wackstone to grainstone were observed in wells 7 and 11. The bottom of the limestone in well 7 shows dolomite limestone interval (Lsd) that calcifies upwards.	2, 7, 11
Iron-rich oolitic shoal (FA5b)	Fining upward trends with calcareous sandstone (Sc) or ooid-rich ironstone (Ore) at the bottom that transition up to calcareous Mudstone (Msc).	1, 5, 7, 8, 9, 13

Table 3.2: Summary of the facies associations defined in this study along with their occurrence with respect to well locations.

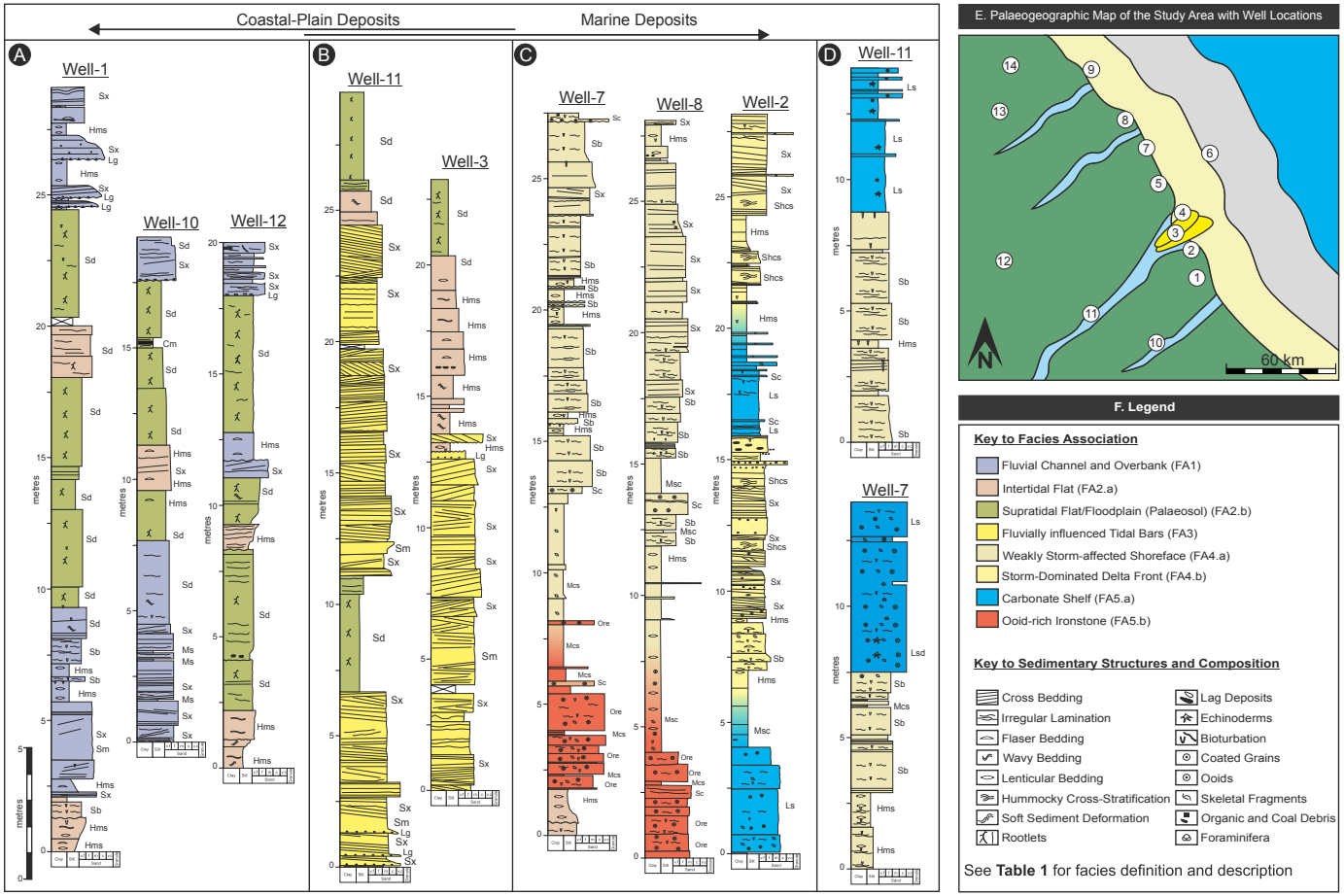

Figure 3.2: Representative sedimentary logs depicting the different facies associations defined in the lower Dhruma Formation and their vertical relationships. A) 'Fluvial channels' and 'intertidal flats and pedogenically modified supratidal or floodplain facies associations B) 'fluvial-influenced tidal bars' facies associations, C) 'weakly storm-affected shoreface and offshore transition zone' and ' fluvial-influenced storm-dominated delta-front and prodelta' facies associations; note the occurrence of the oolitic ironstone facies association Fa5 below the shoreface successions; D) carbonate shelf facies associations occurring in the uppermost part of the cored section; E) simplified paleogeographic map of the lower unit of the lower Dhruma Formation based on this study; F) Legend with color codes for facies associations and symbols used in the sedimentary logs. See text for further explanation.

3.4.1 Fluvial-channel deposits (FA1)

3.4.1.1 Description

This facies association was cored in 7 wells (see Table 3.2) and commonly has an erosional base and occurs on top of FA2 (described below). FA1 is composed of fining-upward packages of massive (Sm) and cross-bedded sandstone (Sx) that always pass upward to thinner beds of heterolithic mudstone and sandstone (Hms) and mudstone (Ms). These deposits are sand dominated and occur as a single package (e.g. middle of well 12 in Figure 3.2), else as repeated cyclically arranged packages (e.g. top of well 1 and base of well 12 in Figure 3.2). A single package of strata representing this facies association is 0.5-4 m in thickness. The sandy units are commonly thicker (0.2 to 3.5 m) than the overlying heterolithic facies (0.1 to 0.8 m). The sandstone units exhibit erosional bases that are commonly overlain by lag sediments (Lg), mainly of very coarse sand grains whereas the overlying heterolithic and mudstone facies show gradational or sharp bases. There also exists rare small scale (0.2 m) alternating sandstone (Sx) and heterolithic facies (Hms) towards the upper part of the overall sandy section (Figure 3.3C).

Generally, the sandstone facies grade upward into planar-bedded medium- to fine-grained sandstone and siltstone units. The massive and cross-bedded sandstone consistently has sparse floating mud chips (1.2 to 5 mm diameter) present within it, as well as sparse clasts of organic and coaly debris (Figure 3.3A and B). FA1 exhibits millimetre-scale, carbonaceous laminae draping the cross-stratified sets in wells 10, 12 and 13. These laminae are faint in the lower parts of the sandy units but more pronounced upwards. Localized double mud drapes occur in well 13 at the transition between the sandstone and the

overlying heterolithic facies (Figure 3.3D). The heterolithic units in this association are mud-dominated (mainly clay) and contain thin beds and lenses of sand and common wavy to lenticular bedding. They cap and/or separate units composed of the sandy facies (Figure 3.3E). Localized vertical burrows (*Skolithos*) are observed at the upper contact of sandstone units that are directly overlain by the heterolithic facies; these burrows likely originate at the interface with the overlying finer-grained sediments. Within the heterolithic facies, small sporadic forms of *Planolites* and other unidentified burrows are present. The heterolithic facies is commonly overlain by the deposits identified in FA2b (Figure 3.3F).

3.4.1.2 Interpretation

The numerous erosional beds indicate repeated high-energy currents eroding the underlying sediments. The massive coarse sandstone with lack of pronounced sedimentary structures and bioturbation suggests rapid deposition by deceleration of high-energy, heavily sediment-laden currents (Martin, 1995; Collinson et al., 2006; Dalrymple et al., 2015). The abundance of clasts of mudstone, organic matter and coaly debris suggests reworking of pre-existing sediments, and perhaps transportation by fluvial currents. The vertical trend of the succession, with lag sediments resting on an erosional base and passing upward into massive sandstone, is a characteristic that is common of channel-fill deposits (Martini and Aldinucci, 2017). The more cyclic occurrence of thick sandstone overlain by thin intervals of heterolithic deposits is interpreted to represent alternation of high and low river flow stages. The thick sandstone units were likely deposited during river-flood periods (high river discharge), whereas the overlying heterolithic interval was likely deposited during inter-flood periods (low river discharge) (Dalrymple et al., 2015). Possible tidal effect is

indicated by the presence of double mud drapes in well 13. Overall, this facies association is interpreted to represent fluvial-channel and overbank deposits. The fluvial-channel deposits observed in well 13 with the possible tidal effect may represent deposition within the upstream region of the FMTZ.

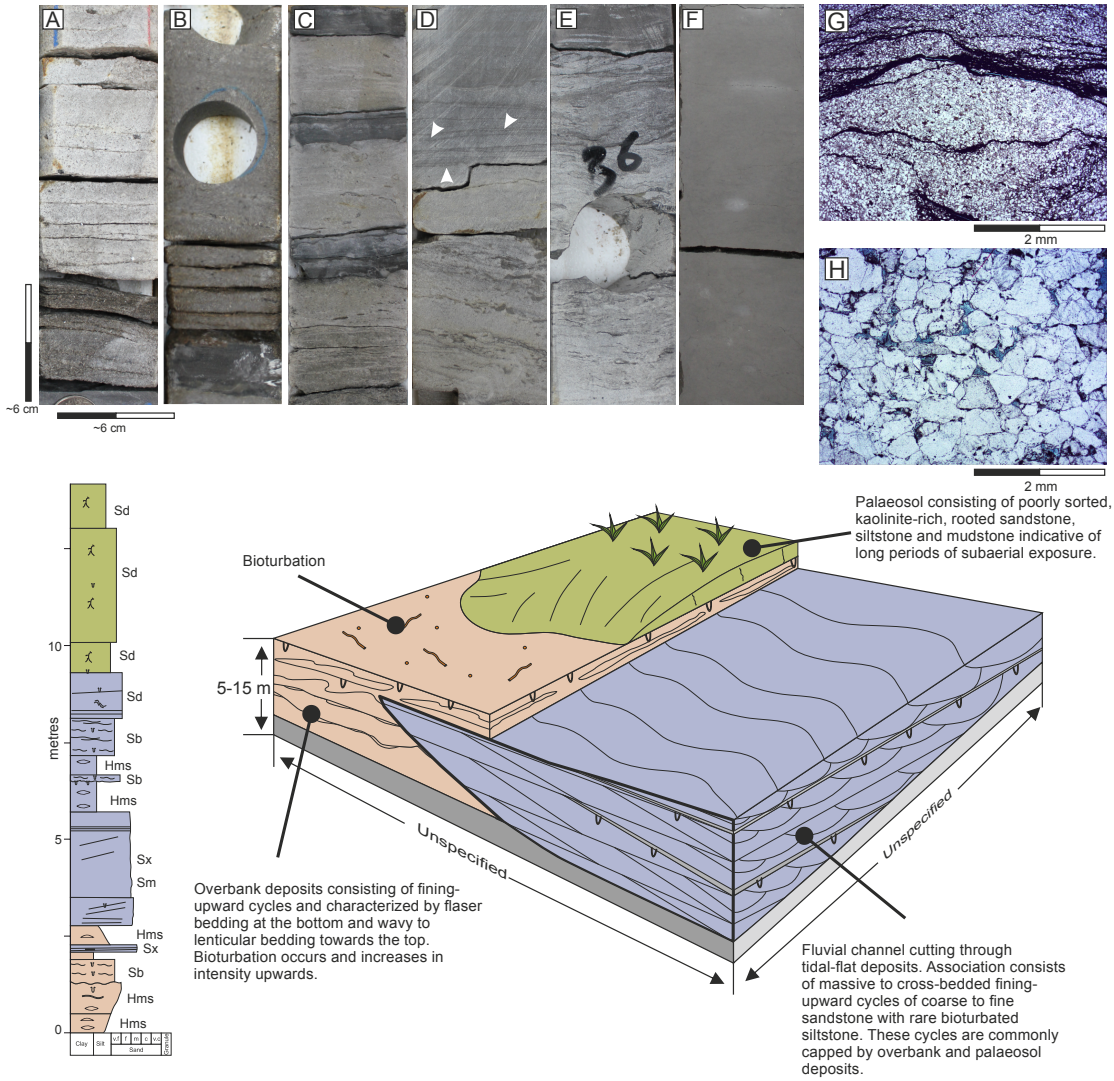

Figure 3.3: Representative core photographs of 'fluvial channel' facies association (FA1). A-B) massive to faintly bedded sandstone with lag sediments at the bottom and common floating coal debris and mud chips; B) Alternating sandstone and heterolithic facies D-E) transition between sandstone and heterolithic facies (white arrows indicate double mud drapes in (D); F) destratified facies of FA2b overlying the FA1, G-H) thin sections representing the petrography of the sandstone facies (G) and heterolithic facies (H) defined in FA1; note grain size and mud content variation.

3.4.2 Intertidal and pedogenically modified supratidal flat or floodplain (FA2): intertidal flat deposits (FA2a)

3.4.2.1 Description.

This facies association was cored in 8 wells (see Table 3.2). It was observed at the bottom of the formation, where cored, across much of the study area. It unconformably overlies the lower Jurassic carbonate deposits of the upper Marrat Formation. This facies association overlies the fluvial deposits of FA2b in many wells. It mainly consists of fining-upward packages (up to 5-m thick with an average of ~3 m) of heterolithic fine to medium-grained muddy sandstone that transitions to sandy mudstone facies (mainly clay) (Hms). The sandy part contains cross-lamination and stacked bidirectional ripple forms (Collinson and Mountney, 2019) that decrease in frequency and become isolated towards the muddy part (Figure 3.4A). Unidirectional ripples also exist within the sandy facies. Repeated double mud drapes are observed in various parts within this facies association (Figure 3.4A). It also shows common flaser, wavy and lenticular bedding as well as abundant thin, very fine sand lenses within the finer interval (Figure 3.4B). Distorted beds locally occur at the bottom of the sandstone facies. In places, shrinkage cracks are observed in the muddy parts of this facies association; they taper downward and are filled with sediment. Low to intense bioturbation is observed within sand-mud alternations, with bioturbation index values ranging from 1 to 5 (Figure 3.4C).

3.4.2.2 Interpretation

The presence of sand-mud alternation in the form of rippled sandstone, together with the flaser, wavy and lenticular bedding, suggests deposition during fluctuating energy levels (Reineck and Wunderlich 1968; Ginsburg 1975; Klein 1985). In this context, sand grains are typically deposited as bedload during the more energetic flows of a tidal cycle, generating bidirectional ripple

forms (Boggs, 1995). By contrast, mud particles settle out of suspension on the underlying rippled sand during low-velocity flows or at slack-water, giving rise to the occurrence of flaser, wavy and lenticular bedding (Klein, 1985; Boggs, 1995). The observed shrinkage cracks are interpreted to be desiccation cracks that resulted from periodic subaerial exposure of the muddy deposits in the upper intertidal zone (Dalrymple, 2010). They are not likely to be syneresis cracks, given their downward tapering form (Collinson and Mountney, 2019). The vertical succession of this facies association, with its fining-upward trends is similar to those interpreted as deposition in channel-related tidal flats (e.g. Dalrymple, 2010; Desjardins et al., 2012a). Possible fluvial influence is indicated by the presence of unidirectional ripple forms. This facies association may represent tidal flat setting within the inner FMTZ considering the possible tidal and fluvial indicators.

3.4.3 Intertidal and pedogenically modified supratidal flat or floodplain (FA2):pedogenically modified supratidal flat or floodplains (FA2b)

3.4.3.1 Description

This facies association was cored in 9 wells (see Table 3.2). The heterolithic mudstone and sandstone of FA2a and those defined in FA1 repeatedly transition upward to thick (few metres to 10 m) intervals of greenish-grey destratified very-fine sandstone, siltstone and mudstone (Sd), with intensive rooting (Figure 3.4D). It also shows variegated mottling in some wells, with a brownish-red colour interchanging with a greenish-grey colour (Figure 3.4E). Within the highly oxidized facies, there exists cm-scale blocky volume that is separated by mm-scale iron-rich matrix (Figure 3.4E). This destratified facies commonly shows thin beds of coal (~20-80 mm) (Figure 3.4F and G), coarse- to

pebble-size coal clasts and organic debris, and up to 0.8 m-thick coaly mudstone beds (Cm). Pyrite nodules and disseminations are observed in this FA and are associated with the presence of coal and organic material. Furthermore, thin sections of this facies indicate high content of kaolinite and of organic carbonaceous material. A low diversity of ichnogenera, mostly *Planolites*, is observed with a bioturbation index that ranges from 1 to 3.

3.4.3.2 Interpretation

The destratified nature of this facies association suggests post-depositional alteration of the sediments prior to lithification. The presence of the rootlets across most of the facies suggests vegetation forming on top of the deposits. Kaolinite is commonly formed during intense chemical weathering in warm and humid climate conditions (Weaver, 1989; Robert and Chamley, 1991); its high abundance in this facies association suggests that FA2b deposits were subjected to intense chemical alteration. The variegated form of red and brown colours suggests oxidation of iron-bearing sediments, possibly during subaerial exposure (Bromley, 1975; Pemberton and Frey, 1985; Pemberton et al., 1992, 2001; MacEachern et al., 1992, 2012). Pedogenic processes are also indicated by the presence of the blocky volumes that is separated by iron-rich matrix which suggest soil formation. Coaly debris and organic material observed within this facies association in most of the locations may have been reworked from localized vegetated swamps and accumulated under reducing conditions. This facies association is interpreted as subaerially exposed supratidal deposits in the seaward position of the region (wells 1, 2, 4, 5 ,7, 8) and may represent altered floodplain deposits in more landward positions (wells 10, 12).

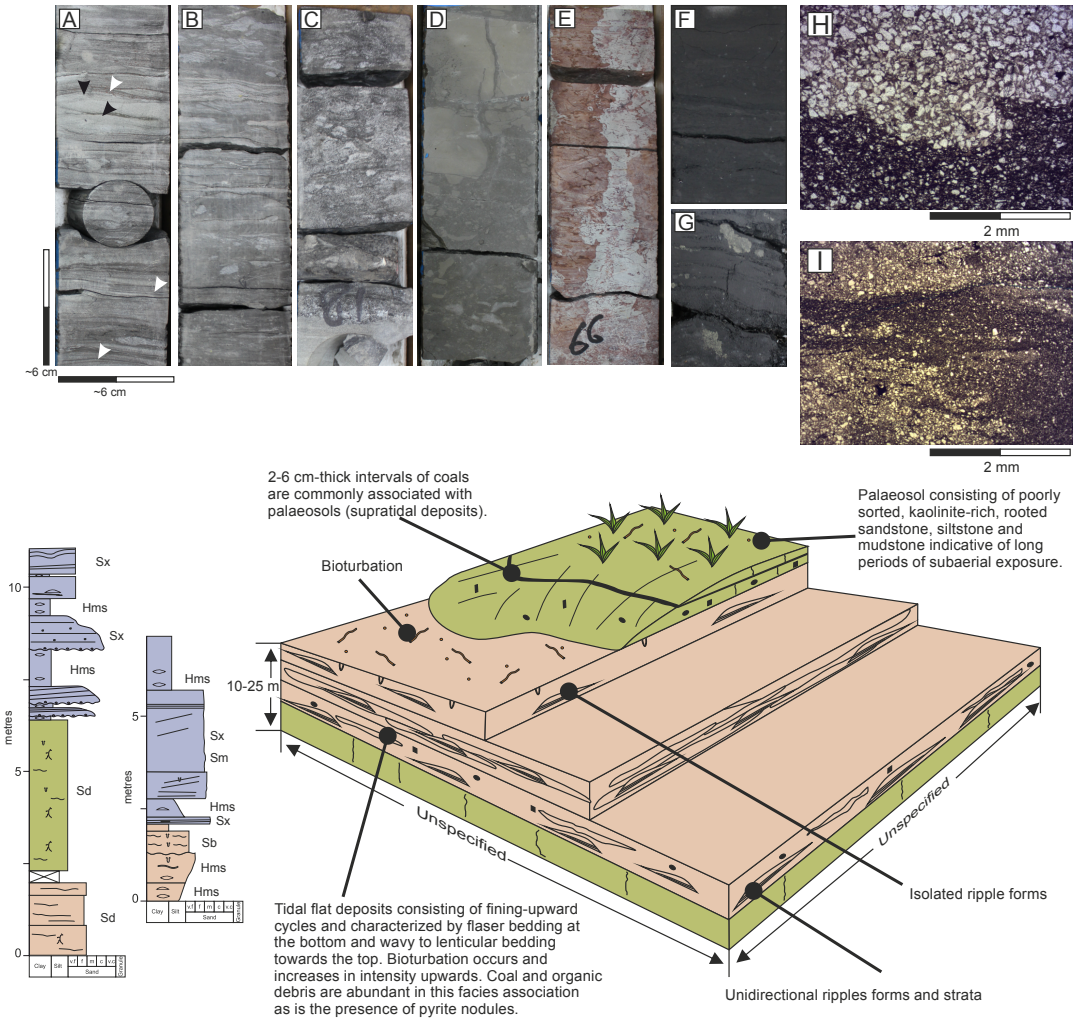

Figure 3.4: Representative core photographs of 'tidal flat' (FA2a, A-C) and 'paleosol' (FA2b, D-G) facies associations. A-B) heterolithic sand and mud facies; note the stacked bidirectional ripple forms (black arrows) and double mud drapes (white arrows); C) intense bioturbation within the sand-mud alternation; D-E) kaolinite-rich sandstone, siltstone and mudstone with intense rooting; note the color mottling in photograph E; F-G) coaly mudstone. H-I) representative thin sections of the heterolithic facies of FA2a.

3.4.4 Fluvial-influenced tidal bars (FA3)

3.4.4.1 Description

This facies association was cored in 3 wells (see Table 3.2) and observed overlying and underlying the intertidal and supratidal deposits of FA2. It is composed of normally graded, centimetre- to decimetre-beds of non-stratified very coarse to medium quartz-dominated sandstone (Sm), commonly with scoured bases overlain by coarse-grained lag sediments (Lg). This massive sandstone shows relatively thicker beds and with more frequent erosional bases in well 11 compared to wells 3 and 4. It generally grades upward to stacked sets of medium-grained trough and planar cross-bedded sandstone (Sx). Sedimentary structures observed within Sx include planar cross-stratification, with foresets that possess thin (up to 5 mm) single and double mud drapes (mainly clay). Sand and mud couplets were also observed within bundles (Figure 3.5A). Furthermore, the cross-stratified sets are observed bounded by non-bioturbated erosional surfaces (reactivation surfaces). Within Sx, there exist thin beds (20 to 40 mm) of non-stratified very coarse sandstone that generally grade upwards to coarse and medium grain size (Figure 3.5B and C). These are commonly overlain by double mud drapes that generally increase in frequency and decrease in spacing upwards (Figure 3.5C). Towards the top of FA3, heterolithic and destratified facies were observed overlying the sandstone facies (Figure 3.5D and E). The sandstone facies is dominantly composed of monocrystalline quartz with lesser polycrystalline quartz, with rare lithic fragments and heavy minerals (Figure 3.5F). Thin sections record limited presence of kaolinite in Sx (Figure 3.5G). Bioturbation is generally rare in FA3. This facies association exhibits a high proportion of carbonaceous organic material.

3.4.4.2 Interpretation

Where they co-occur, single and double mud drapes, reactivation surfaces and sand-mud couplets are considered as possible tidal indicators (Visser, 1980; Dalrymple and Choi, 2007; Dalrymple, 2010; Davis, 2012). Mud drapes typically represent deposition from suspension during low-velocity tidal flow or at slack-water periods (Visser, 1980), whereas reactivation surfaces indicate pause planes (discontinuities in sedimentation) or reversing tidal currents (Boersma and Terwindt, 1981). Alternation of sand and mud beds in the form of bundles is commonly described as the product of flood-ebb tidal cycles (Visser, 1980). However, recent work demonstrates that such bundles may originate in tide-modulated fluvial settings (Martinius and Gowland, 2011) or in purely fluvial settings (Ainsworth et al., 2011). The thin, normally graded beds indicate deposition by high-energy currents, possibly by streamflow. The overlying double mud drapes and their upward increase in frequency of occurrence supports an interpretation of increase in tidal influence over time. The coaly fragments, organic material and kaolinite present in this facies association imply reworking of sediments from a coeval adjacent vegetated setting.

This facies association indicates interaction of tide and fluvial currents. Tidal currents are interpreted to be the dominant process overall, though significant fluvial influence is evident in places. Overall, the deposit of FA3 are interpreted as fluvial-influenced tidal bars in a potentially estuarine setting.

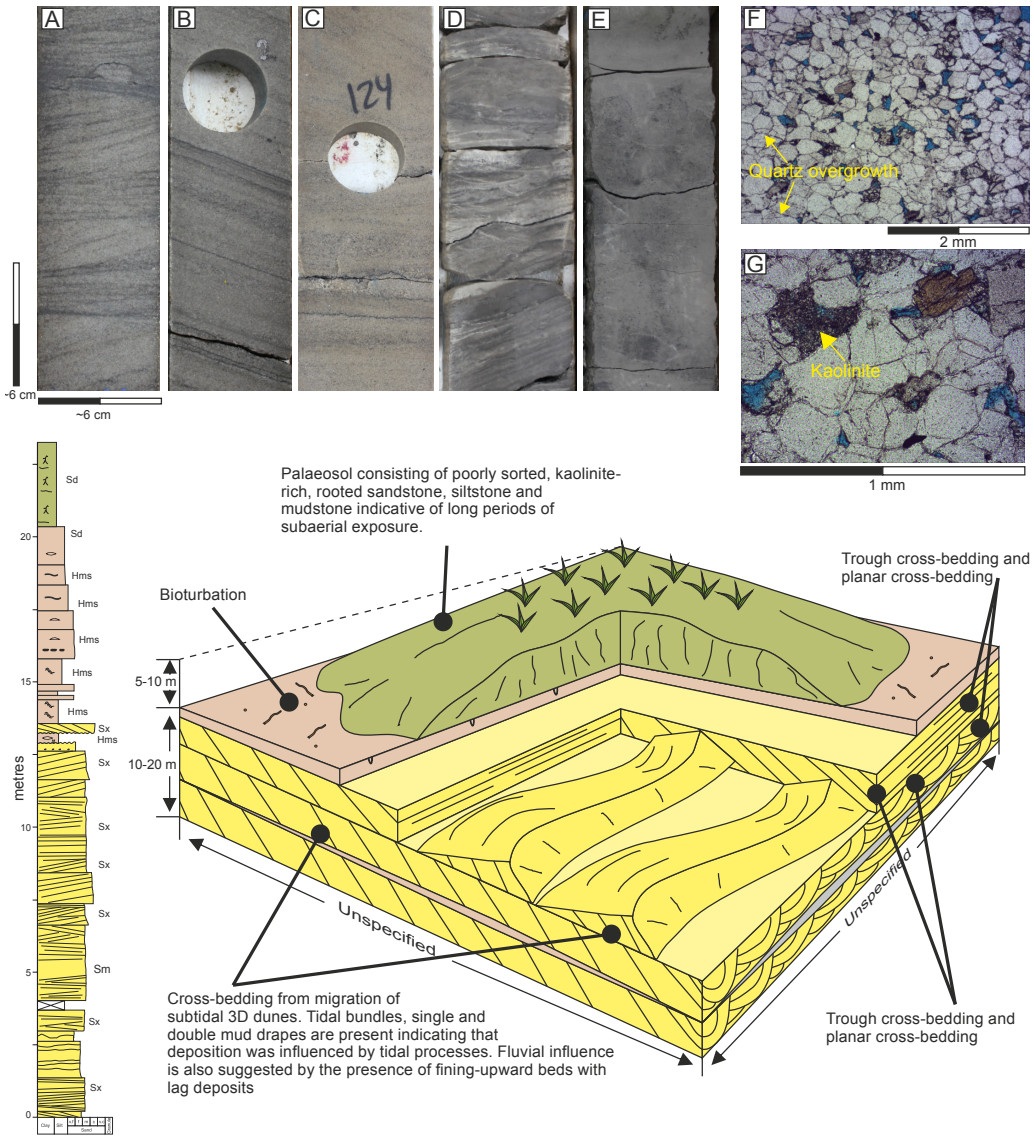

Figure 3.5: Representative core photographs of the 'fluvial-influenced tidal bars' facies association (FA3). A) cross-bedded sandstone with apparent bundled bedsets showing internal mud drapes; B-C) cross-stratified sandstone showing thin beds of very coarse sand within medium-grained sandstone; note the double mud drapes in (B). D-E) heterolithic and kaolinite-rich deposits that overlie the tidal bar deposits; F-G) representative thin sections of tidal-bar facies; note the kaolinite in photograph G.

3.4.5 Shoreface to offshore transition and delta-front to prodelta (FA4): weakly storm-affected shoreface to offshore-transition zone (FA4a)

3.4.5.1 Description

This facies association was cored in 8 wells (see Table 3.2), where it consistently overlies the oolitic ironstone of FA5b. This facies association comprises amalgamated coarsening- and thickening-upward packages (0.5 m to few metres thick) of massive mudstone (partly calcareous), heterolithic mudstone and sandstone (Hms), and fine to medium-grained hummocky cross-stratified sandstone (Shcs) and bioturbated sandstone (Sd). These packages show increasing dominance of sand upwards. The mudstone units (Ms) are rather homogeneous, with rare apparent sedimentary structures. The heterolithic part is composed of mudstone and very fine- to fine-grained sandstone and exhibits an upwards increase in sand proportion (Figure 3.6A). Locally, slightly asymmetrical lenticular ripples with gently inclined internal cross-lamination were observed within the heterolithic unit (Figure 3.6B). In facies Hms, rare thin sandstone beds with erosional bases and internal fine laminations are present in places. In its upper part, FA4a is dominated by the presence of weakly to intensely bioturbated, dominantly fine-grained sandstone of Sb (Figure 3.6C), which commonly grades up to cleaner (relatively lower mud content) lightly bioturbated sandstone with apparent hummocky cross-stratification (Shcs). The bioturbated sandstone is composed of poorly sorted grains and shows rare preserved cross bedding. Abundant rounded to elongate, concentrically lined iron-rich ooids are scattered in various parts of this facies association (Figure 3.6D). A moderately diverse assemblage of ichnogenera is present in FA4a: *Skolithos*, *Planolites*, *Ophiomorpha*, *Teichichnus*; the bioturbation index varies from 2 to 5.

3.4.5.2 Interpretation

The coarsening-upwards packages of mudstone, heterolithic strata and sandstone indicate increasing energy levels as a result of decreasing depositional water depth (van Wagoner et al. 1990 and Howell et al., 2008). The observed ripple forms are likely products of wave activity above fair-weather wave base, where propagating waves produce a slight landward shift of sediment forming the asymmetrical shape (Reineck and Singh, 1980). The observed intensity and diversity of bioturbation present in FA4a successions suggest broad organism colonization, in low-energy settings (e.g. Pemberton et al. 2003; MacEachern et al. 2005). The decrease in bioturbation in the sandstone facies and the presence of hummocky cross-stratification is attributed to periods of strong wave activity, likely between the fair-weather and the storm wave bases (Harms et al., 1975; Collinson and Mountney, 2019). Variations in bioturbation may also reflect changes in sedimentation rate, whereby organisms colonize the sediments during periods of low sedimentation rate (Bromley, 1996; Melnyk and Gingras, 2020). The abundance of iron-rich ooids in this facies association is attributed to reworking of pre-exiting ooids. Overall, this facies association is interpreted as a prograding storm-affected offshore-transition zone to shoreface environment.

3.4.6 Shoreface to offshore transition and delta-front to prodelta (FA4): storm-dominated river-influenced prodelta to delta-front deposits (FA4b)

3.4.6.1 Description

This facies association was only cored in well 2; however, gamma-ray signatures in two nearby wells (wells 3 and 4) show striking resemblance with the corresponding gamma-ray signatures of well 2. FA4b was observed overlying the open-marine carbonate deposits of FA5a in two coarsening- and thickening-upwards packages (that are ~9 and 10 m thick). These packages consist of mudstone (Ms), heterolithic mudstone and sandstone (Hms) and fine to medium-grained sandstone (Sx and Shcs). The mudstone unit is blocky, sub-fissile homogeneous in nature. The mudstone facies (Ms) shows numerous fine sandstone lenses and thin to medium beds (up to 150 mm) of finely laminated very fine sandstone, commonly with erosional bases, and exhibit moderate to weak bioturbation (Figure 3.6E and F). These deposits grade up to faintly laminated to low-angle cross-bedded fine to medium-grained sandstone (Sx) and hummocky and swaley cross-stratified fine to medium-grained sandstone (Shcs) (Figure 3.6G and H). The facies association becomes more sand-dominated upwards. Furthermore, several inversely graded beds (50-120 mm) are observed with well-rounded medium to granular grains, floating mud chips and rare preserved gastropod shells. These beds occur towards the upper parts of the sandstone units. The sandstone units are composed primarily of sub-rounded to sub-angular, well sorted monocrystalline quartz grains with common interstitial greenish chlorite cement (Figure 3.6J). Bioturbation is generally rare within the sandstone units, but a low diversity of ichnogenera (e.g. diminutive forms of *Planolites*, *Skolithos* and fugichnia) was observed within Sx, disturbing the original sedimentary structures.

3.4.6.2 Interpretation

Similar to FA4a, deposits of FA4b are indicative of increasing energy levels, likely associated with a decrease in water depth, which is recorded by the coarsening- and thickening-upwards trends. The mud within Ms and Hms in the lower part of each package generally suggests deposition from suspension under quiet water conditions. Periods of storm events eroding the muddy substrate are indicated by the presence of numerous erosionally based sandy beds and lenses (Baniak et al., 2014). The bioturbated heterolithic strata are indicative of energy level fluctuations (cf. Collins et al., 2020). Hummocky and swaley cross-strata present in this facies association are typically wave-generated structures resulting from combined flows (e.g. Harms et al., 1975; Meene et al., 1996). The inverse grading that occurs towards the upper parts of the sand-dominated units may indicate deposition by hyperpycnal flows during waxing river discharge (Bhattacharya and MacEachern, 2009). The overall scarcity of bioturbation indicates environmental conditions that prevented organisms from flourishing. Such conditions might have been due to high rates of sediment influx into the system, freshwater input and/or high-energy wave currents. The local presence of low-index and low-diversity ichnogenera assemblages observed within the sand units is attributed to periods of lower wave action and/or lower sedimentation rate, which might have enabled the temporary activity of organisms (Bromley, 1996; Pemberton et al., 2012). Subsequent episodes of rapid sedimentation would have required the organisms to escape upward to reach the seabed (Pemberton and MacEachern, 1997; Bann et al., 2008; MacEachern and Bann, 2008, Pemberton et al., 2012). The observed ichnofossil assemblage represents an impoverished and distal expression of the Skolithos ichnofacies (MacEachern &

Bann, 2008). Overall, this facies association is interpreted to have formed in a prograding storm-dominated river-influenced delta-front to prodelta setting (cf. Collins et al., 2020).

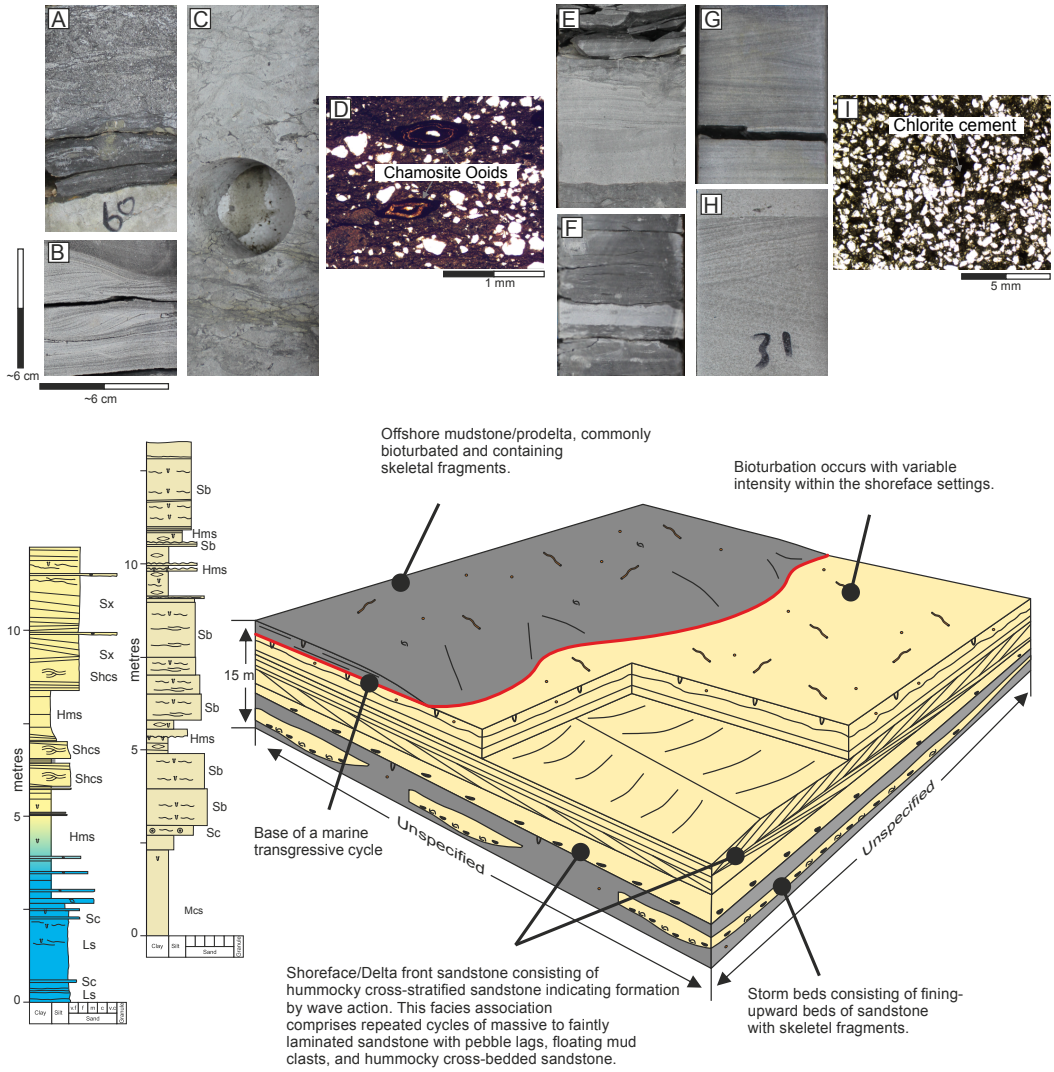

Figure 3.6: Representative core photographs of 'offshore-transition zone to shoreface' (FA4a; A-D) and prodelta to delta-front (FA4b; E-I) facies associations. A) heterolithic facies overlying bioturbated sandstone; B) slightly asymmetrical wave ripple; C) bioturbated sandstone; D) representative thin section showing deformed chamosite ooids within heterolithic facies; E-F) thin sandstone intervals interbedded with heterolithic and mudstone facies; G-H) hummocky cross stratification; I) thin section showing abundant chlorite cement within hummocky cross-stratified sandstone.

3.4.7 Open-marine shelf (FA5): carbonate shelf (FA5a)

3.4.7.1 Description

This facies association was cored in 3 wells (see Table 3.2). It forms the lower part of the two packages defined in FA4b in well 2 and marks the top of the cored section in wells 7 and 11. Packages of carbonate facies overlie FA4b and FA4a in well 2 and FA4b in wells 7 and 11. Generally, this association comprises limestone (Ls) that grades upwards to calcareous mudstone (Msc). The limestone is fine- to medium-grained and is grain dominated (packstone to grainstone; Dunham, 1962). The limestone facies occur as amalgamated bedsets of approximately 4 m thickness, or as thinner interbeds (50 to 150 mm) between packages of facies Msc. The grain composition includes common outsized quartz grains, abundant ooids, shell and skeletal fragments that are commonly replaced by dolomite rhombs. At the base of the deepest occurrence of this limestone, ooids and skeletal grains are highly fragmented. This facies shows moderate to intense bioturbation (BI: 3 to 5) (Figure 3.7A and B). The overlying mudstone beds are marly at their base but become less calcareous toward their top. Mudstone beds are blocky, sub-fissile to fissile, and show many drilling-induced fractures (Figure 3.7C). In places mudstone beds reveal fine parallel lamination, limited wavy to lenticular bedding and can exhibit an increasing proportion of sand upwards. In addition, Msc shows scattered shell fragments in a clayey matrix. Bioturbation within Msc is generally sporadic and is developed most intensely near lithological boundaries. Unlike the limestone units observed in well 2, coarsening- and thickening-upward beds are preserved in wells 7 and 11 with smaller packages of mud-dominated to grain-dominated limestone (wackestone to grainstone). The grain types observed are primarily coated grains, ooids, intraclasts, and shell and skeletal fragments.

Dolomite cement dominates the lower part of the section (Lsd) and decreases in abundance as it is replaced by calcite upwards.

3.4.7.2 Interpretation

The calcite-rich sediments together with the abundant ooids, shells and skeletal fragments indicate periods of carbonate sedimentation. The ooids formed in agitated shallow-water settings (Davies et al., 1978; Rankey and Reeder, 2012). The overall dominance of grainstone within the carbonate facies is indicative of high-energy shoal environments. The presence of skeletal and grain fragmentation at the base of the limestone in well 2 suggests reworking by high-energy currents to leave a lag deposit, possibly during transgression. The overlying mudstone is interpreted to be deposited from settling out of suspension in quiet water conditions, possibly during a subsequent flooding (i.e. deepening) event.

3.4.8 Open-marine shelf (FA5): iron-rich oolitic shoal (FA5b)

3.4.8.1 Description

This facies association was cored in 6 wells (see Table 3.2). It is observed overlying the tidal flat and supratidal deposits of FA2 and the fluvial channel deposits of FA1, with sharp bases. These deposits are always capped by the mudstone of FA4a. They show an overall fining-upward trends and consists primarily of calcareous sandstone (Sc), ooid-rich ironstone (Ore) and calcareous mudstone (Msc). The calcareous sandstone is carbonaceous and composed of poorly sorted fine to medium quartz grains with abundant bioclasts and scattered chamosite ooids (Figure 3.7D and F). The ooid-rich ironstone is composed primarily of orange-brown ooids, skeletal fragments and sparse

detrital quartz grains that are of fine to medium sand size (Figure 3.7E and G). The ooids show concentric laminae around various types of nuclei, including clay, quartz and skeletal fragments. They are mostly rounded to slightly elongate in shape and deformed in some instances (Figure 3.7G). Some of these ooids are completely or partly dissolved and replaced by dolomitic rhombs. The calcareous mudstone is observed interbedded with and/or overlying the calcareous sandstone and the ooid-rich ironstone. The mudstone facies comprises sparse ooids and skeletal fragments at the base of beds; these decrease in abundance upward within beds.

3.4.8.2 Interpretation

The dominance of ooids in this facies association indicates accumulation in high-energy, shallow water settings (Chen et al., 2017). The iron in these accumulations could have been transported from the continent to the sea as Fe-bearing detritus or Fe-clay colloid by river currents (Maynard, 1983; Einsele, 2000). The calcareous sandstone with the abundant ooids and fragmented bioclasts also suggest reworking by wave activity in close proximity to a carbonate source. The stratigraphic position of this facies association, overlying the nearshore deposits of FA1 and FA2, and being overlain by marine deposits of FA4a, suggests deposition during a transgressive episode. This is in accord with how these types of ooidal ironstones are commonly interpreted to form under transgressive conditions (cf. Bayer et al. 1985; van Houten 1985).

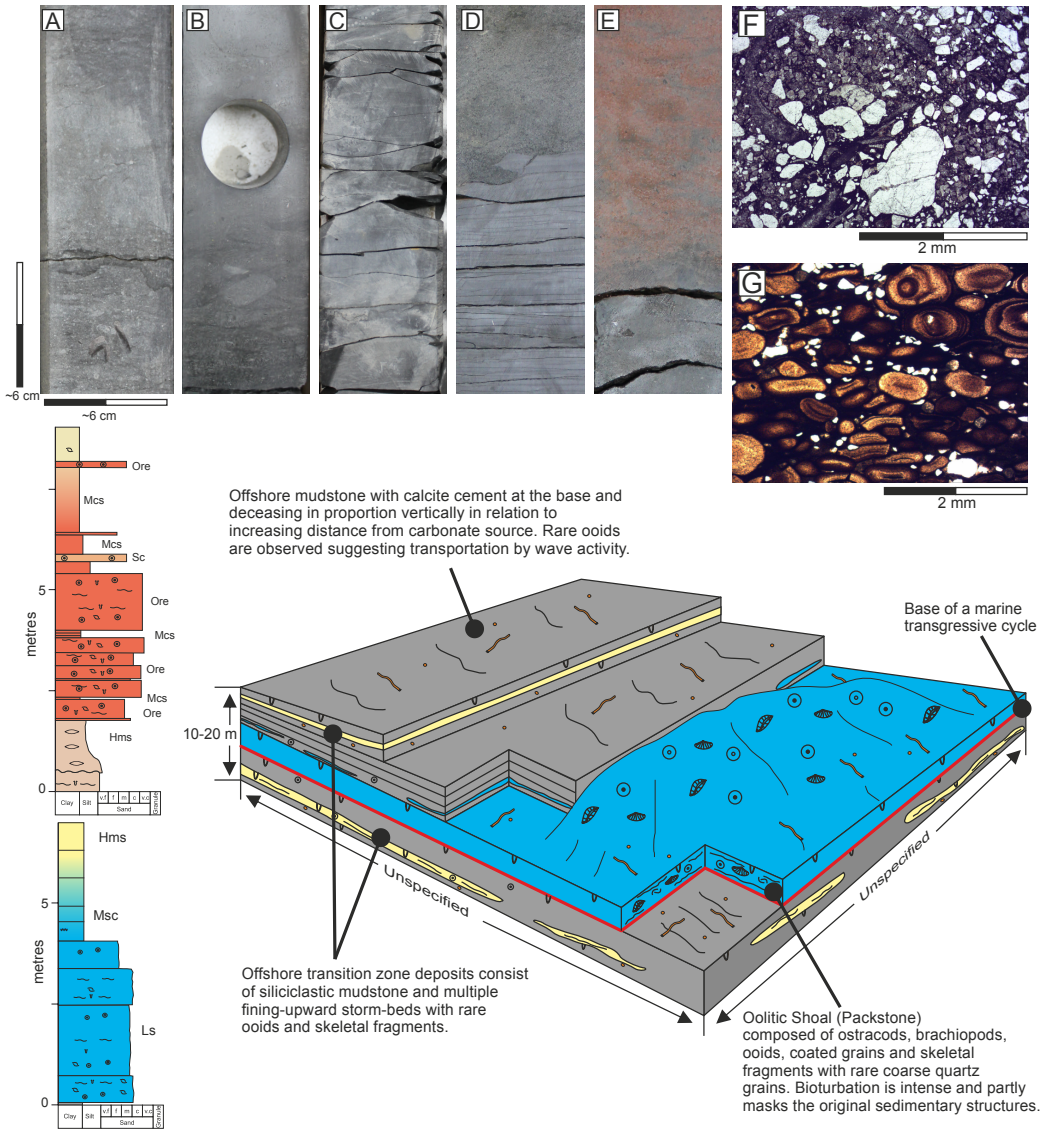

Figure 3.7: Representative core photographs of 'open-marine shelf carbonate' facies association (FA5). A-B) bioturbated limestone; C) calcareous mudstone; D) calcareous sandstone overlying massive mudstone; E) ooid-rich ironstone; F-G) representative thin section examples showing calcareous sandstone (F) and ooid-rich ironstone (G).

3.4.9 Palaeocurrent analysis

Subsurface cores do not reveal information required for palaeocurrent identification as the cores are not oriented. Rather, image logs of the boreholes provide the prevalent type of data used to infer palaeocurrent directions. In this study, FMI image logs acquired from 4 wells were used to interpret the palaeocurrent directions for the defined facies associations. Interpretations of image logs are summarized in rose diagrams (Figure 3.8), which report the dip directions of foresets of cross-bedded sandstones from shoreface (FA4a) deltaic (FA4b), tidal-bar (FA3) and fluvial-channel (FA1) deposits. The foreset dip directions of the shoreface sandstone cross-bedded sets from well 8 and the deltaic sandstone from well 2 show broadly consistent north-northeast (present day) dip directions. Inclined forests of tidal-bar deposits also show a broad northeast dip direction with limited variability. This broad unidirectional bedding of tidal bars might indicate an ebb-dominant tidal currents that is driven by dominant river input at the estuary mouth. However, the position of the tidal bars with respect to the channel remains uncertain. Overall, these observations indicate a broad north-eastward progradation and direction of sediment dispersal. However, the dip directions of fluvial channel deposit interpreted from well 13 vary and indicate east, southeast and northwest (present day) dip directions, which could be due to the formative channel being sinuous and/or to in-channel secondary, or possibly reversing, flow.

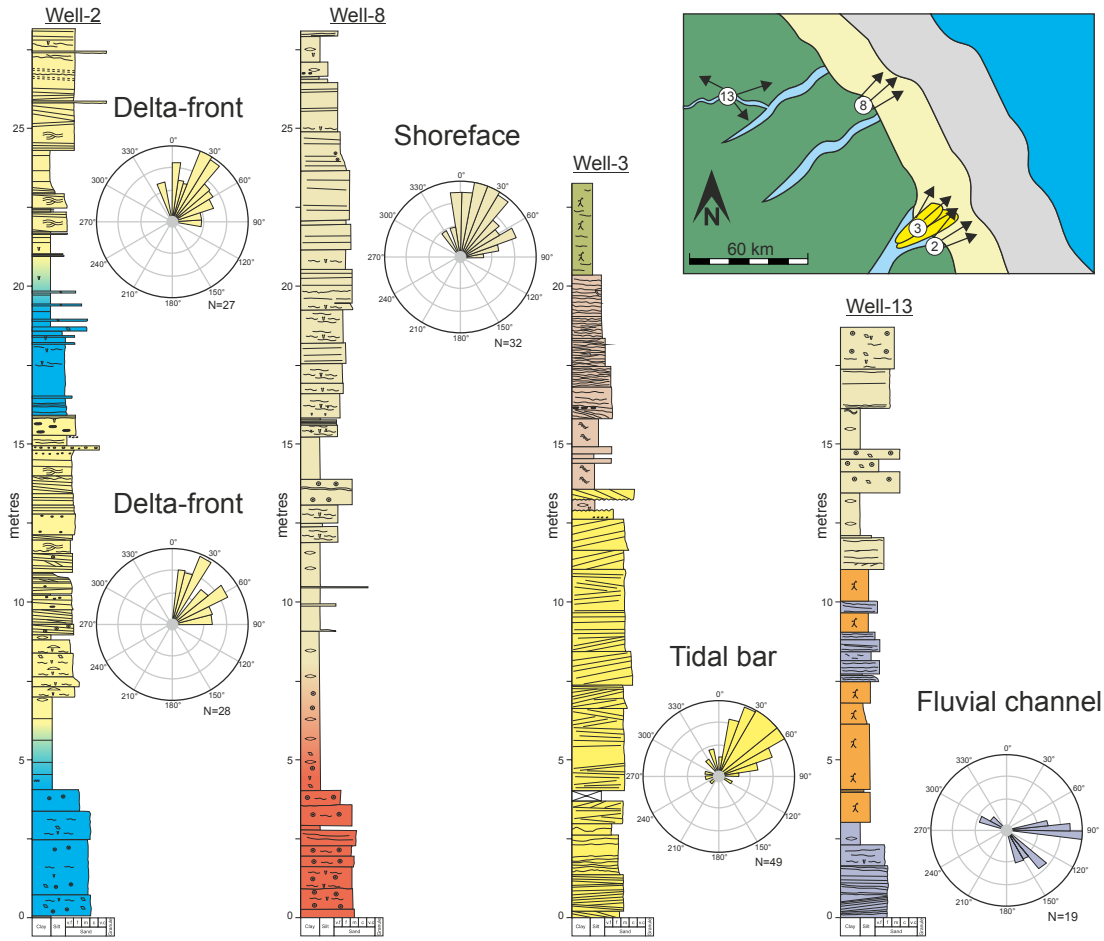

Figure 3.8: Rose diagrams showing the dominant dip direction of cross-stratification in different sandstone units, based on analysis of image logs. See Figure 4 for keys to facies associations and symbols.

3.4.10 Spatial distribution of facies associations

The studied cores are divided into two main facies belts: coastal-plain deposits comprising FA1, FA2 and FA3 facies associations and marine deposits including the FA4 and FA5 facies associations. To illustrate the spatial distribution of the facies, three correlation panels have been constructed across the area of interest (A-A', B-B', and C-C'), principally based on the available sedimentary logs and well-log gamma-ray signatures, but also supported by secondary analogue data from the SMAKS database; a data summary is provided in Figure 3.9. The non-cored intervals have been interpreted based on

their gamma-ray signatures, which typically yield information on the rock characteristics and enable lithological interpretations (Emery and Myers, 1996). The data obtained from SMAKS show thickness vs dip length relationship of numerous shoreface and shallow-marine sand belts, tidal bar and tidal flats. Thickness-dip length relationships of shallow-marine sand belts (Figure 3.9A) indicate a 10 m thick sandstone (analogous to the sandstone observed in FA4b) ranges in dip length from a few hundreds of metres to nearly 40 km. Limited data related to tidal flats and tidal bars were obtained, from which a trend does not emerge (Figure 3.9B). However, some instances of metre-thick tidal flats can be several hundreds of metres long in dip direction, and may reach up nearly 2 km. For example, one 7.5 m-thick tidal bar is 1.5 km in dip length. These data have been applied to help constrain expected sandbody architectures in the correlation panels of Figure 3.10.

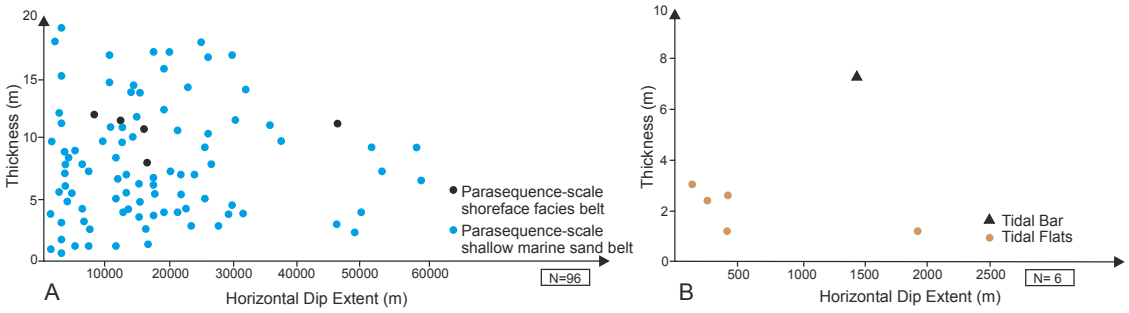

Figure 3.9: Cross plots showing thickness and lateral dip extent for analog sedimentary units that broadly match with the defined facies associations, as derived from a sedimentological database (Colombera et al., 2016a). A) Data relating to parasequence-scale sedimentary units representing the product of regression of shoreface and more generally shallow marine (i.e., encompassing sand-prone offshore transition) sand belts (Colombera et al., 2016a and b); Colombera & Mountney, 2020); B) Data relating to architectural elements classified as 'tidal bar' and 'tidal flat'

Sections A-A’ and B-B’ have been constructed in an orientation approximately parallel to the depositional strike of the system. These sections show an overall vertical transition from a coastal-plain succession at the base to a marine succession at the top. Section A-A’ (Figure 3.10) reveals a thicker succession of marine deposits overlying the coastal-plain deposits, compared to cross section B-B’ (Figure 3.11), which is itself interpreted to have occupied a position further landward (towards the west) by virtue of a thicker coastal-plain succession and thinner marine succession. Section C-C’ (Figure 3.12) has been constructed in an orientation approximately parallel to the depositional dip of the system (and intersecting panels A-A’ and B-B’). This section reveals a dominance of coastal-plain deposits in the southwest of the area and predominantly marine deposits in the northeast. This section demonstrates an overall deepening-upward trend. However, six smaller-scale transgressive-regressive packages superimposed upon the overall deepening trend are identified. These packages are most clearly developed in the middle of the section C-C’ (Figure 3.12).

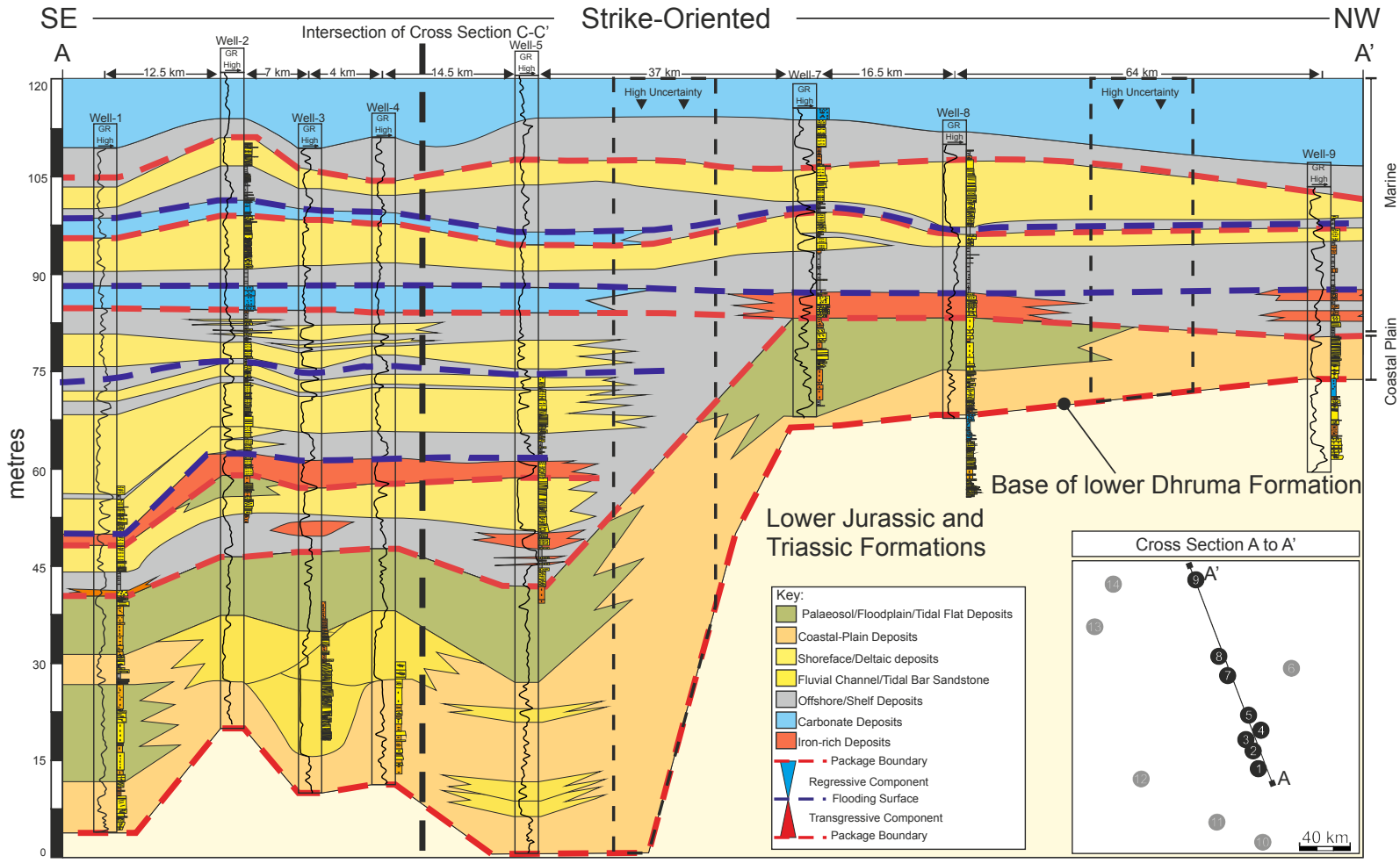

Figure 3.10: Strike-oriented stratigraphic cross-section (A-A') showing the distribution of facies associations and key stratigraphic surfaces as correlated along strike in a seaward position.

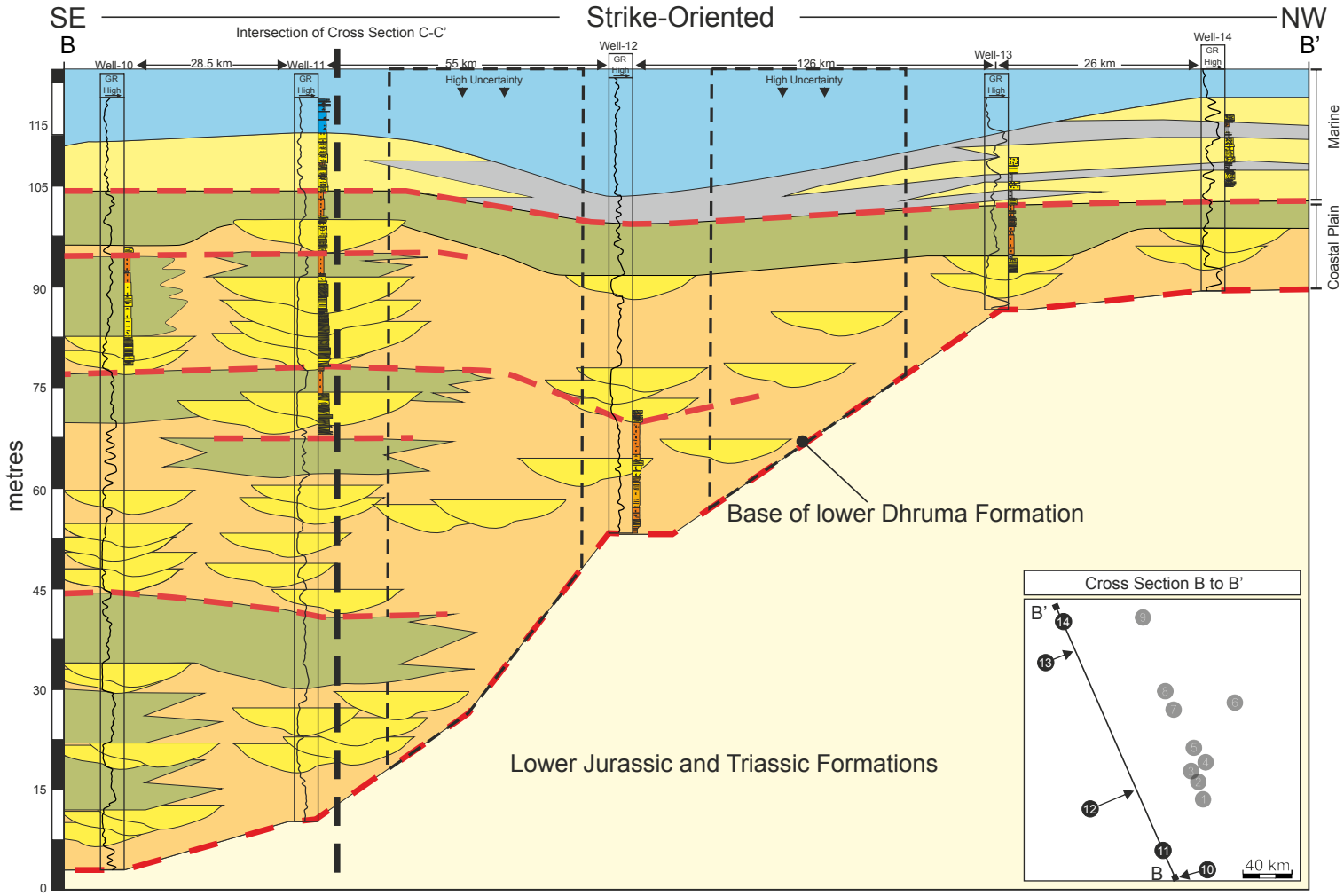

Figure 3.11: Strike-oriented stratigraphic cross-section (B-B') showing facies associations and stratigraphic surfaces as correlated along strike in a landward position compared to cross-section A-A'.

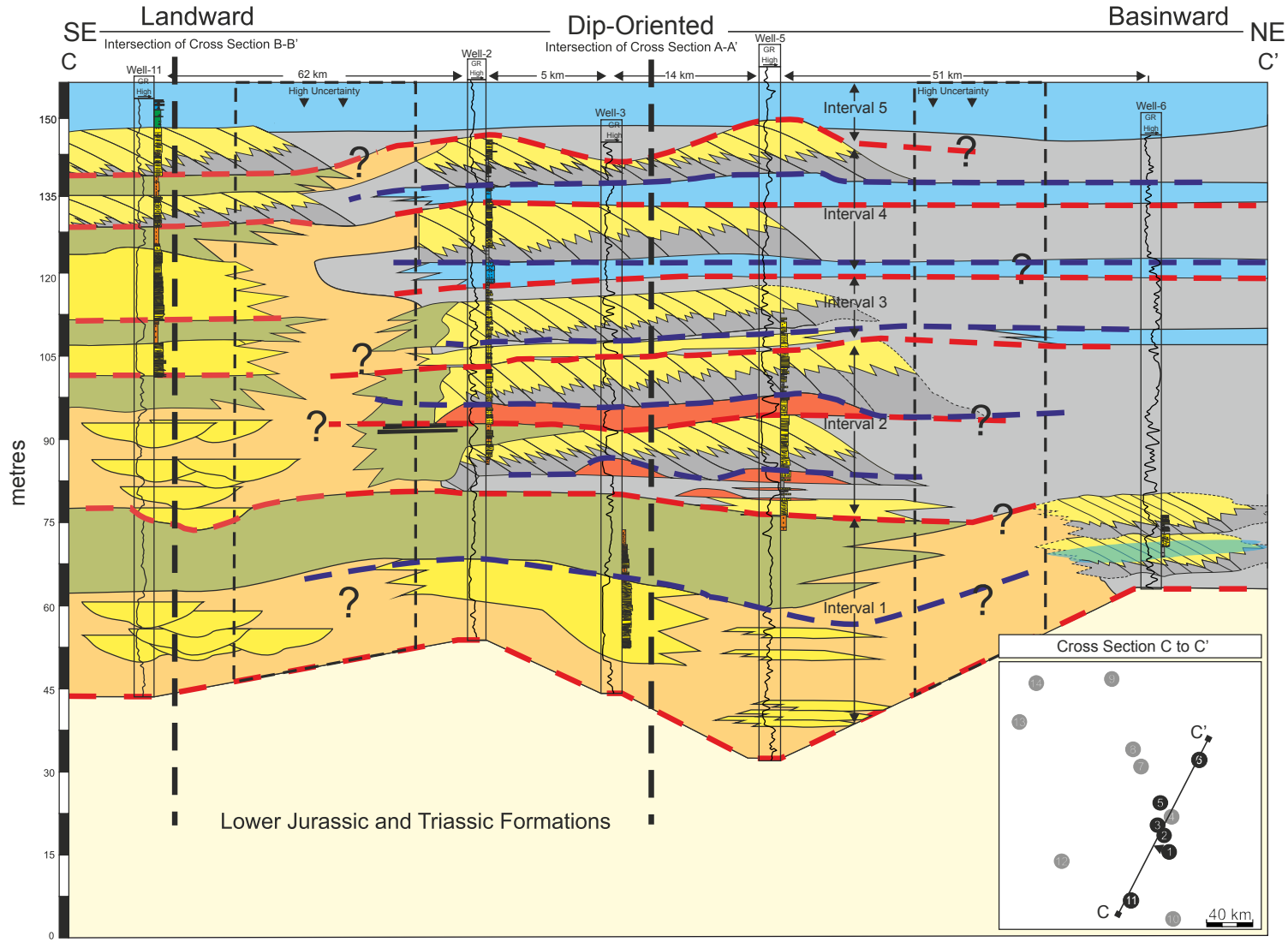

Figure 3.12: Dip-oriented stratigraphic cross-section (C-C') intersecting the two strike-oriented cross sections (A-A' and B-B') showing the distribution of facies associations and key stratigraphic surfaces as correlated along depositional dip, and documenting the increase in marine deposits towards the northeast (basinward).

3.5 Discussion

3.5.1 Controls on sedimentation in the lower Dhruma Formation

A depositional model depicting the evolution of the Middle Jurassic lower Dhruma Formation over five intervals is presented in Figure 3.13. Vertically, the study succession records an overall transition from coastal-plain deposits at the base to marine deposits at the top, as demonstrated in Figure 3.10 and 3.11. The overall stratigraphic architecture of the lower Dhruma Formation is interpreted to be controlled by relative sea-level fluctuations, as well as by fluvial, tidal and wave processes, as documented above.

The lower part of the section (interval 1) is dominated by fluvial and fluvial-tidal sedimentation, which resulted in the deposition of fluvial channel deposits (FA1), channel-associated tidal flats (FA2a) and fluvial-influenced tidal bars. The deposits of FA2 and FA3 possibly represent deposition within FMTZ in a mixed energy estuary. Extensive palaeosols (FA2b) are present across much of the study area which indicate a prolonged period of subaerial exposure. This is overlain by two transgressive-regressive packages (interval 2). The transgressive components in these packages comprise reworked iron-rich oolitic shoal sediments (FA5b). The ooidal ironstone in this example are commonly interpreted to form from reworking of iron-rich coastal plains during transgressive events as documented above (cf. Bayer et al. 1985; van Houten 1985). The regressive components are composed of progradational, weakly storm-affected offshore-transition and shoreface units (FA4a). Interval 3 incorporates a package that is similar to those defined in interval 2, but with the transgressive component displaying reduced iron content in wells 2 and 5; this indicates the presence of carbonate sediments accumulation towards the

northeast. Following the accumulation of interval 3, interval 4 is represented by two successive carbonate-mudstone-sandstone packages. The transgressive components of the two packages are represented by the fining-upwards limestone of FA5a. These are overlain by the regressive components represented by the prodelta and delta-front deposits of FA4b. These packages indicate two episodes of encroachment and retreat of carbonate-producing shelf areas. This is attributed to variations in the balance between the rate of relative sea-level change and the rate of supply of terrigenous sediment. Carbonate sedimentation developed most widely during episodes of limited siliciclastic influx or relative sea-level rise. By contrast, carbonate production was curtailed during episodes of increased rates of terrigenous sedimentation, or relative falls of sea level. The same factors acted to drive changes in shoreline position, which were paralleled by landward and basinward shifts in the foci of carbonate deposition (cf. Tirsgaard, 1996). Interval 5 incorporates the weakly storm influenced shoreface deposits of FA4a in a more proximal position, further southwest of the study area. These deposits are themselves overlain by carbonates that are apparently present across the entire study area.

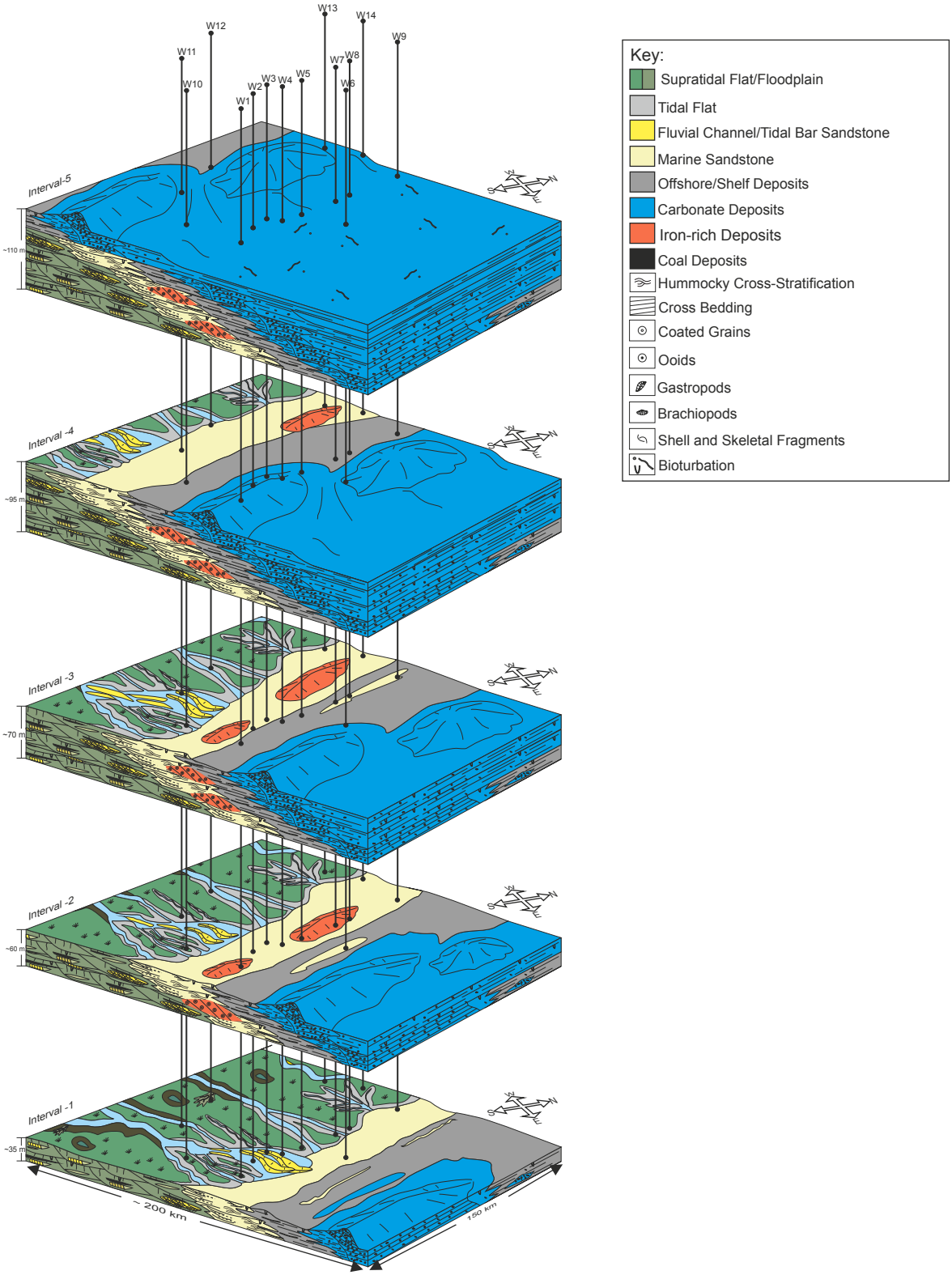

Figure 3.13: A depositional model depicting the evolution of the Middle Jurassic lower Dhruma Formation over five intervals. Each interval represents a synthesis

3.5.2 Climate and sediment source

The Arabian plate occupied a position near or at the equator during the Jurassic (Stampfli and Borel, 2002; Golonka, 2007; Seton et al., 2012; Stewart et al., 2016). Al-Aswad (1995) suggested that the climate of the Arabian plate during the Jurassic was humid to semi-humid. This has also been supported by the increased presence of small fern spores (Classopollis) along with an abundance of kaolinite within palaeosols (e.g. Al-Hussaini, 2019). In the studied area, the defined supratidal/floodplain deposits also show enrichment of kaolinite, which is indicative of intense chemical alteration under humid to semi-humid climate (Weaver, 1989; Robert and Chamley, 1991).

The source of the clastic sediments of the Middle Jurassic succession has been interpreted by a number of authors. The eastern Mediterranean back-arc rifting in the Early Jurassic caused uplifts to the residual highs of western and southern parts of the Arabian Plate (Beydoun, 1991; Ziegler, 2001). In the Middle Jurassic, the Hadramaut-Oman Arches were the only elevated hinterlands that could have perhaps acted as a source of sediments into various parts of the Arabian Peninsula, and which could have been drained by extensive channel networks (Al-Aswad, 1995). Al-Aswad (1995) suggests that southern central Arabia was traversed by alluvial tributaries draining the Hadramaut-Oman Arch, mainly from the south towards the north. The location of the study area and the broad north-eastern palaeoflow direction recorded in FMI image logs suggest that the siliciclastic sediments were likely sourced from the same southern Arabian hinterlands to the south and southwest.

3.6 Conclusions

A core-based sedimentological analysis of the Middle Jurassic lower Dhruma Formation in Saudi Arabia is presented. The study reveals that the lower Dhruma Formation was deposited in a varied range of fluvial to shallow-marine environments that interacted in a complex way over both space and time. Five lithofacies associations are identified based on the analysis of the core data; each is considered indicative of sedimentation within a particular palaeoenvironment. The facies associations represent different palaeoenvironments: fluvial channels, intertidal to pedogenically modified supratidal flats or floodplains, fluvial-influenced tidal bars, deltaic and shoreface to offshore transition, and an open-marine carbonate-dominated shelf. The deposits of the facies associations are interpreted to be controlled by the interaction of fluvial, tide and wave processes. At a larger scale, the pattern of sedimentation is controlled by the interplay of sea-level change and rate of sediment supply, causing zones of sedimentation to shift with changes in the position of the palaeoshoreline. The vertical successions of the lower Dhruma Formation record an overall transition from coastal-plain deposits at the base to marine deposits at the top. As such, the succession records a long-term transgressive, deepening-upward event. However, this overall deepening trend was punctuated by at least six progradational events whereby coastal deposits prograded basinward episodically.

4 Quantitative analysis of tidal bars in tide-dominated estuaries: modern systems and ancient preserved successions

4.1 Introduction

Tidal bars are notable features of tidal estuaries (e.g. Dalrymple and Rhodes, 1995; Fenies and Tastet, 1998; Dalrymple et al., 2003). They are also present in other tide-dominated or tide-influenced environments, such as deltas (e.g. Maguregui and Tyler, 1991; Willis et al., 1999; McCrimmon and Arnott, 2002; Willis and Gabel, 2003) and shelf environments (e.g. Houbolt, 1968; Berné et al., 2002). Estuarine tidal bars most commonly form in the middle and outer parts of an estuary where they are supplied principally by marine-derived sediments (Boyd et al., 1992; Dalrymple, 1992). However, in mixed-energy estuaries, tidal bars also commonly form in the inner parts where they are supplied chiefly by river-derived sediments and are subsequently reworked by tidal currents (Dalrymple et al., 1992). Tidal bars develop over a wide range of scales, from tens of metres to tens of kilometres in both width and length, and a few to several tens of metres in height (Tang et al., 2019).

Estuarine environments have considerable long-term sediment preservation potential due to the sheltering nature of their morphology (Meade 1972; Biggs and Howell, 1984; Demarest and Kraft, 1987). Furthermore, being systems that are most readily developed in transgressive settings, estuaries with tidal bars have significant potential for burial by subsequent highstand mud-prone deposits (e.g. shelf mudstone in Shanmugam et al. (2000) or prodelta mudstone in Chen et al. (2014)). Improving the understanding of their geometry,

sedimentary architecture and facies distribution is therefore important for both hydrocarbon exploration and development.

Characterising estuarine tidal-bar reservoirs is difficult from subsurface data alone (Wood, 2004), principally due to the one-dimensional nature of core and well-log data, which precludes direct determination of the 3D geometry of architectural elements. As such, applied geoscientists routinely utilise analogue studies from outcrops and modern environments to predict and assess the 3D dimensions and facies organisation of sedimentary bodies present in the subsurface. However, each sedimentary system possesses its own unique characteristics and the use of single analogues may be suitable only in highly specialised and limited cases (Howell et al., 2014). For this reason, this study utilises a database-driven approach to analyse many analogues; it combines cases from many different studies of ancient and modern analogues stored in a relational database, the Shallow-Marine Architecture Knowledge Store (SMAKS; Colombera et al., 2016).

The aim of this study is to quantitatively document and depict the nature of tidal bars in tidal-dominated estuaries from modern and ancient systems, and to discuss controls on their development and preservation. Specific objectives are as follows: i) to investigate the geometry and size of tidal bars known from modern systems and their deposits preserved in ancient outcropping successions; ii) to illustrate their sedimentological characters (internal facies organisation, external form and architectural geometry); iii) to investigate the nature of juxtaposition of tidal bars in association with other estuarine and shallow-marine elements; iv) to highlight tidal-bar development and preservation; and vi) to present implications of the results for reservoir prediction and characterisation.

4.2 Background

Estuaries are funnel-shaped bodies of water that have an inflow from a fluvial source at their upstream end and that are open to the sea at their downstream end. In some examples, estuaries are blocked from the seaward end by barrier systems (e.g. South Carolina Coastline). Estuaries are environments subject to dynamic water flow and sediment transport. A number of classifications have been proposed for estuaries over the last few decades, mostly based on the relative importance of tide, wave and fluvial processes (e.g. Fairbridge, 1980; Roy et al., 1980; Dalrymple, 1992). A widely used scheme that recognises tide- and wave-dominated estuaries is that proposed by Dalrymple (1992). Tide-dominated estuaries are those in which sedimentation is primarily controlled by tidal processes. In such environments, wave and river influences are subordinate, and are largely restricted to the outer and inner ends of estuaries. The hydrodynamics and sedimentology of tidal estuaries have been predominantly studied from the assessment of modern systems; examples include the Cobequid Bay-Salmon River Estuary in Eastern Canada (Dalrymple et al., 1990), the South Alligator Estuary in North Australia (Woodroffe et al., 1989), the Gironde Estuary in SW France (Allen, 1991; Fenies et al., 1999; Virolle et al., 2020), the Seine Estuary in NW France (Lesourd et al. 2003) and the Gulf of Khambhat in India (Saha et al., 2016 and Saha et al., 2018). Tidal estuaries from ancient successions are less well documented; however, valuable examples include the Quaternary Dong Nai River Succession in Vietnam (Kitzawa, 2007), the Eocene Aspelingtoppen Formation in Spitsbergen, Norway (Plink-Björklund, 2005), the Neogene Morne L'Enfer Formation in SW Trinidad (Chen et al., 2014).

Tidal bars develop mostly within distributary channels, in estuaries and along delta fronts (Dalrymple and Choi, 2007). An approach to recognise tidal bars in ancient sedimentary successions of estuarine origin was proposed by a study of coarsening-upward, sand-dominated successions in the Ager basin, NE Spain (Mutti et al., 1985). This approach to interpretation was adopted by many succeeding studies (e.g. Sullivan et al., 1997; Wood, 2004; Feldman and Demko, 2015). These Spanish successions were reinterpreted by Olariu et al. (2012) who argued that they most likely represent forward accreting tidal compound dunes (tidal sandwaves) and that the term tidal bars should be reserved for laterally migrating sandbodies. Among the main distinguishing features between tidal bars and tidal compound dunes is that dunes migrate forward relative to the dominant flow direction, whereas tidal bars migrate in a lateral or oblique fashion relative to the dominant flow current (Figure 4.1; Dalrymple et al., 2003; Dalrymple and Choi, 2007; Desjardins et al., 2012a; Olariu et al., 2012).

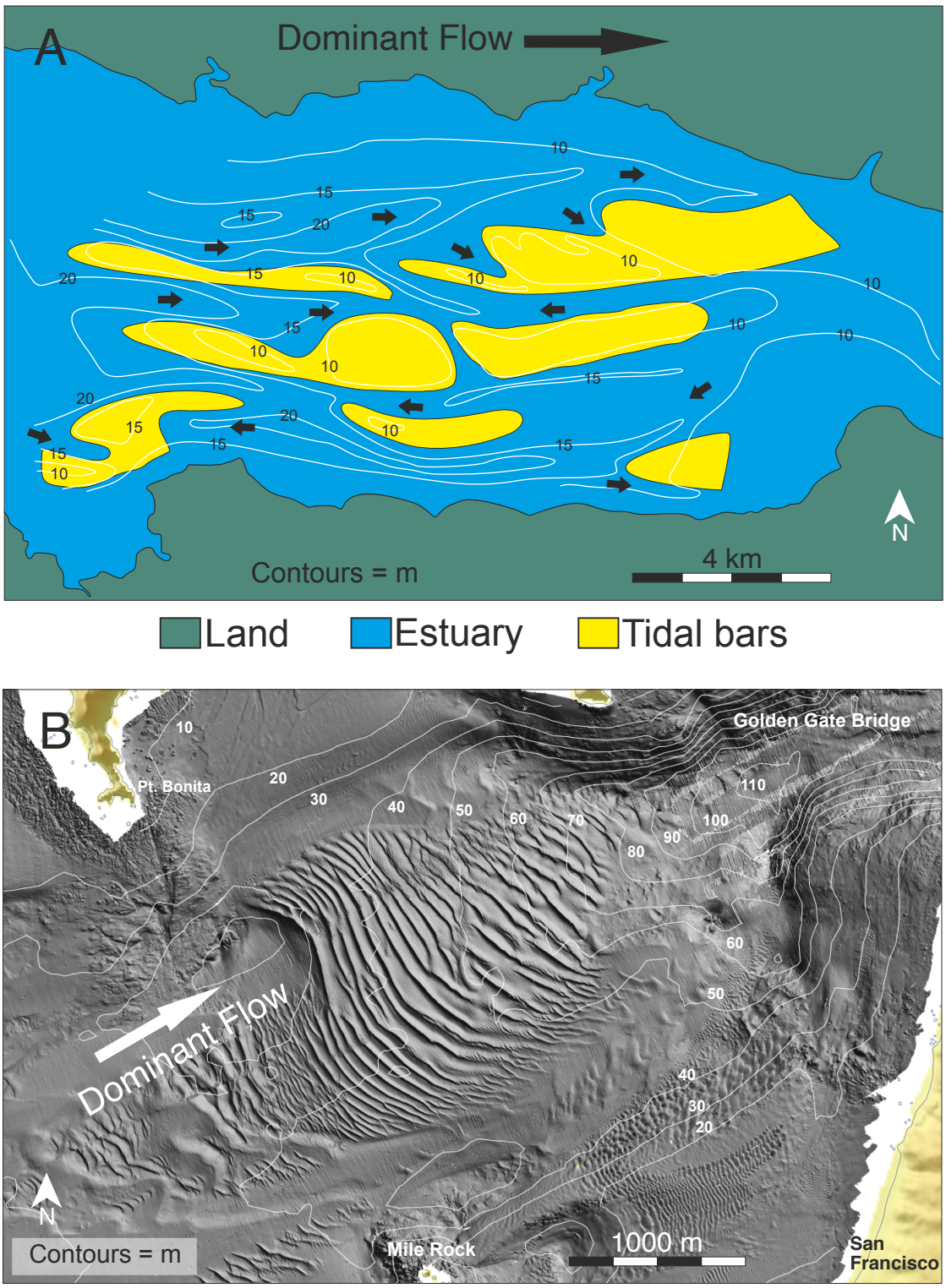

Figure 4.1: Organisation of tidal sand bars in Cobequid Bay, Bay of Fundy, adapted from Dalrymple and Rhod (1995) and B) Bathymetric map showing an oblique landward view of the arrangement of tidal dunes in San Francisco Bay (Barnard et al., 2006). Note the relationship between the dominant flow direction and the organisation of tidal bars and tidal dunes.

Tidal bars are typically associated with channels and migrate or expand laterally following the migration trajectory of the channel in which they are developed (Desjardins et al., 2012b). Laterally accreted tidal-bar deposits overlie an erosional surface created by the floor of the associated channel (Desjardins et al., 2012a; Yu et al., 2012). Their deposits exhibit fining- and thinning-upward trends (Figure 4.2A; Desjardins et al., 2012b; Olariu et al., 2012). However, they may coarsen upwards in some cases, notably where fluid mud occupies the base of the channel, a common feature of tidal estuaries (Dalrymple et al., 2003). By contrast, tidal compound dunes are characterised by coarsening upward trends (Figure 4.2B: Olariu et al., 2012).

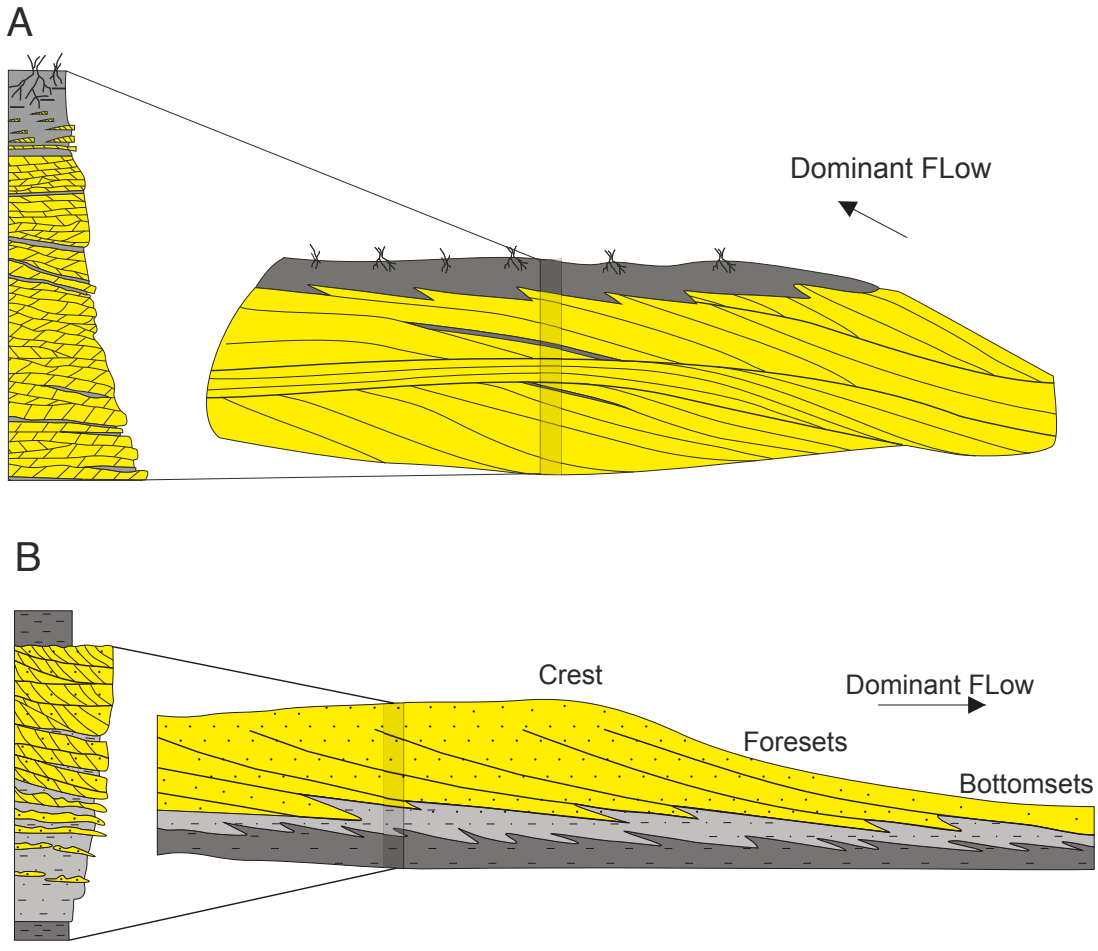

Figure 4.2: Comparison of the architecture and vertical succession of A) tidal bars, modified from Dalrymple (2010) and B) tidal dunes, modfied from Mutti et al. (1985).

Estuaries are subject to fluctuations in salinity as they receive river freshwater from their upstream end and marine saline water from their downstream end. This can greatly influence the presence of ichnofauna in their deposits. Estuarine tidal bars typically contain a low diversity of ichnofossils and may exhibit generalist forms such as *Teichichnus*, *Planolites* and *Ophiomorpha* (MacEachern and Pemberton, 1994; MacEachern and Gingras, 2007; Gingras et al. 2012).

4.3 Data and Methods

4.3.1 Overview

This work employs a quantitative approach based on a synthesis of sedimentological data from many published studies. Collected data are included in a relational database, the Shallow-Marine Architecture Knowledge Store (SMAKS), and standardised accordingly (Appendix II, Colombera et al., 2016). SMAKS stores data related to sedimentary architecture, geomorphic organisation and facies units of shallow-marine and paralic depositional systems. The SMAKS database includes quantitative and qualitative data extracted from published sources related to geological entities of different types and scales (e.g. facies units, architectural elements, geomorphic elements, sequence stratigraphic units), each of which is classified based on multiple parameters (e.g. thickness, strike and dip dimensions) and metadata (data type, data source, geographic location). As of January 2021, SMAKS contains data on 227 case studies, extracted from 370 literature sources or derived from 4 unpublished investigations; SMAKS includes data on >5,000 architectural elements, >2,000 geomorphic elements, >2,000 sequence-stratigraphic units and >38,000 facies

units. As part of this Thesis, 15 analogue case studies have been coded for database input and loaded on SMAKS.

The data used in this study are related to tidal bars in estuaries that are dominated or influenced by tidal processes. The collected data have been classified into two broad divisions: geomorphic and architectural datasets. The geomorphic dataset includes data on the geometry of 213 tidal bars in 51 estuaries around the world (this includes pre-exisitng data from 187 tidal bars stored in SMAKS and newly collected data from 26 tidal bars and are added to the SMAKS database). The shapes of tidal bars are classified according to categories proposed by Dalrymple and Choi (2007) and Leuven et al. (2016): elongate, lobate, sidebars and complex bars (Figure 4.3).

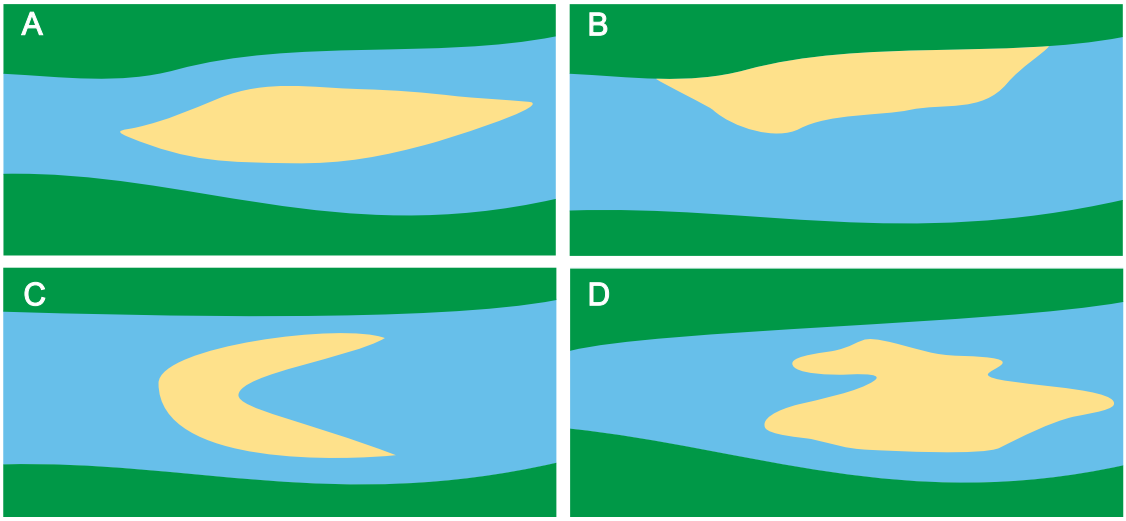

Figure 4.3: Representative sketch of tidal bar types defined in Dalrymple and Choi, (2007) and Luven et al. (2016). A) elongate, B) sidebar, C) lobate and D) complex bars. Modified after Luven et al. (2016).

The architectural datasets comprise 13 case studies of modern and ancient estuarine tidal bar systems and preserved successions, relating to 53 tidal bar elements (these are all newly collected for the purpose of this research and are added to the SMAKS database). Architectural elements that are termed ‘tidal bars’ in this work are flow-parallel or oblique elongate bars that typically migrate through lateral accretion (*sensu* Olariu et al., 2012). The focus of this research

is specifically on tidal bars that form in tidal-dominated estuaries, and excludes bars that form on shelves in open-marine environments. The locations of both geomorphic and architectural datasets are presented in Figure 4.4 and summarised in Table 4.1 (Geomorphic data) and Table 4.2 (Architectural data).

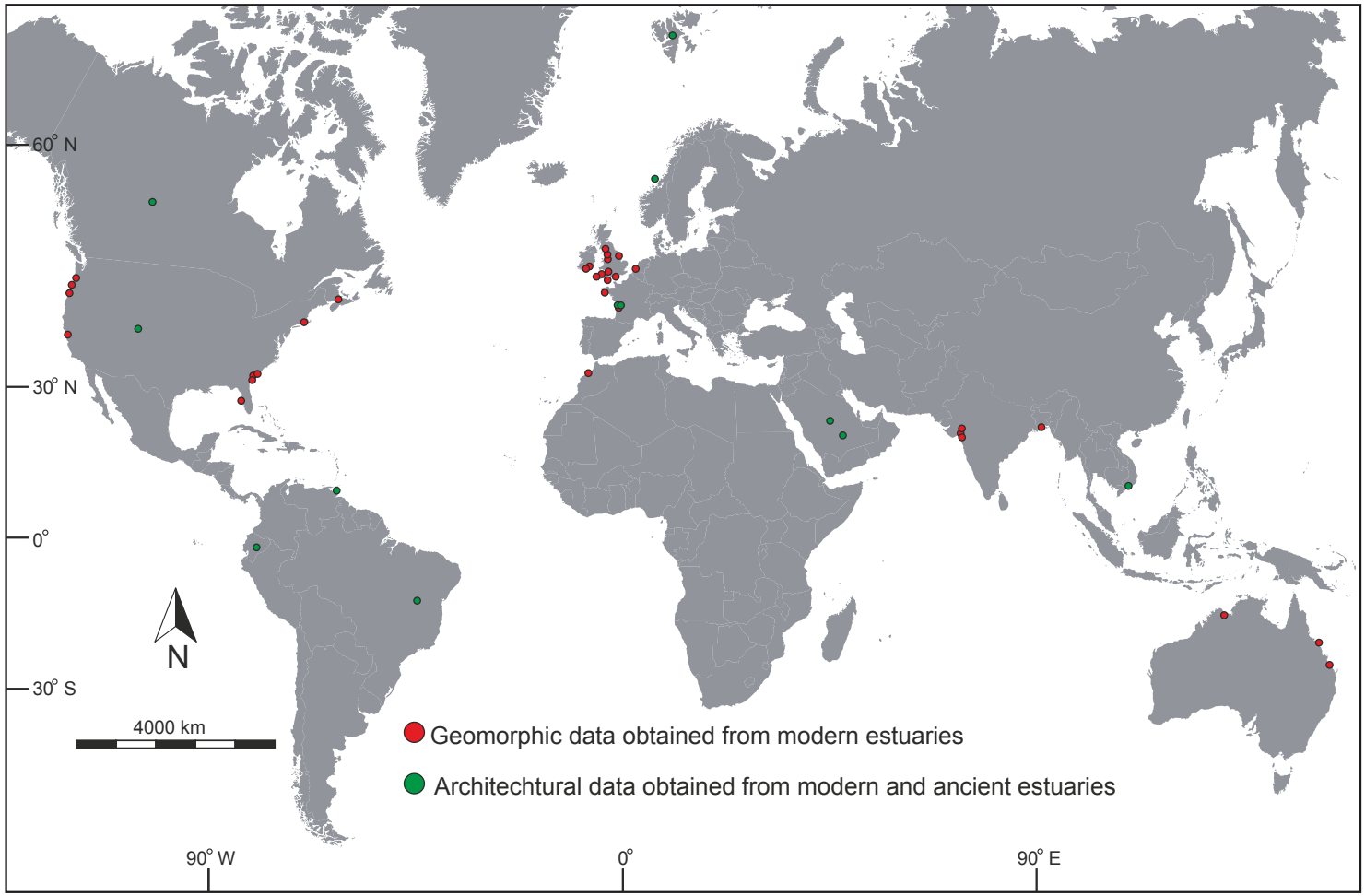

Figure 4.4: Geographic location of estuaries considered in this study. Red circles represent locations of geomorphic data and green circles represent locations of architectural data from both modern and ancient estuaries.

Estuary	Source	Location	N
Alsea Bay	Database of Leuven et al (2016)	Oregon, USA	2
Ambika Estuary	Own Study	Gulf of Khambat, India	3
Unknown estuary	Database of Leuven et al (2016)	Queensland, Australia	3
Bannow Bay	Database of Leuven et al (2016)	Wexford, Ireland	3
Broad River estuary	Database of Leuven et al (2016)	South Carolina, USA	5
Camel estuary	Database of Leuven et al (2016)	Cornwall (North coast), UK	10
Charlotte Harbor Estuary	Database of Leuven et al (2016)	Florida, USA	4
Clwyd estuary	Database of Leuven et al (2016)	North Wales, UK	5
Cobequid Bay (Bay of Fundy)	Database of Leuven et al (2016)	Nova Scotia, Canada	6
Columbia River	Database of Leuven et al (2016)	Oregon, USA	8
Conwy estuary	Database of Leuven et al (2016)	North Wales, UK	8
Coosaw River estuary	Database of Leuven et al (2016)	South Carolina, USA	6
Courtsmacsherry	Database of Leuven et al (2016)	Cork, Ireland	1
Dart estuary	Database of Leuven et al (2016)	South Devon, UK	3
Dovey estuary	Database of Leuven et al (2016)	West Wales, UK	10
Exe estuary	Database of Leuven et al (2016)	South Devon, UK	5
Gannel estuary	Database of Leuven et al (2016)	North Cornwall, UK	2
Gironde	Own Study	SW France	3
Glaslyn estuary	Database of Leuven et al (2016)	NW Wales, UK	5
Gulf of Khambhat Bay	Own Study	Gulf of Khambat, India	5
Humber	Database of Leuven et al (2016)	Yorkshire, UK	3
Jabusar Estuary	Own Study	Gulf of Khambat, India	1
La Laïta	Database of Leuven et al (2016)	West France	1
Loughor estuary	Database of Leuven et al (2016)	SW Wales, UK	10
Mahi Estuary	Own Study	Gulf of Khambat, India	1
Mawddach estuary	Database of Leuven et al (2016)	West Wales, UK	3
Meghna delta estuary	Database of Leuven et al (2016)	Bengal Bay, Bangladesh	4
Merja Zerga	Database of Leuven et al (2016)	North Morocco	2
Mersey estuary	Database of Leuven et al (2016)	Cheshire, UK	7
Narmada Estuary	Own Study	Gulf of Khambat, India	10
Nestucca Bay	Database of Leuven et al (2016)	Oregon, USA	2
Netarts Bay	Database of Leuven et al (2016)	Oregon, USA	4
Nyfer estuary	Database of Leuven et al (2016)	West Wales, UK	1
Ord River estuary	Database of Leuven et al (2016)	Australia	6
Parrett estuary	Database of Leuven et al (2016)	Somerset, UK	4
Poole estuary	Database of Leuven et al (2016)	Dorset, UK	2
Purna Estuary	Own Study	Gulf of Khambat, India	2
San Joachim Bay	Database of Leuven et al (2016)	California, USA	3
Sandy Neck Colony	Database of Leuven et al (2016)	Massachusetts, USA	1
Savannah River	Database of Leuven et al (2016)	Georgia, USA	1
Siuslaw River	Database of Leuven et al (2016)	Oregon, USA	1
Solway estuary	Database of Leuven et al (2016)	Cumbria, UK	13
Tapti Estuary	Own Study	Gulf of Khambat, India	1
Taw-Torridge estuary	Database of Leuven et al (2016)	North Devon, UK	6
Teifi estuary	Database of Leuven et al (2016)	West Wales, UK	2
Teign estuary	Database of Leuven et al (2016)	Devon (South coast), UK	2
The Retreat	Database of Leuven et al (2016)	Cork, Ireland	3
Traeth Melynog estuary	Database of Leuven et al (2016)	NW Wales, UK	5
Westerschelde	Database of Leuven et al (2016)	Netherlands	9
Whitehaven beach	Database of Leuven et al (2016)	Queensland, Australia	6

Table 4.1: Showing the geographic location of modern estuaries from which tidal bras were examined. 'N' denotes the number of tidal bars.

Succession	Data Source	Data Type	N	Age
Richard Tidal Bar, Gironde Estuary, SW France	Virolle et al. (2020)	Maps, Cores, Cross sections	1	Holocene
Plassac Tidal Bar, Gironde Estuary, SW France	Chaumillon et al. (2013), Virollea et al. (2020)	Maps, Cores, Cross sections	1	Holocene
Troumloupe Tidal Bar, Gironde Estuary, SW France	Fenies and Tastet (1999)	Maps, Cores, Cross sections	1	Holocene
Aspelintoppen Formation, Spitsbergen, Norway	Piret Plink-Bjorklund (2005)	Outcrop	7	Eocene
Ba Mieu Formation, Dong Nai River, Vietnam	Kitazawa (2007)	Outcrop	3	Pleistocene
Thu Duc Formation, Dong Nai River, Vietnam	Kitazawa (2007)	Outcrop	5	Pleistocene
Lower Tombador Formation, East of Brazil	Magalhaes et al. (2014)	Outcrop	9	Precambrian
Morne l'Enfer Formation, SW Trinidad	Chen et al. (2014)	Cores	6	Pliocene
McMurray Formation, Alberta, Canada	Tang et al. (2019)	Cores	7	Lower Cretaceous
Hollin and Napo Formations, Oriente Basin, Ecuador	Shanmugam et al. (2000)	Cores	4	Lower and Upper Cretaceous
Tilje Formation, Halten Terrace, Norway	Martinius et al. (2001)	Cores	4	Lower Jurassic
Lower Dhruma Formation, Southeast Saudi Arabia	Alshammari et al. (2020)	Cores	4	Middle Jurassic
Anchor Mine–Upper Sego–Neslen Formations, Book Cliff Utah, USA	Olariu et al. (2015)	Outcrop	1	Upper Cretaceous

Table 4.2: Shows the name of the formation, the geographic location, age, data type and sources of the case studies considered in this study from the architectural point of view. 'N' denotes the number of tidal bars.

4.3.2 Data Collection and Data Types

Data on the morphology of modern estuarine tidal bars included in SMAKS comprise of (i) literature-derived data on 187 tidal bars, and (ii) newly collected data (from analysis of bars evident on satellite imagery) on 26 tidal bars seen in the Gulf of Khambhat estuaries in India and in the Gironde estuary in France. The planform geometry of these bars was digitised using Google Earth satellite images (accessed between March and May 2020). The geometric measurements were taken from the apparent planforms seen on Google Earth images; however, these bars are partly submerged and may be larger in width and length than those reported in this study, especially in cases where suspended sediment load arising from the turbidity maximum in estuaries precludes observation through the water column. Examples of tidal bars examined from modern estuaries are presented in Figure 4.5. The attributes of modern tidal bars that have been characterised include the local width of the

estuaries in which they sit (treated as elements of a higher order in the database hierarchy), the type of estuary, their maximum dip length (length hereafter) and width, and the types of neighbouring elements (treated as elements to which tidal bars transition laterally).

Figure 4.5: Satellite images showing examples of modern estuarine tidal bars. Locations are indicated at the top left corner of each example. Images are courtesy of Google Earth.

Data relating to the sedimentary architecture of tidal-bar elements were all newly collected from published studies, and were derived from texts, tables and/or measured from figures. The attributes of tidal bars that were characterised include their thickness, width, dip-length (length hereafter) and the transition of tidal bars to the other estuarine associated elements (treated as elements to which tidal-bar elements transition in three dimensions). Data concerning the sedimentology of tidal bars were also collected; data types

include grain size, rock type, sedimentary structures, thickness, vertical profile and the arrangement of sedimentary facies within each tidal bar. The containment of tidal bars within sequence stratigraphic systems tracts were also recorded.

Data extracted in this study include units (e.g. facies, architectural elements, geomorphic elements) whose dimensional data reflect true (maximum diemnsion), apparent or partial observations. These have been all included in the analysis with no discrimination of their type, principally because no differences were seen across these types.

4.3.3 Statistical Analysis

Statistical analyses of the datasets were completed using Microsoft Excel 2016 and Minitab 18. The analyses have been undertaken to (i) establish relationships between variables, determining the type and magnitude of the relationships based on Pearson (Rp) and Spearman (Rs) correlation coefficients, and to (ii) test hypotheses concerning differences in means or distributions across sets of variables.

Analyses of statistical significance of differences in means across sets of variables have been performed based on a two-sample t-test when comparing two sets of variables and based on one-way analysis of variance (ANOVA) when comparing three or more sets of variables. Normality of data distribution across sets of variables has been examined prior to computing these tests (by Anderson-Darling normality test) and variables have been transformed by Johnson transformation in the case of non-normal distributions. The statistical significance of differences across groups, expressed as P-values (P), are determined by resulting test statistics of t-tests (t), ANOVA (F) and the number

of degrees of freedom (df). The statistical significance is therefore compared with significance levels (α) that equal 0.05 to determine whether the null hypothesis is rejected.

4.4 Results

4.4.1 Geomorphic Dataset from Modern Estuaries

This section presents relationships between tidal-bar dimensions, variations in dimensions of tidal bars of different types, and a comparison between types of estuaries and their tidal bars, based on data on geomorphic elements.

4.4.1.1 Tidal Bar Dimensions

Tidal bars accumulated in estuaries show a wide range of width and length measurements that range from tens of metres to tens of kilometres. They are generally larger in length than width. Size measurements are as follows: width (minimum = 20 m, maximum = 11,490 m, average = 735 m), length (minimum = 60 m, maximum = 29,790 m, average = 2,929). Furthermore, heights of estuarine tidal bars range between 3 m to 20 m with the average being 10.4 m. Tidal bars overall display strong to moderate positive relationship between their dimensions, and these are statistically significant. Relationships are as follows: width and length relationship R = 0.82 and P = 0.000; length and height R = 0.74 and P = 0.000; and width and height R= 0.61 and P = 0.000. Plots of these relationships are presented in Figure 4.6.

Lengths, widths and heights of tidal bars of different types are investigated. No statistically significant difference is seen in the means of bar lengths and heights, across the four groups of bar types, based on one-way analysis of

variance (ANOVA) (length P = 0.214, F (3,163) = 1.51 and depth P = 0.948, F (3,40) = 0.12, (Figure 4.7A and C). However, mean values of width differ significantly across the different types of bars (P = 0.019, F (3,163) = 3.40) (Figure 4.7B).

Relationships between domensions of tidal bars of different types are also investigated. All tidal bar types show strong to moderate positive relationships between their dimensions and are all statistically significant. Results are summarised in Figure 4.8 and Table 4.3.

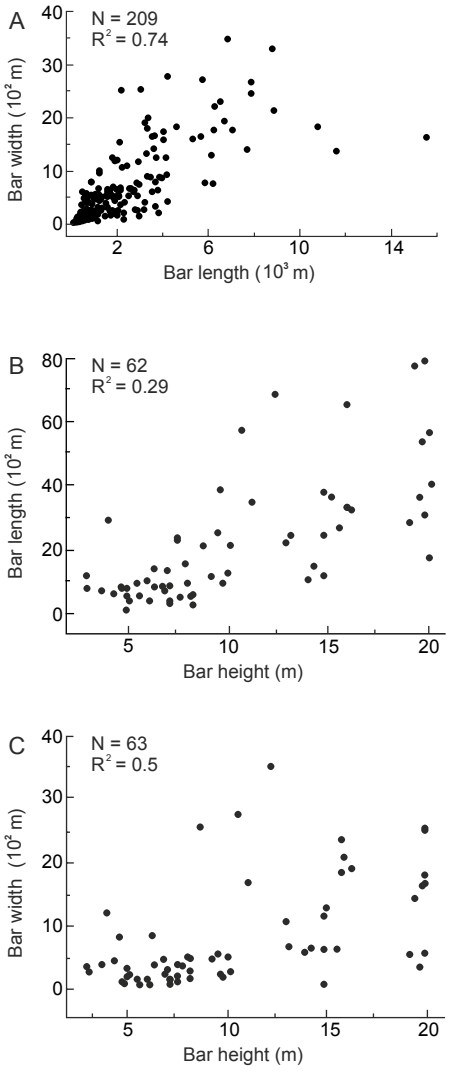

Figure 4.6: Cross plots showing the relationships of tidal bar dimensions, A) width-length, B) length-height and C) width-height relationships.

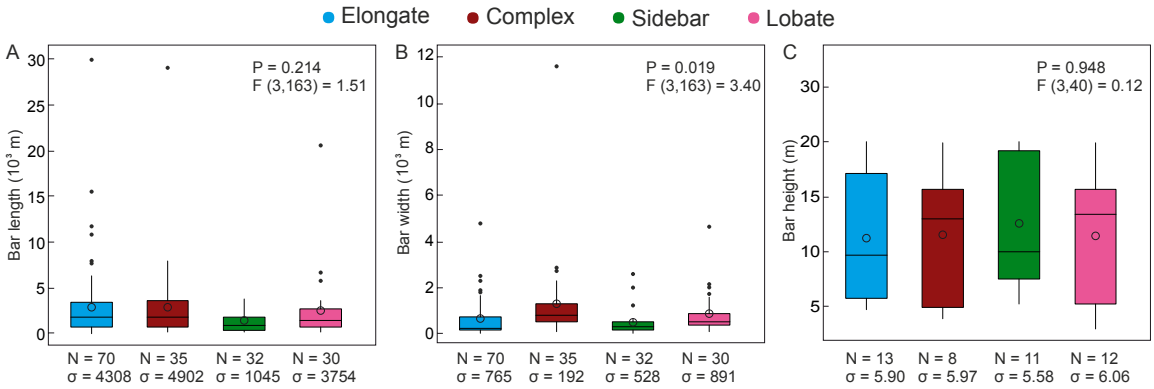

Figure 4.7: Box-plots show ranges of readings relating to A) lengths, B) widths and C) heights of tidal bars of different types (Elongate, Complex, Sidebar and Lobate). For each box-plot, boxes represent interquartile ranges, open circles represent mean values, horizontal bars within the boxes represent median values, and black dots represent outliers (values that are more than 1.5 times the interquartile range). 'N' denotes the number of readings. 'σ' denotes the standard deviation. 'F' denotes the one-way analysis of variance (Anova). 'P' denotes P-value.

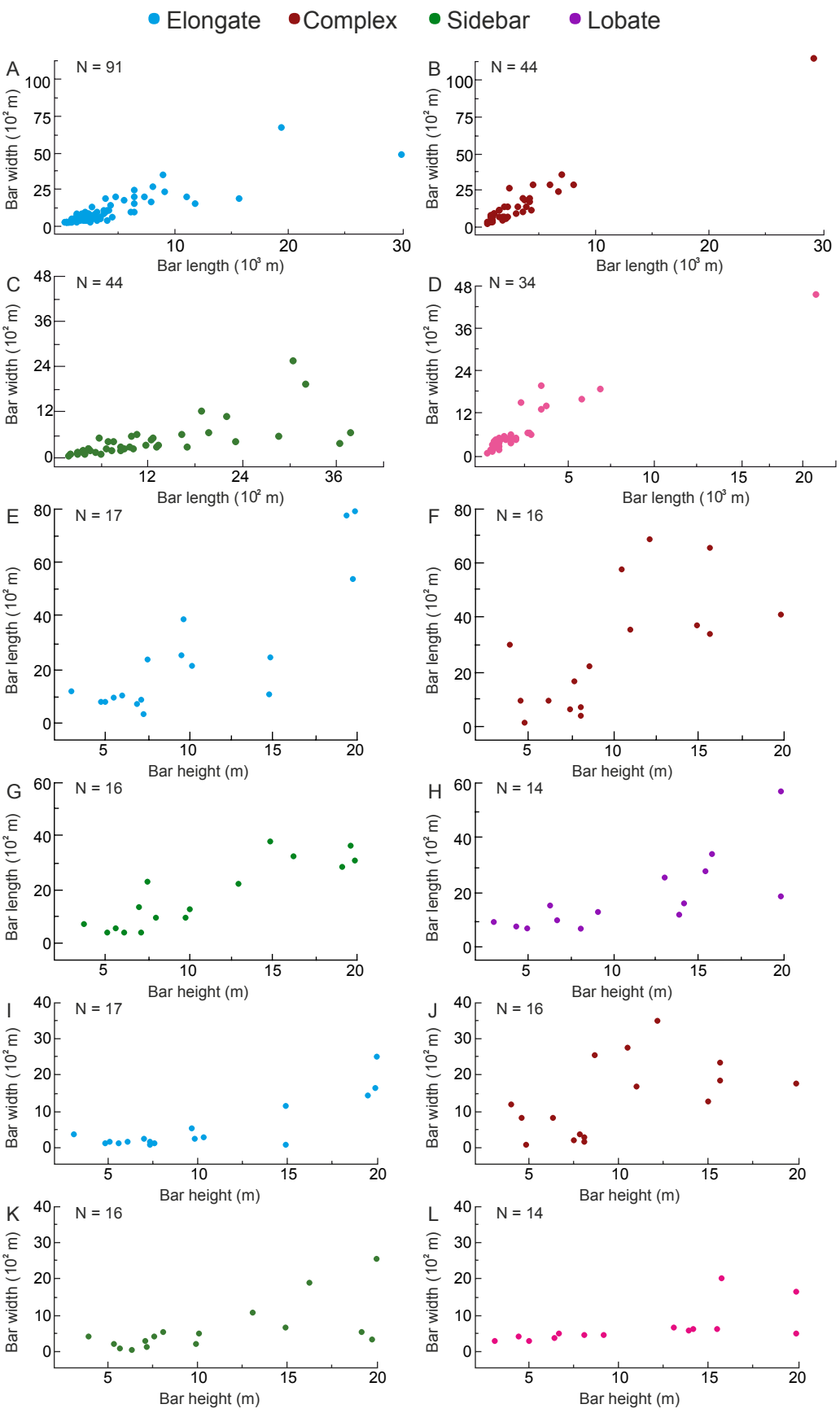

Figure 4.8: Cross plots showing the relationships of tidal bar dimensions, A-D) width-length, E-H) length-height and I-L) width-height relationships.

	Length and Width	Length and Height	Width and Height
All bar types	N = 213 Rp = 0.86, P < 0.001 Rs = 0.82, P < 0.001	N = 63 Rp = 0.70, P < 0.001 Rs = 0.74, P < 0.001	N = 63 Rp = 0.55, P < 0.001 Rs = 0.61, P < 0.001
Linear	N = 91 Rp = 0.87, P < 0.001 Rs = 0.89, P < 0.001	N = 17 Rp = 0.84, P < 0.001 Rs = 0.77, P < 0.001	N = 17 Rp = 0.84, P < 0.001 Rs = 0.53, P = 0.028
Complex	N = 44 Rp = 0.97, P < 0.001 Rs = 0.89, P < 0.001	N = 16 Rp = 0.65, P = 0.006 Rs = 0.72, P = 0.002	N = 16 Rp = 0.52, P = 0.038 Rs = 0.64, P = 0.008
Sidebar	N = 44 Rp = 0.66, P < 0.001 Rs = 0.85, P < 0.001	N = 16 Rp = 0.88, P < 0.001 Rs = 0.72, P = 0.002	N = 16 Rp = 0.63, P = 0.008 Rs = 0.70, P = 0.003
Lobate	N = 34 Rp = 0.95, P < 0.001 Rs = 0.89, P < 0.001	N = 14 Rp = 0.75, P < 0.001 Rs = 0.81, P = 0.002	N = 14 Rp = 0.62, P = 0.018 Rs = 0.86, P < 0.001

Table 4.3: Relationships between tidal-bar dimensions based on Pearson (Rp) and Spearman (Rs) correlation coefficients.'N' denotes the number of tidal bars. 'P' denotes the statistical significance (P-value).

4.4.1.2 Tidal Bars Size vs Estuary Size

Relationships of estuaries and tidal bars contained within them are investigated. Results show that there is a strong positive relationship between estuary depth and mean bar height, which is statically significant (Rp = 0.85, P = 0.000 and Rs = 0.85, P = 0.000) (Figure 4.9A). Estuary width and mean bars width show a moderate to strong positive relationship, which is also statistically significant (Rp = 0.48, P = 0.004 and Rs = 0.70, P = 0.000 (Figure 4.9B).

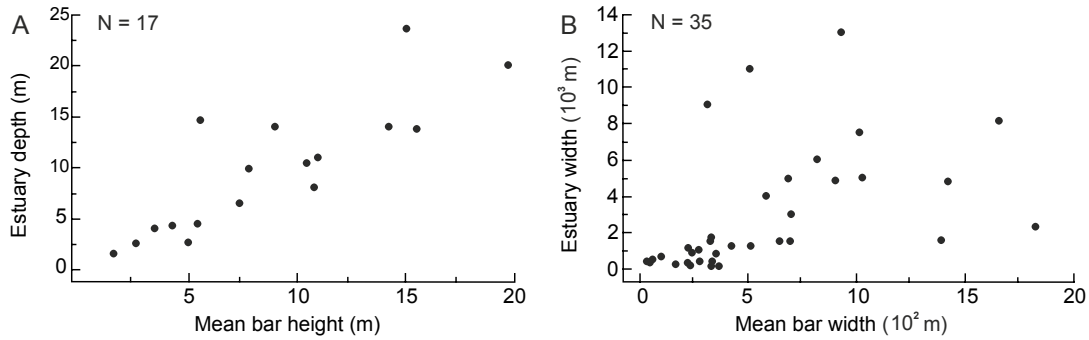

Figure 4.9: Cross plots showing the relationships between size of estuaries and tidal bars. A) relationship of mean estuary depth and mean bar height and B) relationship of mean estuary width and mean bar width. 'N' denotes the number of readings.

Estuaries differ morphologically and are classified into a number of different types, two of which are considered in detail in this chapter: bar-built and coastal-plain estuaries. Bar-built estuaries are semi-enclosed or have bars built at their mouths and coastal-plain estuaries occupy drowned river valleys (Figure 4.10; Pritchard, 1967; Davidson et al., 1991).

Figure 4.10: Examples of estuary types compared in this study, A) bar-built estuaries (Columbia River, Oregon, USA) and B) coastal-plain (Themes River, UK).

The size of bar-built and coastal-plain estuaries and the size of tidal bars contained within them are investigated. Coastal-plain estuaries are larger in size than the bar-built estuaries, and they show a wider range of width and depth measurements. Coastal-plain estuaries are 2.7 times deeper and 2.6 times wider on average than bar-built ones. Coastal-plain estuaries (N = 11) range in width between 200 m and 11,000 m, with the average being 4,347 m; the depth values (N = 8) range from 0.9 m to 23.6 m, with the average being 13.2 m (Figure 4.11A and B). In contrast, bar-built estuaries have a smaller range in width (N = 19), between 100 and 6,000 m, with an average of 1,678 m. Their depth (N = 10) ranges from 1.5 m to 10.9 m with an average of 6.5 m (Figure

4.11A and B). The differences in mean values of width and depth across these two types of estuaries are statistically significant based on two-sample t-test (width: t = -3.44, P = 0.002, df = 28; depth: t = -2.53, P = 0.022, df = 16) (Figure 4.11A and B).

Tidal bars accumulated in coastal-plain and bar-built estuaries are seen to scale well with their respective estuaries. Tidal bars in coastal-plain estuaries are 2.5 times higher, 2 times wider and 2.5 times longer on average than those in bar-built estuaries. The differences in mean values of tidal-bar dimensions in the two different types of estuaries are statistically significant based on two-sample t-test (length t = -3.81, P = 0.000, df = 165; width t = -3.08, P = 0.002, df = 165; height t = -9.16, P = 0.000, df = 42) (Figure 4.11C, D and E).

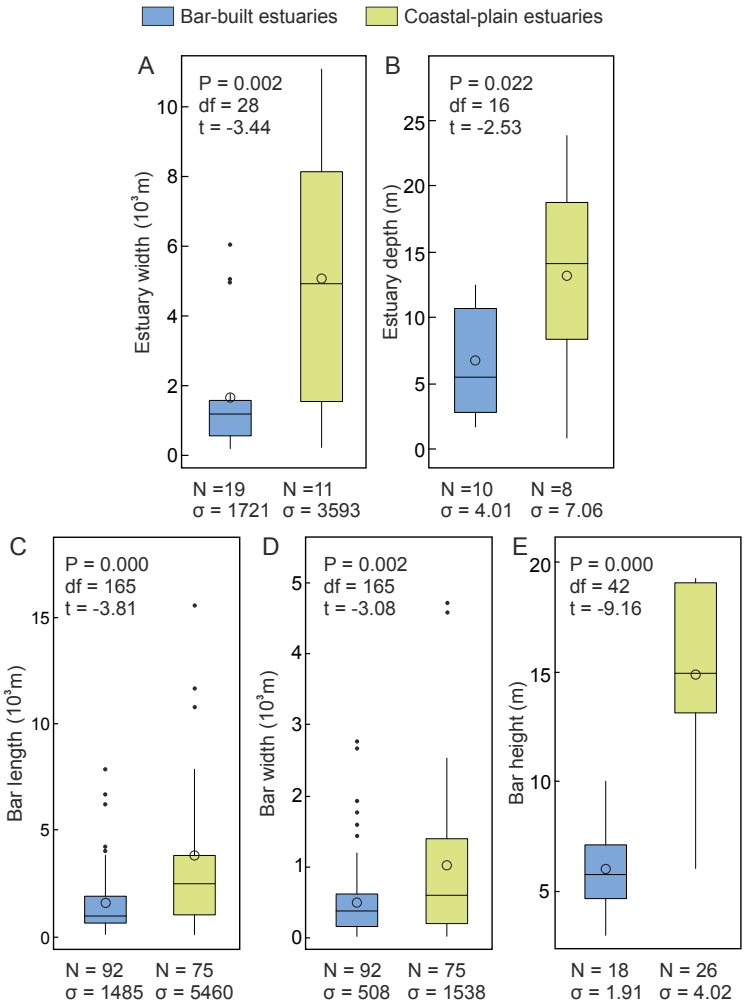

Figure 4.11: Box-plots show ranges of size readings relating to A) estuary width, B) estuary depth, C) bar length, D) bar width and E) bar heights across bar-built and coastal-plain estuaries. For each box-plot, boxes represent interquartile ranges, open circles represent mean values, horizontal bars within the boxes represent median values, and black dots represent outliers (values that are more than 1.5 times the interquartile range). 'N' denotes the number of readings. 'σ' denotes the standard deviation. 't' denotes the two-sample t-test. 'df' degrees of freedom. 'P' denotes P-value.

4.4.2 Architectural Dataset from Modern and Ancient Estuaries

This section presents results of analyses relating to the size and the internal architecture of tidal-bar architectural elements from ancient and modern examples.

4.4.2.1 Tidal Bar Size

Relationships between the width and length of tidal-bar architectural elements cannot be established in this study because of data paucity. However, the thickness of tidal bars (N = 53) ranges from 0.2 m to 28.8 m with the average of 6.6 m and median of 5 m (Figure 4.12). Differences of means in thicknesses of tidal bars in each case study are statistically significant based on ANOVA ($F(13, 39) = 2.32$, $P = 0.022$).

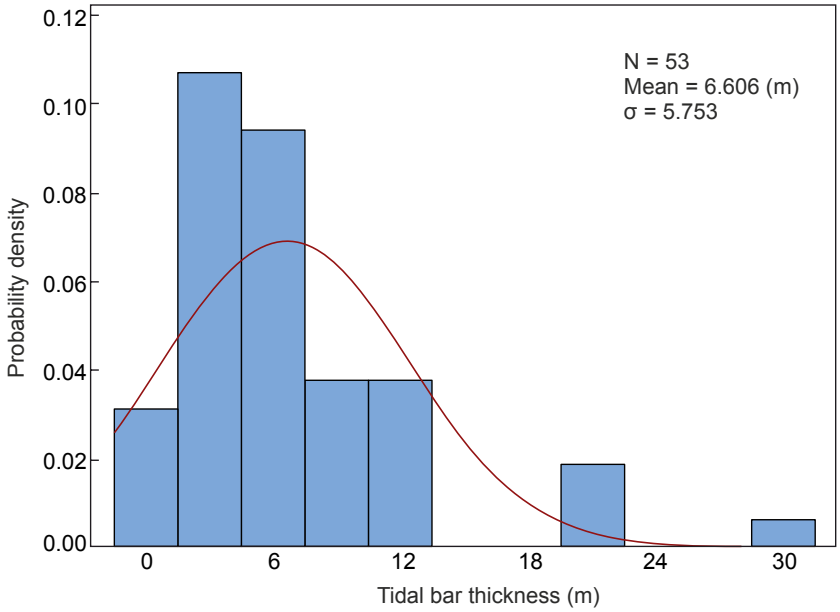

Figure 4.12: Histogram shows tidal bar thickness distribution across 53 tidal bars. 'N' denotes number of readings. 'σ' denotes the standard deviation.

4.4.2.2 Grain size

Tidal bars are primarily composed of sandstone with a significantly lesser proportion of heterolithic sand and mud, siltstone and claystone (Figure 4.13A). Gravel components were observed only in 3 tidal bars (two in the Eocene Aspelintoppen Formation in Spitsbergen, Norway, and one in the Pleistocene Ba Mieu Formation in Vietnam). The differences in means of thicknesses and proportions of the gravel, sand, silt and clay are statistically significant ($F(6,602) = 2.65$, $P = 0.015$ and $F(3,54) = 41.22$, $P = 0.000$, respectively).

The grain size of the sandstone present in the cumulative tidal bars is mostly fine-grained and medium-grained (43.7 % and 38.2%, respectively), with very fine-grained sandstone occurring in a much lower proportion (12.4%). Coarse-grained sandstone is present in some tidal bars, and this accounts for 5.6% of the total, whereas very coarse sandstone is rare (Figure 4.13B).

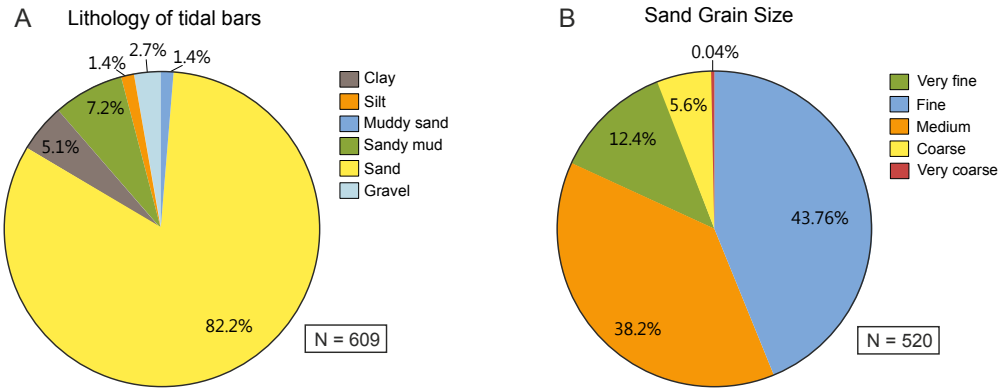

Figure 4.13: Pie charts illustrating A) proportion of lithiotypes and B) proportion of sand grainsize across tidal bars. 'N' denotes the number of readings.

The lithology of the bars with respect to their locations within the estuary is investigated. In this study, this was only done for examples from the Gironde estuary since both their sedimentology and location within the estuary are known (Fenis and Tasete, 1998; Virolle et al., 2020). The Plassac and Trompeloup tidal bars are located in the inner estuary, whereas the Richard tidal bar is located further seaward in the outer estuary (Virollet et al., 2020 - Figure 1). These three bars are sand-dominated (76-86%). However, the sand grain size differs between the bars. In the proximal bars (Plassac and Trompeloup), the sandstone is dominated by medium-grained sand, whereas the Richard tidal bar is dominated by fine-grained sand.

4.4.2.3 Sedimentary Facies and Vertical Profile

Sedimentary facies reported in tidal bars have been categorised into 16 separate facies based on the dominant sedimentary structures, most of which are sand dominated (facies are shown in Figure 4.14 and 4.15). Means of the thickness of sandstone and mudstone facies are investigated. Differences in mean thicknesses of the different sandstone facies are statistically significant based on ANOVA test ($P = 0.000$, $F(10,509) = 6.51$) (Figure 4.14B).

Differences between the mean thicknesses of the different mudstone facies are also statistically significant (P = 0.000, F (4,71) = 13.28) (Figure 4.15B).

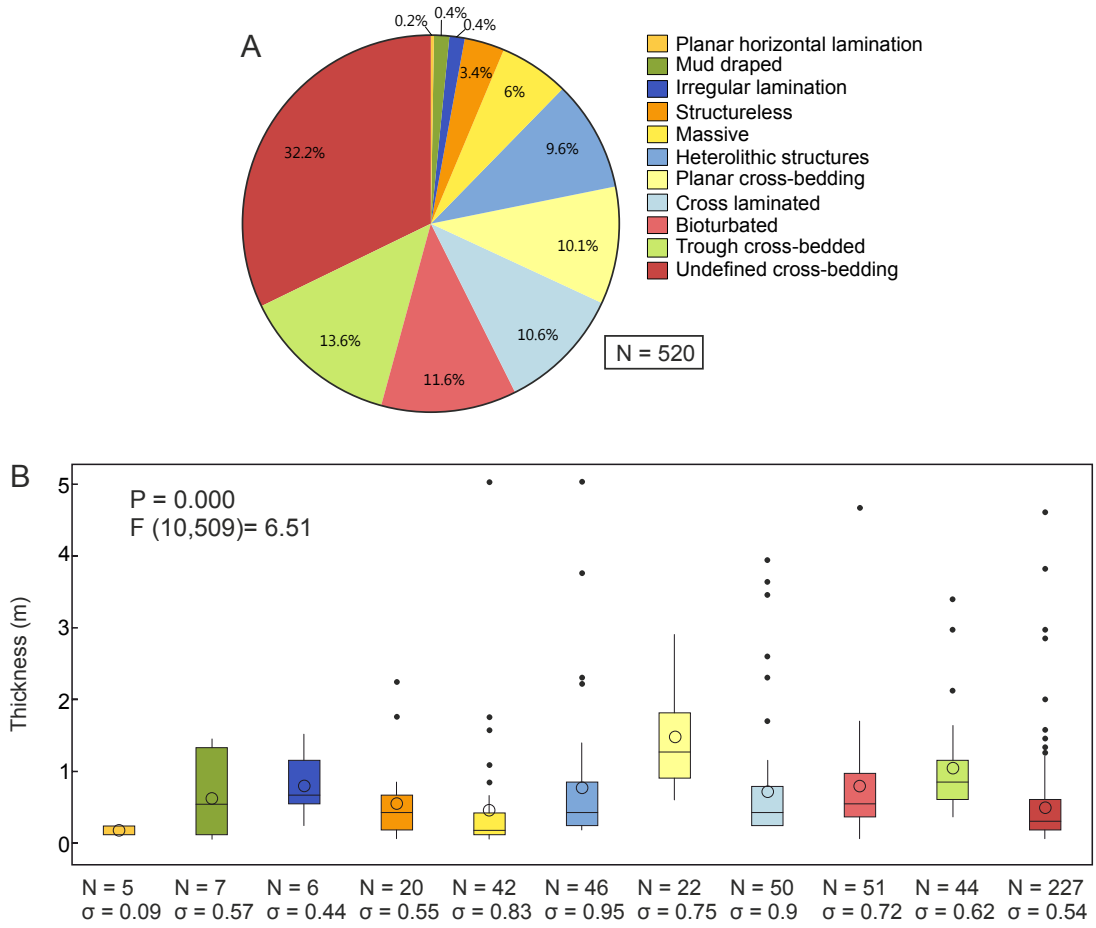

Figure 4.14: A) Pie charts illustrating the proportion of sandstone facies across tidal bars and B) Box-plots illustrating the variation in means of thickness of sandstone facies. the grain size variation in planar and trough-cross bedding sandstone. For each box-plot, boxes represent interquartile ranges, open circles represent mean values, horizontal bars within the boxes represent median values, and black dots represent outliers (values that are more than 1.5 times the interquartile range). 'N' denotes the number of readings. 'σ' denotes the standard deviation. 't' denotes the two-sample t-test. 'df' degrees of freedom. 'P' denotes P-value.

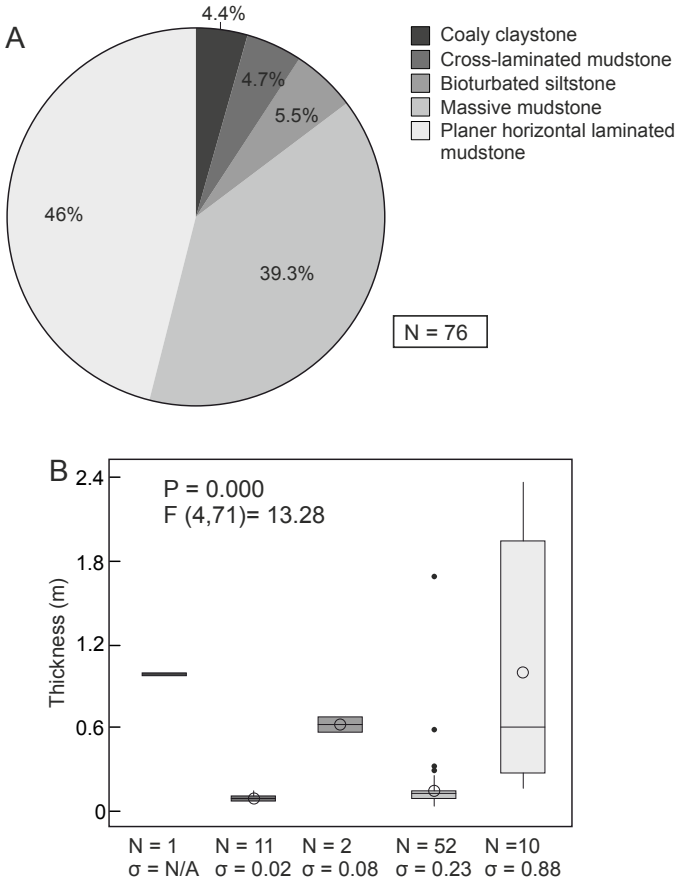

Figure 4.15: A) Pie chart illustrating the proportion of mudstone facies across tidal bars and B) Box-plots illustrating the variation in means of thickness of mudstone facies. the grain size variation in planar and trough-cross bedding sandstone. For each box-plot, boxes represent interquartile ranges, open circles represent mean values, horizontal bars within the boxes represent median values, and black dots represent outliers (values that are more than 1.5 times the interquartile range). 'N' denotes the number of readings. 'σ' denotes the standard deviation. 't' denotes the two-sample t-test. 'df' degrees of freedom. 'P' denotes P-value.

The most common sedimentary facies, which is consistently present in tidal bars, is cross-bedded sandstone; this facies collectively accounts for over 56% of the sandstone thickness (32.0% undefined cross-bedding, 13.6% trough cross-bedding and 10.1% planar cross-bedding) (Figure 4.16 A, B and C). The trough cross-bedded facies is dominated by medium sand, whereas the planar cross-bedded facies is predominantly fine sand.

Bioturbation in tidal bars is generally uncommon; it was only recorded in 5 tidal bars (out of 35). Where present, it occurs most commonly within fine sandstone and very fine sandstone (74.7% and 21.3%, respectively) but occurs only rarely

in medium-grained sandstone (Figure 4.16D). Bioturbation most frequently occurs within sandstone that alternate with numerous thin intervals of mudstone. However, this mudstone appears not to be bioturbated (e.g. tidal bars in Morne L'Enfer Formation).

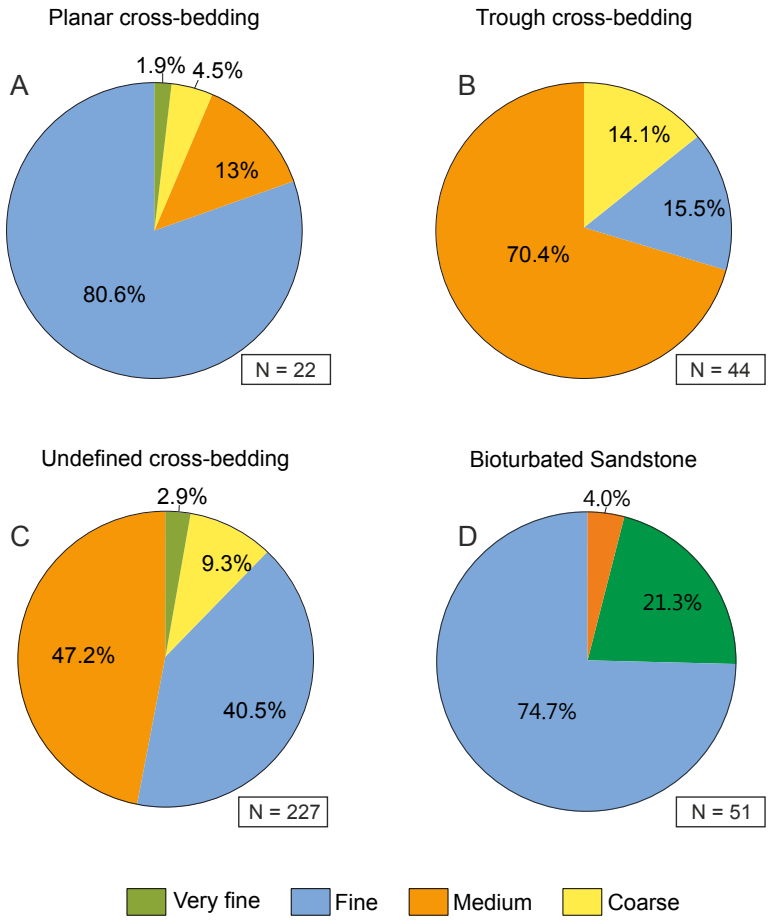

Figure 4.16: Pie charts illustrating the grain size variation in A) planar, B) trough, C) undefined cross-bedded sandstone while D) show the variation in grain size in bioturbated sandstone. 'N' denotes the number of readings.

4.4.3 Vertical Succession and Nature of Juxtaposition of Elements

The vertical succession of tidal bars is commonly represented by fining-upward trends. In few cases, tidal bars exhibit mudstone at their bases that coarsen into heterolithic mud and sand beds passing upwards into sand-dominated bedsets. Sandstone packages are seen to be separated by metre-scale mudstone or

heterolithic deposits in their middle parts and appear to be laterally continuous (e.g. Gironde estuary, Morne L'Enfer Formation).

The majority of tidal bars are characterised by extensive sets of cross-bedded sandstone with only minor mud content in their lower part; they comprise finer sand and more mud content in their upper part. The upper part of bars is commonly characterised by heterolithic or mudstone deposits.

Modern tidal bars are seen to interact with and to be juxtaposed by other estuarine geomorphic elements. They are commonly covered by vegetation and bounded by tidal and or tidal-fluvial channels. The sidebars are by definition bank-attached; therefore, they are bounded by bank sediments, primarily tidal flats, on one side and by channels on the other side. Tidal-bar deposits are associated with a range of architectural elements. They are seen overlying deposits of tidal flat, shoreface, tidal channel, tidal bar or fluvial channel origin (Figure 4.17 A). Also, they are overlain by the deposits of tidal flat, tidal bar, shoreface and tidal-channel sub-environments (Figure 4.17 B). Tidal-bar elements from successions for which a sequence stratigraphic framework was erected are always seen as components of transgressive systems tracts. A major (maximum?) flooding surface or marine mud directly covers (i.e. overlies) either the tidal bars themselves or the overlying finer-grained tidal flat deposits in 12 examples.

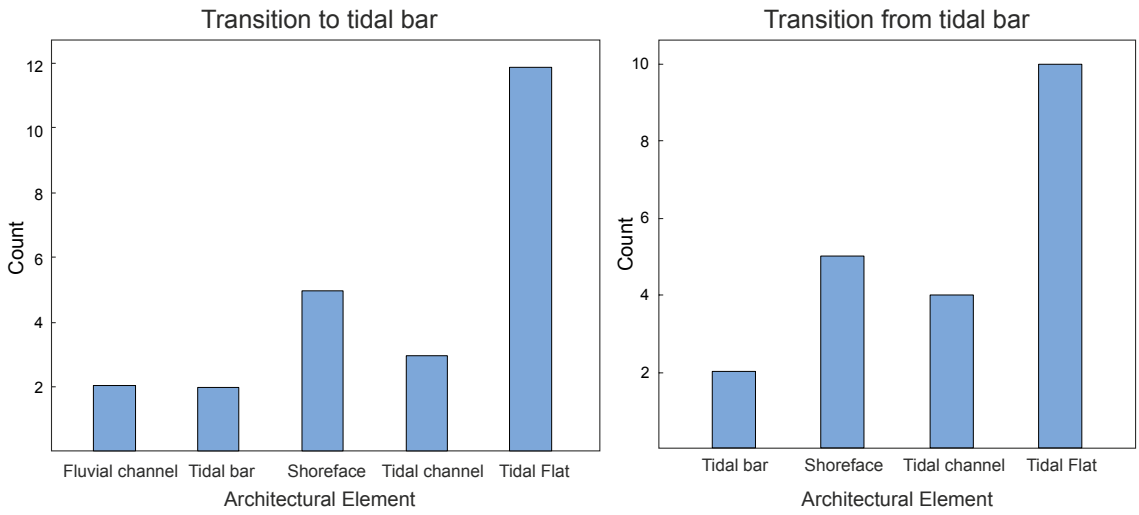

Figure 4.17: Graphs show the count of elements that tidal bars interact with in tidal estuaries. A) shows the elements occur below tidal bars and B) show the elements that occur on top of tidal bars.

4.5 Discussion

4.5.1 Controls on Tidal Bar Size and Architecture

4.5.1.1 Size of Estuaries and Tidal Bars

The comparison between the sizes of bar-built and coastal-plain estuaries shows clear variation in their depth and width values. Coastal-plain estuaries are wider and deeper on average than their bar-built counterparts. This is related to the size of tidal bars within them, which appear to be larger in coastal-plain estuaries compared to bar-built ones. Bars of different types seem to scale well with their respective estuaries. This demonstrates that the bar size is related to the depositional depth of the container in which they form. Tidal bars are vertically limited by water depth and they expand laterally when they reach the water surface during active sedimentation (Dalrymple and Choi, 2007).

4.5.1.2 Sedimentary Architecture of Tidal bars

In most cases, tidal bars exhibit fining-upward trends from their sand-dominated lower part, largely deposited in the subtidal zone. In areas of active deposition, tidal bars can aggrade into the intertidal zone where heterolithic sediments can accumulate and vegetation colonize their upper part (Dalrymple et al., 2003). In a limited number of cases, heterolithic and vegetated deposits are not present, which indicates that either the tidal bars did not aggrade to the water surface, preventing accumulation of those deposits, or that they were deposited but not preserved.

Tidal bars examined in this study can be broadly divided into two types according to the arrangement of sand and mud intervals and the presence of bioturbation. Most of the tidal bars exhibit extensive cross-bedding across much

of their vertical succession produced by the migration of 2D and/or 3D dunes. These tidal bars record a continuous sandy section in their lower parts that transitions upward to thinner heterolithic and mudstone sediments. These types of tidal bars display rare or limited mud intervals within the sandy section. By contrast, fewer examples (5 tidal bars) show more frequent mud intervals within the lower sandy parts and exhibit bioturbation that increases in intensity upwards. Bioturbation present in these tidal bars is expressed by generalist ichnoforms (*Thallassinoides* and *Ophiomorpha*), which are typically produced by organisms that can survive salinity fluctuations in estuaries (MacEachern and Pemberton, 1994; MacEachern and Gingras, 2007; Gingras et al. 2012). The difference between these two types could be interpreted to be function of sedimentation rate. The tidal bars with a continuous sandy section and rare mud intervals indicate deposition during high rate of sediment supply, expressed by rapid dune migration (Amos et al., 1980; Yeo and Risk, 1981), which prevented the deposition of mud layers and the sediment-churning activities of organisms. In contrast, low sedimentation rate allows the deposition of mud layers and provides calmer conditions for organisms to colonise tidal bars.

4.5.2 Grain size Distribution within Estuaries

The Gironde estuary, although being macrotidal, is considered to be a mixed wave and tidal energy system (Allen and Posamentier, 1994; Féniès et al., 2010), and is characterised by the tripartite facies model (sand-mud-sand zones) (Allen, 1991; Dalrymple et al., 1992). The Trompeloup and Plassac tidal bars lie in the proximal sand-dominated zone, whereas the Richard tidal bar is located in the mud-dominated zone. However, all of these bars are sand-

dominated. The sandstone is observed to decrease in grain size from proximal to distal estuary. The Trompeloup and Plassac tidal bars are dominated by medium sand, whereas the Richard tidal bar is dominantly made of fine sand. This can be explained by an overall decrease in grain size from the estuary head towards the sea within the funnel zone of the estuary. A seaward-fining trend is documented in an estuarine tidal bar in the Devonian Baltic basin where the tidal bar is composed of coarser sandstone at its proximal end and finer sandstone at its distal end (Pontén and Plink-Björklund, 2009). However, it could be argued that the Richard tidal bar, being located in the mud-dominated zone and in close proximity to the mouth of estuary, may comprise sediments sourced from the outer sand-dominated zone; therefore, it might not represent a seaward-fining trend.

4.5.3 Preservation and Reservoir Potential

Many of the studied ancient examples demonstrate a thick section of tidal-bar deposits overlain by finer-grained tidal-flat sediments, which represents a complete subtidal to intertidal succession. In other examples, tidal bars transition from fluvial or tidal channels at their bases and into tidal channel or tidal flats. This indicates that estuarine tidal bars in ancient estuaries can be largely preserved. In addition, estuaries are usually subject to relative rise in sea level, which causes submergence of the tidal bars and increases the depositional water depth in estuaries. As a result, tidal bars become abandoned and eventually preserved (Figure 4.18; Pontén and Plink-Björklund, 2009). In other cases, they become stranded as shelf sand ridges during sea-level rise which may or may not be preserved depending on the prevalent process regime

during transgression (Demarest and Kraft, 1987). For example, wave activity during transgression can rework such deposits in some settings.

The sandstone intervals recorded in most of the tidal bar deposits is commonly continuous and can be up to 10 m. They are composed predominantly of sand grains and are commonly reported to contain well-sorted grains (Plink-Björklund, 2005; Virolle et al., 2020), which typically implies porous sediments. Also, tidal bars are largely of significant size, which together with being porous, can potentially have large storage capacity for fluids, notably hydrocarbons. The average length (2,929 m), width (735 m) and height (10.4 m) of the studied tidal bars along with a poor porosity of 5% may would provide around one million cubic metres of storage capacity. However, the heterogeneity that occurs in the internal architecture of tidal bars may impact their reservoir potential and reservoir performance. Heterogeneity is observed to occur at multiple scales within tidal bars. In several examples, although sand-dominated, sandstone packages are separated by decimetre- to metre-thick muddy or heterolithic intervals that extend across much of the tidal bar (e.g. tidal bars in the Gironde estuary and Morne L'Enfer Formation). This may limit the contact between sandstone intervals, and thereby compartmentalise a tidal bar into two or more separate reservoir units or compartments. Alternatively, they may act as baffles depending on the lateral continuity of mud-prone beds. At a smaller scale, the frequent mud laminae draping the sandstone bedsets could affect the vertical and horizontal connectivity of the reservoirs.

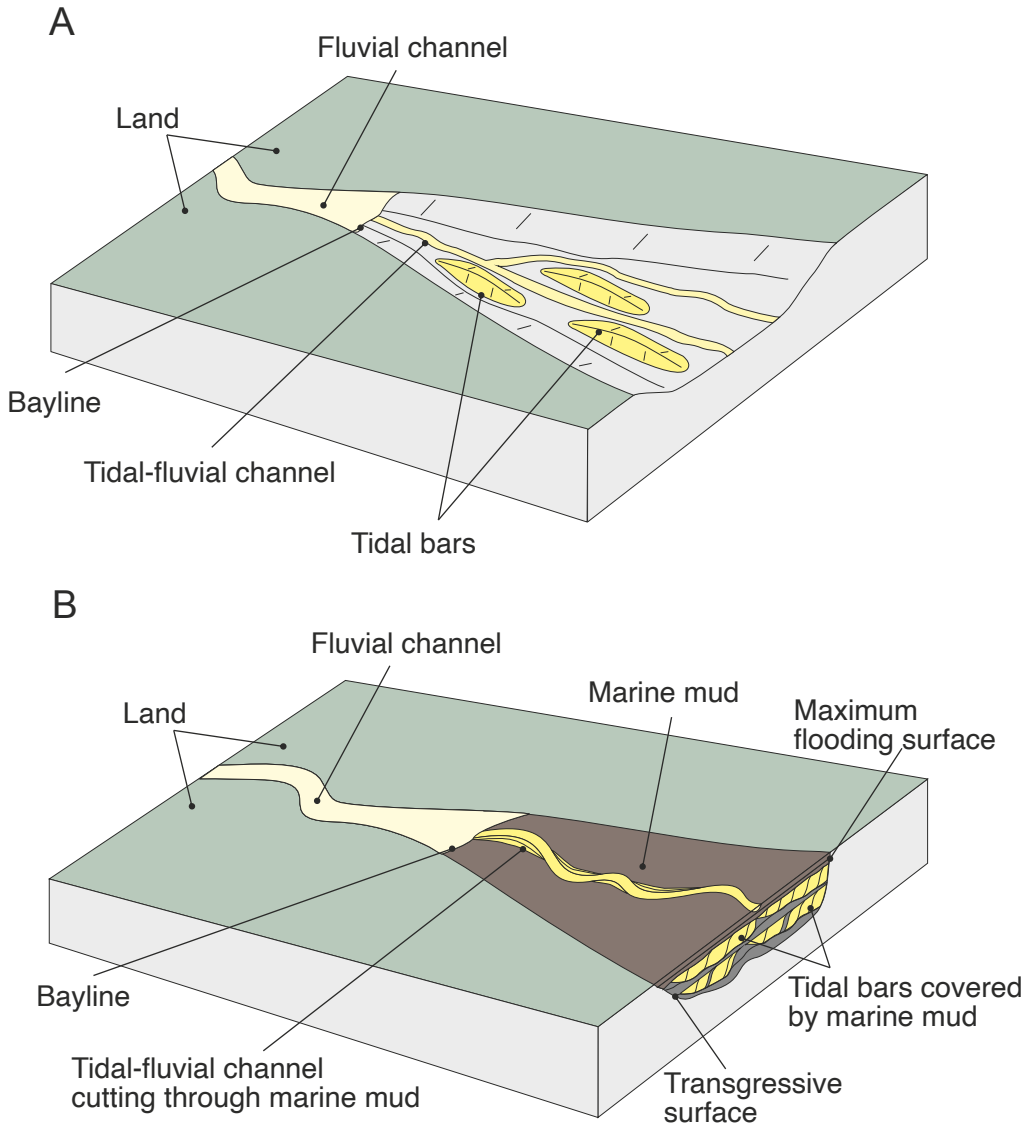

Figure 4.18: Schematic diagrams showing how marine mud fills the estuary bay and subsequently preserve tidal bars, adapted from (Plink-Björklund, 2005).

4.6 Conclusions

This study employs a quantitative approach by which the nature of estuarine tidal bars is investigated. Tidal bars range from tens of metres to tens of kilometres in width and length. The size of tidal bars is related to the size of their respective estuaries. They are limited vertically by the water surface of the estuary and their width values scale well with the width of their respective estuaries. They exhibit fining-upward trends and are characterised by cross-bedded sandstone across much of the succession. Tidal bars that aggrade near

or to the water surface commonly incorporate heterolithic or mudstone deposits in their upper section, recording intertidal and supratidal conditions. Two types of tidal bars are identified; both are sand-dominated but one shows a continuously sandy vertical facies succession, whereas the other contains frequent intervals of mudstone alternating with the sandstone bedsets. Tidal bars are commonly largely preserved mostly intact, as shown by the presence of their subtidal and intertidal sections. Since they contain sand-dominated and moderately sorted deposits, tidal bars may exhibit good reservoir quality, which may however be impacted negatively by heterogeneity that exists within them.

5 Discussion

This chapter integrates the results from the subsurface study of the lower Dhruma Formation (chapter 3) and the quantitative study of estuarine tidal bars and their deposits (chapter 4) to develop and present a discussion of factors that influence patterns of sedimentation and the nature of the stratigraphic record in paralic sedimentary systems. Specifically, this chapter seeks to answer and address the research questions posed in the Introduction (chapter 1). In the following sections, explanation and discussion of the content related to each of the fundamental research questions are provided.

5.1 What controls sedimentation in fluvial to shallow-marine settings? What controls the interaction between siliciclastic and carbonate deposition?

This section addresses the above-stated questions principally through reference to the study of the subsurface datasets relating to the lower Dhruma Formation, Saudi Arabia (Chapter 3). The section is divided into a consideration of controls that influence deposition and evolutionary patterns of sedimentation in fluvial to shallow-marine successions, and the types of interaction between siliciclastic and carbonate deposits, both of which are important in the lower Dhruma Formation. Examples from modern systems that are considered analogous to the environments interpreted for the lower Dhruma Formation succession are presented.

5.1.1 Controls on the Deposition of Fluvial to Shallow-Marine Sediments

The overall succession represented by the lower Dhruma Formation records deposition in fluvial and shallow-marine environments that interacted over both space and time. Five principal facies associations representative of particular sub-environments are identified: fluvial channels (FA1); intertidal flats and pedogenically modified supratidal or floodplains (FA2); fluvial-influenced tidal bars (FA3); shoreface and delta (FA4); open-marine and shelf carbonates (FA5).

5.1.1.1 Regional Scale Controls

At a regional scale, relative changes in sea level are interpreted to have played a major role in controlling the overall pattern of deposition in the lower Dhruma Formation within the study area. The proximal region in the southeast records thicker coastal-plain succession; here a relatively greater proportion of the succession is represented by FA1, FA2 and FA3; by contrast, a relatively lesser proportion is represented by marine deposits (FA4 and FA5). The thickness of coastal-plain deposits decreases progressively towards the northeast to a point where they are entirely replaced by marine deposits (see cross-sections in Figure 3.11). The area of interest is dominated by coastal plain deposits in the southeast and transitions to marine deposits in the northeast.

The depositional patterns in the lower Dhruma Formation record a regional marine transgression represented by an overall shift of facies belts of marine origin towards the southeast of the region. For example, the oolitic shoal deposits of FA5 are present at the top of the lower Dhruma Formation in the proximal southeast area (well 11) overlying a thick succession of coastal-plain deposits. However, this regional marine transgression is punctuated by six

smaller scale transgressive-regressive packages. This is recorded by the presence of prograding shoreface and deltaic deposits of FA4 overlying the open-marine shelf carbonate deposits of FA5 (Figure 5.1A).The net basinward sediment progradation can be produced by periods of increased terrigenous influx that outpaces the rate of relative sea level rise or during periods of stillstands (i.e. normal regression) or by periods of minor falls in relative sea level, where the shoreline is forced to regress basinwards (i.e. forced regression) (Catuneanu et al., 2011 and 2012).

The distinction between these two scenarios is not necessarily straightforward. Both of the scenarios result in a seaward shift of the shoreline trajectory and can produce progradational depositional trends. However, normal regression may produce progradational depositional trend with aggradation, depending on the rate of sea-level rise while the forced regression produces progradation in a downstepping manner (Catuneanu et al., 2012). The depositional trends from both scenarios may be readily apparent in three-dimensional views of facies architecture in outcropping successions or in high-resolution seismic images, but is typically rather difficult to establish from limited one-dimensional core data. In such cases, the distinction between the two regression types would typically be performed through recognition of the characters of regressive surfaces of marine erosion (RSME) (Catuneanu, 2006).

5.1.1.2 Local Scale Controls

The interaction of fluvial, tidal and wave processes is evident in the lower Dhruma Formation and interpreted to have controlled the deposits at a local scale. The interaction of fluvial and tidal processes has been recognised in the channel-fill, intertidal flats and tidal-bar deposits. For example, the fluvial

channel-fill deposits record sedimentation influenced primarily by fluvial currents. However, a possible tidal effect is indicated by the presence of localised double mud laminae draping cross-stratified sets. The intertidal deposits are dominated by tidal processes expressed by bidirectional ripple marks, lenticular to flaser bedding, but also influenced by fluvial currents represented by unidirectional ripple forms. The tidal bars are characterised by fining-upward cross-stratified sandstone bedsets that transition upwards to heterolithic mud and sand. Frequent single and double mud drapes, and reactivation surfaces are observed within the sandy section. There also exist thin intervals of coarse sediments interpreted to be a record of fluvial influence. Fluvial currents have also been recognised to interact with wave actions in the deltaic deposits of FA4. These deposits are dominated by wave processes and are characterised by hummocky and swaley cross-stratification. The sedimentation of these wave-generated deposits was interrupted by periods of fluvial hyperpycnal flows during river waxing stage (cf. Bhattacharya and MacEachern, 2009), which produced inversely graded beds with well-rounded grains and gastropod shells. The interaction of fluvial, tide and wave processes is interpreted to have influenced the shape of the shoreline in the studied area. A synthetic representation of how the shoreline evolved is presented in Figure 5.1B.

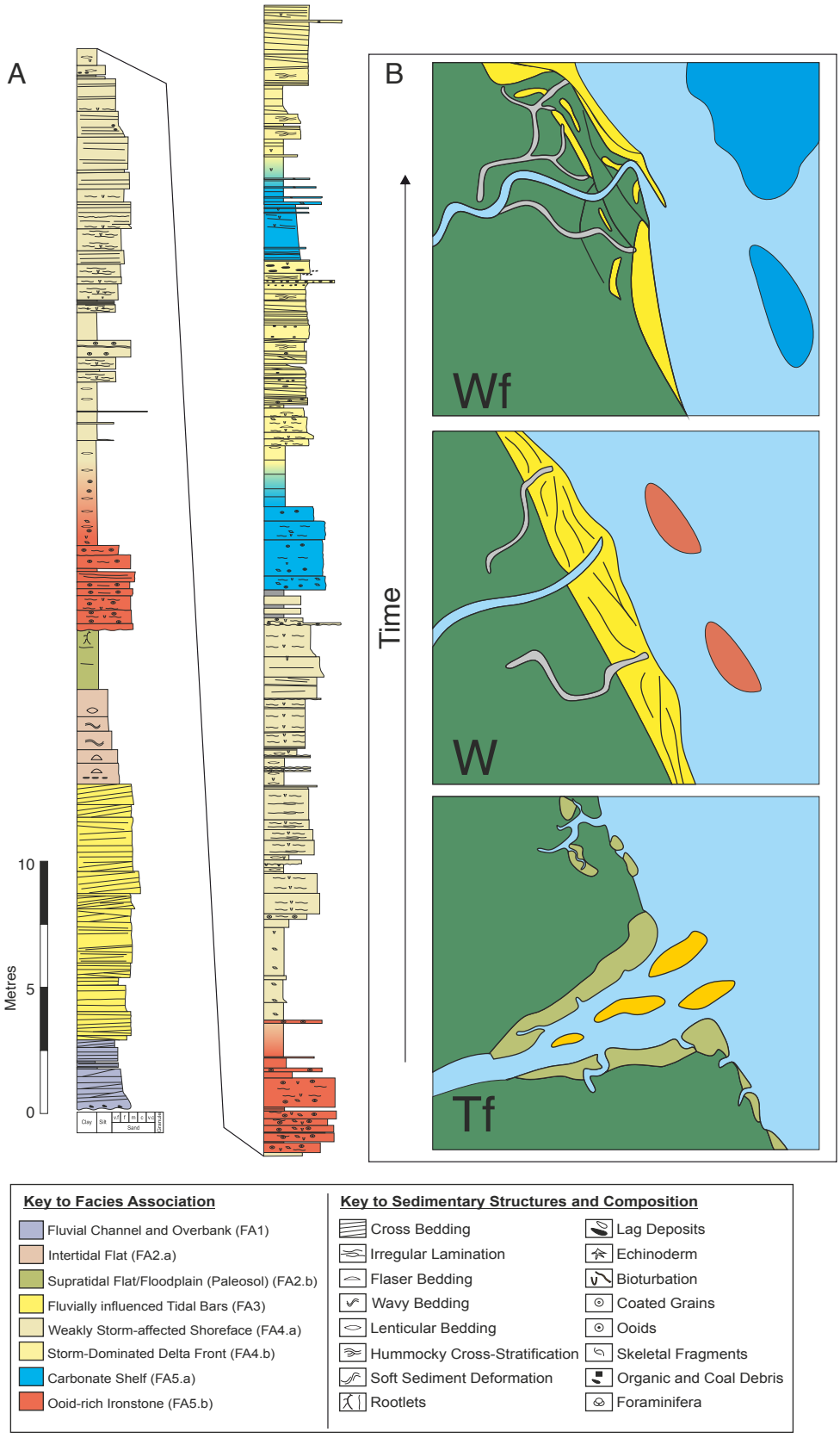

Figure 5.1: A) generalised vertical section showing the vertical stratigraphic evolution of lower Dhruma Formation, B) series of schematic representation of change in shoreline morphology during the Middle Jurassic in the study area. The letter on the maps indicate the processes by which the shoreline was affected (T= tide, F= fluvial and wave= w. the capital letter indicate the dominant control while the lower case letter indicate the subsequent control.

5.1.2 Controls on the Interaction of Siliciclastic and Carbonate Deposits

Siliciclastic and carbonate sediments interact in both space and time. The spatial interaction occurs when siliciclastic and carbonate deposits coexist in a sedimentary system and lie laterally adjacent to each other. The temporal interaction is recorded by the vertical alternation of siliciclastic and carbonate deposits through the same succession (Chiarella et al., 2017). The interaction of siliciclastic and carbonate deposits documented in the literature occur at multiple scales that range from compositional core-plug scale to stratigraphic seismic scale (Chiarella et al., 2017). Observed scales of interaction noted in the lower Dhruma Formation occur at a lithofacies-unit scale and at an architectural-element scale (Figure 5.2 and 5.3). The siliciclastic and carbonate mixing at a lithofacies scale consists of interbedding of siliciclastic and carbonate layers whereas the mixing at an architectural element scale consists of alternating carbonate and siliciclastic architectural elements.

The base of the succession records siliciclastic deposits of fluvial and tidal origins across the study area. The correlative strata seen in the most distal well in the northeast (well-6) records interbedding siliciclastic and carbonate deposits at the scale of lithofacies-unit (Figure 5.2). At this scale, siliciclastic and carbonate mixing can occur as a result of extreme weather conditions (e.g. storms) during the deposition of siliciclastic sediments (Halfar et al., 2004) in which storms transport detrital carbonate sediments into the system from a nearby carbonate source. Mixing at the architectural-element scale in the lower Dhruma Formation is seen in several wells where deposits of carbonate facies association of FA5a alternate vertically with siliciclastic deposits of FA4b. This architectural-element mixing forms part of the transgressive-regressive packages where it can be a result of terrigenous sediment input rate that

outpaces the rise in relative sea-level or during stillstands (scenario 1) or it can be a product of relative fall in sea level (scenario 2) (Figure 5.3). The uppermost interval of the lower Dhruma Formation is characterised by carbonate deposits, which appear to be present across most of the overlying middle and upper Jurassic succession. This indicates sea-level rise and transgression across the entire study area, and perhaps across a much larger region beyond its limits.

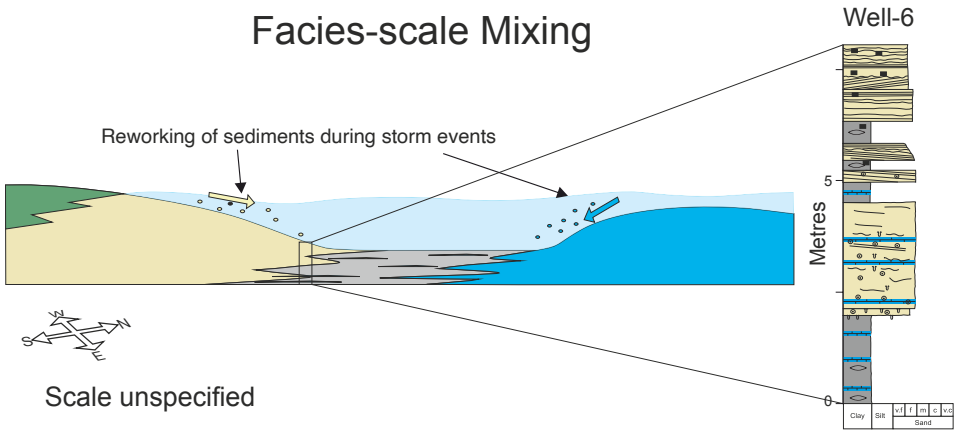

Figure 5.2: Schematic diagram showing the facies-scale interaction between siliciclastic and carbonate deposits, adapted after Chiarella et al. (2017). Refer to Figure 5.1 for key to facies and facies association.

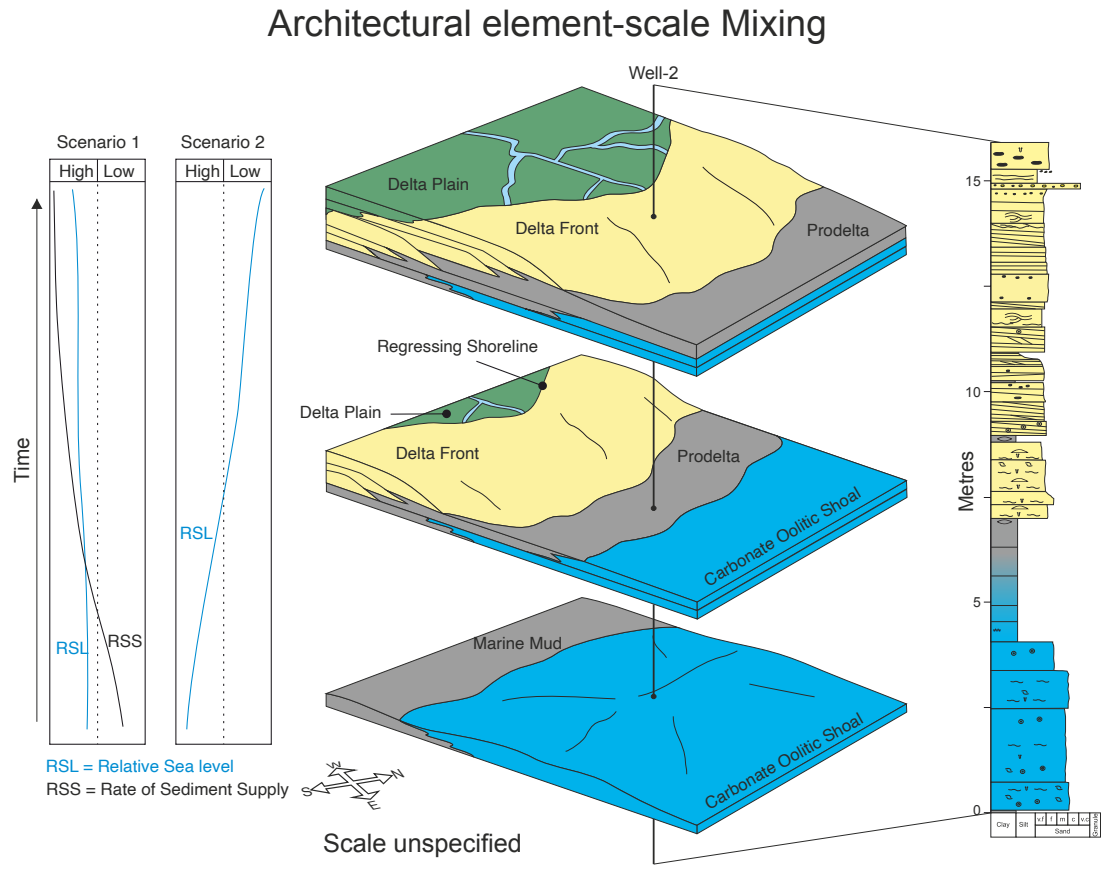

Figure 5.3: Schematic diagram showing the architectural element-scale interaction between siliciclastic and carbonate deposits. The interaction can a result of increased rate of sediment supply that outpaces relative sea-level rise or during stilstand periods (Scenario 1) or it can be produce during relative fall in sea level irrespective of rate of sediment supply (scenario 2). Refer to Figure 5.1 for key to facies and facies association.

5.1.3 Modern Environments

The facies associations defined in the lower Dhruma Formation represent a range of palaeoenvironments. Fluvial channels and the finer sediments overlie them (FA1) represent channel-fill and overbank deposits, and indicate deposition in fluvial environments. The deposits of FA1 show possible localised tidal effect represented by double mud-drapes; this may suggest tidal intrusion in the proximal part of the system. The intertidal deposits of FA2a are interpreted to have formed in a tidal-flat environment. These two facies associations are commonly overlain by similar intensely rooted successions (FA2b). These are interpreted as pedogenically modified floodplains (where they overlie FA1) and supratidal environments (where they overlie FA2b). FA3 represents tidal-bar successions that are influenced by fluvial processes. The upper section of tidal-bar elements is represented by heterolithic deposits that are likely a signature of intertidal conditions. Collectively, these three facies associations, being controlled by tidal and fluvial processes, may represent deposition within an FMTZ. A modern example that is considered to be partially analogous to these environments is the Conwy estuary (UK) (Figure 5.4A and B). The Conwy estuary exhibits multiple elongate sand bars in the middle of the estuary adjacent to intertidal flats, both are exposed during low tides and covered with water during high tides (Figure 5.4B and C). This system is likely to accumulate intertidal deposits on the banks of the estuary and on top of tidal bars in a style similar to those defined in FA2a and FA3. Also, the floodplains and supratidal flats in the Conwy estuary show dense vegetation, which may resemble the paleoenvironment of the floodplains and supratidal flats defined in FA2b.

The prograding deposits of FA4a represent weakly wave-influenced shoreface and offshore transition zone deposits represented by bioturbated sandstone with apparent remnants of hummocky cross-stratification overlying mudstone and heterolithic deposits. These successions may represent deposition in a protected area where wave action is weak and possibly at a considerable distance from the main sediment source (fluvial source). An example that could be considered analogous to this is the east coast of India near the city of Balasore (Bengal Bay) (Figure, 5.5A). The shoreface in this example lies in an area that is semi-protected from major wave action and is located at least 30 km from any sediment source.

FA4b indicate prograding wave-dominated river-influenced delta front and prodelta settings, expressed by coarsening upward trends of mudstone and sandstone facies. Being dominated by wave action and influenced by river currents, the shoreline during deposition of FA4 is interpreted to have possibly outlined an open coast that was subject to strong wave action with low river input, similar to that present in the eastern Madagascar coast (close to the town of Salehy) (Figure 5.5B). The example shown reveals straight and parallel shoreface deposits with minor river influence (Nyberg and Howell, 2016). The river influence does not cause the delta to protrude seawards and sediments delivered by river are likely modified by waves (Nyberg and Howell, 2016).

FA5a indicates deposition in wave-agitated shoal environments near the carbonate source, as revealed by the presence of abundant calcite and skeletal fragments. The palaeoclimate of the study area during the deposition of the lower Dhruma Formation is interpreted as humid to semi-humid based on the presence of small fern spores (Classopollis) (Al-Aswad, 1995; Al-Hussaini, 2019). The carbonate of FA5a is overlain by the prodelta mudstone of FA4b.

This indicates that the carbonate shoal formed at a considerable distance from the siliciclastic source (cf. Roberts, 1986). The shoal environment situated in the west of the Great Bahama Bank (Figure 5.6A and B) is composed of carbonate deposits that are rich in oolite and skeletal fragments (Cruz and Eberli, 2019), which are formed a considerable distance (~ 100 km) from any siliciclastic source (Roberts, 1986). In addition, the climate at the Bahamas is humid for several months of the year, and locally it is especially so where the shoal complex is surrounded by water (Hardie, 1977; Rankey, 2002), which is a situation similar to that interpreted for the lower Dhruma Formation in the study area. The grain composition, the location (distant from any siliciclastic sediment source) and the climate of the Northwest Bahama shoal complex could be considered analogous to the environmental setting represented by FA5a. Similar to FA5a, FA5b indicates deposition in a wave-agitated shoal environment adjacent to a carbonate source. However, in this case, the system represented by the deposits was rich in iron, which is most likely to have been transported to the depositional area by river currents. A modern example of iron-rich river water flowing into the sea is the Rio Tinto (SW Spain) (Figure 5.7A and B).

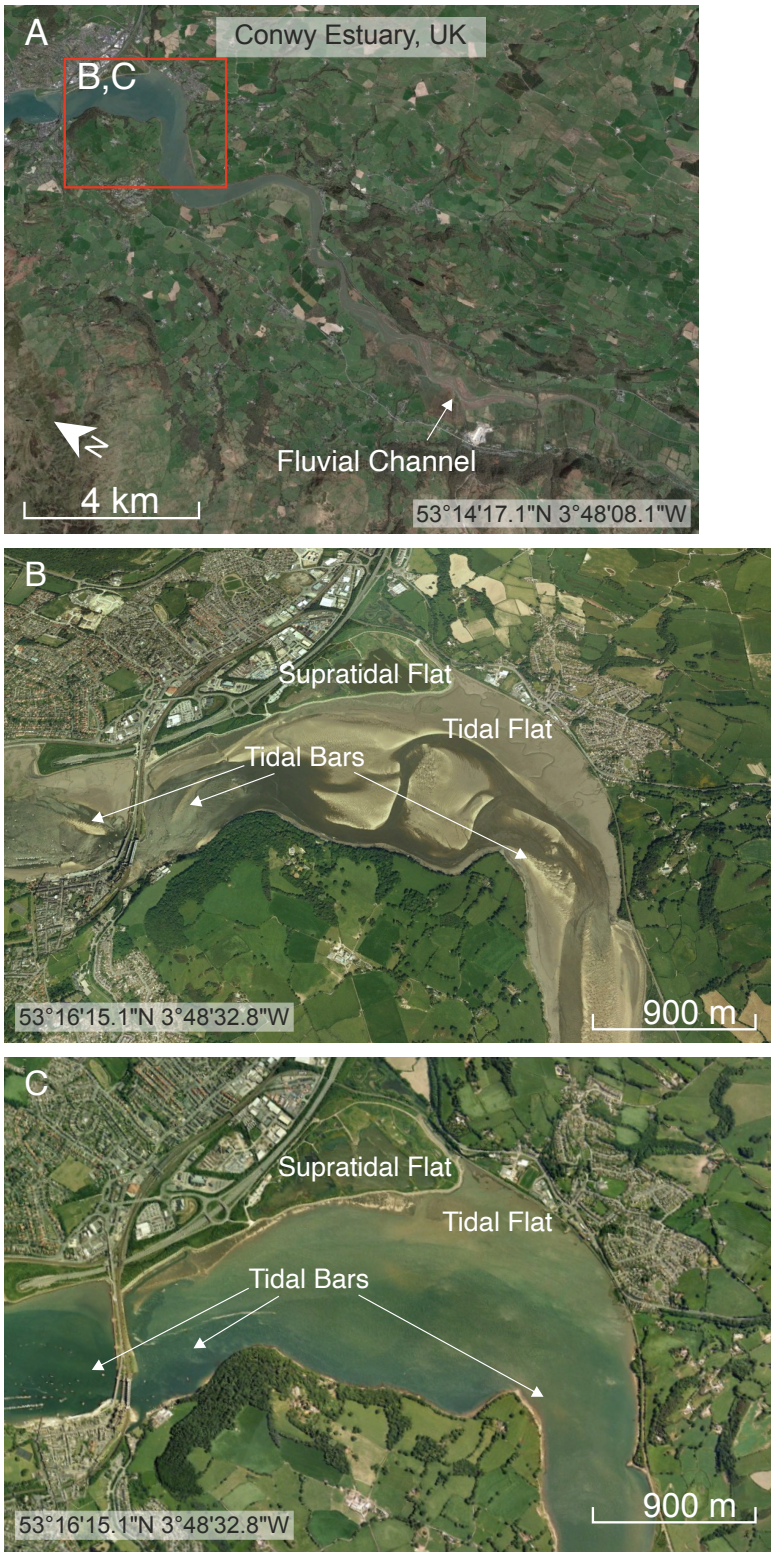

Figure 5.4: A-C) Possible modern example from the Conwy estuary (UK) that is deduced to be analogous to the facies FA1, FA2 and FA3. Note that image B shows the estuary during low tides while C shows it during high tide. Images are courtesy of Google Earth.

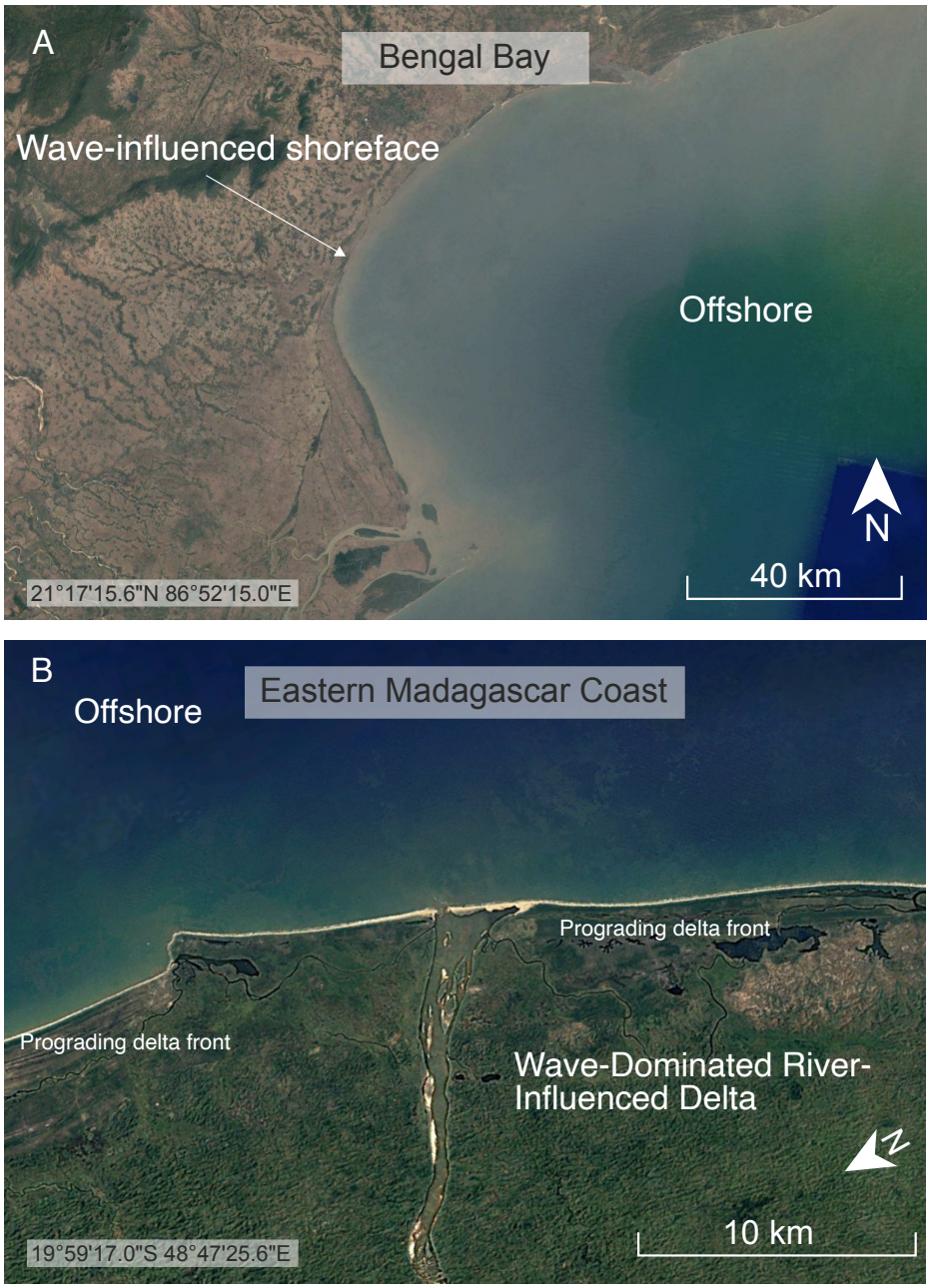

Figure 5.5: Possible modern analogues to A) FA4a and B) FA4b. Images are courtesy of Google Earth.

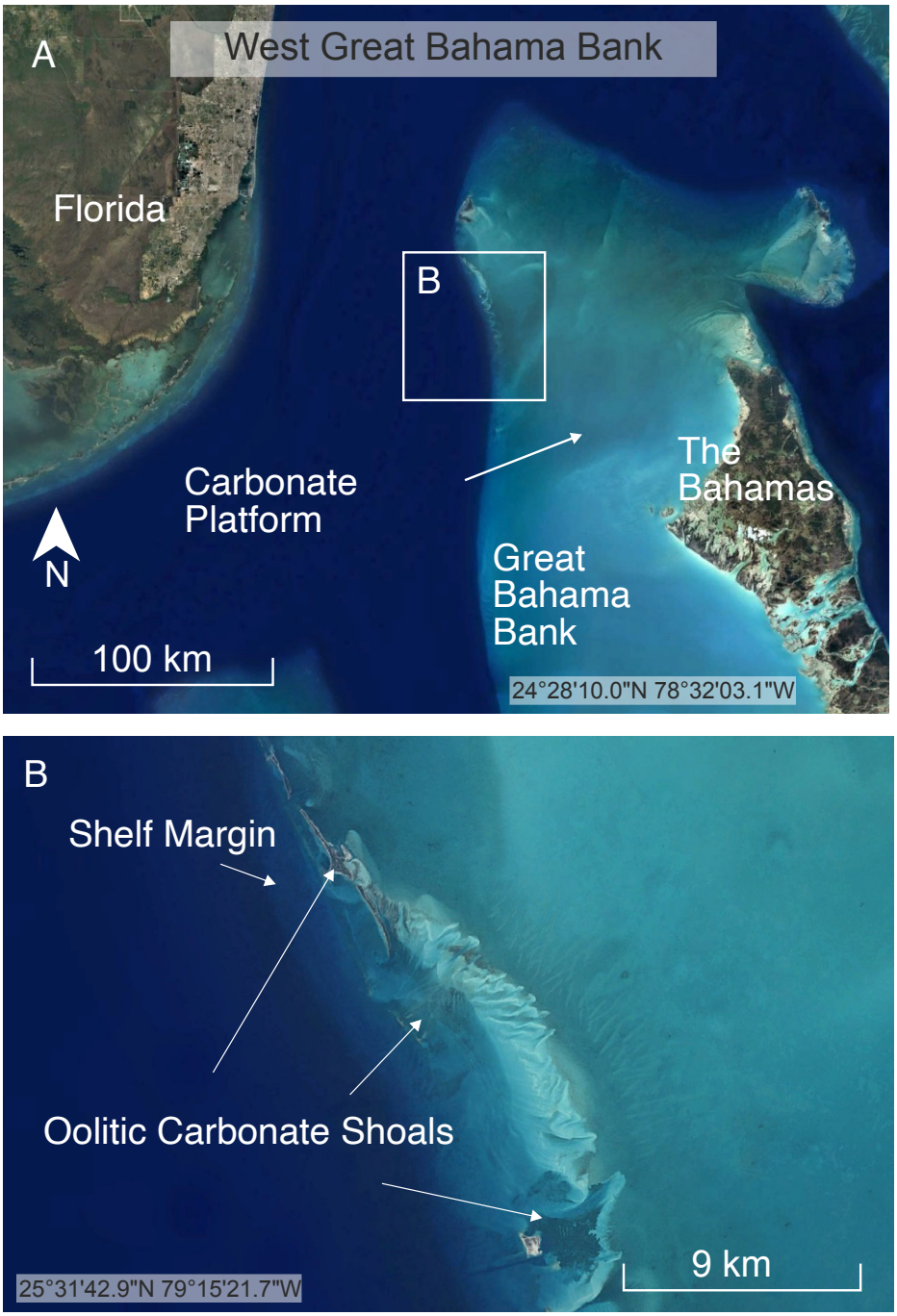

Figure 5.6: A) Possible modern example for the oolitic shoal deposits defined in FA5a from the west of Great Bahama Bank, B) zoomed-in image of B. Images are courtesy of Google Earth.

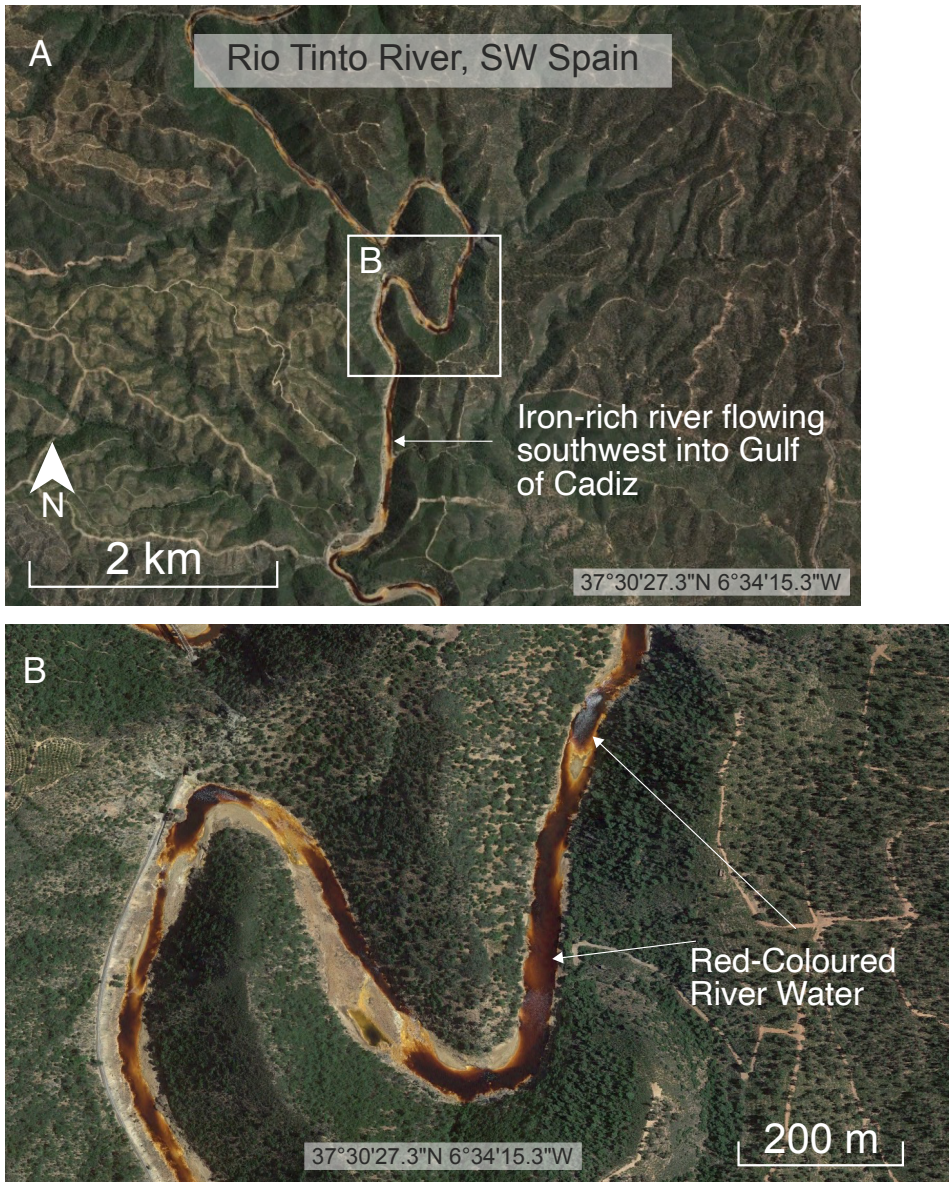

Figure 5.7: A) Iron-rich river water flowing into the sea, which may resemble the processes by which the iron was delivered to the oolitc shoals defined in FA5b. B) zoomed-in image of A. Images are courtesy of Google Earth.

5.2 What controls the deposition and preservation of tidal bars? How are they different from each other? What types of heterogeneity exist within them?

This section is split into 3 parts, each of which answers one of the preceding research questions related to the deposition, preservation and heterogeneity of estuarine tidal bars based on the quantitative analysis presented in chapter 4.

5.2.1 Controls on the Deposition and Preservation of Tidal Bars

The architecture of estuarine tidal-bar successions is typically expressed as an overall fining-upwards trend with an extensive cross-bedded lower part and heterolithic or mud-dominated upper parts. Some tidal bars may exhibit mud-dominated intervals in their lower parts possibly due to a well-developed turbidity maximum zone (see 5.3.2 below). The thickness of tidal bars is controlled by the depth of the estuary in which the bars are developed, where water depth limits their potential for vertical accretion (Dalrymple et al., 2003). During active sedimentation, bars are able to accrete to a level close to the water surface where they develop a heterolithic alternation in response to the influence of changing energy levels associated with intertidal conditions. During active sedimentation, these bars expand laterally in cases where there is a lack of vertical accommodation space due to a limitation imposed by the water depth. Vegetation may occupy the top of the tidal bars; thereby plant rooting and deposition of organic material may occur. The width of the bars is seen to correlate positively with the size of the estuaries they occupy (Chapter 4; Leuven et al., 2016).

Tidal bars accumulate in different areas of an estuary ranging from the inner zone onto the outer zone. Thus, their sedimentary expressions can be different due to the effects of turbidity maximum zone, whereby bars within the zone of turbidity maximum may exhibit more and thicker mudstone layers compared to those located distally from it (see 5.3.2 below). The tidal bars may typically interact with other estuarine elements, including fluvial channels, tidal channels and tidal flats. In rare cases (e.g., the Precambrian Tombador Formation in the East of Brazil; Magalhães et al., 2014), tidal bars (or their preserved deposits) are seen alternating with shoreface deposits. This may be limited to tidal bars that occupy the outer parts of estuaries where wave processes have a greater influence on sedimentation.

Estuaries are commonly considered to have high preservation potential (Meade 1972; Biggs and Howell, 1984; Demarest and Kraft, 1987). Ancient estuarine tidal-bar deposits considered in this research commonly show a complete succession represented by a subtidal sand-dominated lower section and an intertidal heterolithic upper section. Together, these features indicate substantial preservation of the majority of the original bar morphology. In some examples, tidal-channel deposits are seen to overlie tidal bars; this implies that those channels might have eroded parts of the bars. Tidal bars are always associated with channels (Desjardins et al., 2012a; Olariu et al., 2012), but are most commonly developed laterally adjacent to channels in most of the estuaries examined in this research. Moreover, tidal bars are influenced by diagonally oriented tidal channels known as swatchways (Robinsons, 1960) which cut through tidal bars and separate them into multiple individual smaller bars (Dalrymple and Rhodes, 1995). Tidal channels can also erode the upper parts of the underlying tidal bars. These types of interaction between tidal bars

and tidal channels (and their deposits) have been documented from both outcropping successions (e.g. Devonian Baltic Basin; Pontén and Plink-Björklund, 2009) and modern systems (e.g. Ribble Estuary (UK); Van Der Wal et al., 2002).

5.2.2 Types of tidal bars

From a sedimentological standpoint, estuarine tidal bars are broadly categorised into two types: one that shows a thick continuous section of sandstone and another that shows bioturbated sandstone that is interbedded with frequent mud intervals; both types are characterised by extensive cross-bedding but the amount of mud and bioturbation is seen to vary. Estuaries are typically characterised by a well-developed zone of turbidity maximum, which results from turbulence driven by the interaction of seawater and river freshwater (Allen, 1991; Dalrymple and Choi, 2007). The zone of turbidity maximum is characterised by high concentration of suspended sediments that settle out of suspension during tidal slacks. Tidal bars that accumulate in different locations with respect to the zone of turbidity maximum may produce different sedimentary expressions. In relatively more landward locations to the zone of turbidity maximum, freshwater and sediments are introduced into estuaries by rivers. This reduces the salinity and promotes a high rate of dune migration in the proximal zone, which restricts opportunities for colonisation of the substrate by organisms, and limits mud deposition. The more distal position, near or within the zone of turbidity maximum, is characterised by a high concentration of mud content and a relatively lower rate of sedimentation, which typically results in the deposition of thicker mud intervals. Also, the salinity in this zone is greater because the relatively distal position is closer to the

neighbouring open-marine setting. This encourages bioturbation through the burrowing and sediment churning activity of organisms (Figure 5.8; Dalrymple and Choi, 2007; Dalrymple et al., 2015; Melnyk and Gingras, 2020).

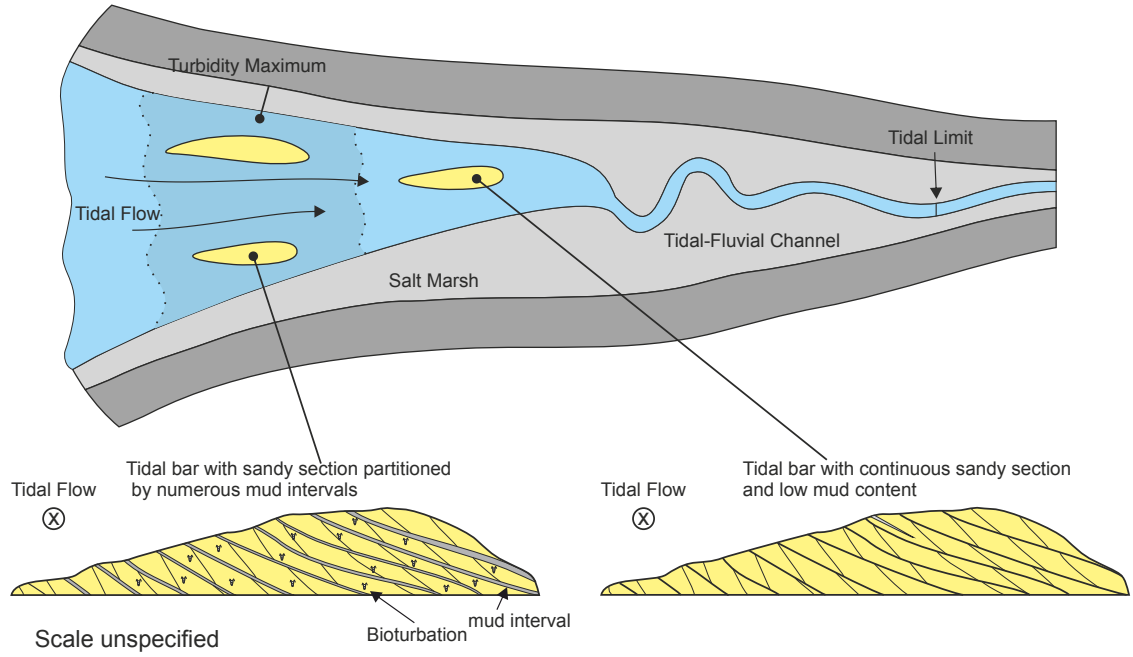

Figure 5.8: Schematic diagram presenting the types of tidal bars defined in estuaries. Estuary model modified after Dalrymple et al. (1992). Note the location of each bar with respect to the tidal maximum zone.

The zone of turbidity maximum is dynamic in the sense that its location within an estuary is subject to shifts to relatively more landward or more seaward positions depending on the relative importance and dominance of river and tidal processes (e.g. Gironde Estuary; Fenies et al., 1999). During episodes of high river discharge, the proximal zone is dominated by fluvial currents and this results in a net seaward sediment transfer (Dalrymple et al., 1992). Under these conditions, the location of the turbidity maximum is pushed seaward, sand is transported principally through bedload and the mud is held aloft in suspension where fluvial and tidal current meet. The mud concentration increases in the turbidity maximum; here, the generation of fluid mud deposits occurs (Dalrymple and Choi, 2007) and thick mud layers tend to preferentially accumulate in the

zone of turbidity maximum. By contrast, during low river discharge, tides play the dominant control in the sand bedload transport and may result in transport in either (or both) a landward or seaward direction depending on the relative power of flood and ebb tides (Dalrymple and Choi, 2007). The zone of heightened sediment suspension and the zone of turbidity maximum both shift landwards (Culver, 1980). However, the mud concentration is considerably lower than in the case of high river discharge, and thinner mud layers may be deposited. This suggests that tidal sand bars in proximal estuarine locations may be characterised by relatively thin mud layers within an otherwise sand prone succession, whereas those occupying more distal (i.e. outboard or marine influenced) locations may exhibit thicker and more abundant and frequent mud layers (Melnyk and Gingras, 2020).

5.2.3 Lithological Heterogeneities in Tidal Bars

Lithological heterogeneity in tidal sediments typically occurs in response to the common intercalation of mudstone and sandstone known in tidal environments. This heterogeneity occurs at a wide range of scales and is an important factor that controls the reservoir performance (Lake and Jensen, 1991). Estuarine tidal bars examined in this research are of significant size and are mostly composed of sandstone. However, different types of lithological heterogeneity (at different scales) are observed within these elements. Lithological heterogeneities observed in the examined tidal bars in this research can be categorised into 3 main classes.

First, a megascopic (kilometre-scale) heterogeneity occurs between different tidal bars that accumulated in an estuary. It is observed that tidal bars may form a bar complex where they accumulate in close proximity to each other;

however, they are more commonly separated by a large distance from each other. If bars are preserved, they may be overlain by deposits associated with marine flooding or prodelta muds, in which case they form isolated reservoirs or reservoir compartments. An example of such a stratigraphic relationship is the preserved estuarine tidal bars of the Pliocene Morne L'Enfer Formation (Chen et al., 2014) where tidal bars are overlain by marine and prodelta mud. Furthermore, tidal bars may accumulate on top of older pre-existing tidal bars, which themselves possess heterolithic or mud-dominated upper parts. This style of juxtaposition of bar elements could form a partition zone that precludes direct contact between the sand-dominated sections of two bars (Figure 5.9A). Second, lithological heterogeneity can occur at a macroscopic scale (decimetre to metre scale). This is most obviously developed in the form of frequent mud layers alternating with sandstone bedsets (e.g. Morne L'Enfer Formation; Chen et al., 2014) or as thick mud layers in the middle of a tidal bar, thereby splitting a tidal bar sandy section into two or more sandy units (Figure 5.9B). An example of the latter is the thick mudstone interval accumulated in the middle of the Trompeloup tidal bar in Gironde estuary (Fenies and Tastet, 1998).

Third, mesoscopic heterogeneity is represented by millimetre- to centimetre-scale tidal mud laminae and beds that drape the cross-stratified sets. These mud drapes can influence fluid flow (Figure 5.9C). Tidal bars exhibit mud drapes in variable contents. Mud drapes, if preserved, can be laterally continuous and possibly thick (e.g. those deposited during neap tides; Trompeloup tidal bar in Fenies and Tastet, 1998) and also vertically continuous. As such, mud drapes act as small-scale barriers to fluid flow (Figure 5.10A-C). In other cases, they may develop at the front of barforms; however, they pinchout above its base, and this provides laterally connected lower section and

forms readily drinable volumes (Figure 5.10D). Mud drapes can also be laterally discontinuous due to patchy deposition of mud or due to erosion by subsequent currents. The gaps in such mud drapes provide permeable zones for fluid flows (Figure 5.10E). Examples of discontinuous mud drapes are present in the Middle Devonian Baltic Basin tidal bars (Pontén and Plink-Björklund, 2009), in the Cretaceous Hollin and Napo Formations (Shanmugam et al., 2000) and include the Plassac and Richard tidal bars in the Gironde estuary (Virolle et al., 2019). Tidal bars may also lack mud drapes due to rapid or high dune migration rate which prevent mud deposition (e.g. the Eocene Aspelingtoppen Formation; Plink-Björklund, 2005). Lithological heterogeneity in tidal bars at a mesoscopic scale is therefore contingent on the deposition and preservation of mud drapes across tidal bars.

Lithological heterogeneity also occurs at a microscopic scale in tidal bars, such that the lithology of tidal bars is characterised by aggregated clay particles that may impact the porosity of tidal bars. This scale of lithological heterogeneity lies beyond the remit of this study and, therefore, is not discussed in this chapter.

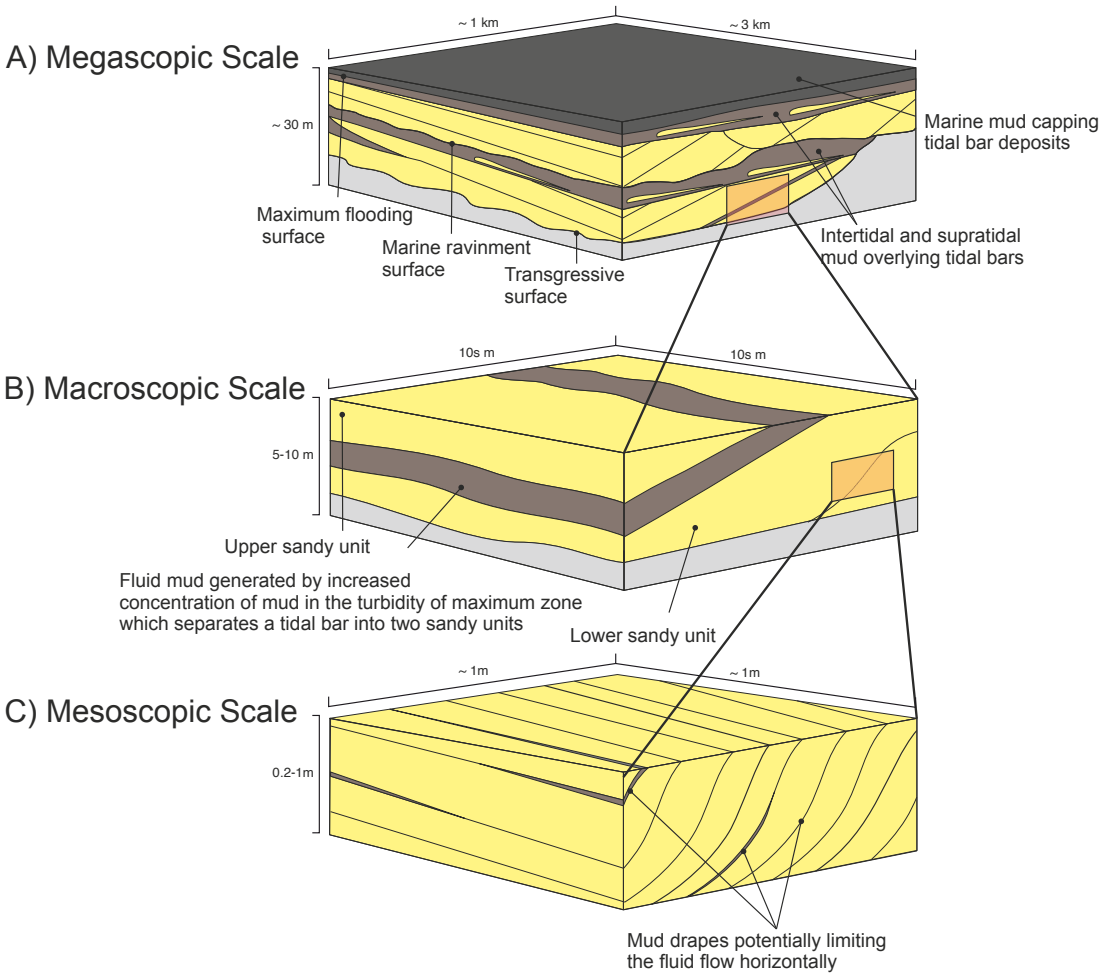

Figure 5.9: Block diagrams presenting the scale of lithological heterogeneity in tidal bars. The Mesoscopic heterogeneity in Figure C is further discussed in the following Figure (Figure 5.10).

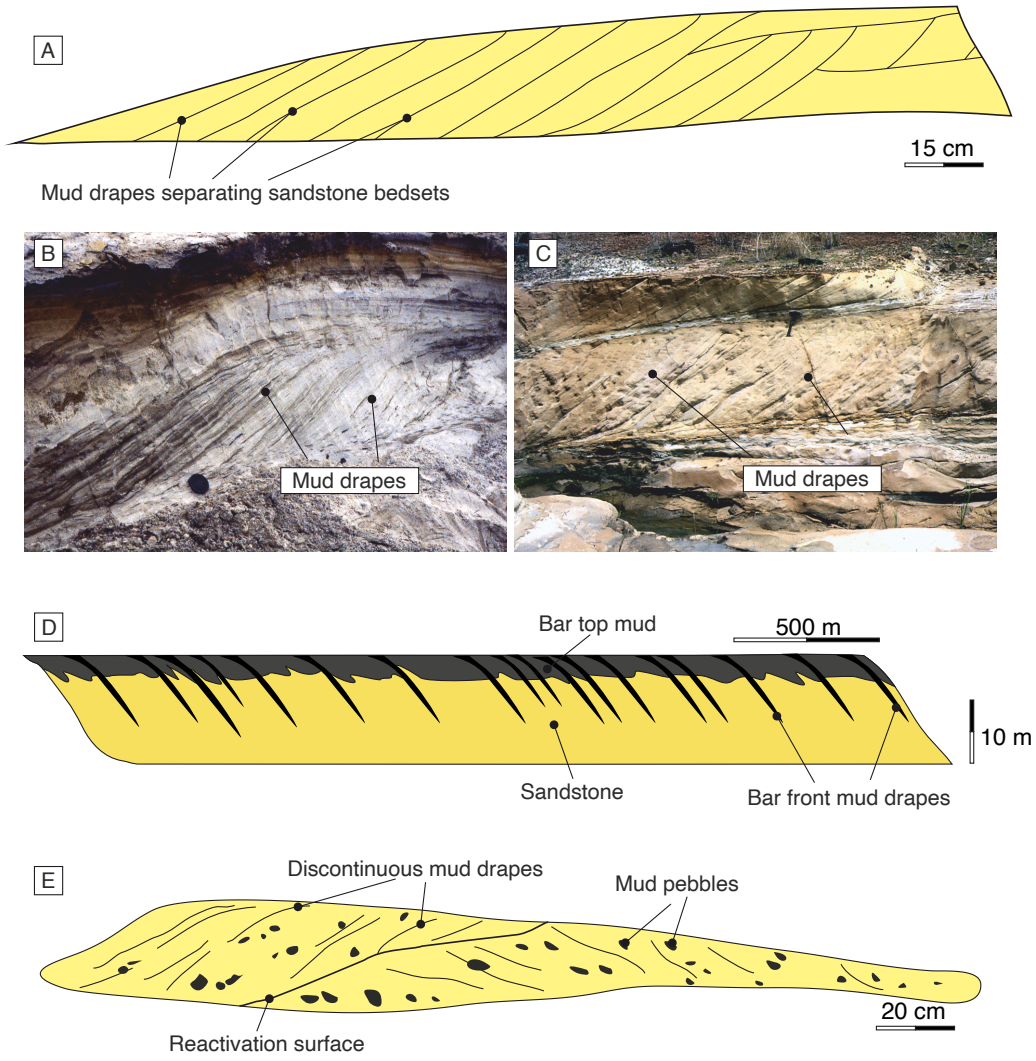

Figure 5.10: Examples of the occurrence of mud drapes in tidal deposits. A) continuous mud drapes that separate sandstone bedsets in the Trompeloup tidal bar in Gironde estuary, adapted from Fenies and Tastet (1998), B-C) examples showing continuous mud drapes at dunes foresets, after Collinson et al. (2016), D) synthetic example of mud drapes at the front of barform that taper from the bar top and pinchout above its base which provides laterally-connected lower section, adapted from Colombera et al. (2018) and E) discontinuous mud drapes across the top of the Plassac tidal bar in Gironde estuary, adapted from Virolle et al. (2019).

6 Conclusions and future work

This chapter summarises the main findings in this research and provides recommendations for future research.

6.1 Conclusions

Fluvial, coastal and shallow-marine systems host a wide range of sub-environments that interact in both space and time. These range from fluvial dominated sub-environments in relatively inland and upstream settings, to marine dominated in relatively offshore settings. The interaction of fluvial, tidal and wave processes controls sedimentation in these environments; complex process interactions govern sediment erosion, transport and deposition. As such, resultant accumulated facies patterns and relationships are complex. Facies arrangements are additionally controlled by the longer-term and regional interplay of rate of sediment supply, rate and magnitude of change in sea level, and their role in dictating how sediment might fill available accommodation. The study of the Middle Jurassic lower Dhruma Formation in Saudi Arabia is based on subsurface datasets. The study revealed that the lower Dhruma Formation was deposited in a wide range of environments that collectively are representative of fluvial to shallow-marine settings. These environments interacted over space and time. Facies associations defined in this study are considered representative of sub-environments within fluvial to shallow-marine settings, and notably in a sub-art of this – the so-called fluvial-to-marine transition zone (FMTZ). These are interpreted to represent fluvial channels affected by tidal processes (FA1), intertidal flats (FA2a), pedogenically modified supratidal flats and floodplains (FA2b), fluvial-influenced tidal bars (FA3),

shoreface and offshore transition zone (FA4a); delta front and prodelta (FA4b), oolitic shoal and open-marine environments (FA5). The FA1, FA2 and FA3 are interpreted to have been deposited in different areas of an FMTZ whereas FA4 and FA5 are considered indicative of marine environments.

The interaction of fluvial, tidal and wave processes controlled the sedimentation of the lower Dhruma Formation at a small-scale. The facies associations accumulated within the FMTZ are controlled by the interaction of fluvial and tidal processes. Fluvial signatures dominate the upstream part with no or only limited evidence for tidal influence. By contrast, the downstream part indicates more tidal influence than fluvial one. The facies associations representative of marine environments are controlled primarily by wave processes, with possible minor fluvial influence. At a larger scale, the interplay of sea-level change and rate of sediment supply controlled the overall evolution of the lower Dhruma succession. A major marine transgression is evident based on recognition of an overall shift from fluvial and nearshore deposits at the base of the succession to progressively more marine-influenced deposits up succession. Episodes of minor relative sea-level fall or high rates of sediment supply are evident based on the recognition of repeated alternation of oolitic shoal deposits and shoreface and deltaic deposits. These are interpreted to be products of shoreline transgression which was responsible for the deposition of oolitic shoal deposits (FA5 a and b) and regression due to sea level fall or increased sedimentation rate that outpaces the rise in sea level which allowed for the deposition of shoreface and deltaic facies associations (FA4a and b)

Estuarine tidal bars, which form a notable sub-environment component of the lower Dhruma Formation (as represented by facies association FA3), are quantitatively examined based on data extracted from published sources that

describe a series of analogous from modern systems and ancient preserved successions. Tidal-bar deposits exhibit a fining-upward succession with extensive cross-bedding with limited mud content in their lower part, and heterolithic or mud dominated facies in their upper part. The size of the tidal bars is scaled to the size of the estuaries in which they are developed and accumulated, and also by the depth of the estuary (i.e. level water surface), which limits their capacity for vertical accretion. Tidal bars show high preservation potential and their deposits possess characteristics required for the development of good reservoir quality. However, the heterogeneity types present in tidal-bar deposits may impact reservoir performance. Such heterogeneity types need to be accounted for carefully when assessing overall reservoir quality and expected behaviour and performance.

6.2 Future Work

The following opportunities for future follow-on research are identified as a direct outcome of this study.

- Determining a high-resolution palynological zonation may enhance the understanding of facies distribution across space and time in the lower Dhruma Formation, and might provide an opportunity for higher-resolution correlation between depositional sequences. This may allow for deciphering the interplay between sea-level change and sedimentation rate at a finer scale.
- Some aspects of the quantitative data used for the study of the lower Dhruma Formation are limited. For example, the tidal flat and tidal channel data reveal from core and well-log data cannot be used to directly constrain the lateral extent of the architectural elements present

in the subsurface. Conducting additional quantitative studies on modern and outcropping examples that are considered analogous to the facies association defined would improve our understanding of their likely distribution and interaction in the subsurface.

- The banks of tidal estuaries are subject to intertidal and supratidal conditions, and these settings are sites for the deposition of sandstone, heterolithic and mudstone facies. The upper parts of tidal bars are also subject to intertidal conditions and processes, and this can result in similar deposits to those of tidal flats. Further investigations could be conducted to ascertain whether the intertidal deposits that form the upper parts of tidal bars and the intertidal deposits of tidal flats are sedimentologically different and, if so, what distinguishes these types of deposits from each other in the ancient rock record.
- The sedimentology, internal architecture, external geometry and dimensions of tidal bars from modern examples provides information about their features before preservation and burial. These are inevitably different after the process of accumulation, preservation, burial and compaction. Further work on quantitively defining their architectural shapes and dimensions by seismic, magnetic or gravity data can improve understanding of the mechanisms by which such bars are preserved. Thus, this will lead to more accurate geological models that can be used to better inform hydrocarbon prospectivity.

References

Ainsworth, R.B., Vakarelov, B.K., and Nanson, R.A., 2011, Dynamic spatial and temporal prediction of changes in depositional processes on clastic shorelines: Toward improved subsurface uncertainty reduction and management: American Association of Petroleum Geologists, Bulletin, v. 95, p. 267-297.

Ainsworth, R.B., 2010, Prediction of stratigraphic compartmentalization in marginal marine reservoirs, *in* Jolley, J.S., Fisher, Q.J., Ainsowrth, R.B., Vrolijk, P.J., Delisle, S., eds., Reservoir Compartmentalization: Geological Society of London, Special Publications, v. 347, p. 199-218.

Al-Aswad, A.A., 1995, Middle Jurassic non-marine siliciclastic facies in Southern Central Saudi Arabia: African Earth Sciences, v. 20, p. 253–262.

Al-Eidan, A.J., Wethington, W.B., Davies, R.B., 2001, Upper Burgan Reservoir Description, Northern Kuwait: Impact on Reservoir Development: GeoArabia, v. 6, p. 179-208.

Al-Hussaini, A., Steel, R.J., Melvin, J., Olariu, C., Ertug, K., Hooker, N., 2019, New evidence of regressing and transgressing Jurassic siliciclastic coastlines within the Dhruma Formation in Northern Central Arabia, Saudi Arabia: Sedimentary Geology, v. 379, p. 114–137.

Al-Husseini, M., 2009, Update to Late Triassic-Jurassic stratigraphy of Saudi Arabia for the Middle East geologic time scale: GeoArabia, v. 14, p. 145–186.

Al-Masrahy M.A., 2017, Modelling Temporal and Spatial Sedimentary Architectural Complexity in Mixed Aeolian-Fluvial Reservoir Successions: SPE-8802.

Al-Masrahy M.A., and Mountney N.P., 2015, Quantitative Approach to the Characterization of Sedimentary Architecture in Mixed Eolian-Fluvial Reservoir Successions: American Association of Petroleum Geologists, Search and Discovery, Article 41669.

Allen, G.P., Posamentier, H.W., 1994, Transgressive facies and sequence architecture in mixed tide-and wave-dominated incised valleys: example from the Gironde Estuary, France, *in* Dalrymple, R.W., Boyd, R., Zaitlin, B.A., eds., Incised-valley Systems: Origins and Sedimentary Sequences: SEPM Special Publication v. 51., p. 225–240.

Allen, G.P., 1991, Sedimentary processes and facies in the Gironde estuary: a recent model for macrotidal estuarine systems, *in* Rahmani, R.A, Smith D.G., Reinson G.E and Zaitlan B.A., eds., Clastic Tidal Sedimentology: Canadian Society of Petroleum Geologist, V. 16, p. 29-39.

Amos, C.L., Buckley, D.E., Daborn, G.R., Dalrymple, R.W., McCann, S.B. and Risk, M.J. 1980, Geomorphology and Sedimentology of the Bay of Fundy, *in*

Guidebook, Geological Association of Canada, Annual Meeting, Halifax, trip 23, p. 82.

Arkell, W.J., 1952, Jurassic ammonites from Jebel Tuwaiq, Central Arabia. Philosophical Transactions of the Royal Society B, Biological Sciences, v. 236, p. 241–313.

Ashley, G.M. and Zeff, M.L.,1988, Tidal channel classification for a low-mesotidal salt marsh: Marine Geology, v. 82, p. 17–32

Ayranci, K., Lintern, D.G., Hill, P.R. and Dashtgard, S.E., 2012, Tide-supported gravity flows on the upper delta front, Fraser River delta, Canada. Marine Geology, v. 326, p. 166–170.

Baniak, G.M., Gingras, M., Burns, B., and Pemberton, S.G., 2014, An example of a highly bioturbated, storm-influenced shoreface deposit: Upper Jurassic Ula Formation, Norwegian North Sea: Sedimentology, v. 61, p. 1-25.

Bann, K.L., Tye, S.C., MacEachern, J.A., Fielding, C.R., and Jones, B.G., 2008, Ichnological and sedimentologic signatures of mixed wave- and storm-dominated deltaic deposits: examples from the early Permian Sydney Basin, Australia, *in* Hampson, G.J., Steel, R.J., Burgess, P.M., and Dalrymple, R.W., eds., Recent Advances in Models of Siliciclastic Shallow Marine Stratigraphy: SEPM, Special Publication 90, p. 293–332.

Barnard, P.L., Hanes, D.M., Rubin, D.M., Kvitek, R.G., 2006, Giant sand waves at the mouth of San Francisco Bay: EOS Transactions of the American Geophysical Union, v. 87, p. 285–289.

Bayer, U., Altheimer, E., Deutschle, W., 1985, Environmental evolution in shallow epicontinental seas: sedimentary cycles and bed formation, *in* Bayer, W. and Seilacher, A., eds., Sedimentary and Evolutionary Cycles: New York, Springer-Verlag, p. 347-81.

Berne, S., Vagner, P., Guichard, F., Lericolais, G., Liu, Z., Trentesaux, A., Yin, P. and Yi, H.I., 2002, Pleistocene forced regressions and tidal sand ridges in the East China Sea: Marine Geology, v. 188, p. 293-315.

Beydoun, Z.R., 1991, Arabian Plate Hydrocarbon Geology and Potential: A Plate Tectonic Approach. American Association of Petroleum Geologists, Studies in Geology, v. 33, 77 p.

Bhattacharya, J.P. and MacEachern, J.A., 2009, Hyperpycnal rivers and prodeltaic shelves in the Cretaceous seaway of North America: Journal of Sedimentary Research, v. 79, p.184-209.

Bhattacharya, J.P., 2010, Deltas, *in* James, N.P., and Dalrymple, R.W., eds., Facies Models 4: Geological Association of Canada, p. 233-264.

Bhattacharya, J.P., 2006, Deltas, *in* Walker, R.G., and Posamentier, H., eds., Facies Models revisited: SEPM Special Publication, p. 237-292.

Biggs, R.B. and Howell, B.A., 1984, The estuary as a sediment trap: Alternative approaches to estimating its filtering efficiency: *in* Kennedy V.S., ed., The Estuary as a Filter: Academic Press, Orlando, Florida, p. 107–129.

Boersma, J.R. and Terwindt, J.H.J., 1981, Neap-spring tide sequences of intertidal shoal deposits in a mesotidal estuary: Sedimentology, v. 28, p. 151-170.

Boggs, S. JR., 1995, Principles of sedimentology and stratigraphy, 2nd Edition: New Jersey, Upper Saddle River, Prentice Hall, 774 p.

Boothroyd, J.C., Friedrich, N.E., McGinn, S.R., 1985, Geology of microtidal coastal lagoons: Rhode Island: Marine Geology, v. 63, p. 35–76

Boyd, R., Dalrymple, R.W., Zaitlin, B.A., 1992, Classification of clastic coastal depositional environments: Sedimentary Geology, v. 80, p. 139–150.

Bridge, J.S., 1993, Description and interpretation of fluvial deposits: a critical perspective: Sedimentology, v. 40, p.801-810.

Bromley, R.G., 1975. Trace fossils at omission surfaces, *in* Frey, R. W., ed., the Study of Trace Fossils: A Synthesis of Principles, Problems, and Procedures in Ichnology: Berlin, Springer-Verlag, p. 399-428.

Bromley, R.G., 1996, Trace Fossils. Biology, Taphonomy and Applications, 2nd Edition: London, Chapman & Hall, 361 p.

Burton, D., and Wood, L.J., 2013, Geologically-based permeability anisotropy estimates for tidally-influenced reservoirs using quantitative shale data: Petroleum Geoscience, v. 9, p. 3-20.

Catuneanu, O. Kendall, C.G. Henry Posamentier,H. and Strasser, A., 2011, Sequence Stratigraphy: Methodology and Nomenclature: Newsletter on Stratigraphy, Special Issue, v. 44, p. 173-245.

Catuneanu, O., Abreu, V., Bhattacharya, J.P., Blum, M.D., Dalrymple, R.W., Eriksson, P.G., Fielding, C.R., Fisher, W.L., Galloway, W.E., Gibling, M.R. and Giles, K.A., 2009, Towards the standardization of sequence stratigraphy: Earth-Science Reviews, v. 92, p. 1-33.

Chaumillon, E., Féniès, H., Billy, J., Breilh, J-F., and Richetti, H., 2013, Tidal and fluvial controls on the internal architecture and sedimentary facies of a lobate estuarine tidal bar (The Plassac Tidal Bar in the Gironde Estuary, France): Marine Geology, v. 346, p. 58-72.

Chen, L., Lu, Y.C., Fu, X.F., Xing, F.C., Wang, C., Luo, C., 2017, Oolitic shoal complexes characterization of the lower Triassic Feixianguan Formation in the Yuanba gas field, northeast Sichuan Basin, China: Marine and Petroleum Geology, v. 83, p. 35–49.

Chen, S., Steel, R.J., Dixon, J.F. and Osman, A., 2014, Facies and architecture of a tide-dominated segment of the Late Pliocene Orinoco Delta (Morne L'Enfer Formation) SW Trinidad: Marine and Petroleum Geology, v. 57, p. 208-232.

Chiarella, D., Longhitano, S.G., 2012, Distinguishing depositional environments in shallow-water mixed bio-siliciclastic deposits on the base of the degree of heterolithic segregation (Gelasian, Southern Italy): Journal of Sedimentary Research, v. 82, p. 962-990.

Chiarella, D., Longhitano, S.G., Tropeano, M., 2017, Types of mixing and heterogeneities in siliciclastic-carbonate sediments: Marine and Petroleum Geology, v. 88, p. 617-627.

Coffey, B.P., Read, J.F., 2004, Mixed carbonate-siliciclastic sequence stratigraphy of a Paleogene transition zone continental shelf, southeastern USA: Sedimentary Geology, v. 166, p. 21-57.

Collins, D.S., Johnson, H.D. and Baldwin, C.T., 2020, Architecture and preservation in the fluvial to marine transition zone of a mixed-process humid-tropical delta: Middle Miocene Lambir Formation, Baram Delta Province, north-west Borneo: Sedimentology, v. 67, p. 1-46.

Collinson, J.D. and Mountney, N.P., 2019, Sedimentary Structures, 4th Edition: Edinburgh, Dunedin Academic Press, 340 p.

Collinson. J.D., Mountney N.P., and Thompson, D.B., 2006. Sedimentary Structures, 3rd Edition: Edinburgh, Dunedin Academic Press, 292 p.

Coleman, J.M., and Prior, D.B., 1982, Deltaic Environments of Deposition, *in* Scholle, P.A. and Spearing, D., eds., Sandstone Depositional Environment: American Association of Petroleum Geologist, Memoir, v. 31, p. 139-178.

Colombera, L., and Mountney, N. P., 2020b, Accommodation and sediment-supply controls on clastic parasequences: a meta-analysis: Sedimentology, online. 67, p. 1667-1709.

Colombera, L., and Mountney, N.P., 2020a, On the geological significance of clastic parasequences: Earth-Science Reviews, v. 201, p. 103-062.

Colombera, L., Yan, N., McCormick-Cox, T. and Mountney, N.P., 2018, Seismic-driven geocellular modeling of fluvial meander-belt reservoirs using a rule-based method: Marine and Petroleum Geology, v. 93, p. 553-569.

Colombera, L., Felletti, F., Mountney, N.P. and McCaffrey, W.D., 2012, A database approach for constraining stochastic simulations of the sedimentary heterogeneity of fluvial reservoirs: American Association of Petroleum Geologist, Bulletin, v. 96, p. 2143-2166.

Colombera, L., Shiers, M.N., Mountney, N.P., 2016b, Assessment of backwater controls on the architecture of distributary-channel fills in a tide-influenced coastal-plain succession: Campanian Neslen Formation, USA: Journal of Sedimentary Research, v. 86, p. 476-497.

Colombera, L., Mountney, N.P., Hodgson, D.M., and McCaffrey, W.D., 2016a, The Shallow- Marine Architecture Knowledge Store: a database for the characterization of shallow- marine and paralic depositional systems: Marine and Petroleum Geology, v. 75, p. 83–99.

Crain, E. R., 2015, Crain's Petrophysical Handbook [Online]: [Accessed 11 October 2019], Available from https://www.spec2000.net/.

Cruz, F.E. and Eberli, G.P., 2019, Co-existence of skeletal and ooid shoals because of antecedent topography—Cat cay shoal complex, Bahamas: The Depositional Record, v. 5, p. 451-468.

Dalrymple, R.W., Kurcinka, C.E., Jablonski, B.V.J., Ichaso, A.A., and MacKay, D.A., 2015, Deciphering the relative importance of fluvial and tidal processes in the fluvial-marine transition, *in* Ashworth P.J., Best J.L., Parsons, D.R., eds., Fluvial-Tidal Sedimentology: Amsterdam, Elsevier, p. 3-40.

Dalrymple, R.W., Baker, E.K., Harris, P.T., and Hughes, M.G., 2003, Sedimentology and stratigraphy of a tide-dominated, foreland-basin delta (Fly River, Papua New Guinea), *in* Sidi, F.H., Nummedal, D., Imbert P., Darman H., and Posamentier, H.W., eds., Tropical Deltas of Southeast Asia—Sedimentology, Stratigraphy, and Petroleum Geology: SEPM, Special Publication, v. 76, p. 147–173.

Dalrymple, R.W., Zaitlin, B.A. and Boyd, R., 1992, Estuarine facies models; conceptual basis and stratigraphic implications: Journal of Sedimentary Research, v. 62, p. 1130-1146.

Dalrymple, R.W., Knight, R.J., Zaitlin, B.A. and Middleton, G.V., 1990, Dynamics and facies model of a macrotidal sand-bar complex, Cobequid Bay—Salmon River Estuary (Bay of Fundy): Sedimentology, v. 37, p. 577-612.

Dalrymple, R.W. and Choi, K., 2007, Morphologic and facies trends through the fluvial-marine transition in tide- dominated depositional systems: a schematic framework for environmental and sequence stratigraphic interpretation: Earth-Science Review, v. 81, p. 135–174.

Dalrymple, R.W. and Rhodes, R.N., 1995, Estuarine dunes and bars, *in* Perillo, G.M.E, ed., Geomorphology and Sedimentology of Estuaries: Developments in Sedimentology, v. 53, p. 359-422.

Dalrymple, R.W., 2010, Tidal depositional systems, *in* James, N.P., and Dalrymple, R.W., eds., Facies Models 4: Geological Association of Canada, p. 201–231.

Dalrymple, R.W., 2006, Incised valleys in time and space: an introduction to the volume and an examination of the controls on valley formation and filling, *in* Dalrymple, R.W., Leckie, D. A., and Tillman, R.W., eds., Incised Valleys in Time and Space: SEPM, Society for Sedimentary Geology, p. 5–12.

Dashtgard, S.E., MacEachern, J.A., Frey, S.E., and Gingras, M.K., 2012, Tidal effects on the shoreface: towards a conceptual framework: Sedimentary Geology, v. 279, p. 42-61.

Dashtgard, S.E., Venditti, J.G., Hill, P.R., Sisulak, C.F., Johnson, S.M., and La Croix, A.D., 2012, Sedimentation across the tidal-fluvial transition in the Lower Fraser River, Canada: SEPM, Sedimentary Record, v. 10, p. 4-9.

Davies, J. L., 1964, A morphogenic approach to world shorelines. Zeitschrift für Geomorphologie, v. 8, p. 127-142

Davies, P.J., Bubela, B., and Ferguson, J., 1978, The formation of ooids: Sedimentology, v. 25, p. 703-730.

Davis, R.A., 2012, Tidal signatures and their preservation potential *in* stratigraphic sequences, *in* Davis Jr., R.A., Dalrymple, R.W., eds., Principles of Tidal Sedimentology: Berlin, Springer-Verlag, p. 35-55.

Davis, R.A., 1985, Coastal Sedimentary Environments, 2nd edition: New York, Springer-Verlag, 716 p.

Demarest, J. M., and Kraft, J. C., 1987, Stratigraphic record of Quaternary sea levels: implications for more ancient strata, *in* Nummedal, D., Pilkey, O.H., Howard, J.D., eds., Sea Level Fluctuation and Coastal Evolution: SEPM Special Publication, v. 41, p. 223–239.

Desjardins, P.R., Buatois, L.A. and Mangano, M.G., 2012a, Tidal flats and subtidal sand bodies, *in* Knaust, D., Bromley, R.G., eds., Trace fossils as indicators of sedimentary environment: Developments in Sedimentology, v. 64, p. 529-561.

Desjardins, P.R., Buatois, L.A., Pratt, B.R. and Mangano, M.G., 2012b, Sedimentological–ichnological model for tide-dominated shelf sandbodies: Lower Cambrian Gog Group of western Canada: Sedimentology, v. 59, p. 1452-1477.

Dorsey, R.J., Kidwell, S.M., 1999, Mixed carbonate-siliciclastic sedimentation on a tectonically active margin: example from the Pliocene of Baja California Sur, Mexico: Geology, v. 27, p. 935-938.

Driese, S.G., Srinivasan, K., Mora, C.I. and Stapor, F.W., 1994, Paleoweathering of Mississippian Monteagle Limestone preceding development of a lower Chesterian transgressive systems tract and sequence boundary, middle Tennessee and northern Alabama: Geological Society of America Bulletin, v. 106, p. 866-878.

Dunham, R.J., 1962, Classification of carbonate Rocks according to depositional texture, *in* Ham, W.E., ed., Classification of carbonate Rocks: American Association of Petroleum Geologists, Memoir 1, p. 108-121.

Einsele, G., 2000, Sedimentary Basins: Evolution, Facies, and Sediment Budget: Berlin, Springer-Verlag, 792 p.

Elliott, T., 1986, Deltas, *in* Reading, H.G., ed., Sedimentary Environments and Facies: Oxford, U.K., Blackwell Scientific Publications, p. 113–154.

Emery, D. and K.J. Myers. 1996, Sequence Stratigraphy: Victoria, Australia, Blackwell Science Ltd., 291 p.

Enay, R., C. Mangold, Y. Alméras and Hughes G.W. 2009, The Wadi ad Dawasir “delta”, central Saudi Arabia: GeoArabia, v. 14, p. 17-52.

Fairbridge, R.W. and RW, F., 1980, The estuary: its definition and geodynamic cycle, *in* Olausson, E. and Cato I, eds., Chemistry and Biogeochemistry of Estuaries: Wiley and Sons, New York, p. 1-36.

Faqira, M., Rademakers, M., and Afifi, A.M., 2009. New insights into the Hercynian Orogeny, and their implications for the Paleozoic hydrocarbon system in the Arabian Plate: GeoArabia, v. 14, p. 199-228.

Feldman, H. and Demko, T., 2015, Recognition and prediction of petroleum reservoirs in the fluvial/tidal transition, *in* Ashworth, P.J., Best, J.L., and Parsons, eds., Fluvial-Tidal Sedimentology: Developments in Sedimentology, v. 68, p. 483-528.

Fenies, H., Lericolais, G., Posamentier, H.W., 2010, Comparison of wave-and tide-dominated incised valleys: specific processes controlling systems tract architecture and reservoir geometry: Bulletin de la Société Géologique de France, v. 181, p. 171–181.

Fenies, H., Resseguier, A.D. and Tastet, J.P., 1999, Intertidal clay-drape couplets (Gironde estuary, France): Sedimentology, v. 46, p. 1-15.

Fenies, H and Tastet J-P, 1998, Facies and architecture of an estuarine tidal bar (the Trompeloup bar, Gironde Estuary, SW France): Marine Geology, v. 150, p. 149–169.

Fisher, W.L., Brown, L.F., Scott, A.J., and Mcgowen, J.H., 1969, Delta systems in the exploration for oil and gas: A research colloquium: Texas Bureau of Economic Geology: University of Texas at Austin, 78 p.

Fisk, H.N., McFarlan, E., Jr., Kolb, C.R. and Wilbert, L.J., Jr., 1954, Sedimentary framework of the modern Mississippi delta: Journal of Sedimentary Research, v. 24, p. 76-99

FitzGerald, D.M., Penland, S., Nummedal, D., 1984. Control of barrier island shape by inlet sediment bypassing: east Frisian Islands, West Germany: Marine Geology, v. 60, p. 355–376.

Frey, R.W., Howard, J.D., 1986, Mesotidal estuarine sequences: a perspective from the Georgia Bight: Journal of Sedimentary Petrology, v. 56, p. 911–924.

Galloway, W.E., 1975, Process framework for describing the morphologic and stratigraphic evolution of deltaic depositional systems, *in* Broussard, M.L., ed., Deltas– Models for exploration: Houston Geological Society, p. 87-98.

Gillespie, J.L., Nelson, C.S., 1997, Mixed siliciclastic-skeletal carbonate facies on Wanganui shelf, New Zealand: a contribution to the temperate carbonate, *in* James, N.P., Clarke, J.A.D., eds. Cool Water Carbonates: Sedimentary Geology, Special Publication, v. 56, p. 127-140.

Gingras, M.K., MacEachern, J.A., Dashtgard, S.E., Zonneveld, J.-P., Schoengut, J., Ranger, M.J., and Pemberton, S.G., 2012, Estuaries, *in* Knaust, D., Bromley, R.G., eds., Trace fossils as indicators of sedimentary environment: Developments in Sedimentology, v. 64, p. 463–505.

Gingras, M.K., MacEachern, J.A., Bromley, R.G., Buatois, L.A., Mángano, G., Genise, J.F., and Melchor, R.N., 2007, Recognition of brackish-water trace fossil suites in the Cretaceous Western Interior Seaway of Alberta, Canada: Society for Sedimentary Geology, Special Publication, v. 88, p. 149-193.

Ginsburg R.N., 1975, Tidal deposits: New York, Springer-Verlag, 428 p.

Godin, G., 1999, The propagation of tides up rivers with special considerations on the Upper Saint Lawrence River: Estuarine, Coastal and Shelf Science, v. 48, p. 307-324.

Golonka, J., 2007, Late Triassic and Early Jurassic palaeogeography of the world: Palaeogeography, Palaeoclimatolology, Palaeoecolology, v. 244, p. 297-307.

Gugliotta, M., Saito, Y., Nguyen, V.L., Ta, T.K.O., and Tamura, T., 2019, Sediment distribution and depositional processes along the fluvial to marine transition zone of the Mekong River delta, Vietnam: Sedimentology, v. 66, p. 146–164.

Gugliotta, M., Saito, Y., Nguyen, V. L., Ta, T. K. O., Nakashima, R., Tamura, T., Uehara, K., Katsuki, K. and Yamamoto, S., 2017, Process regime, salinity, morphological, and sedimentary trends along the fluvial to marine transition zone of the mixed-energy Mekong River Delta, Vietnam, *in* Ogston A. S., Allison M. A., Mullarney J. C., Nittrouer C. A., eds., Sediment- and Hydro-Dynamics of the Mekong Delta: From Tidal River to Continental Shelf: Continental Shelf Research, v. 147, p. 7–26.

Gugliotta, M., Flint, S.S., Hodgson, D.M. and Veiga, G.D., 2016, Recognition criteria, characteristics and implications of the fluvial to marine transition zone in ancient deltaic deposits (Lajas Formation, Argentina): Sedimentology, v. 63, p. 1971–2001.

Halfar, J., Godinez-Orta, L., Mutti, M., Valdez-Holguín, J.E., Borges, J.M., 2004, Nutrient and temperature control on modern carbonate production: an example from the Gulf of California, Mexico: Geology, v. 32, p. 213-216.

Haq, B.U., and Al-Qahtani, A.M., 2005, Phanerozoic cycles of sea-level change on the Arabian Platform: GeoArabia, v. 10, p. 127–160.

Haq, B.U., and Hardenbol, J., and Vail, P., 1988, Mesozoic and Cenozoic chronostratigraphy and cycles of sea-level change, *in* Wilgus, C. K., Hastings, B. S., Kendall, C. G. St. C., Posamentier, H. W., Ross, C. A., and Van Wagoner, J. C., eds., Sea level Changes–an integrated approach: Society of Economic Paleontologists and Mineralogists, Special Publication, v. 42, p. 71–108.

Harms, J.C., Southard, J.B., Spearing, D.R. and Walker, R.G., 1975, Depositional environments as interpreted from primary sedimentary structures and stratification sequences: SEPM, Short Course 2, 161 p.

Harris, P., Heap, A., Bryce, S., Porter-Smith, R., Ryan, D., and Heggie, D., 2002, Classification of Australian clastic coastal depositional environments

based upon a quantitative analysis of wave, tidal, and river power: Journal of Sedimentary Research, v. 72, p. 858-870.

Hayes, M. O., 1979, Barrier island morphology, *in* Leatherma, S. P., ed., Barrier Islands from the Gulf of Mexico to the Gulf of St. Lawrence: New York, Academic Press, p. 1-28.

Hein, F.J., 2015, The Cretaceous McMurray oil sands, Alberta, Canada: A world-class, tidally influenced fluvial–estuarine system—An Alberta government perspective, *in* Ashworth P.J., Best J.L., Parsons, D.R., eds., Fluvial-Tidal Sedimentology: Amsterdam, Elsevier, p. 561-621.

Heldreich, G., Redfern J., Legler B., Gerdes K., and Williams B.P.J., 2017, Challenges in characterizing subsurface paralic reservoir geometries: a detailed case study of the Mungaroo Formation, North West Shelf, Australia, *in* Hampson, G.J., Reynolds, A.D., Kostic, B., Wells, M.R., eds., Sedimentology of Paralic Reservoirs: Recent Advances: Geological Society of London, Special Publications 444, p. 59–108.

Hoekstra, P., ten Haaf, M., Buijs, P.H., Oost, A.P., Klein Breteler, R., van der Giessen, K., van der Vegt, M., 2009, Washover development on mixed-energy, mesotidal barrier island systems: Coastal Dynamics, v. 83, p. 25–32.

Houbolt, J.J.H.C., 1968, Recent sediments in the southern bight of the North Sea. Geology and Mining, v. 47, p. 245-273.

Howell, J.A., Martinius, A.W. and Good, T.R., 2014, The application of outcrop analogues in geological modelling: a review, present status and future outlook, *in* Martinius, A.W, Howell, J.A., and Good, T.R., Sediment-Body Geometry and Heterogeneity: Analogue Studies for Modelling the Subsurface: Geological Society of London, Special Publications, v. 387, p. 1-25.

Howell, J.A., Skorstad, A., MacDonald, A., Fordham, A., Flint, S., Fjellvoll, B., and Manzocchi, T., 2008, Sedimentological parameterization of shallow-marine reservoirs: Petroleum Geoscience, v. 14, p. 17-34.

Hubbard, S.M., Smith, D.G., Nielsen, H., Leckie, D.A., Fustic, M., Spencer, R.J. and Bloom, L., 2011, Seismic geomorphology and sedimentology of a tidally influenced river deposit, Lower Cretaceous Athabasca oil sands, Alberta, Canada. American Association of Petroleum Geologist, Bulletin, v. 95, p. 1123-1145.

Hughes, G.W., 2006, Biofacies and palaeoenvironments of the Jurassic Shaqra' Group of Saudi Arabia, Volumina Jurassica, v.4, p. 89-90.

Jackson, M.D., Yoshida, S., Muggeridge, A.H. and Johnson, H.D. 2005, Three-dimensional reservoir characterisation and flow simulation of heterolithic tidal sandstones: American Association of Petroleum Geologists, Bulletin, v. 89, p. 507–528.

Johnson, H.D. and Baldwin, C.T., 1986., Shallow siliciclastic seas, *in* Reading H.G., ed., Sedimentary Environments and Facies: London, Blackwell, p. 229-282.

Kitazawa, T., 2007, Pleistocene macrotidal tide-dominated estuary–delta succession, along the Dong Nai River, southern Vietnam: Sedimentary Geology, v. 194, p. 115-140.

Klein, G. de V., 1985, Intertidal flats and intertidal sand bodies, *in* Davis, R.A., ed., Coastal Sedimentary Environments, 2nd Edition: New York, Springer-Verlag, p. 187–224.

Kraus, M., 1999, Paleosols in clastic sedimentary rocks: their geologic applications: Earth-Science Reviews, v. 47, p. 41-70.

Kraus, M.J., 2002, Basin-scale changes in floodplain paleosols: implications for interpreting alluvial architecture: Journal of Sedimentary Research, v. 72, p. 500-509.

La Croix, A.D., Dashtgard, S.E. and MacEachern, J.A., 2019, Using a modern analogue to interpret depositional position in ancient fluvial-tidal channels: example from the McMurray Formation, Canada: Geoscience Frontiers, v. 10, p. 2219-2238.

La Croix, A.D. and Dashtgard, S.E., 2015, A synthesis of depositional trends in intertidal and upper subtidal sediments across the tidal-fluvial transition in the Fraser River, Canada: Journal of Sedimentary Research, v. 85, p. 683-698.

La Croix, A. and Dashtgard, S., 2014, Of sand and mud: sedimentological criteria for identifying the turbidity maximum zone in a tidally influenced river: Sedimentology, v. 61, p. 1961–1981.

Lake, L.W. and Jensen, J.L., 1991, A review of heterogeneity measures used in reservoir characterization: In situ, v.15, p. 409-440.

Lander, R.H., Bloch, S., Mehta, S., Atkinson, C.D., 1991, Burial diagenesis of paleosols in the giant Yacheng gas field, People's Republic of China: bearing on illite reaction pathways: Journal of Sedimentary Research, v. 61, p. 256–268.

Lee, H.S., Chough, S.K., 2011. Depositional processes of the Zhushadong and Mantou formations (Early to Middle Cambrian), Shandong Province, China: roles of archipelago and mixed carbonate-siliciclastic sedimentation on cycle genesis during initial flooding of the North China Platform: Sedimentology, v. 58, p. 1530-1572.

Legarreta, L., and Uliana, M.A., 1996, The Jurassic succession in west-central Argentina: stratal patterns, sequences and paleogeographic evolution: Palaeogeography, Palaeoclimatology, Palaeoecology, v. 120, p. 303–330.

Lesourd, S., Lesueur, P., Brun-Cottan, J.C., Garnaud, S. and Poupinet, N., 2003, Seasonal variations in the characteristics of superficial sediments in a macrotidal estuary (the Seine inlet, France): Estuarine, Coastal and Shelf Science, v. 58, p. 3-16.

Leuven, J.R.F.W., Kleinhans, M.G., Weisscher, S.A.H. and Van der Vegt, M., 2016, Tidal sand bar dimensions and shapes in estuaries: Earth-Science reviews, v. 161, p. 204-223.

Levell, B.K., Johnson, H.D., Collins, D. S. and van Cappelle, M., 2020. Deposition and preservation of fluvio-tidal shallow-marine sandstones: A re-evaluation of the Neoproterozoic Jura Quartzite (western Scotland): Sedimentology, v. 67, p. 173-206.

Livera, S.E., and Caline, B., 1990, The sedimentology of the Brent Group in the Cormorant block IV oilfield: Journal of Petroleum Geology, v. 13, p. 367-396.

Loisel, H., Mangin, A., Vantrepotte, V., Dessailly, D., Dinh, D.N., Garnesson, P., Ouillon, S., Lefebvre, J.P., Meriaux, X. and Phan, T. M., 2014. Variability of suspended particulate matter concentration in coastal waters under the Mekong's influence from ocean color (MERIS) remote sensing over the last decade: Remote Sensing of Environment, v. 150, p. 218-230.

Longhitano, S.G., Mellere, D., Steel, R.J., and Ainsworth, R.B., 2012, Tidal depositional systems in the rock record: a review and new insights: Sedimentary Geology, v. 279, p. 2-22.

Longhitano, S.G., 2011, The record of tidal cycles in mixed silici-bioclastic deposits: examples from small Plio-Pleistocene peripheral basins of the microtidal central Mediterranean Sea: Sedimentology, v. 58, p. 691–719

Longhitano, S.G., Sabato, L., Tropeano, M., Gallicchio, S., 2010, A mixed bio-clastic-siliciclastic flood-tidal delta in a microtidal setting: depositional architectures and hierarchical internal organization (Pliocene, southern apennine, Italy): Journal of Sedimentary Research, v. 80, p. 36-53.

MacEachern, J.A., Dashtgard, S.E., Knaust, D., Catuneanu, O., Bann, K.L., and Pemberton, S.G., 2012, Sequence stratigraphy, *in* Knaust, D., Bromley, R.G., eds., Developments in Sedimentology: Amsterdam, Elsevier, p. 157–194.

MacEachern, J.A., Bann, K.L., 2008, The role of ichnology in refining shallow marine facies models, *in* Hampson, G., Steel, R., Burgess, P., Dalrymple, R., eds., Recent Advances in Models of Siliciclastic Shallow-Marine Stratigraphy: SEPM, Special Publication 90, p. 73–116.

MacEachern, J.A., Bann, K.L., Bhattacharya, J.P., and Howell, C.D., 2005, Ichnology of deltas: organism responses to the dynamic interplay of rivers, waves, storms, and tides, *in* Giosan, L., and Bhattacharya, J.P., eds., River Deltas: Concepts, Models, and Examples: SEPM, Special Publication 83, p. 49–85.

MacEachern, J.A., Raychaudhuri, I., and Pemberton, S.G., 1992, Stratigraphic applications of the Glossifungites ichnofacies: delineating discontinuities in the rock record, *in* Pemberton, S.G., ed., Application of Ichnology to Petroleum

Exploration: A Core Workshop: Society of Economic Palaeontologists and Mineralogists, p. 169–198.

MacEachern, J.A., and Pemberton, S.G., 1994, Ichnological aspects of incised valley fill systems from the Viking Formation of the western Canada Sedimentary basin, Alberta, Canada, *in* Boyd, R., Zaitlin,B.A., Dalrymple, R.W., eds., Incised Valley Systems: Origin and Sedimentary Sequences: Society for Sedimentary Geology Special Publication, v. 51, p. 129-157.

Magalhaes, A.J.C, Scherer, C.M.S., Gabaglia, G.P.R., Ballico, M.B., and Catuneanu, O., 2014, Unincised fluvial and tide-dominated estuarine systems from the Mesoproterozoic Lower Tombador Formation, Chapada Diamantina basin, Brazil: Journal of South American Earth Science, v. 56, p. 68-90.

Maguregui, J. and Tyler, N., 1992, Evolution of middle Eocene tide-dominated deltaic sandstones, Lagunillas field, Maracaibo basin, western Venezuela, *in* Miall, A.D. and Tyler, N., eds., Concepts of Sedimentology and Paleontology: SEPM, Special Publication, v. 3, p 233-244.

Manivit, J., Le Nindre, Y., Vaslet, D., 1990. Le Jurassique d'Arabie Centrale Histoire Geologique de la Bordure Occidentale de la Plate-forme Arabe. Documents du Bureau de la Recherche Géologique et Minière.

Martin, C.A.L., 1995, The origin of massive sandstone facies in an ancient braided river deposits [PhD Thesis]: Durham University, Durham, United Kingdom, 329 p.

Martini, I., and Aldinucci M., 2017, Sedimentation and basin-fill history of the Pliocene succession exposed in the northern Siena-Radicofani Basin (Tuscany, Italy): a sequence-stratigraphic approach: Research in Palaeontology and Stratigraphy, v. 123, p. 407-432.

Martinius, A.W. and Gowland, S., 2011, Tide-influenced fluvial bedforms and tidal bore deposits (late Jurassic Lourinhã Formation, Lusitanian Basin, Western Portugal): Sedimentology, v. 58, p. 285-324.

Martinius, A.W., Jablonski, B.V.J., Fustic, M., Strobl, R. and Van den Berg, J.H., 2015, Fluvial to tidal transition zone facies in the McMurray Formation (Christina River, Alberta, Canada), with emphasis on the reflection of flow intensity in bottomset architecture, *in* Ashworth P.J., Best J.L., and Parsons, D.R., eds., Fluvial-Tidal Sedimentology: Amsterdam, Elsevier, v. 68, p. 445–480.

Martinius, A.W., Kaas, I., Naess, A., Helgesen, G., Kjaeresfjord, J.M., Leith, D.A., 2001, Sedimentology of the heterolithic and tide-dominated Tilje Formation (Early Jurassic, Halten Terrace, offshore mid-Norway), *in* Martinsen, O.J., Dreyer, T. eds., Sedimentary Environments Offshore Norway – Palaeozoic to Recent: Norwegian Petroleum Society, special publication, v. 10, p. 103-144.

Martinius, A.W., Ringrose P.S., Brostrom , C., Elfenbein, C., Nass, A., and Ringas, J.E., 2005, Reservoir Challenges of Heterolithic Tidal Sandstone Reservoirs in Halten Terrace, mid-Norway: Petroleum Geoscience, v. 11, p. 3-16.

Massart, B.Y.G., Jackson, M.D., Hampson, G.J. and Johnson, H.D., 2016, Effective flow properties of heterolithic, cross-bedded tidal sandstones, part 2: flow simulation: American Association of Petroleum Geologists, Bulletin, v. 100, p. 723–742.

Maynard, J.B., 1983, Geochemistry of Sedimentary Ore Deposits: New York, Springer-Verlag, 305 p.

McLean, A.Q. and Wilson, B., 2017, Recognizing seasonal fluvial influence in ancient tidal deposits: Geological Society of London, Special Publications, v. 444, p. 287-303.

Meade, R.H., 1972, Transport and deposition of sediments in estuaries, *in* Nelson, B.W, ed., Environmental Framework of Coastal Plain Estuaries: Geological Society of America, v. 133, p. 91-120.

Meene, J.W.H., Boersma, J.R., and Terwindt, J.H.J., 1996, Sedimentary structures of combined flow deposits from the shoreface-connected ridges along the central Dutch coast: Marine Geology, v. 131, p. 151–175.

Melnyk, S and Gingras, M. K., 2020. Using ichnological relationships to interpret heterolithic fabrics in fluvio-tidal settings: Sedimentology, v. 67, p. 1069-1083.

Meyer, R., Engesgaard, P., and Sonnenborg, T.O., 2019, Origin and Dynamics of Saltwater Intrusion in a Regional Aquifer: Combining 3-D Saltwater Modeling with Geophysical and Geochemical Data: Water Resources Research, 55, p. 1792-1813.

Miall, A.D., 2010, Alluvial deposits, *in* Walker, R.G. and James, N.P., eds., Facies Models 4: Response to Sea-Level Change: Geological Association of Canada, p. 119-142.

Miall, A.D., 1985, Architectural-element analysis: a new method of facies analysis applied to fluvial deposits: Earth-Science Reviews, v. 22, p. 261-308.

Miall, A.D., 1976, Facies models 4. Deltas: Geoscience Canada, v. 3, p. 215-227.

Moissette, P., Cornee, J.J., Mannaï-Tayech, B., Rabhi, M., Andre, J.P., Koskeridou, E., Meon, H., 2010. The western edge of the Mediterranean Pelagian Platform: a Messinian mixed siliciclastic-carbonate ramp in northern Tunisia: Palaeogeography, Palaeoclimatology, Palaeoecology,v. 285, p. 85-103.

Mutti, E., Rosell, J., Allen, G., Fonnesu, F. and Sgavetti, M., 1985. The Eocene Baronia tide dominated delta-Sheff system in the Ager Basin. In 6th European Regional Meeting. International Association of sedimentologists, Excursion Guidebook, p. 577-600.

Nguyen, V.L., Ta, T.K.O. and Tateishi, M., 2000, Late Holocene depositional environments and coastal evolution of the Mekong River Delta, Southern Vietnam. Journal of Asian Earth Sciences, v. 18, p. 427-439.

Nichols, M.M., 1989, Sediment accumulation rates and relative sea-level rise in lagoons: Marine Geology, v. 88, p. 201–219.

Nio, S.D. and Yang, C.S., 1991, Diagnostic attributes of clastic tidal deposits: a review, *in* Smith, D.G., Reinson, G.E., Zaitlin, B.A. Rahmani, R.A., eds., Clastic Tidal Sedimentology: Canadian Society of Petroleum Geologists, Memoirs 16, p. 3-28.

Nyberg, B. and Howell, J.A., 2016, Global distribution of modern shallow marine shorelines. Implications for exploration and reservoir analogue studies: Marine and Petroleum Geology, v. 71, p.83-104.

Oertel, G.F., Kearney, M.S., Leatherman, S.P., Woo, H., 1989. Anatomy of a barrier platform: outer barrier lagoon, southern Delmarva Peninsula, Virginia: Marine Geology, v. 88, p. 303–318.

Olariu, C., Steel, R.J., Olariu, M.I. and Choi, K., 2015. Facies and architecture of unusual fluvial–tidal channels with inclined heterolithic strata: Campanian Neslen Formation, Utah, USA. In Developments in Sedimentology (Vol. 68, pp. 353-394). Elsevier.

Olariu, C., Steel, R.J., Dalrymple, R.W. and Gingras, M.K., 2012, Tidal dunes versus tidal bars: The sedimentological and architectural characteristics of compound dunes in a tidal seaway, the lower Baronia Sandstone (Lower Eocene), Ager Basin, Spain: Sedimentary Geology, v. 279, p. 134-155.

Orton, G., Reading, H., 1993, Variability of deltaic processes in terms of sediment supply, with particular emphasis on grain size: Sedimentology, v. 40, p. 475-512.

Pemberton, S.G. MacEachern, J.A., Dashtgard, S.E., Bann, K.L., Gingras M.K., and Zonneveld J-P., 2012, Shorefaces, *in* Knaust, D., and Bromley, R.G., eds., Trace Fossils as Indicators of Sedimentary Environments: Amsterdam, Elsevier, v. 64, p. 563-603.

Pemberton, S.G., and Frey, R.W., 1985, The Glossifungites ichnofacies: modern examples from the Georgia coast, *in* Curran, H.A., ed., Biogenic Structures: Their Use in Interpreting Depositional Environments: Society of Economic Paleontologists and Mineralogists, Special Publication, p. 237–259.

Pemberton, S.G., and MacEachern, J.A., 1997, The ichnological signature of storm deposits: the use of trace fossils in event stratigraphy, *in* Brett, C.E., ed., Paleontological Event Horizons: New York, Columbia University Press, p. 73-109.

Pemberton, S.G., Reinson, G.E., and MacEachern, J.A., 1992, Comparative ichnological analysis of late Albian estuarine valley-fill and shelf-shoreface deposits, *in* Pemberton, S.G., ed., Applications of Ichnology to Petroleum Exploration. Society of Economic Paleontologists and Mineralogists, p. 291–317.

Pemberton, S.G., Spila, M., Pulham, A.J., Saunders, T., MacEachern, J.A., Robbins, D., and Sinclair, I.K., 2003, Ichnology and sedimentology of shallow

marine to marginal marine systems: Ben Nevis & Avalon reservoirs, Jeanne d'Arc Basin: Bulletin of Canadian Petroleum Geology, v. 51, p. 206-211.

Plink-Björklund, P., 2005, Stacked fluvial and tide-dominated estuarine deposits in high-frequency (fourth-order) sequences of the Eocene Central Basin, Spitsbergen: Sedimentology, v. 52, p. 391-428.

Pontén, A. and Plink-Björklund, P., 2009, Regressive to transgressive transits reflected in tidal bars, Middle Devonian Baltic Basin: Sedimentary Geology, v. 218, p.48-60.

Porebsky, S.J., and Steel, R.J., 2006, Deltas and sea-level change: Journal of Sedimentary Research, v. 76, p. 390–403.

Powers, R., Ramirez, L., Redmond, C., and Elberg, E., 1966, Geology of the Arabian Peninsula: Washington, D.C., United States Government Printing Office, 147 p.

Powers, R.W., 1968, Lexique Stratigraphique International: Paris, Centre National de la Recherche Scientifique, p. 73–109.

Prokocki, E.W., Best, J.L., Ashworth, P., Parsons, D.R., Sambrook Smith, G.H., Nicholas, A.P., Simpson, C.J., Wang, H., Sandbach, S. and Keevil, C., 2015, Mid to late Holocene geomorphological and sedimentological evolution of the fluvial–tidal zone: Lower Columbia River, WA/OR, USA, *in* Ashworth P.J., Best J.L., Parsons, D.R., eds., Fluvial-Tidal Sedimentology: Amsterdam, Elsevier, v. 68, p. 193–226.

Rankey, E.C., 2002, Spatial patterns of sediment accumulation on a Holocene carbonate tidal flat, northwest Andros Island, Bahamas: Journal of Sedimentary Research, v. 72, p. 591-601.

Rankey, E.C., and Reeder, S.L., 2012, Tidal sands of the Bahamian archipelago, *in* Davis, R.A., Dalrymple, R.W., eds., Principles of Tidal Sedimentology: Berlin, Springer-Verlag, p. 537–565.

Reading, H.G., Collinson, J.D., 1996, Clastic coasts, *in* Reading, H.G., ed., Sedimentary Environments: Processes, Facies and Stratigraphy: Blackwell Publishing, University of Oxford, ed. 3, p. 154-231

Reineck, H-E., and Singh, I.B., 1980. Depositional Sedimentary Environments - with reference to terrigenous clastic, 2nd Edition: Berlin, Springer-Verlag, 549 p.

Reineck, H-E., and Wunderlich, F. 1968. Classification and origin of flaser, and lenticular bedding: Sedimentology, v. 11, 99–104.

Retallack, G. Soils of the Past, 2001, 2nd Edition: London, Blackwell Science Limited, 404 p.

Reynaud, J.-Y., and Dalrymple, R., 2012, Shallow-marine tidal deposits, *in* Davis, R.A.J., and Dalrymple, R.W., eds., Principles of Tidal Sedimentology: Berlin, Springer, p. 335- 369.

Reynolds, A.D., 2017, Paralic reservoirs, *in* Hampson, G.J., Reynolds, A.D., Kostic, B. and Wells, M.R., eds., Sedimentology of Paralic Reservoirs: Recent Advances: Geological Society of London, Special Publications 444, p. 7-34.

Ringrose, P.S., Nordhal, K., and Wen, R., 2005, Vertical permeability estimation of heterolithic tidal deltaic sandstones: Petroleum Geoscience, v. 11, p. 29–36.

Robert, C., and Chamley, H., 1991, Development of early Eocene warm climates, as inferred from clay mineral variations in oceanic sediments: Global and Planetary Change, v. 3, p. 315–331.

Roberts, H.H., 1987, Modern carbonate-siliciclastic transitions: humid and arid tropical examples: Sedimentary Geology, v. 50, p. 25-65.

Rossi, V.M., and Steel, R.J., 2016, The role of tidal, wave and river currents in the evolution of mixed-energy deltas: Example from the Lajas Formation (Argentina): Sedimentology, v. 63, p. 824-864.

Roy, P.S., Thom, B.G. and Wright, L.D., 1980, Holocene sequences on an embayed high-energy coast: an evolutionary model: Sedimentary Geology, v. 26, p. 1-19.

Saha, S., Burley, S.D. and Banerjee, S., 2018, Mixing processes in modern estuarine sediments from the Gulf of Khambhat, western India: Marine and Petroleum Geology, v. 91, p. 599-621.

Saha, S., Burley, S.D., Banerjee, S., Ghosh, A. and Saraswati, P.K., 2016, The morphology and evolution of tidal sand bodies in the macrotidal Gulf of Khambhat, western India: Marine and Petroleum Geology, v. 77, p. 714-730.

Schlaich, M., and Aigner, T., 2017, Facies and integrated sequence stratigraphy of an Epeiric Carbonate Ramp Succession: Dhruma Formation, Sultanate of Oman: Sedimentology, v. 3, p. 62-132.

Schumm, S., 1985, Patterns of alluvial rivers: Annual Review of Earth and Planetary Sciences, v. 13, p. 5-27

Scotese, C.R., 2001, Atlas of earth history: Palaeogeography 1, 52 p.

Seton, M., Muller, R.D., Zahirovic, S., Gaina, C., Torsvik, T., Shephard, G., Talsma, A., Gurnis, M., Turner, M., Maus, S., and Chandler, M., 2012, Global continental and ocean basin reconstructions since 200 Ma: Earth-Science Reviews, v. 113, p. 212–270.

Shanley, K.W., McCabe, P.J., 1994. Perspectives on the sequence stratigraphy of continental strata: American Association of Petroleum Geologist, Bulletin, v. 78, p. 544-568.

Shanmugam, G., Poffenberger, M., Toro Álava, J., 2000, Tide-Dominated Estuarine Facies in the Hollin and Napo (“T” and “U”) Formations (Cretaceous), Sacha Field, Oriente Basin, Ecuador: American Association of Petroleum Geologists, Bulletin, v. 84, p. 652-682.

Shchepetkina, A., Gingras, M.K., and Pemberton, S.G., 2016, Sedimentology and ichnology of the fluvial reach to inner estuary of the Ogeechee River estuary, Georgia, USA: Sedimentary Geology, v. 342, p. 202–217.

Shiers, M.N., 2016, Controls on the deposition, accumulation and preservation of mixed fluvial and marginal-marine successions in coastal-plain settings [PhD Thesis] University of Leeds, United Kigdom.

Shiers, M.N., Mountney, N.P., Hodgson, D.M. and Cobain, S.L., 2014, Depositional Controls on Tidally Influenced Fluvial Successions, Neslen Formation, Utah, USA: Sedimentary Geology, v. 311, p. 1-16.

Soliman, F.A., Shamlan, A.A., 1982, Review on the geology of the Cretaceous sediments of the Rub' al-Khali, Saudi Arabia: Cretaceous Research, v. 3, p. 187–194.

Soreghan, G.S., Elmore, R.D., Katz, B., Cogoini, M., Banerjee, S., 1997, Pedogenically enhanced magnetic susceptibility variations preserved in Paleozoic loessite: Geology, v. 25, p. 1003–1006.

Stampfli, G.M., and Borel, G.D., 2002, Aplate tectonic model for the Paleozoic and Mesozoic constrained by dynamic plate boundaries and restored synthetic oceanic isochrons: Earth and Planetary Science Letters, v. 196, p. 17–33.

Steel, R.J., Plink-Bjorklund, P. and Aschoff, J., 2012, Tidal deposits of the Campanian Western Interior Seaway, Wyoming, Utah and Colorado, USA, *in* Davis, R.A. and Dalrymple, R.W., eds., Principles of Tidal Sedimentology: Dordrecht, Springer, p. 437-471.

Stewart, S.A., 2016, Structural geology of the Rub' Al-Khali Basin, Saudi Arabia: Tectonics, v. 35, p. 2417–2438.

Stewart, S.A., Reid, C.T., Hooker, N.P., and Kharouf, O.W., 2016, Mesozoic siliciclastic reservoirs and petroleum system in the Rub' Al-Khali basin, Saudi Arabia: American Association of Petroleum Geologists, Bulletin, v. 100, p. 819–841.

Tanavsuu-Milkeviciene, K., Plink-Bjorklund, P., Kirsimae, K. and Ainsaar, L., 2009, Coeval versus reciprocal mixed carbonate–siliciclastic deposition, Middle Devonian Baltic Basin, Eastern Europe: implications from the regional tectonic development: Sedimentology, v. 56, p.1250-1274.

Tandon, S.K., Good, A., Andrews, J.E., Dennis, P.F., 1995, Palaeoenvironments of the dinosaur-bearing Lameta Beds (Maastrichtian), Narmada Valley, Central India. Palaeogeography., Palaeoclimatology., Palaeoecology, v.117, p. 153–184.

Tang, M., Zhang, K., Huang, J. and Lu, S., 2019. Facies and the architecture of estuarine tidal bar in the lower Cretaceous Mcmurray Formation, Central Athabasca Oil Sands, Alberta, Canada: Energies, v. 12, p.1769.

Tawfik, M., Al-Dabbagh, M., and El-Sorogy, A., 2016, Sequence stratigraphy of the late middle Jurassic open shelf platform of the Tuwaiq Mountain Limestone

Formation, central Saudi Arabia: Proceedings of the Geologists' Association, v. 127, p. 395–412.

Taylor, A.M. and Goldring, R., 1993, Description and analysis of bioturbation and ichnofabric: Journal of the Geological Society, v. 150, p. 141-148.

Tessier, B., 1993, Upper intertidal rhythmites in the Mont-Saint-Michel Bay (NW France): perspectives for paleoreconstruction: Marine Geology, v. 110, p. 355–367.

Thrana, C., Talbot, M.R., 2006, High-frequency carbonate-siliciclastic cycles in the Miocene of the Lorca Basin (Western mediterranean, SE Spain): Geological Acta, v. 3, p. 343-354.

Tirsgaard, H., 1996, Cyclic sedimentation of carbonate and siliciclastic deposits on a late Precambrian ramp; the Elisabeth Bjerg Formation (Eleonore Bay Supergroup), East Greenland: Journal of Sedimentary Research, v. 66, p. 699-712.

Vakarelov, B.K. and Ainsworth, R.B., 2013, A hierarchical approach to architectural classification in marginal-marine systems: bridging the gap between sedimentology and sequence stratigraphy: American Association of Petroleum Geologist, Bulletin, v. 97, p .1121-1161.

Van Cappelle, M., Stukins, S., Hampson, G.J. and Johnson, H.D., 2016, Fluvial to tidal transition in proximal, mixed tide-influenced and wave-influenced deltaic deposits: Cretaceous lower Sego Sandstone, Utah, USA: *Sedimentology*, v. *63*, p. 1333-1361.

Van de Lageweg, W.I., Braat, L., Parsons, D.R., and Kleinhans, M. G., 2018, Controls on mud distribution and architecture along the fluvial-to-marine transition: Geology, v. 46, p. 971– 974.

Van den Berg, J.H., Boersma, J.R., Van Gelder, A., 2007, Diagnostic sedimentary structures of the fluvial–tidal transition zone. Evidence from deposits of the Rhine Delta: Netherland Journal of Geoscience, v. 86, p. 253–272.

Van Der Wal, D., Pye, K. and Neal, A., 2002, Long-term morphological change in the Ribble Estuary, northwest England: Marine Geology, v. 189, p. 249-266.

Van Houten, F.B. 1985, Oolitic ironstones and contrasting Ordovician and Jurassic paleogeography: Geology, v. 13, p. 722-24.

Van Wagoner, J.C., Mitchum, R.M., Campion, K.M., and Rahmanian, V.D., 1990, Siliciclastic Sequence Stratigraphy in Well Logs, Cores and Outcrops: Concepts for High-resolution Correlation of Time and Facies: American Association of Petroleum Geologists, Methods in Exploration Series 7, 55 p.

Vaslet, D., Manivit, J., Le Nindre, Y., Brosse, J., Fourniguet, J., Delfour, J., 1983, Explanatory Notes to the Geologic Map of the Wadi Ar Rayn Quadrangle, Kingdom of Saudi Arabia: Saudi Arabian Deputy Ministry for Mineral Resources, Geoscience Map GM-63C.

Vicalvi, M.A. and Milliman, J.D., 1977, Calcium carbonate sedimentation on continental shelf off Southern Brazil, with special reference to Benthic Foraminifera, *in* Frost, S.H., Weiss, M. P., and Saunders, J. B., eds., Reefs and Related Carbonates–Ecology and Sedimentology: American Association of Petroleum Geologists, Studies in Geology 4, p. 313-328.

Virolle, M., Féniès, H., Brigaud, B., Bourillot, R., Portier, E., Patrier, P., Beaufort, E., Jalon-Rojas, I., Derriennic, H., Misk, S., 2020, Facies associations, detrital clay grain coats and mineralogical characterization of the Gironde estuary tidal bars: A modern analogue for deeply buried estuarine sandstone reservoirs: Marine and Petroleum Geology, v. 114, p. 1-25.

Virolle, M., Brigaud, B., Bourillot, R., Féniès, H., Portier, E., Duteil, T., Nouet, J., Patrier, P. and Beaufort, D., 2019, Detrital clay grain coats in estuarine clastic deposits: origin and spatial distribution within a modern sedimentary system, the Gironde Estuary (south-west France): Sedimentology, v. 66, p. 859-894.

Visser, M.J., 1980, Neap-spring cycles reflected in Holocene subtidal large scale bedform deposits: a preliminary note: Geology, v. 8, p. 543-546.

Wakefield, O. J. W., Mountney, N.P., 2013, Stratigraphic architecture of back-filled incised-valley systems: Pennsylvanian-Permian lower Cutler beds, Utah, USA: Sedimentary Geology, v. 298, p. 1-16.

Weaver, C.E., 1989, Clays, Muds, and Shales: Amsterdam, Elsevier, v. 44, 818 p.

Webb, G.E., 1994, Paleokarst, paleosol, and rocky-shore deposits at the Mississipian–Pennsylvanian unconformity, northwestern Arkansas: Geological Society of America Bulletin, v. 106, p. 634–648

Wightman, D. M., and Pemberton, S. G., 1997, The lower Cretaceous (Aptian) McMurray Formation: an overview of the Fort McMurray area, northeastern Alberta, *in* Pemberton, S.G., and James, D.P., eds., Petroleum Geology of the Cretaceous Mannville Group: Canadian Society of Petroleum Geologists, Memoir 18, p. 312–344.

Willis, B.J. and Gabel, S.L., 2003, Formation of deep incisions into tide-dominated river deltas: implications for the stratigraphy of the Sego Sandstone, Book Cliffs, Utah, USA: Journal of Sedimentary Research, v. 73, p. 246-263.

Willis, B.J., Bhattacharya, J.P., Gabel, S.L. and White, C.D., 1999, Architecture of a tide-influenced river delta in the Frontier Formation of central Wyoming, USA: Sedimentology, v. 46, p. 667-688.

Wood, L.J., 2004, Predicting tidal sand reservoir architecture using data from modern and ancient depositional systems, *in* Grammer, G.M., Harris, P.M., and Eberli, G.P., eds., Integration of Outcrop and Modern Analogs in Reservoir Modeling: American Association of Petroleum Geologists, v. 80, p. 1–22.

Woodroffe, C.D., Chappell, J., Thom, B.G. and Wallensky, E., 1989, Depositional model of a macrotidal estuary and floodplain, South Alligator River, Northern Australia: Sedimentology, v. 36, p. 737-756.

Woodroffe, c.d., Chappell, J.M.A., Thom, B.G. & Wallensky, E., 1985, Geomorphology of the South Alligator tidal river and plains, Northern Territory, *in* Bardsley, K. N, Davie, J. D. S., and Woodroffe, C.D, eds., Coasts and Tidal Wetlands of the Australia Monsoon Region: NARU Monograph, ANU Press, Canberra, p. 3-15.

Wright, V.P., Platt, N.H., 1995, Seasonal wetland carbonate sequences and dynamic catenas; a re-appraisal of palustrine limestones: Sedimentary Geology, v. 99, p. 65–71.

Wright, V.P., 1994, Paleosols in shallow marine carbonate sequences: Earth-Science Review, v. 35, p. 367–395.

Yang, B., Dalrymple, R.W., Gingras, M.K., Chun, S. and Lee, H., 2007, Up-estuary variation of sedimentary facies and ichnocoenoses in an open-mouthed, macrotidal, mixed-energy estuary, Gomso Bay, Korea: Journal of Sedimentary Research, v. 77, p. 757-771.

Yeo, R.K. and Risk, M.J., 1981, The sedimentology, stratigraphy, and preservation of intertidal deposits in the Minas basin system, Bay of Fundy: Journal of Sedimentary Petrology, v. 51, p. 245–260.

Yu, Q., Wang, Y., Gao, S. and Flemming, B., 2012, Modeling the formation of a sand bar within a large funnel-shaped, tide-dominated estuary: Qiantangjiang Estuary, China: Marine Geology, v. 299, p. 63-76.

Ziegler, M.A., 2001, Late Permian to Holocene paleofacies evolution of the Arabian Plate and its hydrocarbon occurrences: GeoArabia, v. 6, p. 445–504.

Appendix I

Sedimentology and stratigraphic architecture of a fluvial to shallow-marine succession: the Jurassic Dhruma Formation, Saudi Arabia

BASSAM ALSHAMMARI[a,b], NIGEL P. MOUNTNEY[a], LUCA COLOMBERA[a], MOHAMMED A. AL-MASRAHY[b]

[a] *Fluvial, Eolian & Shallow-Marine Research Group, School of Earth and Environment, University of Leeds, LS2 9JT, UK*

[b] *Exploration Organization, Saudi Aramco, Dhahran 31311, Saudi Arabia*

ABSTRACT

The interaction of fluvial, tidal, and wave processes in coastal and paralic environments gives rise to sedimentary succession with highly varied styles of facies architecture; these are determined by the morphology and evolutionary behavior of the range of coastal sub-environments, which may be difficult to diagnose in subsurface sedimentary successions with limited well control.

This study presents depositional models to account for stratigraphic complexity in a subsurface fluvial to shallow-marine succession, the Middle Jurassic Dhruma Formation, Saudi Arabia. The study achieves the following: (i) it examines and demonstrates sedimentary relationships between various fluvial, nearshore, and shallow-marine deposits; (ii) it develops depositional models to account for the stratigraphic complexity inherent in fluvial to shallow-marine successions; and (iii) it documents the sedimentology and the stratigraphic evolutionary patterns of the lower Dhruma Formation in the studied area of Saudi Arabia. The dataset comprises facies descriptions of approximately 570 m of core from 14 wells, 77 representative core

thin sections, 14 gamma-ray logs, and FMI image logs from 4 wells. These data are integrated with quantitative information from > 50 analogous systems from a wide range of modern and ancient settings, stored in a relational database. Stratigraphic correlations reveal the internal anatomy of the succession.

Facies associations are representative of fluvial channels, intertidal flats, pedogenically modified supratidal flats or floodplains, river-influenced tidal bars, weakly storm-affected shoreface and offshore-transition zones, storm-dominated delta-front and prodelta settings, and an open-marine carbonate-dominated shelf. These sub-environments interacted in a complex way through space and time. The vertical succession of the studied interval records an overall transition from coastal-plain deposits at the base to marine deposits at the top. As such, the succession records a long-term transgressive, deepening-upward trend. However, this general trend is punctuated by repeated progradational events whereby coastal sand bodies of fluvial, wave, and tidal origin prograded basinward during stillstands to fill bays along a coastline. The nature of juxtaposition of neighboring sub-environments has resulted in a sedimentary record that is highly complex compared to that generated by morphologically simple shoreface systems that accumulate more regularly ordered stratal packages.

KEYWORDS

Fluvial, Shallow marine, Mixed-energy coastal system, Mixed siliciclastic and carbonates, Iron ooids.

INTRODUCTION

Coastal fluvial to shallow-marine settings comprise a range of environments including estuaries, lagoons, tidal flats, strandplains, barrier islands, beaches, and deltas; these pass basinward into marine offshore settings. Shoreline environments

are defined and further subdivided by the relative importance of fluvial, wave, and tidal processes (Boyd et al., 1992; Harris et al., 2002). These environments are commonly classified using various simple yet widely employed ternary classifications on the basis of dominant and subordinate process regimes (Galloway, 1975; Johnson and Baldwin, 1986; Boyd et al., 1992; Porebsky and Steel, 2006; Ainsworth et al., 2011).

The interaction of fluvial, tidal, and wave processes in nearshore coastal environments gives rise to the accumulation of depositional bodies that are represented in the sedimentary record by a variety of types of architectural elements (Miall, 1985; Olariu et al., 2012; Vakarelov and Ainsworth, 2013). The internal facies architecture and external preserved geometry of these sedimentary units is determined by the morphology and the evolutionary behavior of the range of formative coastal sub-environments (Dalrymple et al., 2003). The coastal terminus of rivers, where many of the aforementioned physical processes interplay, is termed the fluvial-to-marine transition zone (FMTZ), wherein there typically exists a downstream transition from fluvial dominance to marine dominance (Dalrymple and Choi, 2007; Van den Berg et al., 2007; Gugliotta et al., 2019). This zone can extend for tens to hundreds of kilometers upstream from shorelines at the lower reaches of rivers. Examples of studies that document such reaches include: the present-day Fraser River delta, western Canada (Dashtgard et al., 2012), the Fly River delta, Papua New Guinea (Dalrymple et al., 2003), and the Amazon River, Brazil (Dalrymple et. al., 2015). The influence of fluvial processes can also extend for hundreds of kilometers seaward from the shoreline in front of the river mouths during episodes of high river discharge (Dalrymple and Choi, 2007 and Gugliotta et al., 2019). Several studies have investigated depositional processes operating in this region, including documentation of the gravity-flow deposits of the Fraser River

74 delta front associated with fluvial and tidal interaction (Ayranci et al., 2012), and
75 remote-sensing analysis of the outward delta plume of the Mekong River (Loisel et
76 al., 2014). In recent years, a growing number of studies have examined the detailed
77 sedimentology of FMTZ-related deposits, from both modern systems (e.g., La Croix
78 and Dashtgard, 2014; La Croix and Dashtgard, 2015, Prokocki et al., 2015; Gugliotta
79 et al., 2017; Gugliotta et al., 2019) and from ancient successions (e.g., Van den Berg
80 et al., 2007; Shiers et al., 2014; Martinius et al., 2015; Gugliotta et al., 2016; La
81 Croix et al., 2019a).

82 In shallow-marine settings – given appropriate combinations of latitude,
83 climate, water depth, and a limited supply of nutrients and clastic detritus – carbonate
84 deposition may occur in parts of systems that are elsewhere dominated by clastic
85 sedimentation (Vicalvi and Milliman, 1977).

86 Sand bodies present in various accumulations of fluvial to shallow-marine
87 origin are known in the subsurface chiefly through drill-core and seismic data
88 records. Examples of successions representative of fluvial to shallow-marine sub-
89 environments (including those of the FMTZ) include the Triassic Mungaroo
90 Formation, NW Shelf, Australia (Heldreich et al., 2017), the Jurassic Brent Group,
91 North Sea, UK (Livera and Caline, 1990), the Cretaceous McMurray Formation,
92 Alberta, Canada (Hubbard et al., 2011; Hein, 2015; Jablonski and Dalrymple, 2015),
93 and the Cretaceous Burgan Formation, Kuwait (Al-Eidan et al., 2001). In these
94 settings, sand-body accumulations can be laterally extensive over kilometers where
95 they represent large-scale depositional elements (Wightman and Pemberton, 1997;
96 Shchepetkina et al., 2016; Reynolds, 2017). However, although sand-prone overall,
97 these types of successions tend to be internally lithologically heterogeneous at a
98 variety of smaller scales, for example as exemplified by sandstone beds partitioned
99 by thin but numerous mudstone interbeds (e.g., Reineck and Wunderlich, 1968;

100 Reineck and Singh, 1980; Thomas et al., 1987; Nio and Yang, 1991). As such,
101 developing detailed sedimentological models of fluvial to shallow-marine
102 successions known only from the subsurface is challenging (Jackson et al., 2005;
103 Martinius et al., 2005; Ringrose et al., 2005; Massart et al., 2016). Gaining an
104 improved understanding of the sedimentary facies distribution and anatomy of these
105 types of deposits is therefore important for subsurface characterization. A key part of
106 this is the development of predictive lithofacies models (Dalrymple and Choi, 2007;
107 Burton and Wood, 2013; Al-Masrahy and Mountney, 2015; Al-Masrahy, 2017; Van
108 de Lageweg et al., 2018) based on observations of the lateral extent and continuity of
109 architectural elements in the subsurface, as inferred from subsurface data including
110 cores, wireline logs, seismic data, and, in some cases, pressure data. Nonetheless, it
111 remains a difficult task to reconstruct the geometry and continuity of sandstone
112 bodies representative of fluvial to shallow-marine settings from subsurface data
113 alone. Uncertainty associated with attempts to characterize subsurface successions
114 can be reduced by utilizing analogues based on studies of outcrops and modern
115 systems, and from which quantitative measures of facies and architectural-element
116 proportions, geometries, and distributions can be obtained (e.g., Ainsworth et al.,
117 2008, 2011; Colombera et al., 2012, 2016a).

118 The aim of this study is to document the nature of interaction in fluvial to
119 shallow marine systems. Specific objectives are as follows: (i) examine and
120 demonstrate the relationships between various fluvial, nearshore, and shallow-marine
121 deposits, (ii) construct depositional models to account for the stratigraphic
122 complexity inherent in fluvial to shallow-marine successions, and (iii) document the
123 sedimentology and the stratigraphic evolutionary patterns of the lower Dhruma
124 Formation in the studied area of Saudi Arabia. The aim and objectives are fulfilled
125 through the consideration of a subsurface dataset from the lower Dhruma Formation

126 in Saudi Arabia (Fig. 1; exact well locations cannot be published due to the
127 proprietary nature of the dataset, though well positions relative to one another are
128 indicated). The dataset allow the characterization of sedimentary geobodies
129 considered to represent fluvial to shallow-marine paleoenvironments and allows
130 prediction of the occurrence and arrangement of those geobodies in the subsurface.

131 ## GEOLOGICAL SETTING

132 The Arabian plate, which formed part of the northeastern margin of the
133 Gondwana supercontinent, experienced diastrophic tectonic events throughout much
134 of its geological history (Haq et al., 1988; Haq and Al-Qahtani, 2005; Faqira et al.,
135 2009; Stewart, 2016). In the Permian, it was located at approximately 25° south of
136 the paleoequator, before it progressively shifted northwards during the Triassic and
137 Jurassic (Scotese, 2001; Ziegler, 2001; Schlaich and Aigner, 2017) to occupy a
138 position close to the equator during the Mesozoic (Stampfli and Borel, 2002;
139 Golonka, 2007; Seton et al., 2012; Stewart et al., 2016). This shift of position was
140 accompanied by events that influenced the geology of the Arabian Plate. In the late
141 Permian, the Neo-Tethys Ocean started to form as a result of continental rifting and
142 spreading between the Zagros suture and Gulf of Oman. This led to the formation of
143 a northeast-dipping passive margin (Ziegler, 2001). In the Early Jurassic, back-arc
144 rifting commenced along the eastern Mediterranean basin, and this induced uplift in
145 the western and southern parts of the Arabian plate. This resulted in the development
146 of a new northward-dipping passive margin to the Neo-Tethys Ocean, with an
147 associated open-marine shelf paleoenvironment (Ziegler, 2001).

148 The surface geology of the region is presently covered with aeolian sand dunes,
149 except for bedrock exposures that crop out in the western part of the basin near the
150 Arabian Shield (Fig. 1). The subsurface succession records the basin fill of an

151 elongate basin that plunges to the northeast from south of the Arabian Shield towards
152 the United Arab Emirates (Soliman and Al-Shamlan, 1980; Haq et al., 1988; Tawfik
153 et al., 2016). The study region is bounded by the Qatar Arch to the north and
154 northwest, and by the Hadhramaut-Oman arches to the south and southeast.

155 In the fill of the studied basin, the lower part of the Middle Jurassic Dhruma
156 Formation is the focus of this study. The Dhruma Formation was first identified in
157 outcrop and was originally assigned as a member of the Tuwaiq Mountain Formation
158 by Max Steineke in 1937 (summarized in Powers et al., 1966), but was subsequently
159 ranked as a formation in its own right by Brankamp and Steineke (Arkell, 1952).
160 Later workers have subdivided the Dhruma Formation into Lower, Middle, and
161 Upper members based on distinct lithological changes recognized in outcrop (Powers
162 et al., 1966; Powers, 1968). More recently, the formation has been further subdivided
163 into seven informal units: lowermost D1 to uppermost D7 (Vaslet, et al., 1983; Enay
164 et al., 2009). Where exposed in outcrop, the lower Dhruma Formation is subdivided
165 to units D1 and D2, which are referred to in the literature as the Balum Member and
166 the Dhibi Limestone Member, respectively (Al-Husseini, 2009).

167 In the subsurface, the lower Dhruma Formation of the study area is composed
168 dominantly of a siliciclastic accumulation of coastal-plain and shallow-marine origin,
169 equivalent to the D1 unit (or the Balum Member seen in outcrop). This siliciclastic
170 succession passes vertically to a carbonate-dominated succession, which forms the
171 upper part of the lower Dhruma Formation (equivalent to the D2 unit, Dibi
172 Limestone Member seen in outcrop). The lower Dhruma Formation was reported to
173 represent marginal-marine to paralic environments by Stewart et al. (2016) as part of
174 their review of the Mesozoic subsurface succession. However, no detailed and
175 systematic sedimentological lithofacies analysis of the formation has been published
176 previously.

DATA AND METHODS

Subsurface Datasets

This study integrates techniques in lithofacies analysis, ichnology, and sequence stratigraphy based on analysis of subsurface data from 14 wells that penetrate the lower Dhruma Formation in the studied area, in Saudi Arabia. The dataset includes subsurface core data, representative thin sections from core, gamma-ray logs, and image logs. Cores and thin sections have been described in detail in terms of grain-size distribution, grain texture (clast shape, sorting), sedimentary structures, bed thickness, bed contact types, and bioturbation intensity using the bioturbation index scale (Taylor and Goldring, 1993). Using these descriptive criteria, thirteen distinct lithofacies are identified in the succession. These lithofacies are grouped into five principal facies associations that have been interpreted as being representative of vertical accumulations arising in response to particular suites of depositional processes; each facies association is considered representative of sedimentation in a particular paleoenvironment.

Based on correlations between the studied wells, three stratigraphic cross sections (correlation panels) have been constructed, two in an orientation considered close to parallel to the depositional strike of the sedimentary system, and one along a dip-oriented profile. These three panels have been used to determine the spatial distribution of the defined facies associations. Correlation has been undertaken principally based on analysis of the sedimentary logs and the gamma-ray signatures. Well-log gamma-ray data from the studied wells were placed against the descriptive sedimentary core logs to account for the uncored sections of the lower Dhruma Formation. Logs and cores are commonly mismatched with respect to reported depths due to the tools stretching because of high temperature in the deep boreholes

(Crain, 2015). To address discrepancy between the reported depths of the sedimentary logs (descriptions of the cores) and the gamma-ray logs, a standard core-to-log calibration technique has been applied by matching the core gamma-ray logs (as obtained in the laboratory after cutting the core) with the reference (wireline) gamma-ray logs. This typically required a core shift of up to 7 m downward or upward with respect to the reference gamma-ray log. The gamma-ray signature, which is a proxy for sand and shale in the subsurface, was used to derive insight into vertical lithology trends. The gamma-ray signature of the uncored intervals has been interpreted based on the gamma-ray log responses typical of different depositional settings. For example, the bell-shaped gamma-ray signatures correspond to channel-fill deposits and the funnel-shaped ones correspond to prograding marine shelf or delta-front deposits (cf. Emery and Myers, 1996). Age-diagnostic palynomorphs, described by Stewart et al. (2016), were considered in this study to discriminate the relevant successions of the Middle Jurassic lower Dhruma Formation from the underlying lower Jurassic and/or Upper Triassic formations. FMI image-log analyses (results provided courtesy of Shahzad Ulhaq, Saudi Aramco) from four wells have also been used to determine the paleoflow direction of the defined geobodies (e.g. dip directions of sedimentary structures of different types).

Constraining Uncertainty Associated with Inter-Well Correlation

This study is based primarily on a comprehensive one-dimensional subsurface dataset from wells distributed over an area of approximately 150 km x 150 km (Fig. 1B). The two wells that are closest to each other have a spatial separation of 4 km (wells 3 and 4), whereas the two most widely separated wells are ~ 126 km apart (wells 12 and 13). Therefore, there exists a degree of uncertainty.

In the subsurface study, cores and wireline-log signatures (gamma-ray logs) are the principal data types utilized to infer depositional environments. These types of data indicate the vertical extent of different geobodies, biostratigraphy content, and physical properties of the rock (porosity, permeability etc.), and provide relative age dates through biostratigraphy. However, determining the stacking patterns and the lateral connectivity of geobodies is not straightforward. Uncertainty can be associated with facies interpretation of gamma-ray signatures in cases where cores are unavailable. For example, shoreface and delta-front facies may display similar characteristics and may be difficult to discriminate using well-log data alone.

Geobody geometry has been estimated by employing appropriate modern and ancient analogues from which distributions of geobody length and width can be derived; estimates of geobody lateral extent can be attempted based on knowledge of their thickness. Analogue data were obtained from a relational database detailing sedimentary architectures: the Shallow Marine Architecture Knowledge Store (SMAKS) (Colombera et al., 2016a). The SMAKS database has here been used to provide quantitative information on the architectures and dimensions of geobodies for ancient shallow-marine and paralic siliciclastic successions deemed analogous to the subsurface Dhruma Formation. The database was filtered and queried to derive analog data that are the most suitable to this study. For example, data relating to sedimentary units that represent only one part of a tidal flat (i.e., sand flat or mud flat) were disregarded, as tidal-flat deposits described in this study include a full suite of sand flats, mixed flats, and mud flats. Moreover, data on parasequence-scale shoreface sandstones (cf. Colombera and Mountney, 2020a, 2020b), and on shallow-marine sandstones more generally were considered. Examples of such deposits were filtered on their thicknesses to ensure that only those that are comparable in scale to those observed in core were considered. Relationships between the thickness and

lateral dip extent of sedimentary units (i.e. facies associations) as obtained from SMAKS, have been considered to guide well correlations in the studied subsurface succession.

RESULTS

Fourteen distinctive lithofacies types have been identified from the analyzed cores of the lower Dhruma Formation (Table 1). These have been grouped into five main facies associations based on their arrangement and genetic relations to one another. The five facies associations are categorized as follows: fluvial channels (FA1); intertidal flats and pedogenically modified supratidal or floodplains (FA2); river-influenced tidal bars (FA3); shoreface and delta (FA4); and open-marine and shelf carbonates (FA5). Facies associations FA2, FA4, and FA5 have been further subdivided into two sub-associations each. Representative graphical sedimentary log examples from which facies associations have been identified are shown in Figure 2.

Fluvial-Channel Deposits (FA1)

Description.--- This facies association was observed in 7 wells (see Table 2) and commonly has an erosional base and occurs on top of FA2. FA1 is composed of fining-upward packages of massive (Sm) and cross-bedded sandstone (Sx) that always pass upward to thinner beds of heterolithic mudstone and sandstone (Hms) and mudstone (Ms). These deposits are sand dominated and occur as a single package (e.g., middle of well 12 in Fig. 2), else as repeated cyclically arranged packages (e.g., top of well 1 and base of well 12 in Fig. 2). A single package of strata representing this facies association is 0.5-4 m in thickness. The sandy units are commonly thicker (0.2 to 3.5 m) than the overlying heterolithic facies (0.1 to 0.8 m). The sandstone units exhibit erosional bases that are commonly overlain by lag

sediments (Lg), mainly of very coarse sand grains and mud pebbles (Fig. 3A, B) whereas the overlying heterolithic and mudstone facies show gradational or sharp bases. There also exists rare small-scale (0.2 m) alternating sandstone (Sx) and heterolithic facies (Hms) towards the upper part of the overall sandy section (Fig. 3C).

Generally, the sandstone facies grade upward into planar-bedded medium- to fine-grained sandstone and siltstone units. The massive and cross-bedded sandstone consistently has sparse floating mud chips (1.2 to 5 mm diameter) present in it, as well as sparse clasts of organic and coaly debris (Fig. 3A, B). FA1 exhibits millimeter-scale, carbonaceous laminae draping the cross-stratified sets in wells 10, 12 and 13. These laminae are faint in the lower parts of the sandy units but more pronounced upwards. Localized double mud drapes occur in well 13 at the transition between the sandstone and the overlying heterolithic facies (Fig. 3D). The heterolithic units in this association are mud-dominated (mainly clay) and contain thin beds and lenses of sand (Fig. 3E) and common wavy to lenticular bedding. They cap and/or separate units composed of the sandy facies (Fig. 3C, D, E). Localized vertical burrows (*Skolithos*) are observed at the upper contact of sandstone units that are directly overlain by the heterolithic facies; these burrows likely originate at the interface with the overlying finer-grained sediments. In the heterolithic facies, small sporadic forms of *Planolites* and other unidentified burrows are present. The heterolithic facies is commonly overlain by the deposits identified in FA2b (Fig. 3F).

Interpretation.---The numerous erosional beds indicate repeated high-energy currents eroding the underlying sediments. The massive coarse sandstone with lack of pronounced sedimentary structures and bioturbation suggests rapid deposition by deceleration of high-energy, heavily sediment-laden currents (Martin, 1995; Collinson et al., 2006; Dalrymple et al., 2015). The abundance of clasts of mudstone,

303 organic matter, and coaly debris suggests reworking of pre-existing sediments, and
304 perhaps transportation by fluvial currents. The vertical trend of the succession, with
305 lag sediments resting on an erosional base and passing upward into massive
306 sandstone, is a characteristic that is common of channel-fill deposits (Martini and
307 Aldinucci, 2017). The more cyclic occurrence of thick sandstone overlain by thin
308 intervals of heterolithic deposits is interpreted to represent alternation of high and
309 low river flow stages. The thick sandstone units were likely deposited during river-
310 flood periods (high river discharge), whereas the overlying heterolithic interval was
311 likely deposited during inter-flood periods (low river discharge) (Dalrymple et al.,
312 2015). Possible tidal effects are indicated by the presence of double mud drapes in
313 well 13. Overall, this facies association is interpreted to represent fluvial-channel and
314 overbank deposits. The fluvial-channel deposits observed in well 13 with the
315 possible tidal effect may represent deposition in the upstream region of the FMTZ.

316 *Intertidal and Pedogenically Modified Supratidal Flat or Floodplain (FA2)*

317 *Intertidal-Flat Deposits (FA2a)*

318 **Description.---** This facies association was observed in eight wells (see Table
319 2). It was observed at the bottom of the formation, where cored, across much of the
320 study area. It unconformably overlies the lower Jurassic carbonate deposits of the
321 upper Marrat Formation. This facies association overlies the fluvial deposits of FA1
322 in many wells. It mainly consists of fining-upward packages (up to 5 m thick with an
323 average of ~ 3 m) of heterolithic fine- to medium-grained muddy sandstone that
324 transitions to sandy mudstone facies (mainly clay) (Hms). The sandy part contains
325 cross-lamination and stacked symmetric bidirectional ripple forms (Collinson and
326 Mountney, 2019) that decrease in frequency and become isolated towards the muddy
327 part (Fig. 4A). Unidirectional ripples also exist in the sandy facies. Repeated double

mud drapes are observed in various parts in this facies association (Fig. 4A). It also shows common flaser, wavy, and lenticular bedding as well as abundant thin, very fine sand lenses in the finer interval (Fig. 4B). Distorted beds locally occur at the bottom of the sandstone facies. In places, shrinkage cracks are observed in the muddy parts of this facies association. They taper downward and have infills of sediment derived from the bed above. Low to intense bioturbation is observed in sand-mud alternations, with bioturbation index values ranging from 1 to 5 (Fig. 4C). Identified ichnoforms include *Ophiomorpha*, *Planolites* and *Diplocraterion*.

Interpretation.---The presence of sand-mud alternation in the form of bidirectional rippled sandstone, together with the flaser, wavy, and lenticular bedding, suggests deposition during fluctuating energy levels (Reineck and Wunderlich 1968; Ginsburg 1975; Klein 1985). In this context, sand grains are typically deposited as bedload during the more energetic flows of a tidal cycle, generating bidirectional ripple forms (Boggs, 1995). By contrast, mud particles, possibly flocculated, settle out of suspension on the underlying rippled sand during low-velocity flows or at slack water, giving rise to the occurrence of flaser, wavy, and lenticular bedding (Klein, 1985; Boggs, 1995). The unidirectional ripple forms may represent deposition by ebb- or flood-dominant currents. Alternatively, the unidirectional ripples can possibly be products of fluvial currents. The observed shrinkage cracks are interpreted to be desiccation cracks that resulted from periodic subaerial exposure of the muddy deposits in the upper intertidal zone (Dalrymple, 2010). They are not likely to be syneresis cracks, given their downward tapering form and fill of sediment derived from above (Collinson and Mountney, 2019). The vertical succession of this facies association, with its fining-upward trends, is similar to those interpreted as deposition in channel-related tidal flats (e.g., Dalrymple, 2010; Desjardins et al., 2017). Overall, this facies association may represent channel-

related tidal flat setting which dominated by tidal process. If the unidirectional ripple forms are of fluvial origin, the tidal flat setting may be within the inner FMTZ.

Pedogenically Modified Supratidal Flat or Floodplains (FA2b)

Description.--- This facies association was observed in nine wells (see Table 2). The heterolithic mudstone and sandstone of FA2a and those defined in FA1 repeatedly transition upward to thick (few meters to 10 m) intervals of greenish-gray non-stratified very fine sandstone, siltstone, and mudstone (Sd), with intensive rooting (Fig. 4D). It also shows variegated mottling in some wells, with a brownish-red color interchanging with a greenish-gray color (Fig. 4E). In the highly oxidized facies, there exists centimeter-scale blocky volume that is separated by millimeter-scale iron-rich matrix (Fig. 4E). This non-stratified facies commonly shows thin beds of coal (~ 20-80 mm) (Fig. 4F, G), coarse- to pebble-size coal clasts and organic debris, and up to 0.8-m-thick coaly mudstone beds (Cm). Pyrite nodules and disseminated grains are observed in this FA and are associated with the presence of coal and organic material. Furthermore, thin sections of this facies indicate high content of kaolinite, and organic and carbonaceous material (Fig. 4H, I). A low diversity of ichnogenera, mostly *Planolites*, is observed with a bioturbation index that ranges from 1 to 3.

Interpretation.---The non-stratified nature of this facies association suggests post depositional alteration to the sediments before lithification. The presence of rootlets across most of the facies suggests subaerial exposure which facilitated colonization by plants. Kaolinite is commonly formed during intense chemical weathering in warm and humid climate conditions (Weaver, 1989; Robert and Chamley, 1991); its high abundance in this facies association suggests that FA2b deposits were subjected to intense chemical alteration. The variegated form of red

and brown colors suggests oxidation of iron-bearing sediments, possibly during subaerial exposure (Bromley, 1975; Pemberton and Frey, 1985; Pemberton et al., 1992; MacEachern et al., 1992, 2012). Pedogenic processes are also indicated by the presence of the blocky volumes that is separated by iron-rich matrix which suggest soil formation. Coaly debris and organic material observed in this facies association in most of the locations may have been reworked from localized vegetated swamps. This facies association is interpreted as subaerially exposed supratidal deposits in the seaward position of the region (wells 1, 2, 4, 5, 7, 8) and may represent altered floodplain deposits in more landward positions (wells 10, 12).

River-Influenced Tidal Bars (FA3)

Description.--- This facies association was observed in 3 wells (see Table 2) and observed overlying and underlying the intertidal and supratidal deposits of FA2. The facies association is composed of normally graded, centimeter- to decimeter-beds of non-stratified very coarse to medium quartz-dominated sandstone (Sm), commonly with scoured bases overlain by coarse-grained lag sediments (Lg). This massive sandstone shows relatively thicker beds (0.4 m on average) and with more frequent erosional bases in well 11 compared to wells 3 and 4 where the massive beds are 0.10 m on average. It generally grades upward to stacked sets of medium-grained trough and planar cross-bedded sandstone (Sx). Sedimentary structures observed in Sx include planar cross-stratification, with foresets that possess thin (up to 5 mm) single and double mud drapes (mainly clay). Sand and mud couplets were also observed within bundles (Fig. 5A). Furthermore, the cross-stratified sets are observed bounded by unbioturbated erosional surfaces (reactivation surfaces). In Sx, there exist thin beds (20 to 40 mm) of non-stratified very coarse sandstone that generally grade upwards to coarse and medium grain size (Fig. 5B, C). These are commonly overlain by cross-bedded sandstone with double mud drapes (Fig. 5C).

405 The double mud drapes occur more frequently towards the top of the sandy part of
406 FA3. Towards the top of FA3, heterolithic (Fig. 5D) and non-stratified facies (Fig.
407 5E) were observed overlying the sandstone facies. The heterolithic and non-stratified
408 facies are similar to those observed in FA2. Thin sections record limited presence of
409 kaolinite in Sx (Fig. 5F, G). Bioturbation is generally rare in FA3. This facies
410 association exhibits a high proportion of carbonaceous and organic material.

411 **Interpretation.--- S**ingle and double mud drapes, reactivation surfaces, and
412 sand-mud couplets are considered as possible tidal indicators (Visser, 1980;
413 Dalrymple and Choi, 2007; Dalrymple, 2010; Davis, 2012). Mud drapes typically
414 represent deposition from suspension during low-velocity tidal flow or at slack-water
415 periods (Visser, 1980), whereas reactivation surfaces indicate pause planes
416 (discontinuities in sedimentation) or reversing tidal currents (Boersma and Terwindt,
417 1981). Alternation of sand and mud beds in the form of bundles is commonly
418 described as the product of flood-ebb tidal cycles (Visser, 1980). However, recent
419 work demonstrates that such bundles may originate in tide-modulated fluvial settings
420 (Martinius and Gowland, 2011) or in purely fluvial settings (Ainsworth et al., 2011).
421 The thin, normally graded beds indicate deposition by high-energy currents possibly
422 by fluvial currents. The overlying double mud drapes and their upward increase in
423 frequency of occurrence supports an interpretation of increasing tidal influence over
424 time. The coaly fragments, organic material, and kaolinite present in this facies
425 association imply reworking of sediments from a coeval adjacent vegetated setting.

426 This facies association indicates interaction of tidal and fluvial currents. Tidal
427 currents are interpreted to be the dominant controlling process overall, though
428 significant fluvial influence is evident in places. Overall, the deposit of FA3 are
429 interpreted as fluvial-influenced tidal bars in a potentially estuarine setting.

Shoreface to Offshore Transition and Delta-Front to Prodelta (FA4)

Weakly Storm-Affected Shoreface To Offshore-Transition Zone (FA4a)

Description.--- This facies association was cored in eigth wells (see Table 2), where it consistently overlies the oolitic ironstone of FA5b. This facies association comprises amalgamated coarsening- and thickening-upward packages (0.5 m to a few meters thick) of massive mudstone (partly calcareous), heterolithic mudstone and sandstone (Hms), and fine- to medium-grained hummocky cross-stratified sandstone (Shcs) and bioturbated sandstone (Sd). These packages show increasing proportion of sand upwards. The mudstone units (Ms) are homogeneous, with rare pronounced sedimentary structures. The heterolithic part is composed of mudstone and very fine- to fine-grained sandstone and exhibits an upwards increase in sand proportion (Fig. 6A). Local slightly asymmetrical lenticular ripples were observed in the heterolithic unit (Fig. 6B). In facies Hms, rare thinly laminated sandstone beds with erosional bases are present in places. In its upper part, FA4a is dominated by the presence of weakly to intensely bioturbated, dominantly fine-grained sandstone of Sb (Fig. 6C), which commonly grades up to cleaner (relatively lower mud content) lightly bioturbated sandstone with apparent hummocky cross-stratification (Shcs). The bioturbated sandstone is composed of poorly sorted grains and shows rare preserved cross bedding. Abundant rounded to elongate, concentrically lined iron-rich ooids are scattered in various parts of this facies association (Fig. 6D). A slightly diverse assemblage of ichnogenera is present in FA4a: *Skolithos*, *Planolites*, *Ophiomorpha*, and *Teichichnus*; the bioturbation index varies from 2 to 5.

Interpretation.---The coarsening-upwards packages of mudstone, heterolithic strata, and sandstone indicate increasing energy levels as a result of decreasing depositional water depth (Van Wagoner et al. 1990 and Howell et al., 2008). The

455 defined ripple forms observed are likely products of wave activity above fair-weather
456 wave base where propagating waves produce a slight landward shift of sediment
457 forming the asymmetrical shape (Reineck and Singh, 1980). The observed intensity
458 and diversity of bioturbation present in FA4a successions suggest broad organism
459 colonization, in low-energy settings (e.g., Pemberton et al. 2003). The decrease in
460 bioturbation in the sandstone facies and the presence of hummocky cross-
461 stratification is attributed to periods of storm wave activity, likely between the fair-
462 weather and the storm wave bases (Harms et al., 1975; Collinson and Mountney,
463 2019). Variations in bioturbation may also reflect changes in sedimentation rate,
464 whereby organisms colonize the sediments during periods of low sedimentation rate
465 (Bromley, 1996). The abundance of iron-rich ooids in this facies association is
466 attributed to reworking of pre-existing ooids. Overall, this facies association is
467 interpreted as a prograding storm-affected offshore-transition zone to shoreface
468 environment.

469 *Storm-Dominated River-Influenced Prodelta to Delta-front Deposits (FA4b)*

470 **Description.---** This facies association was observed only in well 2; however,
471 gamma-ray signatures in two nearby wells (wells 3 and 4) show striking resemblance
472 with the corresponding gamma-ray signatures of well 2. FA4b was observed
473 overlying the open-marine carbonate deposits of FA5a in two coarsening- and
474 thickening-upwards packages (that are ~ 9 and 10 m thick). These packages consist
475 of mudstone (Ms), heterolithic mudstone and sandstone (Hms), and fine to medium-
476 grained sandstone (Sx and Shcs). The mudstone unit is blocky and homogeneous in
477 nature. The mudstone facies (Ms) shows numerous fine sandstone lenses and thin to
478 medium beds (up to 150 mm) of thinly laminated very fine sandstone, commonly
479 with erosional bases, and exhibit moderate to weak bioturbation (BI:1-3) (Fig. 6E,
480 F). These deposits grade up to faintly laminated to low-angle cross-bedded fine to

481 medium-grained sandstone (Sx) and hummocky and swaly cross-stratified fine to
482 medium-grained sandstone (Shcs) (Fig. 6G, H). The facies association becomes more
483 sand-dominated upwards. Furthermore, several inversely graded beds (50-120 mm)
484 are observed with well-rounded medium to angular grains, floating mud chips and
485 rare preserved gastropod shells. These beds occur towards the upper parts of the
486 sandstone units. The sandstone units are composed primarily of quartz grains with
487 common interstitial greenish chlorite cement (Fig. 6J). Bioturbation is generally rare
488 in the sandstone units, but a low diversity of ichnogenera (e.g., diminutive forms of
489 *Planolites*, *Skolithos,* and fugichnia) was observed in Sx, disturbing the original
490 sedimentary structures.

491 **Interpretation.---**Similar to FA4a, FA4b deposits are indicative of increasing
492 energy levels, likely associated with a decrease in water depth, which is recorded by
493 the coarsening- and thickening-upwards trends. The mud in Ms and Hms in the lower
494 part of each package generally suggests deposition from suspension under quiet
495 water conditions. Periods of storm events eroding the muddy substrate are indicated
496 by the presence of numerous erosionally based sandy beds and lenses (Baniak et al.,
497 2014). The bioturbated heterolithic strata are indicative of storm power fluctuations
498 (cf. Collins et al., 2020). Hummocky and swaly cross-strata present in this facies
499 association are typically wave-generated structures (e.g., Harms et al., 1975; Meene
500 et al., 1996). The inverse grading that occurs towards the upper parts of the sand-
501 dominated units may indicate deposition by hyperpycnal flows during waxing river
502 discharge (Bhattacharya and MacEachern, 2009). The overall scarcity of bioturbation
503 indicates environmental conditions that prevented organisms from flourishing. Such
504 conditions might have been due to high rates of sediment influx into the system,
505 freshwater input, and/or high-energy wave currents (MacEachern et al., 2007a, and
506 2007b). The local presence of low-index and low-diversity ichnogenera assemblages

observed in the sand units is attributed to periods of lower wave action and/or lower sedimentation rate, which might have enabled the temporary activity of organisms (Bromley, 1996; Pemberton et al., 2012). Subsequent episodes of high rates of sedimentation would have required the organisms to escape upward to reach the water-substrate interface (Pemberton and MacEachern, 1997; Bann et al., 2008; MacEachern and Bann, 2008, Pemberton et al., 2012). The observed ichnofossil assemblage represents an impoverished and distal expression of the *Skolithos* ichnofacies (MacEachern and Bann, 2008). Overall, this facies association is interpreted to have formed in a prograding storm-dominated river-influenced delta-front to prodelta setting (cf. Collins et al., 2020).

Open-Marine Shelf (FA5)

Carbonate Shelf (FA5a)

Description.--- This facies association was observed in three wells (see Table 2). It forms the lower part of the two packages defined in FA4b in well 2 and marks the top of the cored section in wells 7 and 11. Packages of carbonate facies overlie FA4b and FA4a in well 2 and FA4b in wells 7 and 11. Generally, this association comprises limestone (Ls) that changes in composition and grain size upwards to calcareous mudstone (Msc). The limestone facies is grain dominated (packstone to grainstone; Dunham, 1962). The limestone facies occur as amalgamated bedsets of approximately 4 m thickness, or as thinner interbeds (50 to 150 mm) between packages of facies Msc. The grain composition includes common outsized quartz grains, abundant ooids, and shell and skeletal fragments that are commonly replaced by dolomite rhombs. At the base of the deepest occurrence of this limestone, ooids and skeletal grains are highly fragmented. This facies shows moderate to intense bioturbation (BI: 3 to 5) (Fig. 7A, B). The overlying mudstone beds are marly at their

532 bases but become less calcareous toward their tops. Mudstone beds are blocky and
533 show many drilling-induced fractures (Fig. 7C). In places mudstone beds reveal thin
534 parallel lamination, and limited wavy to lenticular bedding and can exhibit an
535 increasing proportion of sand upwards. In addition, Msc shows scattered shell
536 fragments in a clayey matrix. Bioturbation in Msc is generally sporadic and is
537 developed most intensely near lithological boundaries. Unlike the limestone units
538 observed in well 2, coarsening- and thickening-upward beds are preserved in wells 7
539 and 11 with smaller packages of mud-dominated to grain-dominated limestone
540 (wackestone to grainstone). The grain types observed are primarily coated grains,
541 ooids, intraclasts, and shell and skeletal fragments. Dolomite cement dominates the
542 lower part of the section (Lsd), and decreases in abundance as it is replaced by
543 calcite upwards.

544 **Interpretation.---**The calcite-rich sediments together with the abundant ooids,
545 shells, and skeletal fragments indicate periods of carbonate sedimentation. The ooids
546 formed in agitated shallow-water settings (Davies et al., 1978; Rankey and Reeder,
547 2012). The overall dominance of grainstone in the carbonate facies is indicative of
548 high-energy shoal environments. The presence of skeletal and grain fragmentation at
549 the base of the limestone in well 2 suggests reworking by high-energy currents to
550 leave a lag deposit, possibly during transgression. The mudstone that occurs on top
551 of the limestone is interpreted to be deposited from settling out of suspension in quiet
552 water conditions, possibly during a subsequent flooding (i.e., deepening) event.

553 *Iron-Rich Oolitic Shoal (FA5b)*

554 **Description.---** This facies association was observed in six wells (see Table 2).
555 It is observed overlying the tidal-flat and supratidal deposits of FA2 and the fluvial
556 channel deposits of FA1, with sharp bases. These deposits are always capped by the

557 mudstone of FA4a. They show an overall fining-upward trends and consists
558 primarily of calcareous sandstone (Sc), ooid-rich ironstone (Ore), and calcareous
559 mudstone (Msc). The calcareous sandstone is carbonaceous and composed of poorly
560 sorted fine to medium quartz grains with abundant bioclasts and scattered chamosite
561 ooids (Fig. 7D, F). The ooid-rich ironstone is composed primarily of orange-brown
562 ooids, skeletal fragments, and sparse detrital quartz grains that are of fine to medium
563 sand size (Fig. 7E, G). The ooids show concentric laminae around various types of
564 nuclei, including clay, quartz, and skeletal fragments. They are mostly rounded to
565 slightly elongate in shape and are deformed in some instances (Fig. 7G). Some of
566 these ooids are completely or partly dissolved and replaced by dolomitic rhombs.
567 The calcareous mudstone is observed interbedded with and/or overlying the
568 calcareous sandstone and the ooid-rich ironstone. The mudstone facies comprises
569 sparse ooids and skeletal fragments at the base of beds; these decrease in abundance
570 upward within beds.

571 **Interpretation.---**The dominance of ooids in this facies association indicates
572 accumulation in high-energy, shallow-water settings (Chen et al., 2017). The iron in
573 these accumulations could have been transported from the continent to the sea as Fe-
574 bearing detritus or Fe-clay colloids by river currents (Maynard, 1983; Einsele, 2000).
575 The calcareous sandstone with the abundant ooids and fragmented bioclasts also
576 suggest reworking by wave activity in close proximity to a carbonate source. The
577 stratigraphic position of this facies association, overlying the nearshore deposits of
578 FA1 and FA2, and being overlain by marine deposits of FA4a, suggests deposition
579 during a transgressive episode. This is in accord with how these types of ooidal
580 ironstones are commonly interpreted to form under transgressive conditions (cf.
581 Hallam and Bradshaw, 1979; Bayer et al. 1985; Van Houten 1985; La Croix et al.,
582 2019b).

Paleocurrent Analysis

Subsurface cores do not reveal information required for paleocurrent identification, as in that the cores are not oriented. Rather, image logs of the boreholes provide the prevalent type of data used to infer paleocurrent directions. In this study, Formation Micro Imager (FMI) logs acquired from four wells were used to interpret the paleocurrent directions for the defined facies associations. Interpretations of image logs are summarized in rose diagrams (Fig. 8), which report the dip directions of foresets of cross-bedded sandstones from shoreface (FA4a) deltaic (FA4b), tidal-bar (FA3) and fluvial-channel (FA1) deposits. The foreset dip directions of the shoreface sandstone cross-bedded sets from well 8 and the deltaic sandstone from well 2 show broadly consistent north-northeast (present day) dip directions. Inclined forests of tidal-bar deposits also show a broad northeast dip direction with limited variability. This broad unidirectional bedding of tidal bars might indicate an ebb-dominant tidal current that is driven by dominant river input at the estuary mouth. However, the position of the tidal bars with respect to the channel remains uncertain. Overall, these observations indicate a broad northeastward progradation and direction of sediment dispersal. However, the dip directions of a fluvial channel interpreted from well 13 vary and indicate east, southeast, and northwest (present day) dip directions, which could be due to the formative channel being sinuous and/or to in-channel secondary, or possibly reversing, flow.

Spatial Distribution of Facies Associations

The studied cores are divided into two main facies belts: coastal-plain deposits comprising FA1, FA2 and FA3 facies associations and marine deposits including the FA4 and FA5 facies associations. To illustrate the spatial distribution of the facies, correlations between the defined facies associations have been constructed across the

608 study area principally based on the available sedimentary logs and well-log gamma-
609 ray signatures, but also supported by secondary analog data from the SMAKS
610 database; a data summary is provided in Figure 9. The correlation panels are shown
611 in Figure 10A, B, C. The non-cored intervals have been interpreted based on their
612 gamma-ray signatures, which typically yield information on the rock characteristics
613 and enable lithological interpretations (Emery and Myers, 1996).

614 The data obtained from SMAKS show relationship between thickness and dip
615 length of numerous shoreface and shallow-marine sand belts, tidal bars and tidal
616 flats. Thickness-dip-length relationships of shallow-marine sand belts (Fig. 9A)
617 indicate that a 10 m thick sandstone (analogous to the sandstone observed in FA4b)
618 ranges in dip length from a few hundreds of meters to nearly 40 km. Limited data
619 related to tidal flats and tidal bars were obtained, from which a relationship cannot be
620 obtained (Fig. 9B). However, some instances of meter-thick tidal flats can be several
621 hundreds of meters long in dip direction, and may reach up nearly 2 km. For
622 example, one 7.5-m-thick tidal bar is 1.5 km in dip length. These data have been
623 applied to help constrain expected sand body architectures in the correlation panels
624 of Figure 10.

625 Sections A-A' and B-B' have been constructed in an orientation approximately
626 parallel to the depositional strike of the system. These sections show an overall
627 vertical transition from a coastal-plain succession at the base to a marine succession
628 at the top. Section A-A' (Fig. 10A) reveals a thicker succession of marine deposits
629 overlying the coastal-plain deposits compared to cross section B-B' (Fig. 10B),
630 which is itself interpreted to have occupied a position farther landward (towards the
631 west) by virtue of a thicker coastal-plain succession and thinner marine succession.
632 Section C-C' (Fig. 10C) has been constructed in an orientation approximately
633 parallel to the depositional dip of the system (and intersecting panels A-A' and B-

B'). This section reveals a dominance of coastal-plain deposits in the southwest of the area and predominantly marine deposits in the northeast. This section demonstrates an overall deepening-upward trend. However, six smaller-scale transgressive-regressive packages superimposed upon the overall deepening trend are identified. These packages are most clearly developed in the middle of section C-C' (Fig. 10C).

DISCUSSION

Controls on Sedimentation in the Lower Dhruma Formation

A depositional model depicting the evolution of the Middle Jurassic lower Dhruma Formation over five intervals is presented in Figure 11. Vertically, the study succession records an overall transition from coastal-plain deposits at the base to marine deposits at the top, as demonstrated in Figure 10A and B. The overall stratigraphic architecture of the lower Dhruma Formation is interpreted to be controlled by relative sea-level fluctuations, as well as by fluvial, tidal, and wave processes, as documented above.

The lower part of the section (interval 1) is dominated by fluvial and fluvial-tidal sedimentation, which resulted in the deposition of fluvial channel deposits (FA1), channel-associated tidal flats (FA2a) and river-influenced tidal bars. The deposits of FA2 and FA3 possibly represent deposition in FMTZ in a mixed-energy estuary. Extensive paleosols (FA2b) are present across much of the study area; these indicate a prolonged period of subaerial exposure. This is overlain by two transgressive-regressive packages (interval 2). The transgressive components in these packages comprise reworked iron-rich oolitic shoal sediments (FA5b). The ooidal ironstone in this example is commonly interpreted to form from reworking of iron-rich coastal plains during transgressive events as documented above (cf. Bayer et al.

1985; Van Houten 1985). The regressive components are composed of progradational, weakly storm-affected offshore-transition-zone and shoreface units (FA4a). Interval 3 incorporates a package that is similar to those defined in interval 2, but with the transgressive component displaying reduced iron content in wells 2 and 5; this indicates the presence of accumulation of carbonate sediments towards the northeast. Following the accumulation of interval 3, interval 4 is represented by two successive carbonate-mudstone-sandstone packages. The transgressive components of the two packages are represented by the fining-upwards limestone of FA5a. These are overlain by the regressive components represented by the prodelta and delta-front deposits of FA4b. These packages indicate two episodes of encroachment and retreat of carbonate-producing shelf areas. This is attributed to variations in the balance between the rate of relative sea-level change and the rate of supply of terrigenous sediment. Carbonate sedimentation developed most widely during episodes of limited siliciclastic influx or relative sea-level rise. By contrast, carbonate production was curtailed during episodes of increased rates of terrigenous sedimentation, or falls of relative sea level. The same factors acted to drive changes in shoreline position, which were paralleled by landward and basinward shifts in the foci of carbonate deposition (cf. Tirsgaard, 1996). Interval 5 incorporates the weakly storm-influenced shoreface deposits of FA4a in a more proximal position, farther southwest of the study area. These deposits are themselves overlain by carbonates that are apparently present across the entire study area.

Climate and Sediment Source

The Arabian Plate occupied a position near or at the equator during the Jurassic (Stampfli and Borel, 2002; Golonka, 2007; Seton et al., 2012; Stewart et al., 2016). Al-Aswad (1995) suggested that the climate of the Arabian Plate during the Jurassic was humid to semihumid. This has also been supported by the increased presence of

small fern spores (Classopollis) along with an abundance of kaolinite in paleosols (e.g., Al-Hussaini, 2019). In the studied area, the defined supratidal or floodplain deposits also show enrichment of kaolinite, which is indicative of intense chemical alteration under a humid to semi-humid climate (Weaver, 1989; Robert and Chamley, 1991).

The source of the clastic sediments of the Middle Jurassic succession has been interpreted by a number of authors. The eastern Mediterranean back-arc rifting in the Early Jurassic caused residual highs of western and southern parts of the Arabian Plate (Beydoun, 1991; Ziegler, 2001). In the Middle Jurassic, the Hadramaut-Oman Arches were the only elevated hinterlands that could perhaps have acted as a source of sediments into various parts of the Arabian Peninsula, and which could have been drained by extensive channel networks (Al-Aswad, 1995). Al-Aswad (1995) suggests that southern central Arabia was traversed by alluvial tributaries draining the Hadramaut-Oman Arch, mainly from the south towards the north. The location of the study area and the broad northeastern paleoflow direction recorded in FMI image logs suggest that the siliciclastic sediments were likely sourced from the same southern Arabian hinterlands to the south and southwest.

CONCLUSIONS

A core-based sedimentological analysis of the Middle Jurassic lower Dhruma Formation in Saudi Arabia is presented. The study reveals that the lower Dhruma Formation was deposited in a varied range of fluvial to shallow-marine environments that interacted in a complex way over both space and time. Five lithofacies associations are identified based on the analysis of the core data; each is considered indicative of sedimentation within a particular paleoenvironment. The facies associations represent different paleoenvironments: fluvial channels, intertidal to

pedogenically modified supratidal flats or floodplains, river-influenced tidal bars, deltaic and shoreface to offshore transition, and an open-marine carbonate-dominated shelf. The deposits of the facies associations are interpreted to be controlled by the interaction of fluvial, tide, and wave processes. At a larger scale, the pattern of sedimentation is controlled by the interplay of sea-level change and sediment accumulation rate, causing zones of sedimentation to shift with changes in the position of the paleoshoreline. The vertical successions of the lower Dhruma Formation record an overall transition from coastal-plain deposits at the base to marine deposits at the top. As such, the succession records a long-term transgressive, deepening-upward event. However, this overall deepening trend was punctuated by at least six progradational events whereby coastal deposits prograded basinward episodically.

ACKNOWLEDGMENTS

The authors would like to thank the Saudi Arabian Oil Company (Saudi Aramco) for funding this research and allowing this work to be published. We would like to thank our project partner Petrotechnical Data Systems (PDS) for provision of an academic license for Ava Clastics, which has been used to interrogate the Shallow-Marine Architecture Knowledge Store (SMAKS). We thank Marcello Gugliotta, Andrew La Croix, and an anonymous reviewer for their comments, which have significantly improved the article.

REFERENCES

Ainsworth, R.B., Flint, S.S., and Howell, J., 2008, Predicting coastal depositional style: Influence of Basin Morphology and accommodation/sediment supply regime within a sequence stratigraphic framework, *in* Hampson, G.J., Steel, R.J., Burgess,

735 P.B., and Dalrymple, R.W., eds., Recent Advances in Shallow-Marine Stratigraphy:
736 SEPM, p. 237-263.

737 Ainsworth, R.B., Vakarelov, B.K. and Nanson, R.A., 2011, Dynamic spatial and
738 temporal prediction of changes in depositional processes on clastic shorelines:
739 towards improved subsurface uncertainty reduction and management: American
740 Association of Petroleum Geologists Bulletin, v. 95, p. 267-297.

741 Al-Aswad, A.A., 1995, Middle Jurassic non-marine siliciclastic facies in Southern
742 Central Saudi Arabia: African Earth Sciences, v. 20, p. 253–262.

743 Al-Eidan, A.J., Wethington, W.B., Davies, R.B., 2001, Upper Burgan Reservoir
744 Description, Northern Kuwait: Impact on Reservoir Development: GeoArabia, v. 6,
745 p. 179-208.

746 Al-Hussaini, A., Steel, R.J., Melvin, J., Olariu, C., Ertug, K., Hooker, N., 2019, New
747 evidence of regressing and transgressing Jurassic siliciclastic coastlines within the
748 Dhruma Formation in Northern Central Arabia, Saudi Arabia: Sedimentary Geology,
749 v. 379, p. 114–137.

750 Al-Husseini, M., 2009, Update to Late Triassic-Jurassic stratigraphy of Saudi Arabia
751 for the Middle East geologic time scale: GeoArabia, v. 14, p. 145–186.

752 Al-Masrahy M.A., 2017, Modelling Temporal and Spatial Sedimentary Architectural
753 Complexity in Mixed Aeolian-Fluvial Reservoir Successions: SPE-8802.

754 Al-Masrahy M.A., and Mountney N.P., 2015, Quantitative Approach to the
755 Characterization of Sedimentary Architecture in Mixed Eolian-Fluvial Reservoir
756 Successions: American Association of Petroleum Geologists, Search and Discovery,
757 Article 41669.

758 Arkell, W.J., 1952, Jurassic ammonites from Jebel Tuwaiq, Central Arabia:
759 Philosophical Transactions of Royal Society of London, Series B, Biological
760 Sciences, v. 236, p. 241–313.

761 Ayranci, K., Lintern, D.G., Hill, P.R., and Dashtgard, S.E., 2012, Tide-supported
762 gravity flows on the upper delta front, Fraser River delta, Canada: Marine Geology,
763 v. 326, p. 166–170.

764 Baniak, G.M., Gingras, M., Burns, B., and Pemberton, S.G., 2014, An example of a
765 highly bioturbated, storm-influenced shoreface deposit: Upper Jurassic Ula
766 Formation, Norwegian North Sea: Sedimentology, v. 61, p. 1-25.

767 Bann, K.L., Tye, S.C., MacEachern, J.A., Fielding, C.R., and Jones, B.G., 2008,
768 Ichnological and sedimentologic signatures of mixed wave- and storm-dominated
769 deltaic deposits: examples from the early Permian Sydney Basin, Australia, *in*
770 Hampson, G.J., Steel, R.J., Burgess, P.M., and Dalrymple, R.W., eds., Recent
771 Advances in Models of Siliciclastic Shallow Marine Stratigraphy: SEPM, Special
772 Publication 90, p. 293–332.

773 Bayer, U., Altheimer, E., and Deutschle, W., 1985, Environmental evolution in
774 shallow epicontinental seas: sedimentary cycles and bed formation, *in* Bayer, W., and
775 Seilacher, A., eds., Sedimentary and Evolutionary Cycles: New York, Springer-
776 Verlag, p. 347-81.

777 Beydoun, Z.R., 1991, Arabian Plate Hydrocarbon Geology and Potential: A Plate
778 Tectonic Approach: American Association of Petroleum Geologists, Studies in
779 Geology, v. 33, 77 p.

780 Bhattacharya, J.P., and MacEachern, J.A., 2009, Hyperpycnal rivers and prodeltaic
781 shelves in the Cretaceous seaway of North America: Journal of Sedimentary
782 Research, v. 79, p.184-209.

783 Boersma, J.R., and Terwindt, J.H.J., 1981, Neap-spring tide sequences of intertidal
784 shoal deposits in a mesotidal estuary: Sedimentology, v. 28, p. 151-170.

785 Boggs, S., 1995, Principles of Sedimentology and Stratigraphy, 2nd Edition: Upper
786 Saddle River, New Jersey, Prentice Hall, 774 p.

787 Boyd, R., Dalrymple, R.W., and Zaitlin, B.A., 1992, Classification of clastic coastal
788 depositional environments: Sedimentary Geology, v. 80, p. 139–150.

789 Bromley, R.G., 1975, Trace fossils at omission surfaces, *in* Frey, R.W., ed., the
790 Study of Trace Fossils: A Synthesis of Principles, Problems, and Procedures in
791 Ichnology: Berlin, Springer-Verlag, p. 399-428.

792 Bromley, R.G., 1996, Trace Fossils; Biology, Taphonomy and Applications, 2nd
793 Edition: London, Chapman & Hall, 361 p.

794 Burton, D., and Wood, L.J., 2013, Geologically-based permeability anisotropy
795 estimates for tidally-influenced reservoirs using quantitative shale data: Petroleum
796 Geoscience, v. 9, p. 3-20.

797 Chen, L., Lu, Y.C., Fu, X.F., Xing, F.C., Wang, C., and Luo, C., 2017, Oolitic shoal
798 complexes characterization of the lower Triassic Feixianguan Formation in the
799 Yuanba gas field, northeast Sichuan Basin, China: Marine and Petroleum Geology, v.
800 83, p. 35–49.

801 Collins, D.S., Johnson, H.D., and Baldwin, C.T., 2020, Architecture and preservation
802 in the fluvial to marine transition zone of a mixed-process humid-tropical delta:

803 Middle Miocene Lambir Formation, Baram Delta Province, north-west Borneo:
804 Sedimentology, v. 67, p. 1-46.

805 Collinson, J.D., and Mountney, N.P., 2019, Sedimentary Structures, 4th Edition:
806 Edinburgh, Dunedin Academic Press, 340 p.

807 Collinson. J.D., Mountney N.P., and Thompson, D.B., 2006. Sedimentary Structures,
808 3rd Edition: Edinburgh, Dunedin Academic Press, 292 p.

809 Colombera, L., and Mountney, N.P., 2020a, On the geological significance of clastic
810 parasequences: Earth-Science Reviews, v. 201, p. 103-062.

811 Colombera, L., and Mountney, N.P., 2020b, Accommodation and sediment-supply
812 controls on clastic parasequences: a meta-analysis: Sedimentology, online, v. 67, p.
813 1667-1709.

814 Colombera, L., Felletti, F., Mountney, N.P. and McCaffrey, W.D., 2012, A database
815 approach for constraining stochastic simulations of the sedimentary heterogeneity of
816 fluvial reservoirs: American Association of Petroleum Geologists, Bulletin, v. 96, p.
817 2143-2166.

818 Colombera, L., Mountney, N.P., Hodgson, D.M., and McCaffrey, W.D., 2016a, The
819 Shallow- Marine Architecture Knowledge Store: a database for the characterization
820 of shallow-marine and paralic depositional systems: Marine and Petroleum Geology,
821 v. 75, p. 83–99.

822 Colombera, L., Shiers, M.N., and Mountney, N.P., 2016b, Assessment of backwater
823 controls on the architecture of distributary-channel fills in a tide-influenced coastal-
824 plain succession: Campanian Neslen Formation, USA: Journal of Sedimentary
825 Research, v. 86, p. 476-497.

826 Crain, E.R., 2015, Crain's Petrophysical Handbook [Online]: [Accessed 11 October
827 2019], Available from https://www.spec2000.net/.

828 Dalrymple, R.W., and Choi, K., 2007, Morphologic and facies trends through the
829 fluvial-marine transition in tide- dominated depositional systems: a schematic
830 framework for environmental and sequence stratigraphic interpretation: Earth-
831 Science Review, v. 81, p. 135–174.

832 Dalrymple, R.W., 2010, Tidal depositional systems, in James, N.P., and Dalrymple,
833 R.W., eds., Facies Models 4: Geological Association of Canada, p. 201–231.

834 Dalrymple, R.W., Baker, E.K., Harris, P.T., and Hughes, M.G., 2003, Sedimentology
835 and stratigraphy of a tide-dominated, foreland-basin delta (Fly River, Papua New
836 Guinea), *in* Sidi, F.H., Nummedal, D., Imbert P., Darman H., and Posamentier,
837 H.W., eds., Tropical Deltas of Southeast Asia—Sedimentology, Stratigraphy, and
838 Petroleum Geology: SEPM, Special Publication 76, p. 147–173.

839 Dalrymple, R.W., Kurcinka, C.E., Jablonski, B.V.J., Ichaso, A.A., and MacKay,
840 D.A., 2015, Deciphering the relative importance of fluvial and tidal processes in the
841 fluvial-marine transition, *in* Ashworth P.J., Best J.L., and Parsons, D.R., eds.,
842 Fluvial-Tidal Sedimentology: Amsterdam, Elsevier, p. 3-40.

843 Dashtgard, S.E., MacEachern, J.A., Frey, S.E., and Gingras, M.K., 2012, Tidal
844 effects on the shoreface: towards a conceptual framework: Sedimentary Geology, v.
845 279, p. 42-61.

846 Davies, P.J., Bubela, B., and Ferguson, J., 1978, The formation of ooids:
847 Sedimentology, v. 25, p. 703-730.

Davis, R.A., 2012, Tidal signatures and their preservation potential in stratigraphic sequences, *in* Davis R.A. Jr., and Dalrymple, R.W., eds., Principles of Tidal Sedimentology: Berlin, Springer-Verlag, p. 35-55.

Desjardins, P.R., Buatois, L.A., and Mangano, 2012, Tidal Flats and Subtidal Sand Bodies, *in* Knaust, D., Bromley, R.G., eds., Trace fossils as indicators of sedimentary environment: Developments in Sedimentology, v. 64, p. 529-561

Dunham, R.J., 1962, Classification of carbonate Rocks according to depositional texture, *in* Ham, W.E., ed., Classification of Carbonate Rocks: American Association of Petroleum Geologists, Memoir 1, p. 108-121.

Einsele, G., 2000, Sedimentary Basins: Evolution, Facies, and Sediment Budget: Berlin, Springer-Verlag, 792 p.

Emery, D., and Myers, K.J., 1996, Sequence Stratigraphy: Victoria, Australia, Blackwell Science Ltd., 291 p.

Enay, R., Mangold, C., Alméras, Y., and Hughes G.W., 2009, The Wadi ad Dawasir "delta", central Saudi Arabia: GeoArabia, v. 14, p. 17-52.

Faqira, M., Rademakers, M., and Afifi, A.M., 2009. New insights into the Hercynian Orogeny, and their implications for the Paleozoic hydrocarbon system in the Arabian Plate: GeoArabia, v. 14, p. 199-228.

Galloway, W.E., 1975, Process framework for describing the morphologic and stratigraphic evolution of deltaic depositional systems, *in* Broussard, M.L., ed., Deltas– Models for exploration: Houston Geological Society, p. 87-98.

Ginsburg R.N., 1975, Tidal Deposits: New York, Springer-Verlag, 428 p.

870 Golonka, J., 2007, Late Triassic and Early Jurassic palaeogeography of the world:
871 Palaeogeography, Palaeoclimatolology, Palaeoecolology, v. 244, p. 297-307.

872 Gugliotta, M., Flint, S.S., Hodgson, D.M., and Veiga, G.D., 2016, Recognition
873 criteria, characteristics and implications of the fluvial to marine transition zone in
874 ancient deltaic deposits (Lajas Formation, Argentina): Sedimentology, v. 63, p.
875 1971–2001.

876 Gugliotta, M., Saito, Y., Nguyen, V. L., Ta, T. K. O., Nakashima, R., Tamura, T.,
877 Uehara, K., Katsuki, K., and Yamamoto, S., 2017, Process regime, salinity,
878 morphological, and sedimentary trends along the fluvial to marine transition zone of
879 the mixed-energy Mekong River Delta, Vietnam, *in* Ogston, A.S., Allison, M.A.,
880 Mullarney, J.C., Nittrouer, C.A., eds., Sediment- and Hydro-Dynamics of the
881 Mekong Delta: From Tidal River to Continental Shelf: Continental Shelf Research,
882 v. 147, p. 7–26.

883 Gugliotta, M., Saito, Y., Nguyen, V.L., Ta, T.K.O., and Tamura, T., 2019, Sediment
884 distribution and depositional processes along the fluvial to marine transition zone of
885 the Mekong River delta, Vietnam: Sedimentology, v. 66, p. 146–164.

886 Hallam, A., and Bradshaw, M.J., 1979, Bituminous shales and oolitic ironstones as
887 indicators of transgressions and regressions: Geological Society of London, v. 136, p.
888 157-164.

889 Haq, B.U., and Al-Qahtani, A.M., 2005, Phanerozoic cycles of sea-level change on
890 the Arabian Platform: GeoArabia, v. 10, p. 127–160.

891 Haq, B.U., Hardenbol, J., and Vail, P., 1988, Mesozoic and Cenozoic
892 chronostratigraphy and cycles of sea-level change, *in* Wiglus, C.K., Hastings, B. S.,

893 Kendall, C.G., Posmentier, H.W., Ross, C.A., and Van Wagoner, J. C., eds., Sea-
894 Level Change: an Integrated Approach :SEPM, v. 42, p. 71–108.

895 Harms, J.C., Southard, J.B., Spearing, D.R., and Walker, R.G., 1975, Depositional
896 Environments as Interpreted from Primary Sedimentary Structures and Stratification
897 Sequences: SEPM, Short Course 2, 161 p.

898 Harris, P., Heap, A., Bryce, S., Porter-Smith, R., Ryan, D., and Heggie, D., 2002,
899 Classification of Australian clastic coastal depositional environments based upon a
900 quantitative analysis of wave, tidal, and river power: Journal of Sedimentary
901 Research, v. 72, p. 858-870.

902 Hein, F.J., 2015, The Cretaceous McMurray oil sands, Alberta, Canada: A world-
903 class, tidally influenced fluvial–estuarine system—An Alberta government
904 perspective, *in* Ashworth P.J., Best J.L., and Parsons, D.R., eds., Fluvial-Tidal
905 Sedimentology: Amsterdam, Elsevier, p. 561-621.

906 Heldreich, G., Redfern J., Legler B., Gerdes K., and Williams B.P.J., 2017,
907 Challenges in characterizing subsurface paralic reservoir geometries: a detailed case
908 study of the Mungaroo Formation, North West Shelf, Australia, *in* Hampson, G.J.,
909 Reynolds, A.D., Kostic, B., and Wells, M.R., eds., Sedimentology of Paralic
910 Reservoirs: Recent Advances: Geological Society of London, Special Publications
911 444, p. 59–108.

912 Howell, J.A., Skorstad, A., MacDonald, A., Fordham, A., Flint, S., Fjellvoll, B., and
913 Manzocchi, T., 2008, Sedimentological parameterization of shallow-marine
914 reservoirs: Petroleum Geoscience, v. 14, p. 17-34.

915 Hubbard, S.M., Smith, D.G., Nielsen, H., Leckie, D.A., Fustic, M., Spencer, R.J. and
916 Bloom, L., 2011, Seismic geomorphology and sedimentology of a tidally influenced

917 river deposit, Lower Cretaceous Athabasca oil sands, Alberta, Canada. American
918 Association of Petroleum Geologists, Bulletin, v. 95, p. 1123-1145.

919 Jackson, M.D., Yoshida, S., Muggeridge, A.H., and Johnson, H.D. 2005, Three-
920 dimensional reservoir characterisation and flow simulation of heterolithic tidal
921 sandstones: American Association of Petroleum Geologists, Bulletin, v. 89, p. 507–
922 528.

923 Johnson, H.D., and Baldwin, C.T., 1986., Shallow siliciclastic seas, *in* Reading,
924 H.G., ed., Sedimentary Environments and Facies: London, Blackwell, p. 229-282.

925 Klein, G.V., 1985, Intertidal flats and intertidal sand bodies, *in* Davis, R.A., ed.,
926 Coastal Sedimentary Environments, 2nd Edition: New York, Springer-Verlag, p.
927 187–224.

928 La Croix, A., and Dashtgard, S., 2014, Of sand and mud: sedimentological criteria
929 for identifying the turbidity maximum zone in a tidally influenced river:
930 Sedimentology, v. 61, p. 1961–1981.

931 La Croix, A.D. and Dashtgard, S.E., 2015, A synthesis of depositional trends in
932 intertidal and upper subtidal sediments across the tidal-fluvial transition in the Fraser
933 River, Canada: Journal of Sedimentary Research, v. 85, p. 683-698.

934 La Croix, A.D., Dashtgard, S.E., and MacEachern, J.A., 2019a, Using a modern
935 analogue to interpret depositional position in ancient fluvial-tidal channels: example
936 from the McMurray Formation, Canada: Geoscience Frontiers, v. 10, p. 2219-2238.

937 La Croix, A.D., Wang, J., He, J., Hannaford, C., Bianchi, V., Esterle, J.S., and
938 Underschultz, J.R., 2019b, Widespread nearshore and shallow marine deposition

within the Lower Jurassic Precipice Sandstone and Evergreen Formation in the Surat Basin, Australia: Marine and Petroleum Geology, v. 109, p. 760-790.

Livera, S.E., and Caline, B., 1990, The sedimentology of the Brent Group in the Cormorant block IV oilfield: Journal of Petroleum Geology, v. 13, p. 367-396.

Loisel, H., Mangin, A., Vantrepotte, V., Dessailly, D., Dinh, D.N., Garnesson, P., Ouillon, S., Lefebvre, J.P., Meriaux, X., and Phan, T.M., 2014. Variability of suspended particulate matter concentration in coastal waters under the Mekong's influence from ocean color (MERIS) remote sensing over the last decade: Remote Sensing of Environment, v. 150, p. 218-230.

MacEachern, J.A., and Bann, K.L., 2008, The role of ichnology in refining shallow marine facies models, *in* Hampson, G., Steel, R., Burgess, P., Dalrymple, R., eds., Recent Advances in Models of Siliciclastic Shallow-Marine Stratigraphy: SEPM, Special Publication 90, p. 73–116.

MacEachern, J.A., Raychaudhuri, I., and Pemberton, S.G., 1992, Stratigraphic applications of the *Glossifungites* ichnofacies: delineating discontinuities in the rock record, *in* Pemberton, S.G., ed., Application of Ichnology to Petroleum Exploration: A Core Workshop: SEPM, p. 169–198.

MacEachern, J.A., Bann, K.L., Pemberton, S.G. and Gingras, M.K., 2007a, The ichnofacies paradigm: high-resolution paleoenvironmental interpretation of the rock record, *in* MacEachern, J.A., Bann, K.L., Gingras, M.K. and Pemberton, S.G., eds., Applied Ichnology: SEPM, p. 27-64.

MacEachern, J.A., Pemberton, S.G., Bann, K.L. and Gingras, M.K., 2007b, Departures from the Archetypal Ichnofacies: Effective Recognition of Physico-

962 Chemical Stresses in the Rock Record, *in* MacEachern, J.A., Bann, K.L., Gingras,
963 M.K. and Pemberton, S.G., eds., Applied Ichnology: SEPM, p. 65-93.

964 MacEachern, J.A., Dashtgard, S.E., Knaust, D., Catuneanu, O., Bann, K.L., and
965 Pemberton, S.G., 2012, Sequence stratigraphy, *in* Knaust, D., and Bromley, R.G.,
966 eds., Trace Fossils as Indicators of Sedimentary Environments: Developments in
967 Sedimentology, v. 64, p. 157–194.

968 Martin, C.A.L., 1995, The origin of massive sandstone facies in an ancient braided
969 river deposits [PhD Thesis]: Durham University, Durham, United Kingdom, 329 p.

970 Martini, I., and Aldinucci M., 2017, Sedimentation and basin-fill history of the
971 Pliocene succession exposed in the northern Siena-Radicofani Basin (Tuscany,
972 Italy): a sequence-stratigraphic approach: Research in Palaeontology and
973 Stratigraphy, v. 123, p. 407-432.

974 Martinius, A.W., and Gowland, S., 2011, Tide-influenced fluvial bedforms and tidal
975 bore deposits (late Jurassic Lourinhã Formation, Lusitanian Basin, Western
976 Portugal): Sedimentology, v. 58, p. 285-324.

977 Martinius, A.W., Ringrose P.S., Brostrom , C., Elfenbein, C., Nass, A., and Ringas,
978 J.E., 2005, Reservoir Challenges of Heterolithic Tidal Sandstone Reservoirs in
979 Halten Terrace, mid-Norway: Petroleum Geoscience, v. 11, p. 3-16.

980 Martinius, A.W., Jablonski, B.V.J., Fustic, M., Strobl, R., and Van den Berg, J.H.,
981 2015, Fluvial to tidal transition zone facies in the McMurray Formation (Christina
982 River, Alberta, Canada), with emphasis on the reflection of flow intensity in
983 bottomset architecture, *in* Ashworth P.J., Best J.L., and Parsons, D.R., eds., Fluvial-
984 Tidal Sedimentology: Amsterdam, Elsevier, v. 68, p. 445–480.

985 Massart, B.Y.G., Jackson, M.D., Hampson, G.J., and Johnson, H.D., 2016, Effective
986 flow properties of heterolithic, cross-bedded tidal sandstones, part 2: flow
987 simulation: American Association of Petroleum Geologists, Bulletin, v. 100, p. 723–
988 742.

989 Maynard, J.B., 1983, Geochemistry of Sedimentary Ore Deposits: New York,
990 Springer-Verlag, 305 p.

991 Meene, J.W.H., Boersma, J.R., and Terwindt, J.H.J., 1996, Sedimentary structures of
992 combined flow deposits from the shoreface-connected ridges along the central Dutch
993 coast: Marine Geology, v. 131, p. 151–175.

994 Miall, A.D., 1985, Architectural-element analysis: a new method of facies analysis
995 applied to fluvial deposits: Earth-Science Reviews, v. 22, p. 261-308.

996 Nio, S.D., and Yang, C.S., 1991, Diagnostic attributes of clastic tidal deposits: a
997 review, *in* Smith, D.G., Reinson, G.E., Zaitlin, B.A., and Rahmani, R.A., eds.,
998 Clastic Tidal Sedimentology: Canadian Society of Petroleum Geologists, Memoir 16,
999 p. 3-28.

1000 Olariu, C., Steel, R.J., Dalrymple, R.W. and Gingras, M.K., 2012, Tidal dunes versus
1001 tidal bars: The sedimentological and architectural characteristics of compound dunes
1002 in a tidal seaway, the lower Baronia Sandstone (Lower Eocene), Ager Basin,
1003 Spain: Sedimentary Geology, v. 279, p. 134-155.

1004 Pemberton, S.G., and Frey, R.W., 1985, The *Glossifungites* ichnofacies: modern
1005 examples from the Georgia coast, *in* Curran, H.A., ed., Biogenic Structures: Their
1006 Use in Interpreting Depositional Environments: SEPM, Special Publication 35, p.
1007 237–259.

1008 Pemberton, S.G., Reinson, G.E., and MacEachern, J.A., 1992, Comparative
1009 ichnological analysis of late Albian estuarine valley-fill and shelf-shoreface deposits,
1010 *in* Pemberton, S.G., ed., Applications of Ichnology to Petroleum Exploration: SEPM,
1011 Core Workshop 17, p. 291–317.

1012 Pemberton, S.G., and MacEachern, J.A., 1997, The ichnological signature of storm
1013 deposits: the use of trace fossils in event stratigraphy, *in* Brett, C.E., ed.,
1014 Paleontological Event Horizons: New York, Columbia University Press, p. 73-109.

1015 Pemberton, S.G., Spila, M., Pulham, A.J., Saunders, T., MacEachern, J.A., Robbins,
1016 D., and Sinclair, I.K., 2003, Ichnology and sedimentology of shallow marine to
1017 marginal marine systems: Ben Nevis & Avalon reservoirs, Jeanne d'Arc Basin:
1018 Bulletin of Canadian Petroleum Geology, v. 51, p. 206-211.

1019 Pemberton, S.G., MacEachern, J.A., Dashtgard, S.E., Bann, K.L., Gingras M.K., and
1020 Zonneveld J-P., 2012, Shorefaces, *in* Knaust, D., and Bromley, R.G., eds., Trace
1021 Fossils as Indicators of Sedimentary Environments: Amsterdam, Elsevier, v. 64, p.
1022 563-603.

1023 Porebsky, S.J., and Steel, R.J., 2006, Deltas and sea-level change: Journal of
1024 Sedimentary Research, v. 76, p. 390–403.

1025 Powers, R., Ramirez, L., Redmond, C., and Elberg, E., 1966, Geology of the Arabian
1026 Peninsula: Washington, D.C., United States Government Printing Office, 147 p.

1027 Powers, R.W., 1968, Lexique Stratigraphique International: Paris, Centre National de
1028 la Recherche Scientifique, p. 73–109.

1029 Prokocki, E.W., Best, J.L., Ashworth, P., Parsons, D.R., Sambrook Smith, G.H.,
1030 Nicholas, A.P., Simpson, C.J., Wang, H., Sandbach, S., and Keevil, C., 2015, Mid to

late Holocene geomorphological and sedimentological evolution of the fluvial–tidal zone: Lower Columbia River, WA/OR, USA, *in* Ashworth P.J., Best J.L., and Parsons, D.R., eds., Fluvial-Tidal Sedimentology: Amsterdam, Elsevier, v. 68, p. 193–226.

Rankey, E.C., and Reeder, S.L., 2012, Tidal sands of the Bahamian archipelago, *in* Davis, R.A., and Dalrymple, R.W., eds., Principles of Tidal Sedimentology: Berlin, Springer-Verlag, p. 537–565.

Reineck, H-E., and Wunderlich, F., 1968., Classification and origin of flaser, and lenticular bedding: Sedimentology, v. 11, 99–104.

Reineck, H-E., and Singh, I.B., 1980, Depositional Sedimentary Environments - With Reference to Terrigenous Clastics, 2nd Edition: Berlin, Springer-Verlag, 549 p.

Reynolds, A.D., 2017, Paralic reservoirs, *in* Hampson, G.J., Reynolds, A.D., Kostic, B., and Wells, M.R., eds., Sedimentology of Paralic Reservoirs: Recent Advances: Geological Society of London, Special Publication 444, p. 7-34.

Ringrose, P.S., Nordhal, K., and Wen, R., 2005, Vertical permeability estimation of heterolithic tidal deltaic sandstones: Petroleum Geoscience, v. 11, p. 29–36.

Robert, C., and Chamley, H., 1991, Development of early Eocene warm climates, as inferred from clay mineral variations in oceanic sediments: Global and Planetary Change, v. 3, p. 315–331.

Schlaich, M., and Aigner, T., 2017, Facies and integrated sequence stratigraphy of an Epeiric Carbonate Ramp Succession: Dhruma Formation, Sultanate of Oman: Sedimentology, v. 3, p. 62-132.

Scotese, C.R., 2001, Atlas of Earth History, Vol. 1, Palaeogeography , 52 p., Paleomap Project, Arlington, Texas.

Seton, M., Muller, R.D., Zahirovi c, S., Gaina, C., Torsvik, T., Shephard, G., Talsma, A., Gurnis, M., Turner, M., Maus, S., and Chandler, M., 2012, Global continental and ocean basin reconstructions since 200 Ma: Earth-Science Review, v. 113, p. 212–270.

Shchepetkina, A., Gingras, M.K., and Pemberton, S.G., 2016, Sedimentology and ichnology of the fluvial reach to inner estuary of the Ogeechee River estuary, Georgia, USA: Sedimentary Geology, v. 342, p. 202–217.

Shiers, M.N., Mountney, N.P., Hodgson, D.M. and Cobain, S.L., 2014, Depositional Controls on Tidally Influenced Fluvial Successions, Neslen Formation, Utah, USA: Sedimentary Geology, v. 311, p. 1-16.

Soliman, F.A., and Al-Shamlan, A.A., 1982, Review on the geology of the Cretaceous sediments of the Rub' al-Khali, Saudi Arabia: Cretaceous Research, v. 3, p. 187–194.

Stampfli, G.M., and Borel, G.D., 2002, A plate tectonic model for the Paleozoic and Mesozoic constrained by dynamic plate boundaries and restored synthetic oceanic isochrons: Earth and Planetary Science Letters, v. 196, p. 17–33.

Stewart, S.A., 2016, Structural geology of the Rub' Al-Khali Basin, Saudi Arabia: Tectonics, v. 35, p. 2417–2438.

Stewart, S.A., Reid, C.T., Hooker, N.P., and Kharouf, O.W., 2016, Mesozoic siliciclastic reservoirs and petroleum system in the Rub' Al-Khali basin, Saudi Arabia: American Association of Petroleum Geologists, Bulletin, v. 100, p. 819–841.

1076 Tawfik, M., Al-Dabbagh, M., and El-Sorogy, A., 2016, Sequence stratigraphy of the
1077 late middle Jurassic open shelf platform of the Tuwaiq Mountain Limestone
1078 Formation, central Saudi Arabia: Proceedings of the Geologists' Association, v. 127,
1079 p. 395–412.

1080 Taylor, A.M. and Goldring, R., 1993, Description and analysis of bioturbation and
1081 ichnofabric: Geological Society of London, v. 150, p. 141-148.

1082 Thomas, R.G., Smith, D.G., Wood, J.M., Visser, J., Calverley-Range, E.A., and
1083 Koster, E.H., 1987, Inclined heterolithic stratification - terminology, description,
1084 interpretation and significance: Sedimentary Geology, v. 53, p. 123-179.

1085 Tirsgaard, H., 1996, Cyclic sedimentation of carbonate and siliciclastic deposits on a
1086 late Precambrian ramp: the Elisabeth Bjerg Formation (Eleonore Bay Supergroup),
1087 East Greenland: Journal of Sedimentary Research, v. 66, p. 699-712.

1088 Vakarelov, B.K., and Ainsworth, R.B., 2013, A hierarchical approach to architectural
1089 classification in marginal-marine systems: bridging the gap between sedimentology
1090 and sequence stratigraphy: American Association of Petroleum Geologists,
1091 Bulletin, v. 97, p .1121-1161.

1092 Van de Lageweg, W.I., Braat, L., Parsons, D.R., and Kleinhans, M. G., 2018,
1093 Controls on mud distribution and architecture along the fluvial-to-marine transition:
1094 Geology, v. 46, p. 971– 974.

1095 Van den Berg, J.H., Boersma, J.R., and Van Gelder, A., 2007, Diagnostic
1096 sedimentary structures of the fluvial–tidal transition zone. Evidence from deposits of
1097 the Rhine Delta: Netherland Journal of Geoscience, v. 86, p. 253–272.

1098 Van Houten, F.B., 1985, Oolitic ironstones and contrasting Ordovician and Jurassic
1099 paleogeography: Geology, v. 13, p. 722-24.

1100 Van Wagoner, J.C., Mitchum, R.M., Campion, K.M., and Rahmanian, V.D., 1990,
1101 Siliciclastic Sequence Stratigraphy in Well Logs, Cores and Outcrops: Concepts for
1102 High-resolution Correlation of Time and Facies: American Association of Petroleum
1103 Geologists, Methods in Exploration Series 7, 55 p.

1104 Vaslet, D., Manivit, J., Le Nindre, Y., Brosse, J., Fourniguet, J., and Delfour, J.,
1105 1983, Explanatory Notes to the Geologic Map of the Wadi Ar Rayn Quadrangle,
1106 Kingdom of Saudi Arabia: Saudi Arabian Deputy Ministry for Mineral Resources,
1107 Geoscience Map GM-63C.

1108 Vicalvi, M.A., and Milliman, J.D., 1977, Calcium carbonate sedimentation on
1109 continental shelf off Southern Brazil, with special reference to Benthic Foraminifera,
1110 *in* Frost, S.H., Weiss, M.P., and Saunders, J.B., eds., Reefs and Related Carbonates–
1111 Ecology and Sedimentology: American Association of Petroleum Geologists, Studies
1112 in Geology 4, p. 313-328.

1113 Visser, M.J., 1980, Neap-spring cycles reflected in Holocene subtidal large scale
1114 bedform deposits: a preliminary note: Geology, v. 8, p. 543-546.

1115 Weaver, C.E., 1989, Clays, Muds, and Shales: Amsterdam, Elsevier, Development in
1116 Sedimentology, v. 44, 818 p.

1117 Wightman, D.M., and Pemberton, S.G., 1997, The lower Cretaceous (Aptian)
1118 McMurray Formation: an overview of the Fort McMurray area, northeastern Alberta,
1119 *in* Pemberton, S.G., and James, D.P., ed., Petroleum Geology of the Cretaceous
1120 Mannville Group: Canadian Society of Petroleum Geologists, Memoir 18, p. 312–
1121 344.

1122 Ziegler, M.A., 2001, Late Permian to Holocene paleofacies evolution of the Arabian
1123 Plate and its hydrocarbon occurrences: GeoArabia, v. 6, p. 445–504.

1124

1125 ## TABLE CAPTIONS

1126 Table 1. Summary of lithofacies observed in the lower Dhruma Formation.

1127

1128 Table 2. Summary of the facies associations defined in this study, along with their
1129 occurrence with respect to well locations.

1130 ## FIGURE CAPTIONS

1131 Figure 1. A) Simplified regional geological map of the Arabian Peninsula, adapted
1132 from Stewart et al. (2016). B) Well distribution map in the study area. The exact
1133 geographic location of the wells cannot be published due to the proprietary nature of
1134 the dataset. C) Generalized stratigraphy of Eastern Saudi Arabia.

1135

1136 Figure 2. Representative sedimentary logs depicting the different facies associations
1137 defined in the lower Dhruma Formation and their vertical relationships. A) "Fluvial
1138 channels" and "intertidal flats and pedogenically modified supratidal or floodplain"
1139 facies associations. B) "River-influenced tidal bars" facies associations. C) "Weakly
1140 storm-affected shoreface and offshore transition zone" and "fluvial-influenced storm-
1141 dominated delta-front and prodelta" facies associations; note the occurrence of the
1142 oolitic ironstone facies association FA5 below the shoreface successions. D)
1143 Carbonate shelf facies associations occurring in the uppermost part of the cored
1144 section. E) Simplified paleogeographic map of the lower unit of the lower Dhruma

Formation based on this study. F) Legend with color codes for facies associations and symbols used in the sedimentary logs. See text for further explanation.

Figure 3. Representative core photographs of "fluvial channel" facies association (FA1). A,B) massive to faintly bedded sandstone with lag sediments at the bottom and common floating coal debris and mud chips. B) Alternating sandstone and heterolithic facies. D,E) transition between sandstone and heterolithic facies (white arrows indicate double mud drapes in Part D. F) Non-stratified facies of FA2b overlying the FA1. G,H) Thin sections representing the petrography of the sandstone facies (G) and heterolithic facies (H) defined in FA1; note variation in grain size and mud content.

Figure 4. Representative core photographs of " tidal flat" (FA2a, A-C) and "paleosol" (FA2b, D-G) facies associations. A,B) Heterolithic sand and mud facies; note the stacked bidirectional ripple forms (black arrows) and double mud drapes (white arrows). C) Intense bioturbation in the sand-mud alternation; D, E) Kaolinite-rich sandstone, siltstone, and mudstone with intense rooting; note the color mottling in photograph E. F, G) Coaly mudstone. H, I) representative thin sections of the heterolithic facies of FA2a.

Figure 5. Representative core photographs of the "fluvial-influenced tidal bars" facies association (FA3). A) Cross-bedded sandstone with apparent bundled bedsets showing internal mud drapes. B, C) Cross-stratified sandstone showing thin beds of very coarse sand in medium-grained sandstone; note the double mud drapes in part

B. D, E) Heterolithic and kaolinite-rich deposits that overlie the tidal-bar deposits. F, G) Representative thin sections of tidal-bar facies; note the presence of kaolinite.

Figure 6. Representative core photographs of "offshore-transition zone to shoreface" (FA4a; A-D) and prodelta to delta-front (FA4b; E-I) facies associations. A) Heterolithic facies overlying bioturbated sandstone. B) Slightly asymmetrical wave ripple. C) Bioturbated sandstone. D) Representative thin section showing deformed chamosite ooids in heterolithic facies. E, F) Thin sandstone intervals interbedded with heterolithic and mudstone facies. G, H) Hummocky cross stratification. I) Thin section showing abundant chlorite cement in hummocky cross-stratified sandstone.

Figure 7. Representative core photographs of "open-marine shelf carbonate" facies association (FA5). A, B) Bioturbated limestone. C) Calcareous mudstone. D) Calcareous sandstone overlying massive mudstone. E) Ooid-rich ironstone. F, G) Representative thin-section examples showing calcareous sandstone (F) and ooid-rich ironstone (G).

Figure 8. Rose diagrams showing the dominant dip direction of cross-stratification in different sandstone units, based on analysis of image logs. See Figure 4 for keys to facies associations and symbols.

Figure 9. Cross plots showing thickness and lateral dip extent for analog sedimentary units that broadly match with the defined facies associations, as derived from a sedimentological database (Colombera et al., 2016a). A) Data relating to

parasequence-scale sedimentary units representing the product of regression of shoreface and more generally shallow-marine (i.e., encompassing sand-prone offshore transition) sand belts (Colombera et al., 2016a, 2016b; Colombera and Mountney, 2020a). B) Data relating to architectural elements classified as "tidal bar" and "tidal flat".

Figure 10A. Strike-oriented stratigraphic cross section (A-A') showing the distribution of facies associations and key stratigraphic surfaces as correlated along strike in a seaward position.

Figure 10B. Strike-oriented stratigraphic cross section (B-B') showing facies associations and stratigraphic surfaces as correlated along strike in a landward position compared to cross-section A-A'.

Figure 10C. Dip-oriented stratigraphic cross-section (C-C') intersecting the two strike-oriented cross sections (A-A' and B-B') showing the distribution of facies associations and key stratigraphic surfaces as correlated along depositional dip, and documenting the increase in marine deposits towards the northeast (basinward).

Figure 11. A depositional model depicting the evolution of the Middle Jurassic lower Dhruma Formation over five intervals. Each interval represents a synthesis of the five intervals highlighted in Figure 10C.

Table 1. Summary of lithofacies observed in the lower Dhruma Formation.

Code	Facies	Description	Bioturbation Index (0-6)	Process Interpretation	Depositional Environment
F1 Hms	Heterolithic mudstone and sandstone	Light to dark gray, heterolithic silty very fine to fine sandstone and claystone. Grains are angular to subrounded, and poorly to moderately sorted. Characterized by lenticular, wavy, and flaser bedding. Pyrite nodules are present and are associated with the presence of mudstone.	0-3	Fluctuating energy levels including ebb and flood tidal processes	Intertidal zone, offshore transition zone
F2 Sx	Trough and planar cross-bedded sandstone	Brown, medium to coarse sandstone with sparse fine sand grains, subrounded to subangular, moderately sorted. Characterized by high- and low-angle-inclined cross bedding, rare irregular lamination.	0-1	Migration of 2D and 3D dunes	Compound bars in estuary, tidal bars (subtidal to intertidal zones)
F3 Ms	Mudstone	Dark gray to black blocky mudstone, non-calcareous. No pronounced sedimentary structures were observed. It commonly contains abundant pyrite nodules.	0-1	Fallout of sediment from suspension in quiet-water conditions	Shelf environment, distal prodelta, restricted lagoon, restricted tidal flats
F4 Sd	non-stratified, rooted sandstone and siltstone	Light gray, light greenish gray, spotty reddish in color, siltstone and very fine sandstone grained, subangular to subrounded grains, mostly poorly sorted. Shows irregular non-stratified sedimentary structures and rare planar laminations. Also shows common rootlets and reddish to blackish fracture-like structures (likely shrinkage fractures of paleosols). Rare clustered small pyrite nodules (2-5 mm in diameter).	Rare-3	Chemical alteration during subaerial exposure	Supratidal-plain setting
F5 Cm	Coal and carbonaceous mudstone	Black to dark gray, almost homogeneous deposits with no pronounced sedimentary structures.	Rare		Supratidal-plain setting
F6 Shcs	Hummocky cross-stratified sandstone	Light gray creamy, very fine- to medium-grained sandstone, subangular to subrounded grains, moderately sorted. Characterized by cross lamination, hummocky cross-stratification. Alternating mud and sand rhythmites present. Single and double mud drapes common. Rare 10-15-cm-thick intervals of gravel lag deposits and floating mud chips. Bioturbation can occur but has low intensity of bioturbation.	1-2	Waves; oscillatory currents	Middle and lower shoreface, shelf ridge or barrier island and delta front

F7 Sb	Bioturbated sandstone and silty sandstone	Cream and gray, silty to medium sandstone, angular to subrounded grains, poorly to moderately sorted. Shows deformed and irregular sedimentary structures due to bioturbation. Bioturbation index varies between wells.	2-5	Burrowing of animals in substrate in low- to high-energy environment	Offshore transition zone, below storm wave base, restricted lagoon, estuarine central basin, channel-associated tidal flats
F8 Sm	Massive structureless or faintly laminated sandstone	Gray and brown, medium to coarse grained sandstone, subrounded grains, moderately to well sorted.	0-2	Rapid or continuous sedimentation	Fluvial deposits (channel fill)
F9 Ls	Limestone	Dark gray, packstone and grainstone (Dunham classification). Well-rounded quartz grains present, shell fragments, coated grains, ooids, and aggregate grains. Grains range in size from silt to coarse; poorly sorted. No pronounced sedimentary structures.	3-5	Biogenic activity	Open-marine shelf environment
F10 Lsd	Dolomitic limestone	Dark gray, mudstone to wackstone (Dunham classification). Quartz grains present but decrease upwards, coated grains, intraclasts, shell and skeletal fragments. Poorly sorted. No sedimentary structures. Moderate to intense bioturbation.	3-5	Biogenic activity and diagenesis	Open-marine shelf environment
F11 Msc	Calcareous mudstone	Dark gray to black, blocky mudstone, mostly calcareous (calcite absent toward the top of beds). Abundant replaced shell fragments. Thin interbedding of oolitic siltstone and sandstone. No pronounced sedimentary structures. Pyrite nodules are present.	Rare to 2	Fallout of sediment from suspension in quiet-water conditions	Shelf environment with close proximity to carbonate platform, offshore mud, distal prodelta
F12 Sc	Calcareous sandstone and siltstone	Gray to dark gray, fine to medium-grained, with common sparse coarse quartz grains, scattered ooids, angular to rounded grains, moderately sorted. Faint planar lamination and common deformed sedimentary structures due to moderate to intense bioturbation.	3-5	Mix of detrital input and marine calcium carbonate	Inner shelf, carbonate platform and oolitic shoal
F13 Ors	Oolitic ironstone	Reddish, fine to medium quartz grains, medium to coarse ooid grains. Rare irregular lamination.	1-2	Biogenic activity in a high-energy environment	Shoal complex with periodic subaerial exposure
F14 Lg	Granule and pebble lag	Medium to coarse sandstone with occasional very coarse sand grains and granules, subangular to rounded grains. Very rare small pebbles. Poorly sorted. Normal grading in some cases.	rare	Sedimentation by high-energy currents	Fluvial channels, river-influenced deposits

Table 2. Summary of the facies associations defined in this study along with their occurrence with respect to well locations.

Facies Association	**Facies Association Description**	**Occurrence: well number**
Fluvial-channel deposits (FA1)	Massive sandstone (Sm) and/or cross-bedded sandstone (Sx) that are commonly overlain by heterolithic mudstone and sandstone (Hms) and mudstone (Ms)	1, 2, 4, 7, 10, 12, 13
Intertidal-flat deposits (FA2a)	Dominated by (Hms) with a fining-upward trend from sand-dominated to mud-dominated facies. Local soft-sediment deformation (Sd) occurs in the sand-dominated part.	1, 2, 4, 5, 7, 8, 12, 13
Pedogenically modified supratidal flat or floodplain (FA2b)	Composed dominantly of non-stratified sandstone, siltstone, and mudstone (Sd) with local presence of carbonaceous mudstone intervals (Cm).	1, 2, 4, 5, 7, 8, 10, 12, 13
River-influenced tidal bars (FA3)	Massive sandstone (Sm) with scoured bases that grades up to cross-bedded sandstone (Sx) with abundant mud laminae draping the cross-stratified sets.	3, 4, 11
Weakly storm-influenced shoreface to offshore transition zone (FA4a)	Coarsening-upward packages of mudstone (Ms) and/or heterolithic mudstone and sandstone (Hms) that grade up to bioturbated (Sb) and/or hummocky cross-stratified sandstone.	1, 2, 5, 6, 7, 8, 11, 14
Storm-dominated delta front to prodelta (FA4b)	Coarsening-upward packages of (Ms) and/or heterolithic mudstone and sandstone (Hms) that grade up to cross-bedded (Sx) hummocky cross-stratified sandstone.	2
Carbonate shelf (FA5a)	Fining-upward packages are observed in well 2 with limestone (packstone and grainstone) dominating the base of each package; this generally grades up to calcareous mudstone (Msc). Conversely, coarsening-upward limestone (Ls) packages from wackstone to grainstone are observed in wells 7 and 11. The bottom of the limestone in well 7 shows dolomite limestone interval (Lsd) that becomes more calcareous upwards.	2, 7, 11
Iron-rich oolitic shoal (FA5b)	Fining-upward trends with calcareous sandstone (Sc) or ooid-rich ironstone (Ore) at the bottom that transition up to calcareous mudstone (Msc).	1, 5, 7, 8, 9, 13

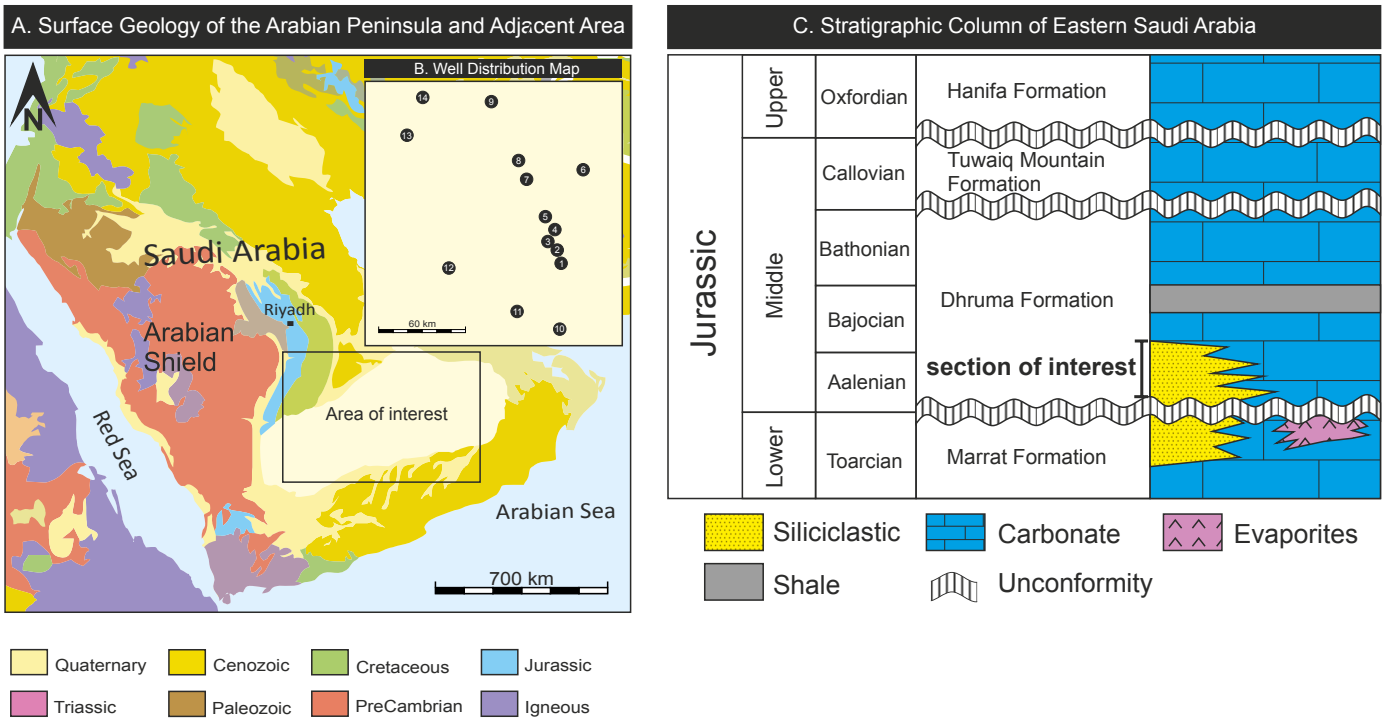
A. Surface Geology of the Arabian Peninsula and Adjacent Area
B. Well Distribution Map
C. Stratigraphic Column of Eastern Saudi Arabia
N
Saudi Arabia
Riyadh
Arabian Shield
Area of interest
Red Sea
Arabian Sea
700 km
60 km
Quaternary
Cenozoic
Cretaceous
Jurassic
Triassic
Paleozoic
PreCambrian
Igneous
Jurassic
Upper
Middle
Lower
Oxfordian
Callovian
Bathonian
Bajocian
Aalenian
Toarcian
Hanifa Formation
Tuwaiq Mountain Formation
Dhruma Formation
section of interest
Marrat Formation
Siliciclastic
Carbonate
Evaporites
Shale
Unconformity

Figure 1

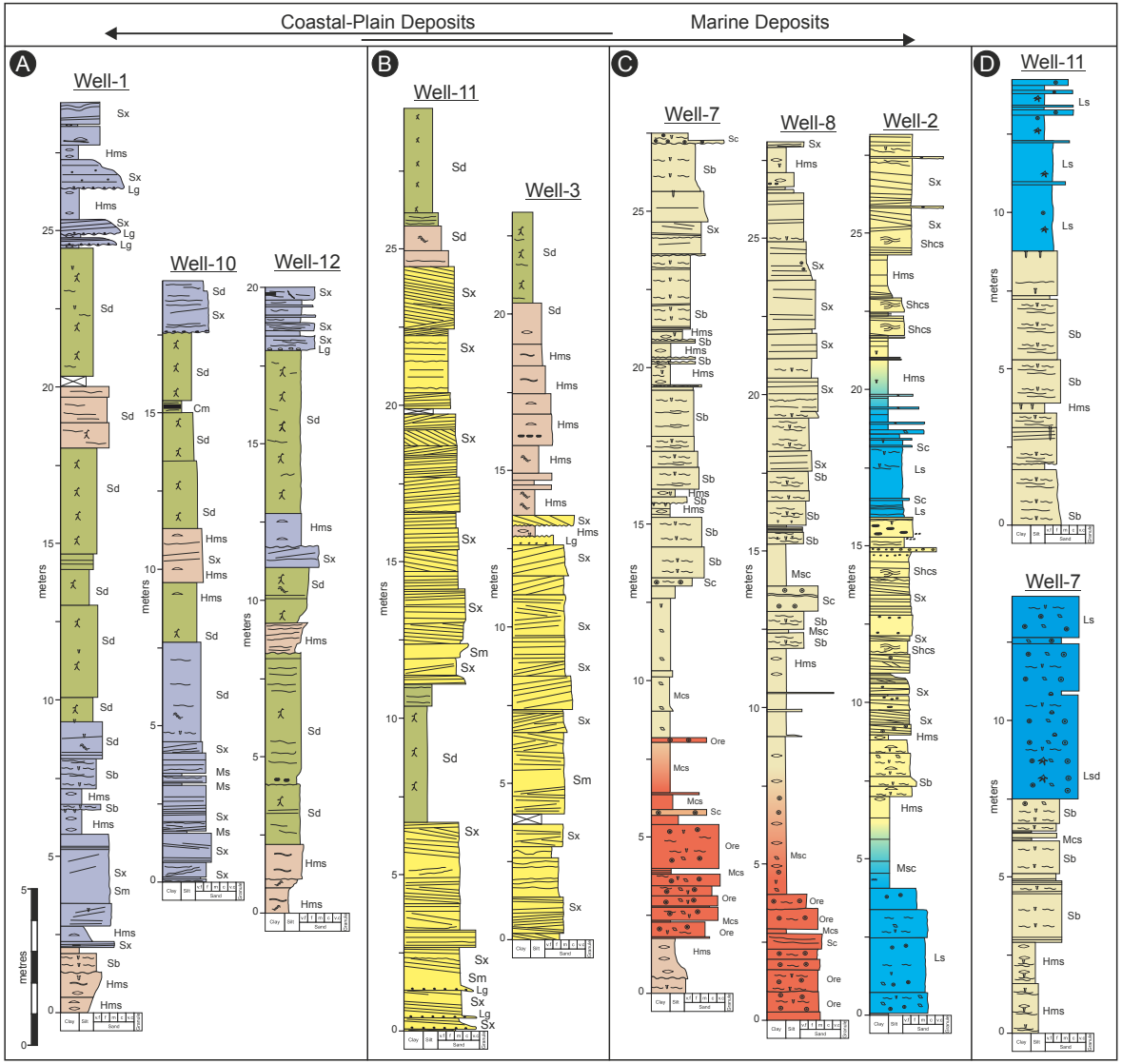

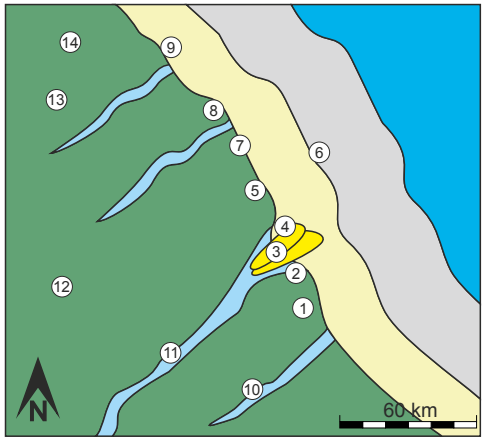

F. Legend

Key to Facies Association

- Fluvial Channel and Overbank (FA1)
- Intertidal Flat (FA2.a)
- Supratidal Flat/Floodplain (Palaeosol) (FA2.b)
- Fluvially influenced Tidal Bars (FA3)
- Weakly Storm-affected Shoreface (FA4.a)
- Storm-Dominated Delta Front (FA4.b)
- Carbonate Shelf (FA5.a)
- Ooid-rich Ironstone (FA5.b)

Key to Sedimentary Structures and Composition

- Cross Bedding
- Irregular Lamination
- Flaser Bedding
- Wavy Bedding
- Lenticular Bedding
- Hummocky Cross-Stratification
- Soft-Sediment Deformation
- Rootlets
- Lag Deposits
- Echinoderms
- Bioturbation
- Coated Grains
- Ooids
- Skeletal Fragments
- Organic and Coal Debris
- Foraminifera

See **Table 1** for facies definition and description

Figure 2

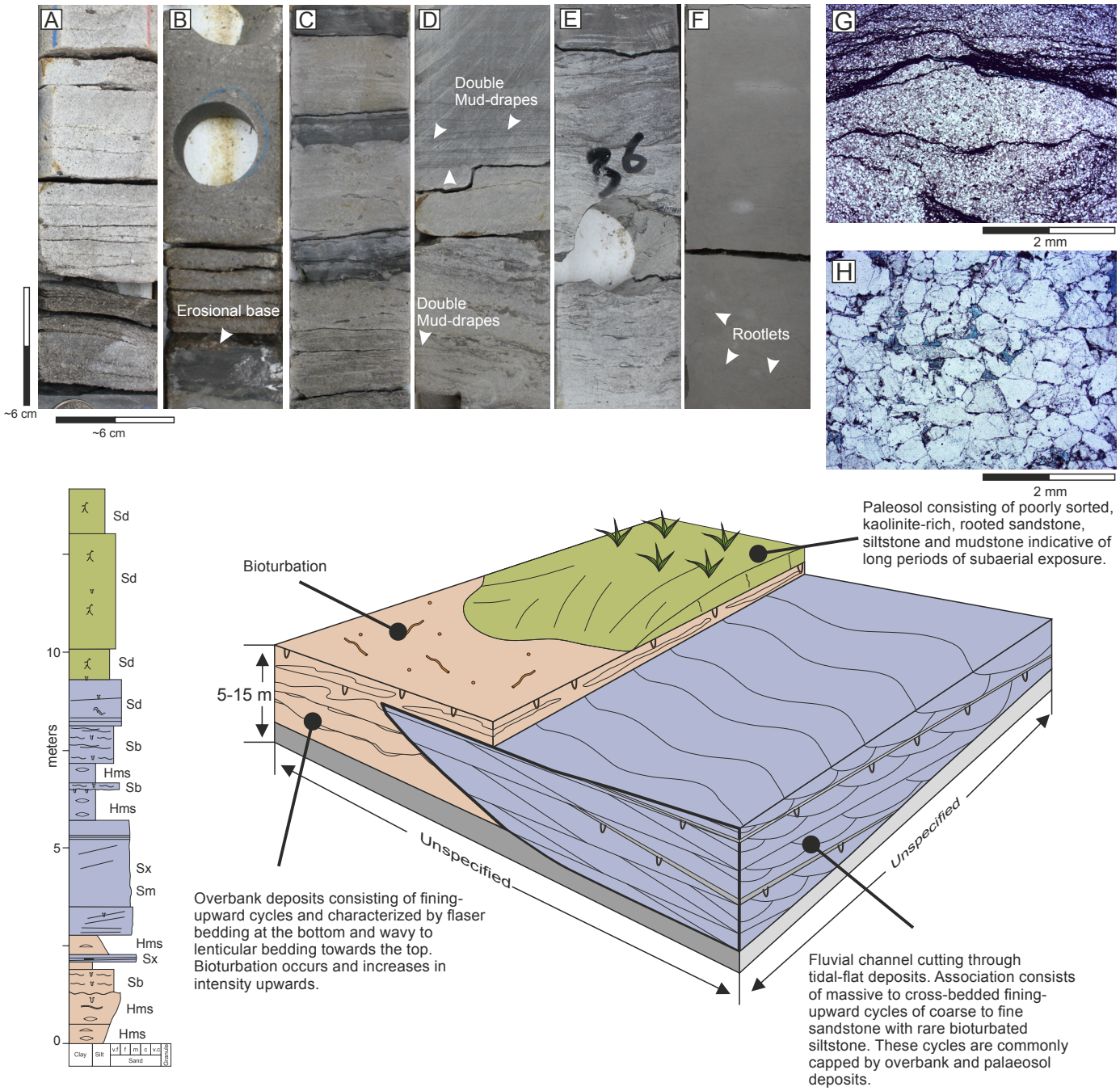
A
B
C
D
E
F
G
H
Double
Mud-drapes
Erosional base
Double
Mud-drapes
Rootlets
36
~6 cm
~6 cm
2 mm
2 mm
Paleosol consisting of poorly sorted, kaolinite-rich, rooted sandstone, siltstone and mudstone indicative of long periods of subaerial exposure.
Bioturbation
5-15 m
Unspecified
Unspecified
Overbank deposits consisting of fining-upward cycles and characterized by flaser bedding at the bottom and wavy to lenticular bedding towards the top. Bioturbation occurs and increases in intensity upwards.
Fluvial channel cutting through tidal-flat deposits. Association consists of massive to cross-bedded fining-upward cycles of coarse to fine sandstone with rare bioturbated siltstone. These cycles are commonly capped by overbank and palaeosol deposits.
meters
10
5
0
Sd
Sd
Sd
Sd
Sb
Hms
Sb
Hms
Sx
Sm
Hms
Sx
Sb
Hms
Hms
Clay
Silt
Sand
Granule

Figure 3

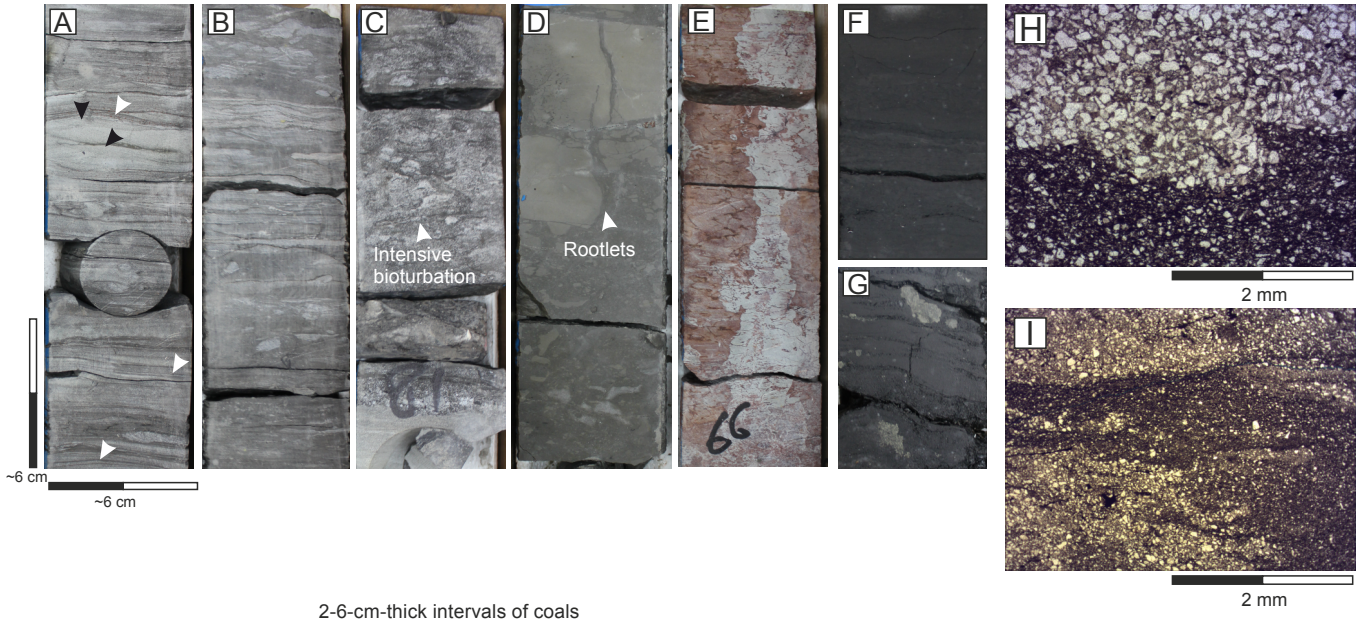
A
B
C
D
E
F
G
H
I
Intensive bioturbation
Rootlets
~6 cm
~6 cm
2 mm
2 mm

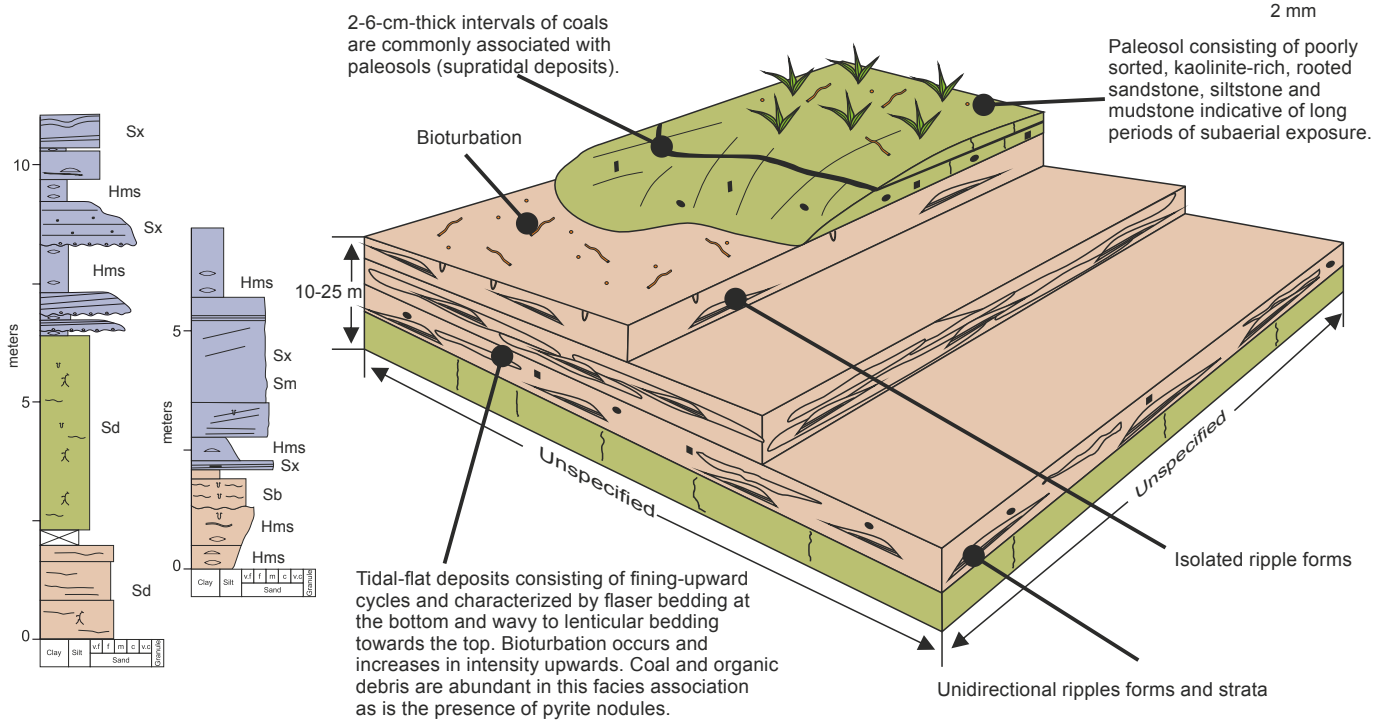
2-6-cm-thick intervals of coals are commonly associated with paleosols (supratidal deposits).
Paleosol consisting of poorly sorted, kaolinite-rich, rooted sandstone, siltstone and mudstone indicative of long periods of subaerial exposure.
Bioturbation
10-25 m
meters
Sx
Hms
Sx
Hms
Sd
Sd
Hms
Sx
Sm
Hms
Sx
Sb
Hms
Hms
Unspecified
Unspecified
Isolated ripple forms
Tidal-flat deposits consisting of fining-upward cycles and characterized by flaser bedding at the bottom and wavy to lenticular bedding towards the top. Bioturbation occurs and increases in intensity upwards. Coal and organic debris are abundant in this facies association as is the presence of pyrite nodules.
Unidirectional ripples forms and strata

Figure 4

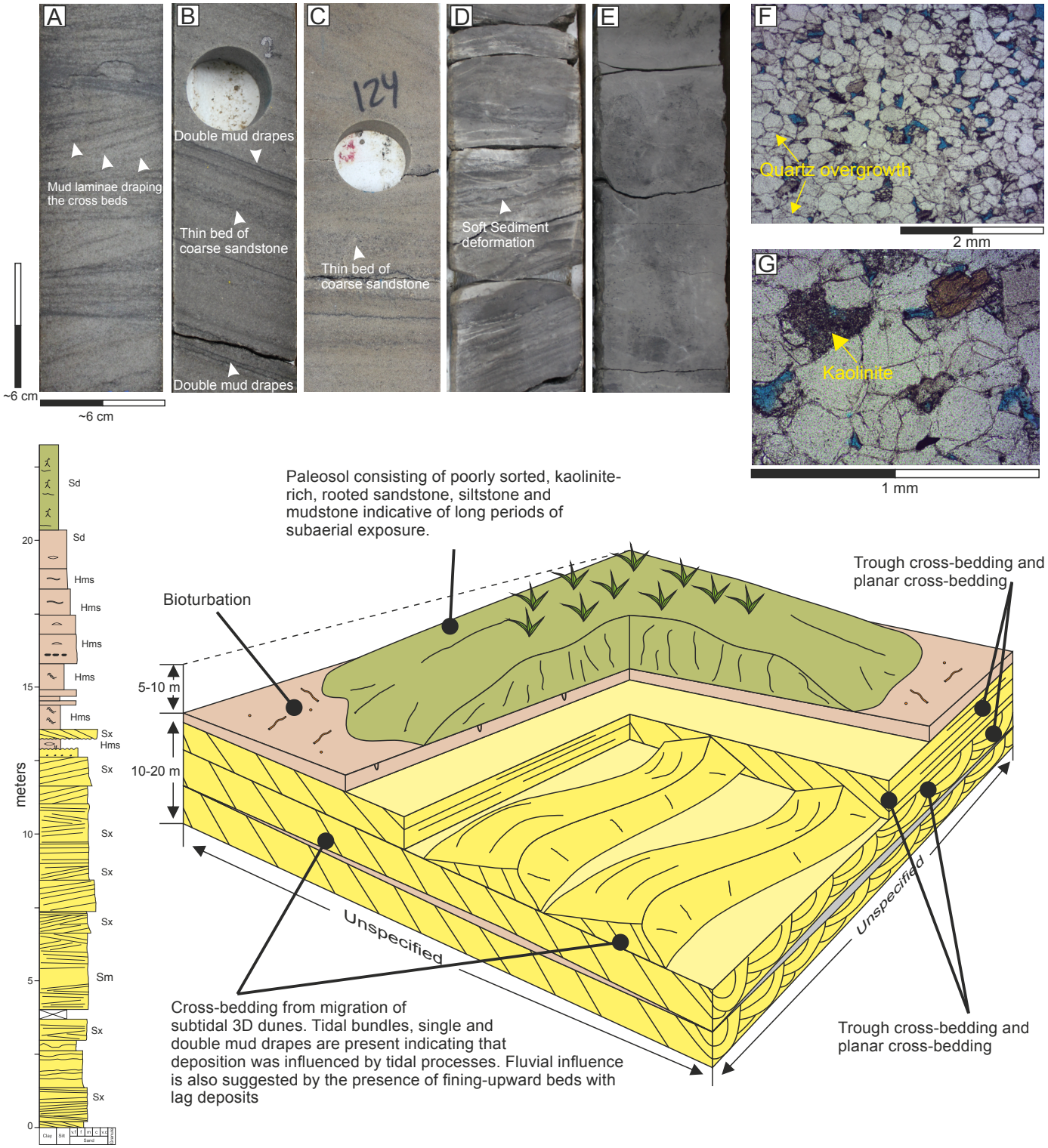
A
B
C
D
E
F
G
Mud laminae draping the cross beds
Double mud drapes
Thin bed of coarse sandstone
Double mud drapes
124
Thin bed of coarse sandstone
Soft Sediment deformation
~6 cm
~6 cm
Quartz overgrowth
2 mm
Kaolinite
1 mm
Paleosol consisting of poorly sorted, kaolinite-rich, rooted sandstone, siltstone and mudstone indicative of long periods of subaerial exposure.
Bioturbation
Trough cross-bedding and planar cross-bedding
5-10 m
10-20 m
Unspecified
Unspecified
Trough cross-bedding and planar cross-bedding
Cross-bedding from migration of subtidal 3D dunes. Tidal bundles, single and double mud drapes are present indicating that deposition was influenced by tidal processes. Fluvial influence is also suggested by the presence of fining-upward beds with lag deposits
meters
0
5
10
15
20
Sd
Sd
Hms
Hms
Hms
Hms
Hms
Sx
Hms
Sx
Sx
Sx
Sx
Sm
Sx
Sx

Figure 5

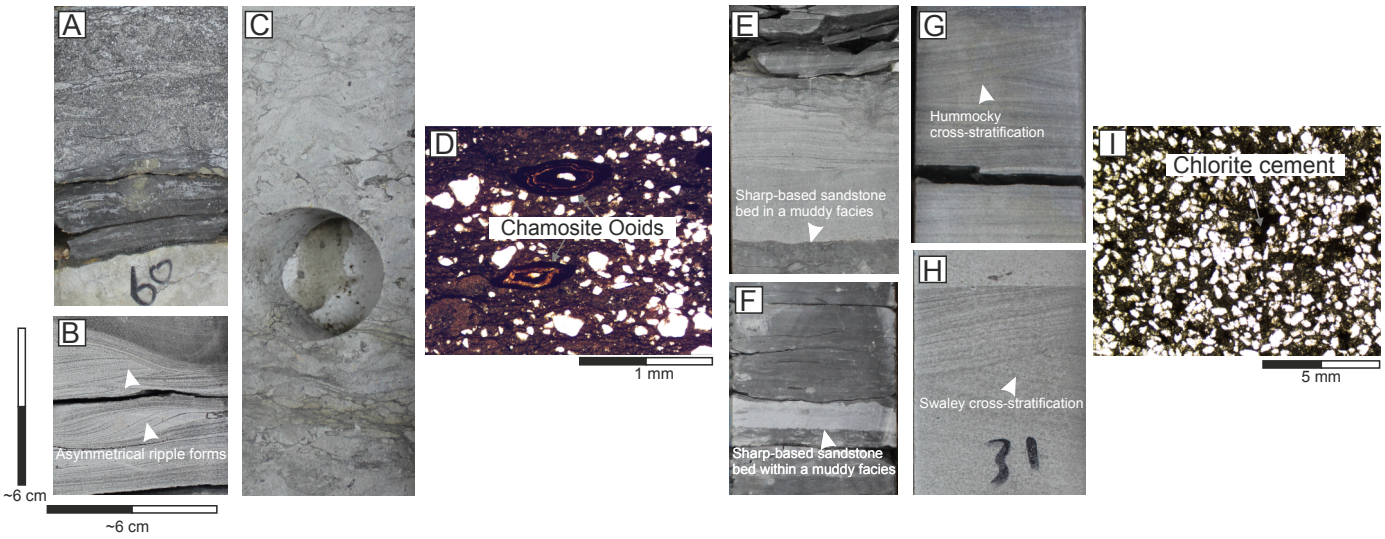
A
B
C
D
E
F
G
H
I
Asymmetrical ripple forms
~6 cm
~6 cm
Chamosite Ooids
1 mm
Sharp-based sandstone bed in a muddy facies
Sharp-based sandstone bed within a muddy facies
Hummocky cross-stratification
Swaley cross-stratification
Chlorite cement
5 mm

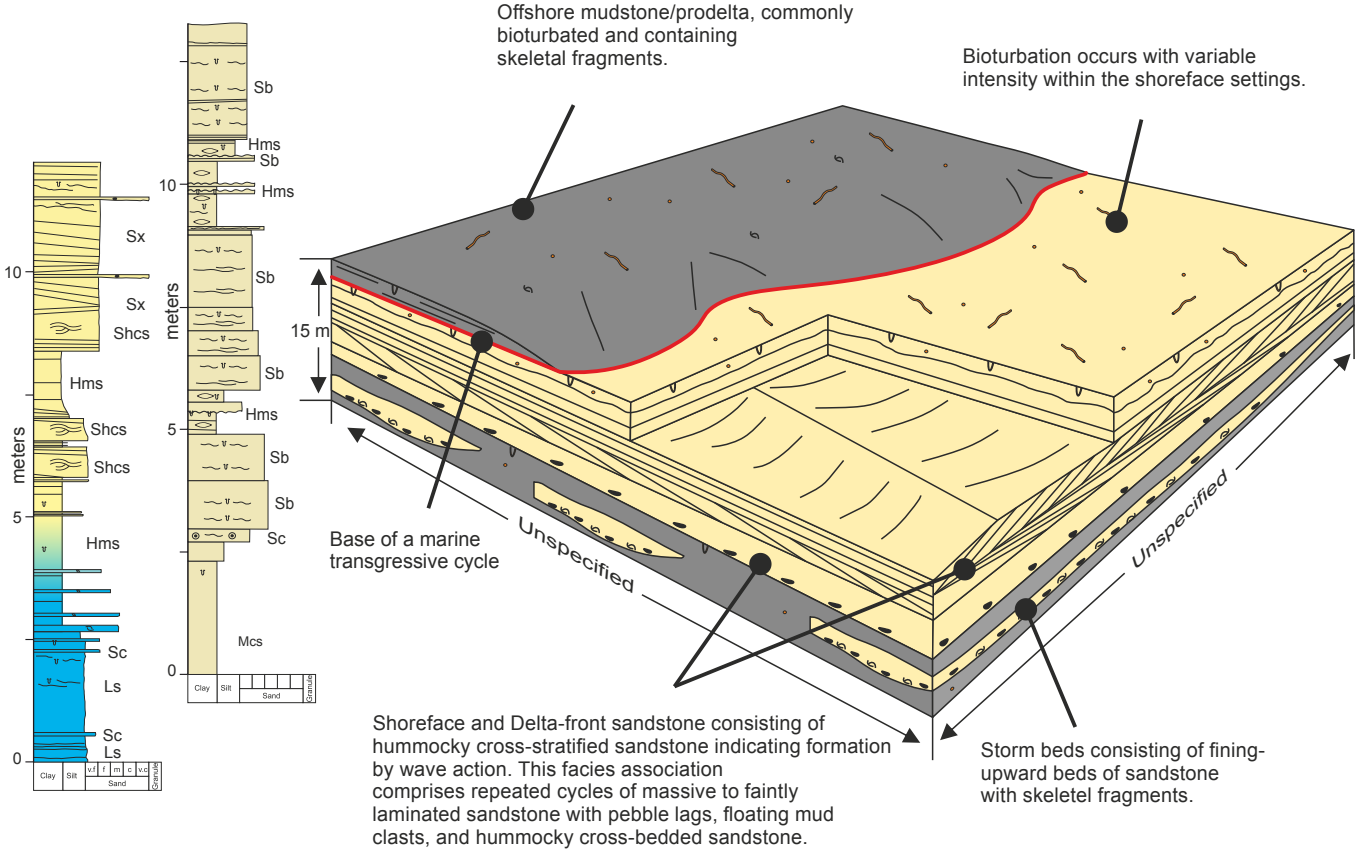
Offshore mudstone/prodelta, commonly bioturbated and containing skeletal fragments.
Bioturbation occurs with variable intensity within the shoreface settings.
meters
Sx
Sx
Shcs
Hms
Shcs
Shcs
Hms
Sc
Ls
Sc
Ls
Sb
Hms
Sb
Hms
Sb
Sb
Hms
Sb
Sb
Sc
Mcs
15 m
Base of a marine transgressive cycle
Unspecified
Unspecified
Shoreface and Delta-front sandstone consisting of hummocky cross-stratified sandstone indicating formation by wave action. This facies association comprises repeated cycles of massive to faintly laminated sandstone with pebble lags, floating mud clasts, and hummocky cross-bedded sandstone.
Storm beds consisting of fining-upward beds of sandstone with skeletel fragments.

Figure 6

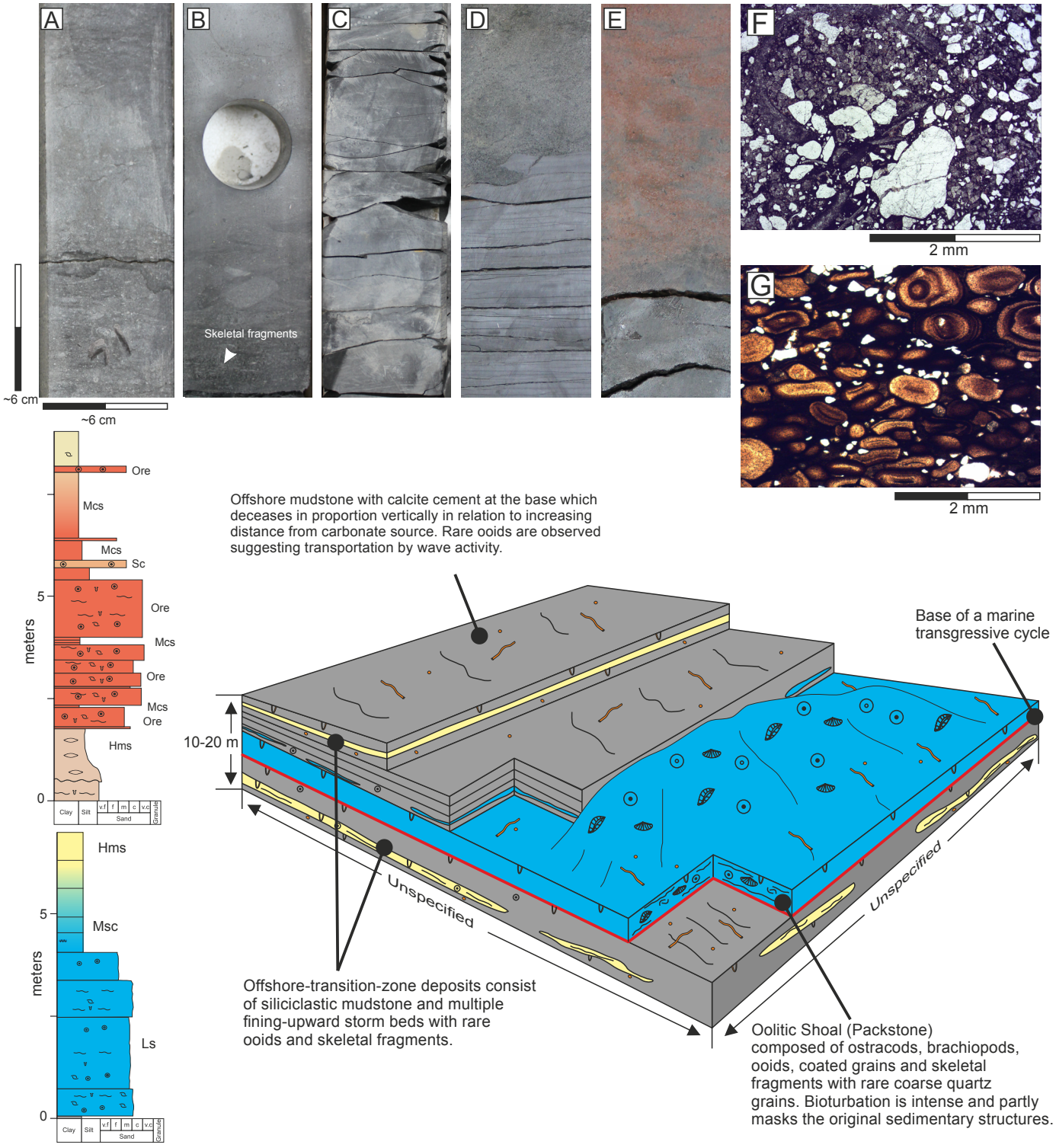
A
B
C
D
E
F
G
Skeletal fragments
~6 cm
~6 cm
2 mm
2 mm
Ore
Mcs
Mcs
Sc
Ore
Mcs
Ore
Mcs
Ore
Hms
meters
5
0
Clay
Silt
v.f
f
m
c
v.c
Sand
Granule
Hms
Msc
Ls
meters
5
0
Offshore mudstone with calcite cement at the base which deceases in proportion vertically in relation to increasing distance from carbonate source. Rare ooids are observed suggesting transportation by wave activity.
10-20 m
Base of a marine transgressive cycle
Unspecified
Unspecified
Offshore-transition-zone deposits consist of siliciclastic mudstone and multiple fining-upward storm beds with rare ooids and skeletal fragments.
Oolitic Shoal (Packstone) composed of ostracods, brachiopods, ooids, coated grains and skeletal fragments with rare coarse quartz grains. Bioturbation is intense and partly masks the original sedimentary structures.

Figure 7

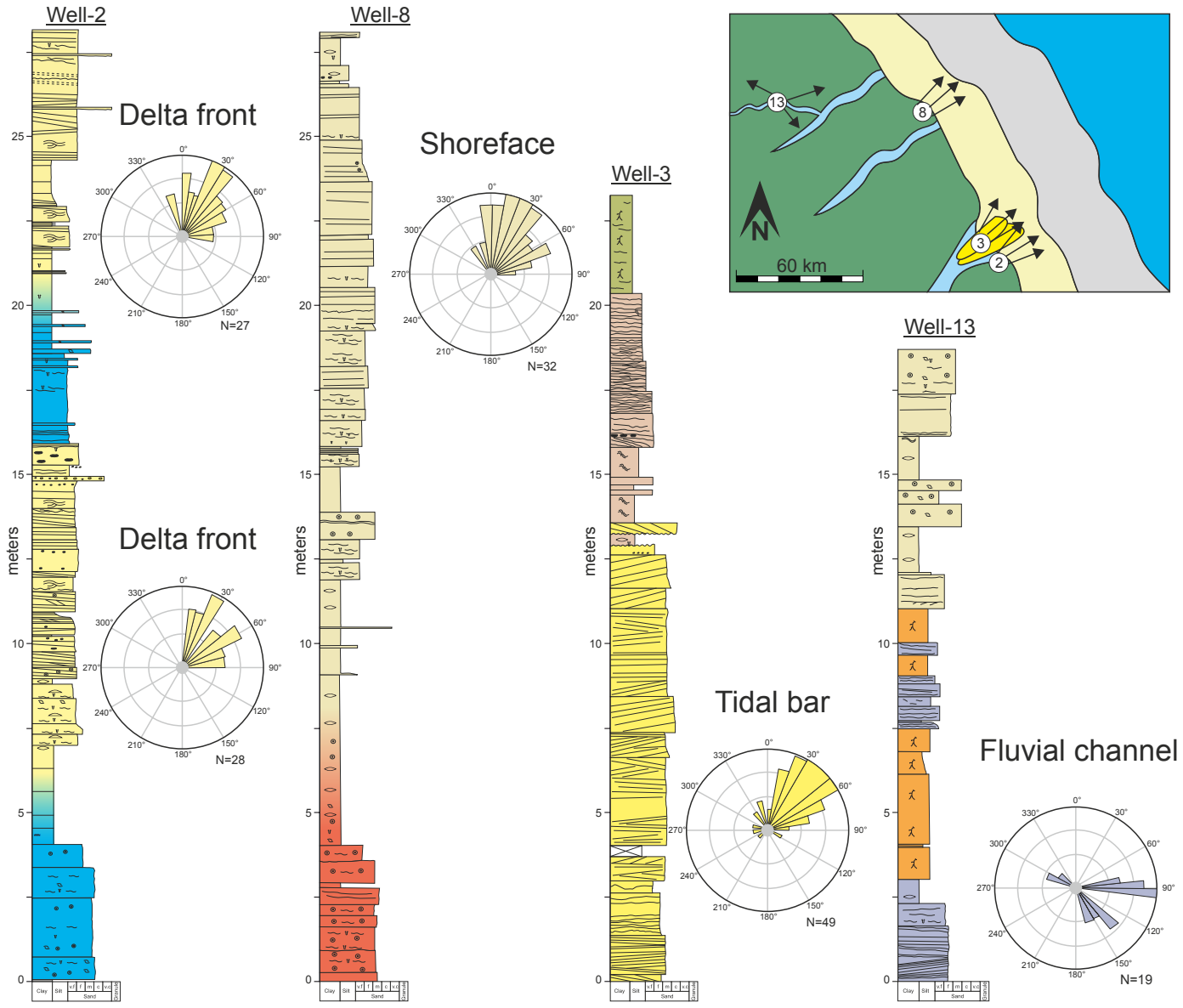
Well-2
Well-8
Well-3
Well-13
Delta front
Delta front
Shoreface
Tidal bar
Fluvial channel
N=27
N=28
N=32
N=49
N=19
meters
60 km
N
13
8
3
2

Figure 8

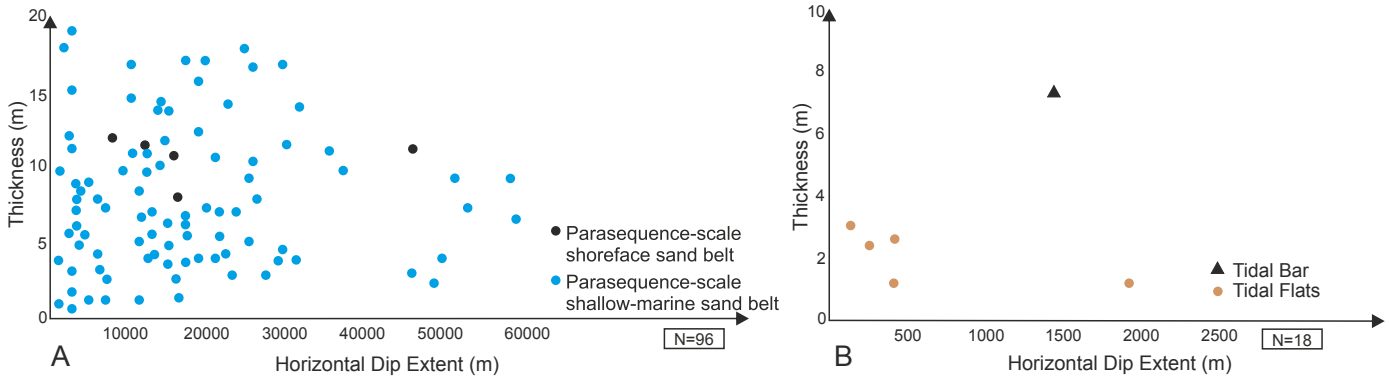
20
15
10
5
0
Thickness (m)
10000
20000
30000
40000
50000
60000
Horizontal Dip Extent (m)
Parasequence-scale shoreface sand belt
Parasequence-scale shallow-marine sand belt
N=96
A
10
8
6
4
2
0
Thickness (m)
500
1000
1500
2000
2500
Horizontal Dip Extent (m)
Tidal Bar
Tidal Flats
N=18
B

Figure 9

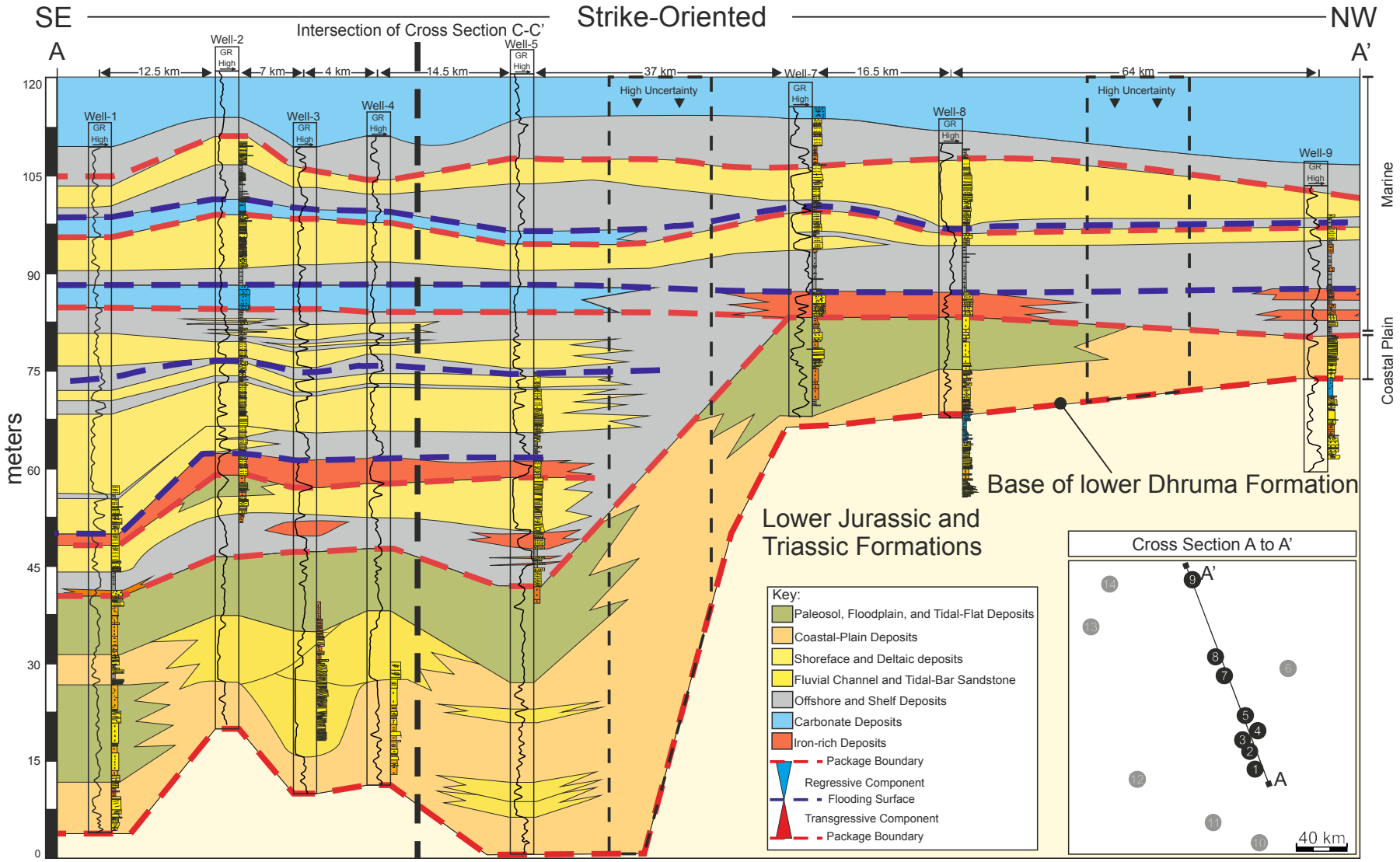
SE
A
Strike-Oriented
NW
A'
Intersection of Cross Section C-C'
Well-1
Well-2
Well-3
Well-4
Well-5
Well-7
Well-8
Well-9
GR
High
12.5 km
7 km
4 km
14.5 km
37 km
16.5 km
64 km
High Uncertainty
High Uncertainty
120
105
90
75
60
45
30
15
0
meters
Marine
Coastal Plain
Base of lower Dhruma Formation
Lower Jurassic and
Triassic Formations
Key:
Paleosol, Floodplain, and Tidal-Flat Deposits
Coastal-Plain Deposits
Shoreface and Deltaic deposits
Fluvial Channel and Tidal-Bar Sandstone
Offshore and Shelf Deposits
Carbonate Deposits
Iron-rich Deposits
Package Boundary
Regressive Component
Flooding Surface
Transgressive Component
Package Boundary
Cross Section A to A'
A'
A
40 km

Figure 10A

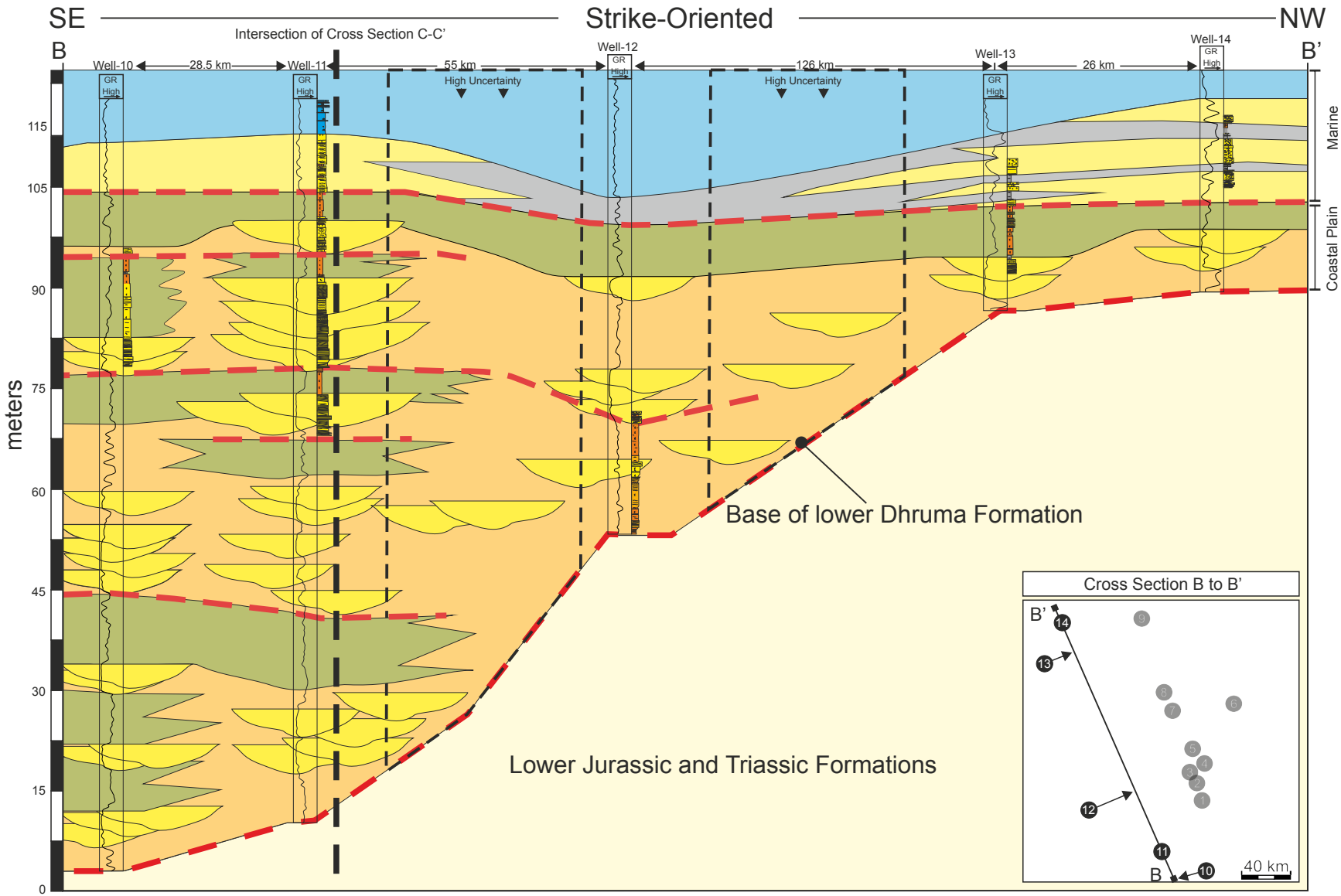
SE
Strike-Oriented
NW
B
B'
Intersection of Cross Section C-C'
Well-10
28.5 km
Well-11
55 km
Well-12
126 km
Well-13
26 km
Well-14
GR
High
High Uncertainty
meters
115
105
90
75
60
45
30
15
0
Marine
Coastal Plain
Base of lower Dhruma Formation
Lower Jurassic and Triassic Formations
Cross Section B to B'
B'
B
40 km

Figure 10B

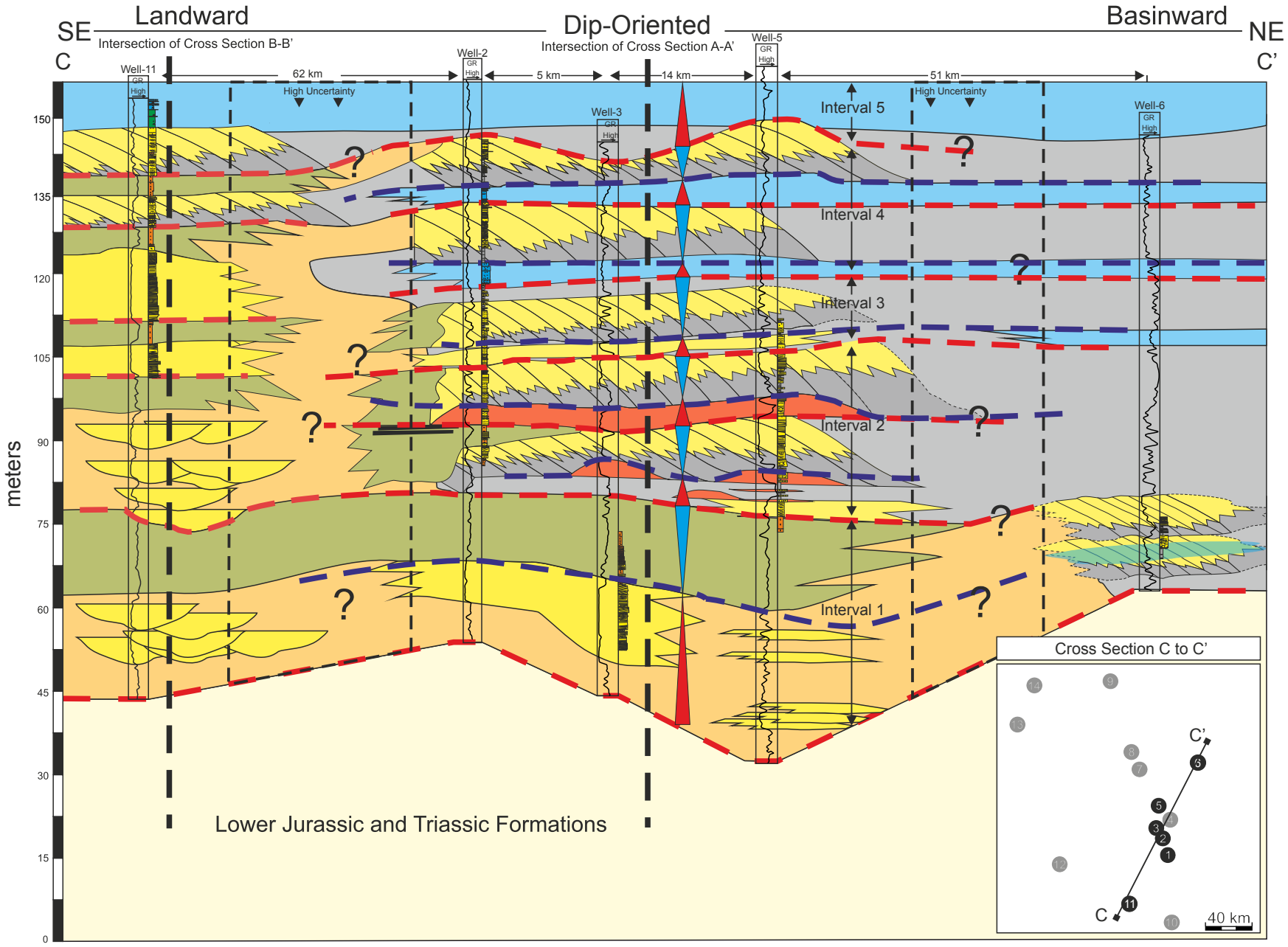
SE
C
Landward
Intersection of Cross Section B-B'
Dip-Oriented
Intersection of Cross Section A-A'
Basinward
NE
C'
Well-11
Well-2
Well-3
Well-5
Well-6
GR
High
62 km
5 km
14 km
51 km
High Uncertainty
High Uncertainty
Interval 5
Interval 4
Interval 3
Interval 2
Interval 1
meters
150
135
120
105
90
75
60
45
30
15
0
Lower Jurassic and Triassic Formations
Cross Section C to C'
C'
C
40 km

Figure 10C

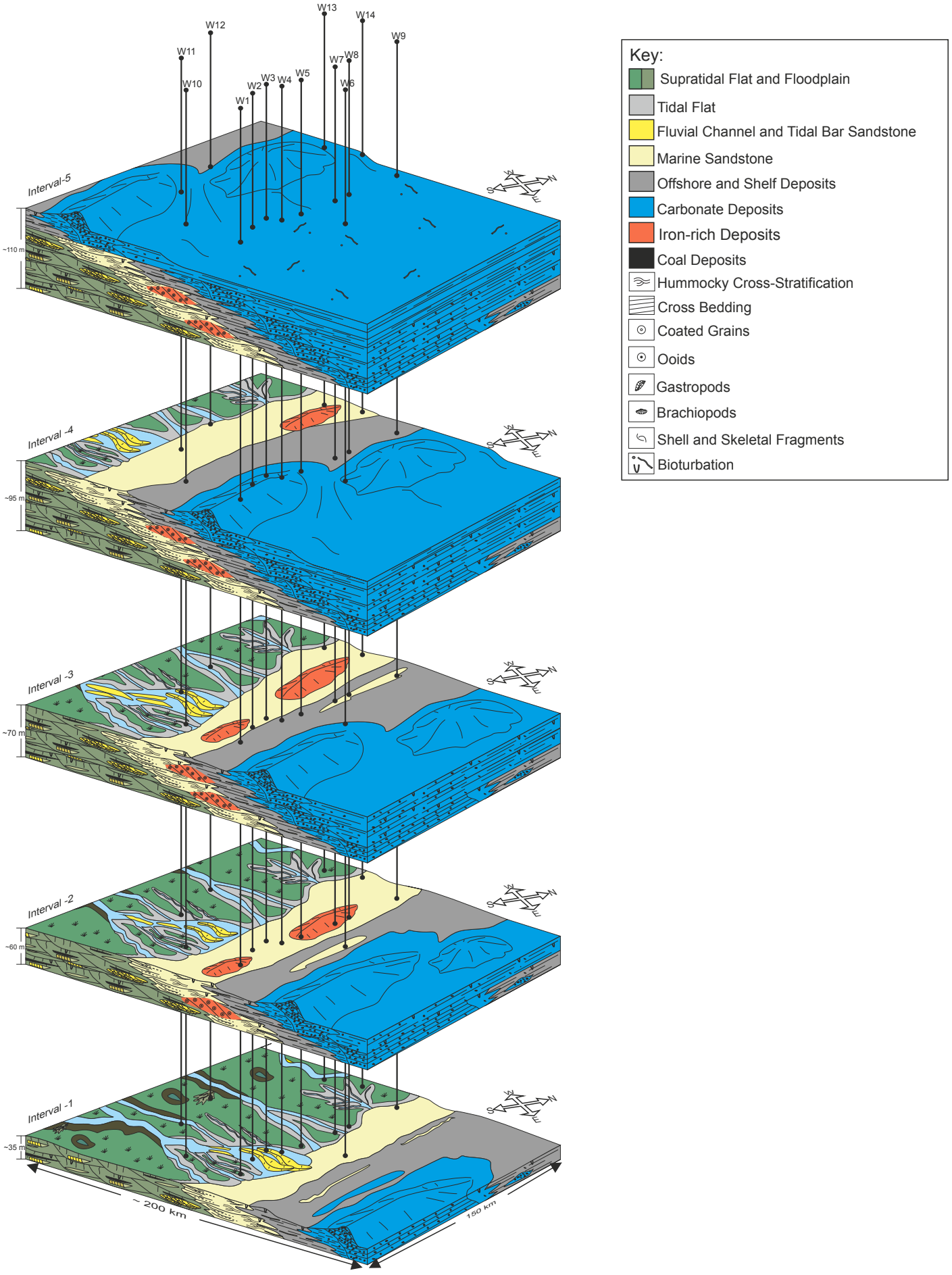
W1
W2
W3
W4
W5
W6
W7
W8
W9
W10
W11
W12
W13
W14
Interval -5
~110 m
Interval -4
~95 m
Interval -3
~70 m
Interval -2
~60 m
Interval -1
~35 m
~ 200 km
150 km
Key:
Supratidal Flat and Floodplain
Tidal Flat
Fluvial Channel and Tidal Bar Sandstone
Marine Sandstone
Offshore and Shelf Deposits
Carbonate Deposits
Iron-rich Deposits
Coal Deposits
Hummocky Cross-Stratification
Cross Bedding
Coated Grains
Ooids
Gastropods
Brachiopods
Shell and Skeletal Fragments
Bioturbation

Figure 11